Monitoring the Excited State Dynamics of Thymine by Time-Resolved IR Spectroscopy

Bert Manuel Pilles

München 2016

Monitoring the Excited State Dynamics of Thymine by Time-Resolved IR Spectroscopy

Bert Manuel Pilles

Dissertation

an der Fakultät für Physik
der Ludwig-Maximilians-Universität
München

vorgelegt von
Bert Manuel Pilles
aus Temeschburg.

München, den 17. Mai 2016

Erstgutachter: Prof. Dr. Wolfgang Zinth
Zweitgutachter: Prof. Dr. Peter Gilch
Tag der mündlichen Prüfung: 01.07.2016

Contents

Kurzfassung

UV-angeregte Zustände von DNS-Basen sind potentiell reaktiv und können daher zu Photoschäden führen. In dieser Arbeit wurden langlebige angeregte Zustände von Mono- und Oligomeren der Base Thymin in wässriger Lösung mittels zeitaufgelöster Infrarotspektroskopie untersucht (TRIR). Thymin ist besonders interessant, da der häufigste Photoschaden, das sogenannte Cyclobutan Pyrimidin Dimer (CPD), durch Cycloaddition von zwei Thyminen gebildet wird. Die Proben wurden durch UV-Photonen angeregt und im Mittelinfrarotbereich (MIR) abgefragt. Die Messungen an Nukleotiden liefern Informationen über deren intrinsische Eigenschaften, während der Einfluss von Wechselwirkungen zwischen benachbarten Basen durch den Vergleich der Photophysik von Oligomeren und Monomeren untersucht wird.

Der niedrigste Triplettzustand $^3\pi\pi^*$ wurde im Hinblick auf seine Entstehung und seinen Zerfall untersucht. Er wird innerhalb von einigen wenigen Pikosekunden, jedoch erst nach dem Zerfall des angeregten $^1\pi\pi^*$ Zustandes, über einen Zwischenzustand gebildet. Dieser wurde nicht direkt beobachtet, kann aber aus theoretischen Gründen als $n\pi^*$ Zustand identifiziert werden. Die Messungen zeigten einen weiteren angeregten Zustand mit einer Lebensdauer von ca. 1 ns, der bislang unbekannt war. Es werden in der vorliegenden Arbeit einige Hypothesen über dessen Identität diskutiert, doch sind zur Klärung weitere Untersuchungen nötig.

Der Zerfall des $^3\pi\pi^*$ Zustandes wurde im Monomer TMP und im Oligomer $(dT)_{18}$ untersucht. Besonders interessant ist letztere Probe, da hieraus CPD-Schäden resultieren können. Hier bindet sich das angeregte Thymin kovalent an eine benachbarte Base, wobei jeweils ein ungepaartes Elektron mit demselben Spin auf jeder Base übrig bleibt. Dieses *Biradikal* zerfällt hauptsächlich in den Grundzustand ($> 85\,\%$), somit ist die Quantenausbeute für die CPD Bildung aus dem $^3\pi\pi^*$ Zustand unter $15\,\%$.

Die Wechselwirkungen gestapelter Basen eröffnen zudem weitere Reaktionskanäle, die in Monomeren nicht vorhanden sind. In dieser Arbeit konnte gezeigt werden, dass im angeregten Zustand im Thymidin Oligomer Ladungstransfer möglich ist, so dass Kation- und Anion-Radikale entstehen können. Diese Zustände sind einerseits reaktiv und könnten somit zu DNS-Schäden führen. Andererseits setzen Ladungstransfer und CPD-Bildung Basenstapelung voraus, so dass beide Prozesse möglicherweise miteinander konkurrieren. Dann würde ein Ladungstransfer indirekt zur Photostabilität der DNS beitragen.

Abstract

UV-excited states of DNA bases are potentially reactive and can lead to photolesions. In this thesis, long-living excited states of monomers and oligomers of the base thymine in aqueous solution were investigated by time-resolved infrared (TRIR) spectroscopy. Thymine is particularly interesting, because the most abundant DNA photolesion, the *cyclobutane pyrimidine dimer*, is formed by a cyclo-addition of two thymines.

The samples were excited by UV photons and probed in the middle infrared (MIR) spectral range. Measurements on nucleotides yield information about their intrinsic properties, while the influence of interactions between neighbouring bases is investigated by comparing the photophysics of oligomers and monomers.

The lowest triplet state $^3\pi\pi^*$ was studied with regard to its formation and its decay. It is formed within a few picoseconds, after the decay of the excited $^1\pi\pi^*$ state via an intermediate state. The latter is not observed directly, but it can be identified as a $n\pi^*$ state by theoretical considerations. The measurements show another excited state with a lifetime of circa 1 ns that was not reported before. Some hypotheses concerning its nature are discussed in the present work, but more investigations are necessary to identify it unequivocally.

The decay of the $^3\pi\pi^*$ state was observed in the monomer and the oligomer. The latter sample is especially interesting, because the $^3\pi\pi^*$ state is a precursor of the CPD lesion. The triplet decay in the thymidine oligomer proceeds via a *biradical* intermediate, where the excited thymine binds covalently to a neighbouring base, leaving an unpaired electron with the same spin on each base. The biradical predominantly returns to the electronic ground state ($> 85\,\%$), hence the quantum yield of CPD formation out of the $^3\pi\pi^*$ state is below $15\,\%$.

The interactions between stacked bases open additional reaction channels that are not present in monomers. In this thesis, charge transfer out of the excited state in the thymidine oligomer was demonstrated, yielding cation and anion radicals. These states are reactive and could lead to DNA lesions. On the other hand, charge transfer and CPD formation require stacked bases, so both processes might be competing with each other. If this is true, then charge transfer could indirectly contribute to DNA photostability.

1. Introduction

The most iconic picture in all of biology is probably that of the DNA double helix. Its paramount status in the collective memory reflects its paramount importance for life on earth. DNA stores the hereditary information of organisms. It contains the genetic code, a building plan for proteins, macromolecules that are involved in almost all vital functions. Proteins are comprised of often more than 1000 amino acids that have to be assembled in the right sequence to be functional [Ber11]. The correct sequence is defined by corresponding sequences of the DNA (genes). These are transcribed into a messenger RNA (*transcription*), which in turn is used as a template to assemble amino acids into proteins (*translation*) [LSO61, Mat62]. The translation of the genetic information into proteins is the central process in biology, because it is virtually impossible to overstate the importance of proteins for life. They catalyse and control vital chemical reactions, they regulate the ion concentration in cells, as membrane receptors they fulfil signalling and transport functions, they enable muscle contractions and thereby movement, they give structure to cells, they make up fabrics like hair and nails and much more [Alb11]. A correct assembly of proteins is therefore of the utmost importance. It requires the genetic code to be intact [Ber11]. Mutations of the genetic code have severe consequences: Dysfunctional or even harmful proteins can be synthesised, resulting in accelerated cell ageing or even cell death. Still worse, mutations of genes that control cell growth can be the first steps leading to cancer [Ber14]. The integrity of the genetic code is constantly threatened by internal and external hazards. Internal hazards include the generation of reactive species like radicals during the normal metabolism. Among the most important external hazards is the UV radiation of the sun. UV radiation is absorbed by the DNA bases, promoting them to potentially reactive excited states. From there, photolesions can be generated that may make the bases unreadable during transcription or even lead to transcription errors. If such lesions occur, most of them are repaired by various mechanisms in different organisms. If too many photolesions are accumulated to be repaired, a programmed cell death is initiated (apoptosis) by mechanisms that are not fully understood at the present time. If these protective measures fail, such photolesions can ultimately lead to skin cancer [Kra97, GKM01, Nor11], as well as immuno suppression [CDM01, PBH05] and certain eye diseases [Gru03, And05]. Unravelling the pathway from UV-induced DNA lesions to those diseases is of major scientific interest and health relevance. The first steps are photophysical and photochemical reactions of DNA. Absorption spectroscopy has proved to be one of the most useful techniques to investigate these processes.

Particularly in the middle-infrared (MIR) spectral range, where the absorbance is caused by vibrations, very detailed spectra can be obtained. They are not only highly specific, but also sensitive to conformational changes that can be induced by the formation of photolesions. Steady state spectroscopy of UV-irradiated DNA samples can identify the accumulated photoproducts and their quantum yields by the induced absorption changes. Time-resolved absorption spectroscopy can track the underlying photophysical processes that typically occur on the timescale of picoseconds.

In this thesis, time-resolved infrared spectroscopy (TRIR) is used to investigate the photophysics of thymidine monophosphate (TMP) and the thymidine oligomer (5'–3') $(dT)_{18}$ on the picosecond to microsecond timescale. Studying the excited state physics of nucleotides can reveal the intrinsic photophysical properties of the bases that can only interact with the solvent. These seemingly simple systems are still not very well understood, as there are conflicting views of the nature of excited states and the mechanisms of their generation and decay (see chapter 7). Since the excited states have a very low quantum yield of formation, they are notoriously hard to observe. In addition, they decay almost exclusively non-radiatively, so they cannot be observed by fluorescence spectroscopy. Transient absorption spectroscopy can address these states with high accuracy.

The complexity increases, if oligomers are studied instead of monomers. In oligomers, the accepted view is that unstacked bases behave like monomers, while stacked bases behave differently [Mid09]. Interactions between neighbouring bases can lead to the delocalization of excitation energy over more than one base. This can happen via dipole-dipole interactions as well as transfers of charges between neighbouring bases. Such delocalised states could be precursors of DNA photolesions [Ban12, Imp12]. However, ultrafast charge transfer could also be an efficient mechanism to deactivate excited states [Buc14a]. Both possibilities are discussed in the present work.

This thesis is structured in the following way:

Chapter 2 introduces the theoretical background of this thesis. The structure and the basic properties of the DNA bases are explained. An introduction to the photophysical properties and the excited states of DNA bases, particularly thymine, is given. A brief overview over the most common UV-induced photolesions concludes this chapter.

Chapter 3 explains the experimental techniques used in this thesis. After a short description of the laser system, the pump-probe setup is explained in more detail. The chapter is concluded by a brief introduction to time-resolved IR spectroscopy (TRIR) and to typical signals that occur in TRIR measurements.

Chapter 4 introduces the UV and IR absorption spectra of thymine and adenine nucleotides and oligonucleotides (the spectra of adenine will be needed in chapter 6). The vibrations that make up the IR spectra are identified. The effects of base stacking on the absorbance spectra (UV and IR) are introduced.

Chapter 5 reports TRIR measurements of the kinetics of the lowest triplet state ($^3\pi\pi^*$) of thymine on the timescale of nanoseconds and microseconds. The photophysics starting from the $^3\pi\pi^*$ state is investigated in TMP and in the all-thymine strand $(dT)_{18}$. The processes that can either lead to CPD formation or to ground state recovery out of the $^3\pi\pi^*$ state are investigated and discussed.

Chapter 6 discusses the possibility of charge transfer between stacked thymine bases out of the excited $^1\pi\pi^*$ state, resulting in a charge separated state. TRIR measurements reveal an excited state that may be of that nature. This possibility is explored by comparing its signature to those of thymine cations and anions.

Chapter 7 discusses the role of $n\pi^*$ states in the excited state physics of thymine, particularly as precursors to the $^3\pi\pi^*$ state. The measurements show a long-living excited state that may be of $n\pi^*$ nature. The transition from the excited $^1\pi\pi^*$ state to the $^3\pi\pi^*$ state is monitored and the underlying mechanism is discussed.

2. Theory DNA

UV radiation is absorbed by DNA and can cause photochemical reactions that endanger the integrity of the genetic code. The underlying photophysical processes have been investigated by time-resolved absorption spectroscopy. This chapter explains the fundamentals of DNA photophysics. The first part briefly introduces the DNA bases and the structure of the DNA double helix. The second and the third parts explain the excited state physics of DNA bases and DNA single strands, respectively. A discussion of some of the UV-induced photolesions that can ultimately result from the DNA excited state physics concludes this chapter.

2.1. DNA Structure

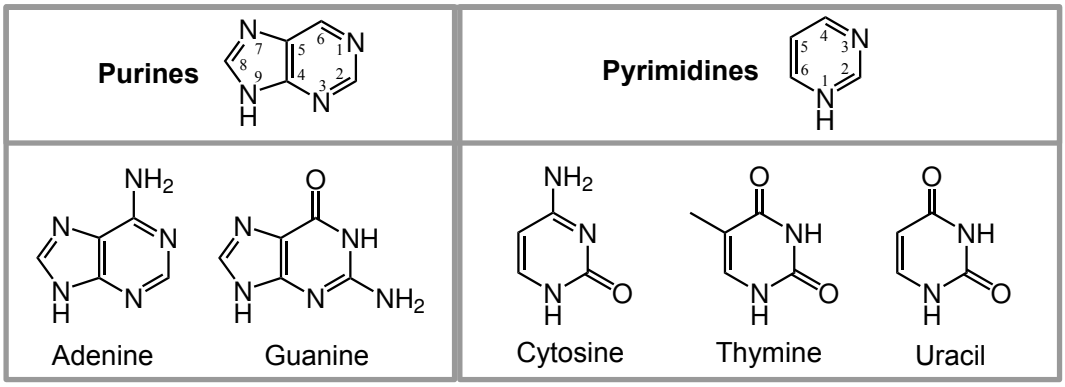

Figure 2.1.: The DNA bases adenine (A), guanine (G), cytosine (C), thymine (T) and the RNA base uracil (U). There are 2 basic structures, purines (A,G) and pyrimidines (C,T,U).

The fundamental building blocks of DNA and RNA are the five bases thymine (T), cytosine (C), adenine (A), guanine (G) and uracil (U). Cytosine, adenine and guanine are used in DNA and RNA alike, uracil only in RNA, thymine only in DNA. The bases are organic, aromatic heterocycles that can be grouped according to their ring structure: Pyrimidines (C, T, U) are 6-membered rings, while purines (A and G) consist of a 6-membered ring and a 5-membered ring. The atoms of pyrimidines and purines are numbered serially as depicted in Figure 2.1.

A DNA single strand is comprised of the bases that are connected by a sugar-phosphate backbone. A base is bound to a sugar (ribose and deoxyribose in RNA and DNA, respectively) to form a *nucleoside*. Ribose and deoxyribose are sugars with

5 carbon atoms (pentoses) that are numbered from 1' to 5' as depicted in Figure 2.2. Deoxyribose is almost identical to ribose, except that the hydroxy group that is attached to the C2' atom of ribose is replaced by hydrogen. Base and sugar are connected via a *N-glycosidic bond* between a nitrogen atom of the base (pyrimidines: N1, purines: N9) and the C1' atom of the sugar. A nucleoside that is connected to phosphoric acid at the 5' atom of the sugar is a *nucleotide*. These structures are displayed in Figure 2.2.

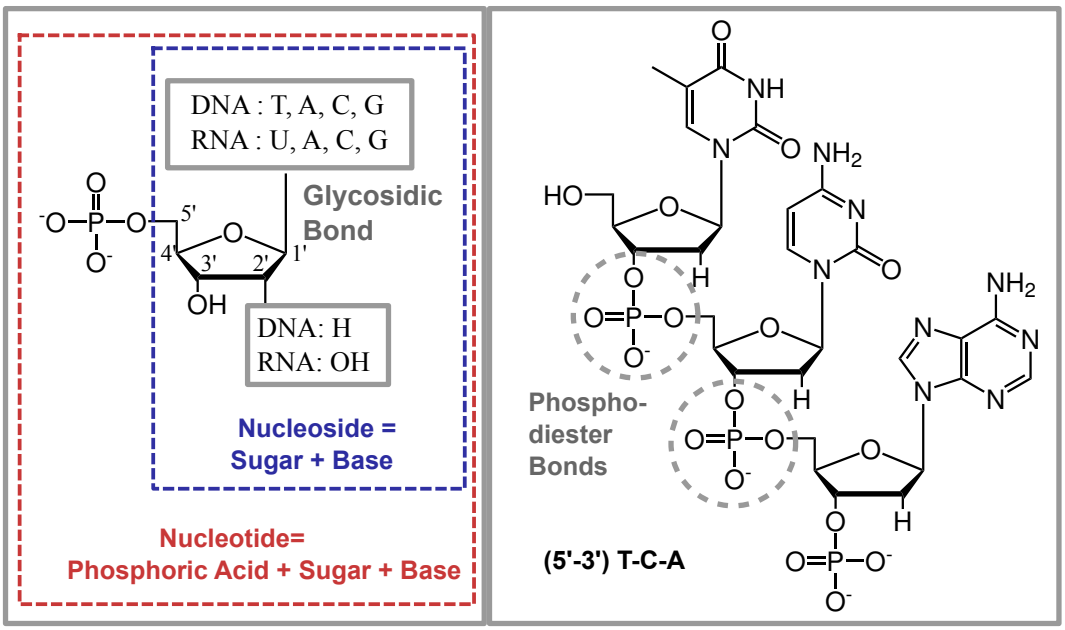

Figure 2.2.: Building blocks of DNA. A base linked by a glycosidic bond to a sugar is called a *nucleoside*. A nucleoside linked to a phosphoric acid at the C5' position is called a *nucleotide*. Nucleotides are connected to each other by phosphodiester bonds to form a DNA strand.

A DNA or RNA strand consists of nucleotides that are linked to each other by phosphodiester bonds of the C5' and C3' atoms of the sugars to the phosphoric acid (see right panel of Figure 2.2).

It may seem that DNA and RNA single strands in solution can coil randomly in any way. In fact they have defined structures because of interactions between the π-systems of neighbouring bases that make a stacked geometry energetically favourable. Hence these interactions are sometimes called *stacking interactions*. They include hydrophobic interactions that make isolated, unstacked bases energetically unfavourable, as well as electrostatic forces between the static dipole moments of the bases and van der Waals forces [BC69, Guc00, Blo00, Koo01].

The stacking properties of dimers and oligomers have been studied extensively by NMR spectroscopy and circular dichroism spectroscopy [WC70, Lee76, Ezr77, JIT72, BC69]. The stacking percentages of DNA heterodimers were found to be between

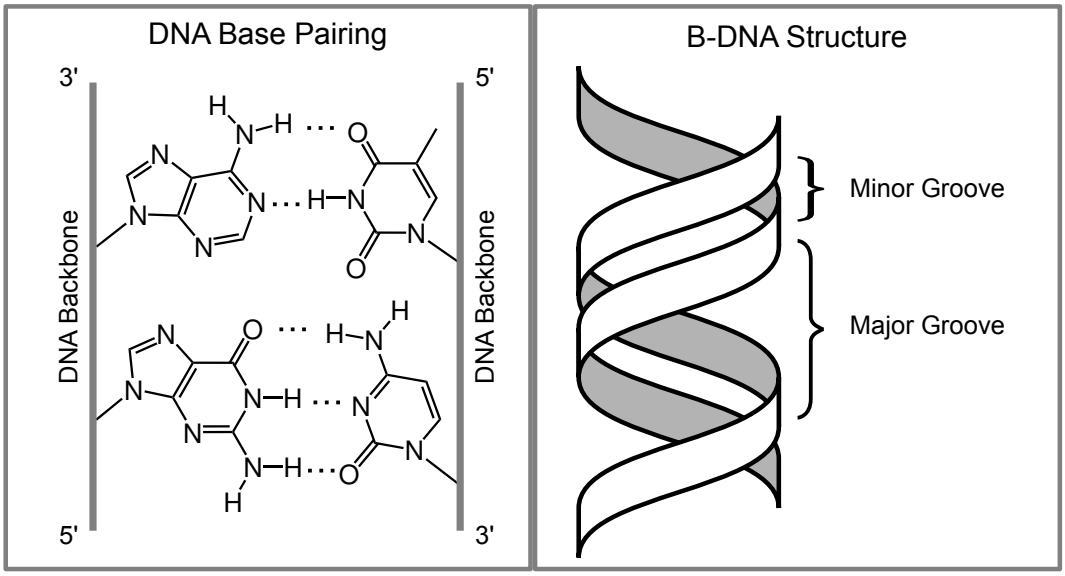

Figure 2.3.: Base pairing scheme of DNA in the double strand. A pairs with T via 2 H-bonds, C with G by 3 H-bonds (left). This base pairing pattern results in the famous double-helical structure of the DNA double strand in the native B-form (right).

10 % and almost 50 %, depending on the bases [Ezr77] and the base sequence. DNA is directional, i.e. the arrangement of stacked bases depends on the base sequence; if for instance a dimer is comprised of two different bases X and Y, the stacked dimers XpY and YpX [1] will have a different arrangement as well as different absorbance spectra [BC69, Pre74].

The DNA double strand is made up of two single strands that are connected by H-bonds between the bases on the inside of the double helix and the sugar-phosphate backbone on the outside. The connections of bases to bases on the opposing strand, referred to as *base pairing*, takes place only between complementary bases. Thymine is complementary to adenine and pairs with it by 2 H-bonds, cytosine pairs with guanine by 3 H-bonds [WC53a, WC53b, FG53, WSW53]. The base pairing pattern and the resulting double helical structure are depicted in Figure 2.3. Different double helical forms of DNA have been identified, two right-handed (so-called B-DNA and A-DNA) and a left-handed double helical structure (Z-DNA) [Wan83, Arn80, DD81, Sha89, HM97, Ber97, Dre81, BW04, WS97]. B-DNA is by far the predominant structure in eucaryontic cells, but A- and Z-DNA have been observed in living organisms, even though the functions of these structures are not yet known precisely [WS97, HM97].

The genetic information is stored in the DNA double helix. DNA nucleotides and single strands are by comparison only of minor biological importance. They are,

[1] The oligomers are by convention always written beginning with the 5' end, so XpY means (5'–3')-XpY.

however, scientifically important as model systems. The photophysical processes in UV-excited DNA double strands are influenced by the intrinsic properties of the bases as well as their intra- and interstrand interactions. The intrinsic photophysical properties of nucleotides can be observed directly. To understand the intrastrand interactions, single strands and the nucleotides that comprise them need to be investigated and compared. Only after these first two steps have been undertaken, comparisons between single- and double-stranded DNA can reveal the effects of interstrand interactions.

This thesis focusses on the first two steps. Though measurements of the DNA double helix have been successfully undertaken, the results are not published yet and will not be addressed here. All measurements discussed in this thesis were performed on bases, nucleotides or single strands.

2.2. Photophysics of the Excited State

All DNA bases absorb in the UVC and UVB spectral range due to strongly allowed $^1\pi\pi^*$ transitions. Figure 2.4 depicts the DNA absorption (black) and the relative intensity of the solar irradiation in the UV-range (light blue).

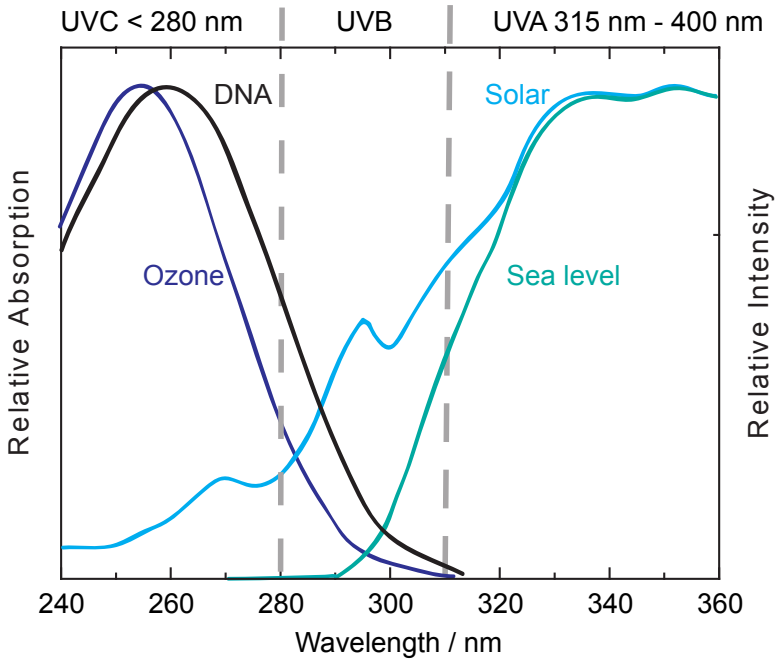

Figure 2.4.: DNA absorbs in the UVC and UVB spectral range (left axis). The UVC radiation of the sun (right axis) is effectively shielded by the ozone layer, but some UVB radiation reaches the earth's surface and can be absorbed by DNA. Data adapted with permission from [Tay94] (copyright American Chemical Society).

As Figure 2.4 shows, UVA radiation is not absorbed by DNA and hence does not harm it directly. However, numerous studies confirm that UVA radiation can cause DNA photolesions [Fre87, Cad86, Mou06, Mou10, Cad12]. They are generated by an indirect mechanism: other molecules, *sensitisers*, absorb UVA photons and undergo a transition to long-living excited states. Subsequently, they can transfer the energy to DNA bases, whereby they reach excited states. Such long-living excited states have been identified, particularly in the case of the base thymine, and proven to be precursors to DNA photolesions [LE68, LY67, EL67].

UVB and UVC radiation below 310 nm is absorbed by DNA. The UVC light, that is absorbed most strongly by DNA, is effectively shielded by the absorption of the ozone layer (dark blue in Figure 2.4). The remaining spectral intensity that reaches sea level (turquoise) has some overlap with the DNA absorbance spectrum between 280 nm and 310 nm. UV radiation excites DNA bases to $^1\pi\pi^*$ states, from where photophysical processes occur that can ultimately result in either the dissipation of the excitation energy or the generation of DNA photolesions [Cad97, CSD05]. Direct excitation of DNA as well as photosensitising of DNA are both highly relevant and have drawn much scientific attention to them.

This thesis focusses on the photophysical processes after direct DNA excitation. A broader discussion of different mechanisms that can damage DNA can be found in [Cad12].

2.2.1. Decay of the Excited State

Upon UV absorption, DNA bases are excited to $^1\pi\pi^*$ states. They can decay to the ground state via radiative and non-radiative mechanisms, as well as undergo transitions to other excited states or directly cause photochemical reactions. Two types of non-radiative transitions should be distinguished: *internal conversion* (IC) is a non-radiative transition between different electronic states that have the same multiplicity, *intersystem crossing* (ISC) is a non-radiative transition that changes the multiplicity, e.g. a transition from a singlet to a triplet state.

The return to the ground state from the $^1\pi\pi^*$ state (internal conversion) deactivates the excited bases and therefore protects DNA from photoreactions. Remaining in the excited state or transitions to other excited states (IC or ISC) increases the probability of photochemical reactions. The excited state lifetime is therefore itself a major factor that influences the photostability of DNA. The $^1\pi\pi^*$ lifetime τ is determined by radiative and non-radiative decay mechanisms according to the following equation [Lak10]:

$$\frac{1}{\tau} = \frac{1}{\tau_{rad}} + \frac{1}{\tau_{nonrad}} \tag{2.1}$$

$1/\tau_{rad}$ is the rate of radiative decay, $1/\tau_{nonrad}$ is the rate of non-radiative decay, and $1/\tau$ is the total excited state decay rate that can be measured by time-resolved

fluorescence spectroscopy. The latter is connected to the radiative lifetime by the fluorescence quantum yield Φ_f [Lak10]:

$$\tau = \Phi_f \cdot \tau_{rad} \tag{2.2}$$

τ_{rad} can be calculated approximatively using the Strickler-Berg equation [SB62]. It is typically in the range of nanoseconds (see for example [CCK04]) for heterocycles like the DNA bases. In 1971, the fluorescence quantum yields were determined to be in the range of 10^{-4} for all DNA bases [DH71], so the excited state lifetime was estimated to be around 1 ps. Later, transient absorption spectroscopy [PPK00, PPK01] and time-resolved fluorescence upconversion spectroscopy [PPK00] showed that the excited state lifetimes of the DNA bases are actually below 1 ps. This remarkably short excited state lifetime is an intrinsic photo-protective mechanism of DNA. It can be explained by assuming a rapid non-radiative decay mechanism involving a *conical intersection* (CI) between the energy surfaces of the $^1\pi\pi^*$ state and the ground state [PPK00]. Figure 2.5 depicts simplified energy surfaces of both states as functions of two reaction coordinates q_1 and q_2. The CI is, as the name suggests, the intersection between both surfaces.

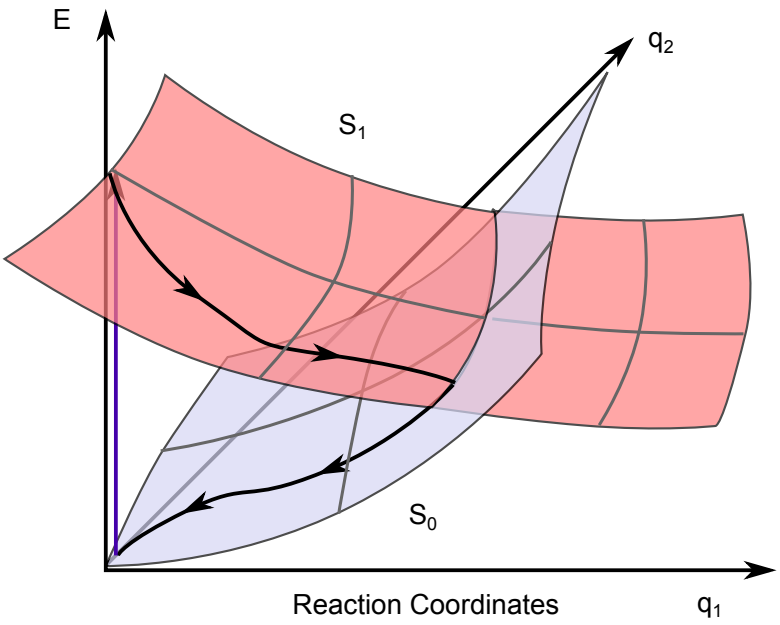

Figure 2.5.: Schematic illustration of conical intersections (CI) between energy surfaces of the excited state S_1 state (red) and the ground state S_0 (blue). The wave packet moves along a path (black) on the S_1 energy surface until the surfaces intersect. At the conical intersection, the wave packet crosses over to the ground state energy surface and subsequently moves on it. In this illustration the surfaces intersect not in a single CI, but rather in a seam of CIs.

After UV- absorption, the molecule moves on a path of the potential energy surface (PES) of the excited state until it reaches the conical intersection (CI). From there it crosses over to the ground state energy surface and subsequently moves on it. After passing the CI, the molecule is in the electronic ground state. The time scale of ground state recovery depends on the shape of the energy surface: if no energy barrier is encountered on the pathway to the CI, the excited state can decay to the ground state within 1 ps [MK11].

Theoretical and experimental evidence for this decay mechanism was gathered in recent years. The pathways of excited DNA bases on the PES of their $^1\pi\pi^*$ states were investigated by numerous theoretical studies. In 2002, a computational study identified a nearly barrierless path of cytosine from the excited state to the ground state via a pair of CIs [Ism02]. Since then, conical intersections between the $^1\pi\pi^*$ state and the electronic ground state of all DNA bases were found, enabling a nearly barrierless passage to the electronic ground state [Gus06a, Mat04, PSD06, SMB06, PSD05] within less than 1 ps. Experimentally, the decay can be investigated by time-resolved absorption spectroscopy.

2.2.2. Vibrational Cooling

After passing through the CI to the electronic ground state, the excitation energy of over 4 eV is deposited in the vibrational modes of the bases, corresponding to a Boltzmann temperature of 1200 °C [PPK01]. This excess energy results in a strongly red-shifted ground state absorption until the vibrational energy is dissipated to the surrounding solvent molecules (*vibrational cooling*, VC).

Experimental evidence for internal conversion and subsequent vibrational cooling was obtained by Middleton et al., who investigated the excited state decay and the ground state recovery of adenine derivatives in various solvents using UV-pump VIS-probe and UV-pump UV-probe spectroscopy [MCK07]. Figure 2.6 shows the results of measurements of 9-methyladenine in water, deuterated water, methanol and acetonitrile.

The sample was excited at 267 nm, and probed at 250 nm to monitor the ground state bleach and at 600 nm to monitor the excited state absorption. The excited state absorption decays with time constants of below 1 ps in all solvents (upper left panel). Ground state recovery (lower left panel) is slower than excited state decay (upper left) in all solvents and depends strongly on the solvent. These findings strongly support the idea of ultrafast internal conversion via a CI and subsequent vibrational cooling:

1. The base returns to a vibrationally excited state via a conical intersection; after this transition, the excited state absorption has vanished. Since CIs are intrinsic properties of the bases, this step is only weakly influenced by the solvent.

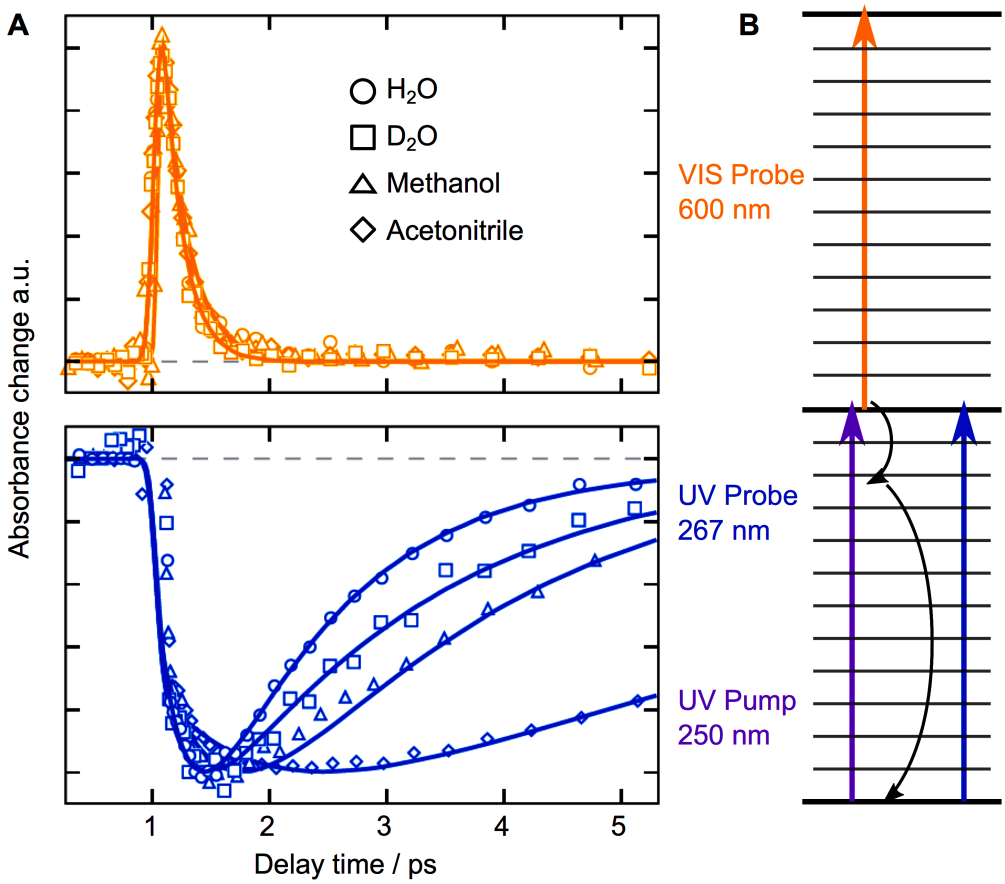

Figure 2.6.: (A) Excited state decay (upper, yellow) and ground state recovery (lower, blue) of 9-methyladenine (pump 266 nm, probe 250 nm and 600 nm) in different solvents. The excited state decays with a time constant that only weakly depends on the solvent, while ground state recovery is slower and strongly solvent dependent. (B) Schematic representation of vibrational cooling (VC). The excited state decays via a CI into a vibrationally excited ground state. Subsequently, the excessive energy is dissipated to the solvent (VC). The ground state absorption recovers with vibrational cooling. Picture adapted with permission from [Mid09] (copyright Annual Reviews).

2. As long as the ground state has excessive energy, the ground state absorption is red-shifted, therefore the ground state bleach at 250 nm remains until the excess energy is dissipated to the solvent. This step explicitly involves the solvent, so the time scale of ground state recovery will depend on the solvent.

2.2.3. Excited States of Monomers

After UV-absorption, the DNA bases are in a $^1\pi\pi^*$ state. From there, most bases return to the ground state via internal conversion. However, a small fraction of

the excited molecules will undergo transitions into other electronic states (for an overview, see for example [Mid09]). In addition to excited states of DNA bases, interactions between neighbouring bases in a strand can lead to long-living states that are not localised on a single base. Excited states that can occur on a single base or nucleotide (monomer) will in the following be called 'localised' or 'monomeric', states that occur only in strands will be called 'delocalised'. In this section, the localised excited states of DNA bases are introduced. The discussion will be focussed on thymine which was investigated in this thesis.

$n\pi^*$ States

Monomeric states include so-called $^1n\pi^*$ states, where a non-binding electron is excited to an anti-binding orbital. Direct excitation of $^1n\pi^*$ states is very unlikely, since these transitions are symmetry forbidden [Mid09]. However, $^1n\pi^*$ and $^3n\pi^*$ states can be populated from an energetically higher $^1\pi\pi^*$ state. The mechanism can be briefly explained using a theoretical study about $^1n\pi^*$ states in cytosine [Ism02]. After UV absorption, if an electron involved in the C=O or C=N double bond is excited into an anti-binding orbital, a non-binding electron of O or N can subsequently occupy the vacant binding orbital, thus forming a $^1n_O\pi^*$ or $^1n_N\pi^*$ state, respectively.

The kinetics of $^1n\pi^*$ states were studied both theoretically and experimentally. Two different possibilities are discussed in the literature: on the one hand, $^1n\pi^*$ have been discussed as part of the ultrafast excited state decay within less than 1 ps [Can05, Bla07, Mar05, Sat06]. Recent studies of uracil [Nac11] and thymine [Szy09] suggest that their $^1\pi\pi^*$ states decay to their ground states via $^1n\pi^*$ intermediates, explaining the relatively long (still below 1 ps) excited state lifetimes of those bases. A more extensive theoretical study of all bases suggested that purines simply decay from the $^1\pi\pi^*$ to the electronic ground state, whereas all pyrimidines involve $^1n\pi^*$ states in the excited state decay [Bar10]. On the other hand, long-living states of pyrimidines have been reported that were assigned to $^1n\pi^*$ states. In cytosine, Keane et al. observed an excited state with a lifetime of 40 ps, which they identified as a $^1n\pi^*$ state [Qui07, Kea11]. In uracil and thymine, Hare et al. reported long-living states that decay on the 100 ps time scale, which they interpreted as $^1n\pi^*$ states [HCK07]. However, the identification of these long-living states as $^1n\pi^*$ states is at this point hypothetical and not supported by conclusive evidence. Moreover, some of the experimental findings themselves were challenged by other groups that found no 100 ps of TMP [KMP08, Pil14b]. The involvement of $^1n\pi^*$ states in the excited state decay of pyrimidines is addressed in more detail in chapter 7.

$^3\pi\pi^*$ States

The $^3\pi\pi^*$ state of thymine is biologically highly important, because it is a precursor to the most common DNA photolesion [EL67, WB70] and because it can be excited

indirectly by UVA radiation, where the intensity of the solar spectrum at sea level is much higher than in the UVB and UVC range. UVA photons do not have enough energy to excite the $^1\pi\pi^*$ state of thymine, but they could excite thymine to its energetically lower $^3\pi\pi^*$ state [ES68], if the transition was not spin-forbidden. However, UVA light might excite other molecules (sensitisers) to singlet states, that subsequently undergo ISC to a triplet state. Upon collision of thymine and a sensitiser of suitable triplet energy, *triplet-triplet energy transfer* (TTET) can occur, yielding thymine in the $^3\pi\pi^*$ state.

Direct excitation of thymine to the $^1\pi\pi^*$ state can also lead to a subsequent transition to the energetically lower lying $^3\pi\pi^*$ state. Transitions from singlet to triplet states (intersystem crossing) are spin-forbidden, but possible due to spin-orbit-coupling. After UV excitation, triplet states can be formed directly out of the $^1\pi\pi^*$ state or out of an intermediate $^1n\pi^*$ or $^3n\pi^*$ state. The rule of El-Sayed [ElS63] states that ISC is quite efficient, if it changes the spatial symmetry of the orbitals and much less efficient if it does not. $^1n\pi^* \rightarrow {}^3\pi\pi^*$ or $^1\pi\pi^* \rightarrow {}^3n\pi^*$ transitions should be more likely than a direct $^1\pi\pi^* \rightarrow {}^3\pi\pi^*$ transition.

Upon UV absorption, a fraction of the excited bases may undergo ISC either directly or via $n\pi^*$ intermediates. Many theoretical studies have suggested that $^1n\pi^*$ or $^3n\pi^*$ states act as major precursors to triplet formation [EFM09, Eti12, Eti13, Gon09, Ser07], while direct ISC from the excited $^1\pi\pi^*$ state only contributes in a minor way to the total triplet yield [Gon10a].

Only few time-resolved experimental studies about the intersystem crossing process and the involvement of $^1n\pi^*$ states in it have been undertaken [HCK07, Har08]. Hare et al. investigated ISC of thymine in acetonitrile, where the high ISC yield (around 10 %) makes experimental observations easier [Har08]. They proposed a model that assumes that a part of the excited thymine molecules undergo internal conversion to a $^1n\pi^*$ state. Initially, the bases in the $^1n\pi^*$ state have excess vibrational energy. They can either dissipate the excess energy to the solvent (VC) or undergo ISC to the $^3\pi\pi^*$ state. After VC is finished, the thermally relaxed $^1n\pi^*$ state bases should be unable to form $^3\pi\pi^*$ states. They return to the ground state on a slower timescale without contributing to ISC any more. Other experimental studies have raised doubt about the data that motivated this model ([KMP08, Pil14b]) so a re-investigation is necessary. This issue is discussed in more detail in chapter 7. The decay of the $^3\pi\pi^*$ state of thymine and its involvement in the generation of DNA photolesions are addressed in chapter 5.

2.3. Excited State Physics of Oligomers

DNA oligomers show more complex photophysics than single nucleotides. Interactions between neighbouring bases can lead to excited states that are not present in monomers. Such interactions depend on the relative orientation of the bases.

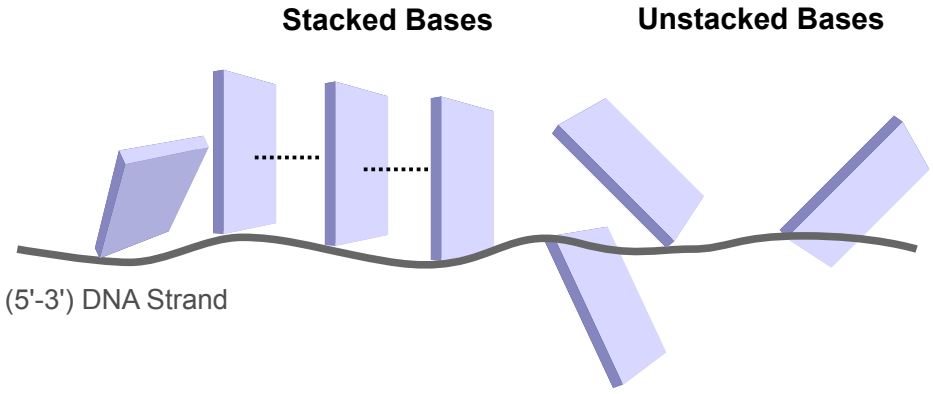

Figure 2.7.: A DNA oligomer consists of a sequence of bases that are partially in a stacked geometry. These can interact with each other and give rise to delocalised excited states.

Figure 2.7 illustrates how a DNA single strand contains stacked and unstacked bases. Unstacked bases lack electronic overlap and therefore do not interact significantly. They are expected to behave like isolated nucleotides [Mid09]. Stacked bases can interact and therefore give rise to excited states that are not localised on one base. Hence these states are sometimes called *delocalised*. The most important delocalised states are explained in the following subsections.

2.3.1. Excitons (Frenkel Excitons)

A Frenkel exciton is an excited state of a multichromophoric system produced by dipolar coupling of the excited states of the neutral excited states of individual molecules [Mid09].
Excitons were first discussed by Frenkel in 1931 [Fre31], where 'excitation waves' are considered (later named 'Frenkel Excitons'), i.e. states that are linear combinations of monomeric states; the exciton is therefore delocalised over several molecules. This model was adapted to molecular spectroscopy in the 1960s by Kasha et al. [KRA65]. The interaction between neighbouring bases causes a splitting of the energy levels [KRA65] that should be observable in the absorbance spectrum. Since the absorbance spectra of oligonucleotides are very similar to those of a mix of the corresponding nucleotides [Cha55], apart from an hypochromic effect [Tin60, Rho61, DT62], excitation seemed to be localised on single bases[ES68]. However, more sophisticated calculations of excitons were performed by the group of D. Markovitsi [Bou02, Bou03, Ema05], where the exciton splitting turns out to be much smaller than the width of the absorbance band. Hence the exciton model is consistent with the absorption data of DNA oligomers [Ema05].

The group of D. Markovitsi, who argued most strongly for the existence of excitons in DNA, pioneered time-resolved spectroscopy by fluorescence upconversion [Gus02, GSM02, Oni02, Sha03]. Using this technique, they were able to observe the fluorescence of DNA mono- and oligomers in the temporal window from sub-picoseconds to a few picoseconds. The fluorescence data of oligomers that they obtained was much more complex and that of the corresponding monomers [Mar06, Mar03]. The exciton model can explain this complexity: Considering that the interactions between bases depend on the base sequence, the multitude of possible sequences should give rise to an multitude of excitonic states, an *exciton band*. An exciton band should give rise to very complex fluorescence data.

Fluorescence upconversion spectroscopy allowed to monitor the fluorescence in the first 10 ps [Vay10] after excitation, but longer-living emission signals were not observed. Very small emission intensities that might be present on longer timescales can be observed by *time-correlated single photon counting* (TCSPC). Vaya et al. used TCSPC and found long-living fluorescence signals that decay on similar timescales as excited states that were observed by time-resolved absorption spectroscopy [Vay10]. Based on the presence of the fluorescence, these states were identified as excitons [Buc07, Mar06]. However, fluorescence measurements are insensitive to 'dark'states (i.e. states that decay nonradiatively), so the long-living states obtained by time-resolved absorption spectroscopy cannot directly be identified as the source of the fluorescence. A different type of long-living delocalised state, an *exciplex* was proposed by other groups to explain the data (see for example [Tak08]).

2.3.2. Excimers/Exciplexes

An excimer/exciplex is an excited electronic state with substantial charge transfer character involving two identical (excimer) or different (exciplex) molecules [Mid09, Bir67, Cre04].

The above definition used by Middleton et al. [Mid09] is applicable to the transfer of partial charges and of complete charges. To distinguish between both possibilities, only transfer processes of complete charges will be called *charge transfer*, resulting in *charge separated states* (CSS). The terms excimers/exciplexes will be used for states that result from the transfer of partial charges.

Eisinger et al. discovered that dimers and oligonucleotides show red-shifted fluorescence spectra compared to the nucleotides that they are composed of [Eis66, ES68, Bir67]. They interpreted this finding by the excimer theory of Förster et al. [FK55], see Figure 2.8. Partial charge transfer results in an attraction of the excimer/exciplex molecules, as depicted in the energy scheme in Figure 2.8. The ground state energy at this intermolecular distance is higher, so the excimer/exciplex lowers the excited state energy and increases the ground state energy, resulting in a red-shifted fluorescence. The long-living state of adenine oligomers that was revealed by TA spectroscopy was assigned to such excimers [CCK05], in agreement with the kinetics of the fluorescence

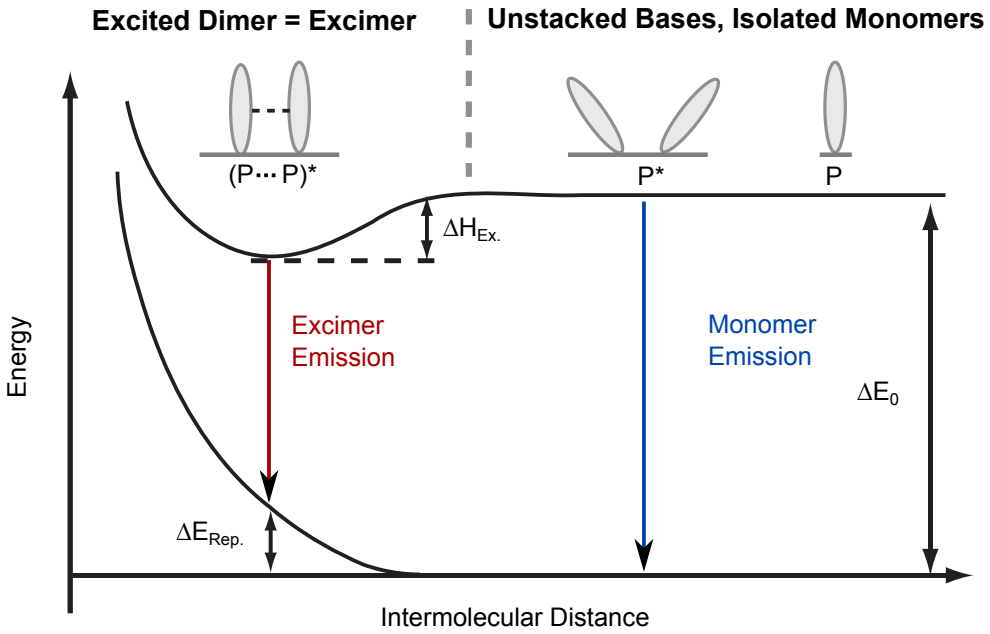

Figure 2.8.: An excited base forms an excimer with a neighbouring ground state, resulting in an attractive force between them. The energy of the excimer is therefore below the excited state energy of the monomer. Additionally, the ground state molecules feel a repulsive force at that distance, resulting in a red-shifted fluorescence. Picture adapted from [Sch08].

of adenine oligomers [Ple00]. The same study showed the red-shifted emission that was attributed to excimers/exciplexes.

2.3.3. Charge Transfer

Recent studies suggest that the long-living excited states observed by TA-spectroscopy are charge separated states [Tak08, Mid09]. Unlike excimers and excitons, charge separated states are 'dark' (see the introduction to charge transfer processes in subsection 2.3.5). If they exist, additional excited states like excitons are necessary to explain the fluorescence data. Indirect evidence for charge transfer was obtained by Takaya et al., who measured excited state lifetimes of DNA dimers and compared them to the thermodynamic 'driving force' for electron transfer [Tak08]. If the long-living states are charge separated, they can decay to the ground state by charge recombination: $D^+pA^- \rightarrow DpA$ (D and A are electron donor and acceptor, respectively). The thermodynamic driving force ΔG is approximately the difference between the ionisation potential of the donor (IP) and the acceptor's electron affinity (EA), both in the vacuum [Mid09]. By this approximation, solvation effects and coulombic stabilisation are neglected. Though these effects are important, the authors

assume that they are roughly the same for all dimers and therefore do not influence the relative recombination rates significantly.

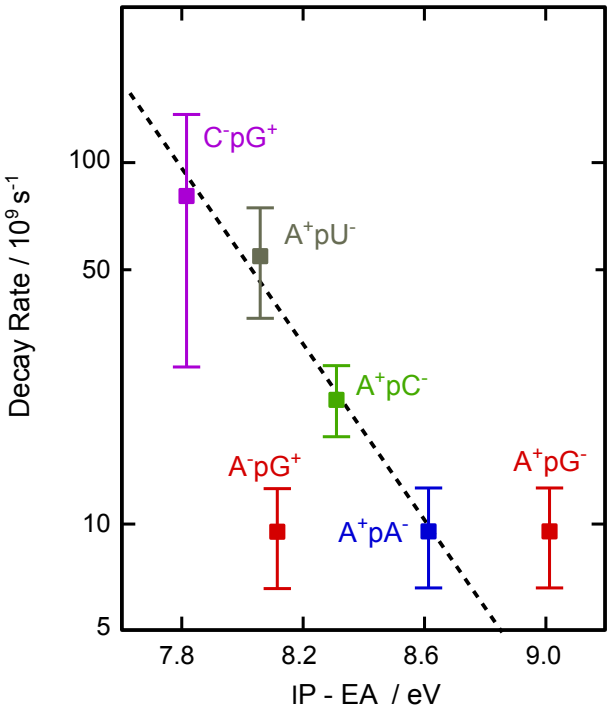

Figure 2.9.: Decay rates of long-living excited states of dimers in relation to the 'driving force' of charge recombination, $IP - EA$ (ionisation potential – electron affinity). With the exception of the two dimers ApG and GpA, the decay rates decrease exponentially with increasing driving force. This dependence is typical of charge transfer processes in the Marcus inverted region (see subsection 2.3.5). Data adapted with permission from [Mid09] (copyright Annual Reviews).

Figure 2.9 shows the lifetimes of the long-living states of dimers; apart from the A^+pG^- and G^+pA^- dimers, the lifetimes decrease exponentially with increasing ΔG. This behaviour is consistent with highly exothermic charge transfer processes like charge recombination [Gou90] (in the so-called 'inverted region' of electron transfer, see subsection 2.3.5) where the charge transfer rate decreases exponentially with increasing 'driving force'([Mar56a, Mar60, Mar63, Mar93]). The dimers A^+pG^- and G^+pA^- do not obey that rule, which might be related to guanine radical deprotonation that competes with charge recombination, or only a partial charge transfer [Mid09].

Conclusive evidence for UV-excited charge transfer in DNA strands was provided only recently. Using time-resolved infrared spectroscopy, Bucher et al. unambiguously identified charge separated states in (hetero-)dimers by identifying the spectral signatures of cations [Buc14a, Buc14b]. These studies showed charge transfer in dimers between different bases. The direction of charge transfer is determined by the

oxidation potential, so the base with the lower oxidation potential acts as electron donor. Evidence for charge separation between two identical bases has not been reported yet. Long-living excited states in cytosine and thymine dimers were reported by different groups [Kea11, Kea12, HCK07, KMP08], but not interpreted as charge separated states.

Recently, a unified model of DNA photophysics involving excitons and charge separated states was proposed that could explain the TA and the fluorescence data [Mid09].

2.3.4. A Unified Model

In this section, a model of DNA photophysics is presented that was proposed in a recent review on DNA photophysics [Mid09]. It is schematically depicted in Figure 2.10. The left side shows the photophysics of isolated nucleotides or unstacked bases. They occupy localised $^1\pi\pi^*$ states upon UV absorption. Purines undergo internal conversion to the ground state within 1 ps without forming long-living excited states. The excited state physics of pyrimidines is more interesting, because they only partly return to the ground state within 1 ps, and partly populate $^1n\pi^*$ states that may subsequently return to the ground state or undergo intersystem crossing to the $^3\pi\pi^*$ state. As already described earlier, some of these findings are controversial: The identification of long-living excited states is not supported by conclusive evidence yet. Moreover, concerning thymine, even the finding of the long-living $^1n\pi^*$ state itself is disputed by other studies [HCK07, KMP08]. The excited state physics of isolated TMP is discussed in more detail in chapter 7.

The right side of Figure 2.10 depicts the behaviour of stacked bases. The arguments for the existence of long-living charge separated states do not rule out the existence of excitons. On the contrary, charge separated states do not explain the complex fluorescence data, so other delocalised states have to exist. Moreover, charge separated states could be formed out of excitons [Mid09, SBI07, SBI09, San13]. So the data obtained from transient absorption and fluorescence measurements can be described in a model that includes both excitons and charge separated states:

Stacked bases (right side of Figure 2.10) populate excitons rather than localised singlet states upon UV-excitation. They cause the complex fluorescence data. Short-living excitons decay into dark charge separated states, that undergo charge recombination on a timescale of 20 ps to 200 ps. This model was proposed by the group of B. Kohler in a review on DNA photophysics [Mid09]. In a recent study by the group of D. Markovitsi, they accepted this model and augmented it slightly by assuming a minor charge recombination pathway from an excimer/exciplex to the $^1\pi\pi^*$ state, leading to a weak delayed fluorescence [Vay12] that was observed by time-correlated single photon counting [Vay10].

However, the experimental evidence is lacking. While charge transfer between heterodimers was reported by Bucher et al. [Buc14a], charge transfer between

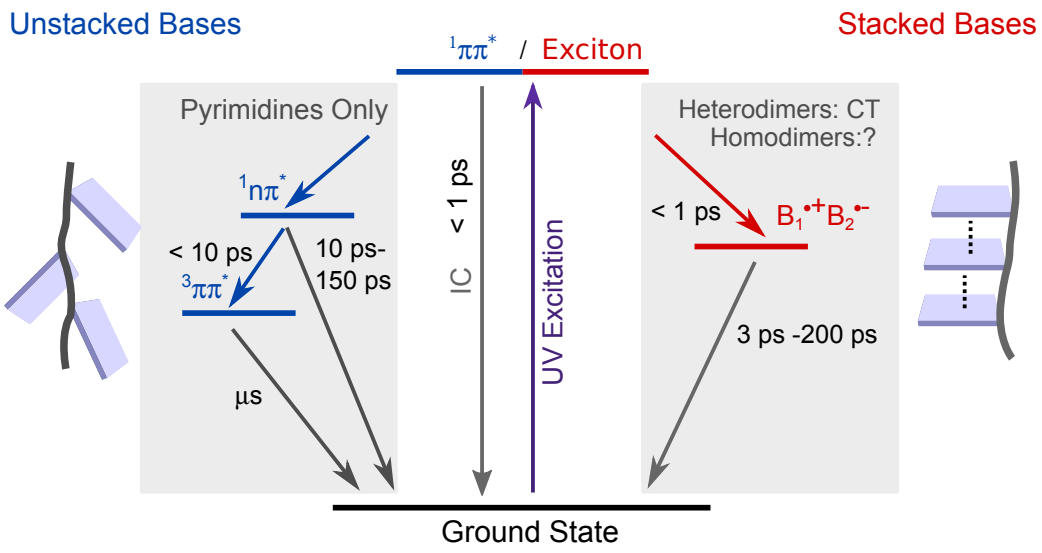

Figure 2.10.: A model of the excited state decay of DNA after UV absorption. Unstacked bases interact negligibly with each other and behave like monomers. Long-living $^1n\pi^*$ and $^3\pi\pi^*$ states of pyrimidines are populated during the $^1\pi\pi^*$ decay. Stacked bases form initially excitons that rapidly decay into long-living charge separated states. It is not yet clear whether charge transfer can occur between identical bases or not.

two identical bases (e.g. two thymines) was not observed yet. Instead, long-living excited states of thymine oligomers were interpreted as $^1n\pi^*$ states [HCK07] or as the formation of photolesions out of the $^3\pi\pi^*$ state [KMP08]. A long-living state of cytosine oligomers was interpreted as a localised $^1n\pi^*$ state [Kea11, Kea12]. Charge transfer processes in thymidine oligomers are discussed in chapter 6. Before this issue can be addressed in more detail in chapter 6, an introduction to the theory of electron transfer is required.

2.3.5. Electron Transfer Theory

Charge transfer (CT) processes of molecules in polar solvents like water are profoundly influenced by the solvent. The polar water molecules orient around a given charge distribution to minimise the energy. Charge transfer processes change the charge distribution, leading to changes not only in the energy levels of the involved charge donors and acceptors, but also in the energy of the surrounding solvent. R.A. Marcus developed a theory of electron transfer (ET) that takes these effects into account [Mar56a, Mar60, Mar63, Mar93]. Electron transfer can occur when random fluctuations of the polarisation of the solvent lead to a configuration that makes electron transfer an isoenergetic process. The Marcus theory models the change in Gibbs free energy ΔG caused by non-equilibrium fluctuations of the solvent

polarisation in three steps: First, an (imaginary) charge Δq is transferred from donor to acceptor, then the solvent adapts to the new charge distribution and finally the charge is transferred back without changing the new solvent polarisation. Thereby the change in the Gibbs free energy ΔG of the polarisation can be described by a single reaction coordinate Δq [Mar56b]:

$$\Delta G = \left(\frac{1}{2r_1} + \frac{1}{2r_2} - \frac{1}{R_{12}}\right) \cdot \left(\frac{1}{\varepsilon_{op}} - \frac{1}{\varepsilon_s}\right) \cdot (\Delta q)^2, \tag{2.3}$$

where r_1, r_2 are the radii of donor and acceptor, R_{12} is their distance, ε_{op} and ε_s are the optical and the static dielectric constant, respectively [Mar56a].

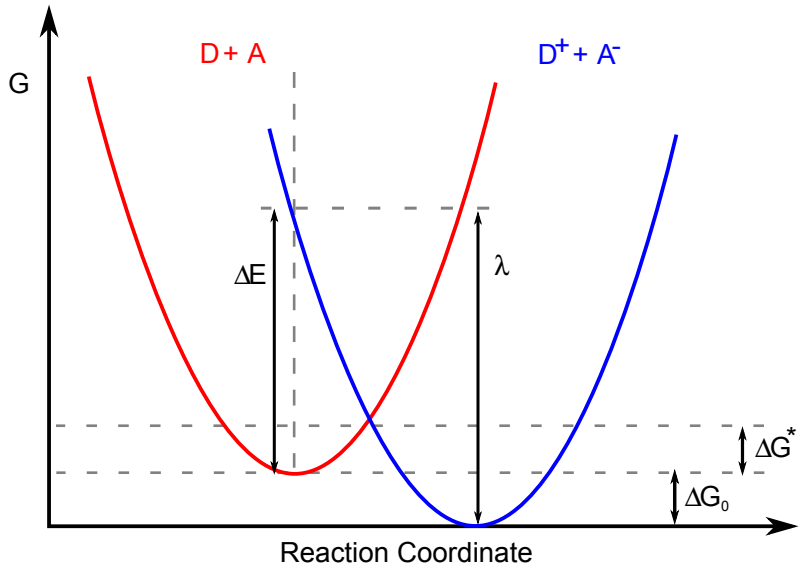

Figure 2.11.: Electron transfer according to Marcus theory. The reaction coordinate is the polarisation of the solvent, described by the transfer of a charge Δq. The parabolas represent the energies of D (donor) + A (acceptor) (red) and D^++A^-(blue). The energy barrier ΔG^* determines the charge transfer rate. It depends on the Gibbs energy difference ΔG_0 and the reorientational energy λ.

The parabolas in Figure 2.11 represent the Gibbs free energy of (Donor + Acceptor) (red) and (Donor^+ + Acceptor^-) (blue). The Gibbs free energy changes along the red parabola as the polarisation randomly fluctuates. For electron transfer to happen, the intersection of both parabolas must be reached. The energy barrier ΔG^* between the energy minimum and the intersection of both parabolas limits the transfer rate according to an Arrhenius equation:

$$k(\Delta G^*) = k_0 \cdot exp\left(-\frac{\Delta G^*}{k_B T}\right) \tag{2.4}$$

The reorientational energy of electron transfer λ is calculated according to Equation 2.3 with $\Delta q = e$. The Gibbs free energy barrier can be written as

$$\Delta G^* = \frac{(\lambda + \Delta G_0)^2}{4\lambda k_B T} \tag{2.5}$$

The quadratic form has an interesting consequence: the maximum rate (corresponding to $\Delta G^* = 0$) is obtained if $\Delta G_0 = -\lambda$. From there, the electron transfer rate decreases, if ΔG_0 increases or decreases. So, if $\Delta G_0 + \lambda > 0$ (Marcus normal region), increasing the free energy difference decreases the energy barrier and thereby accelerates the electron transfer. If $\Delta G_0 + \lambda < 0$ (Marcus inverted region), increasing the energy difference increases the energy barrier and therefore slows down ET. Figure 2.12 illustrates the energy barrier in the Marcus normal (left graph) and the Marcus inverted region (right graph).

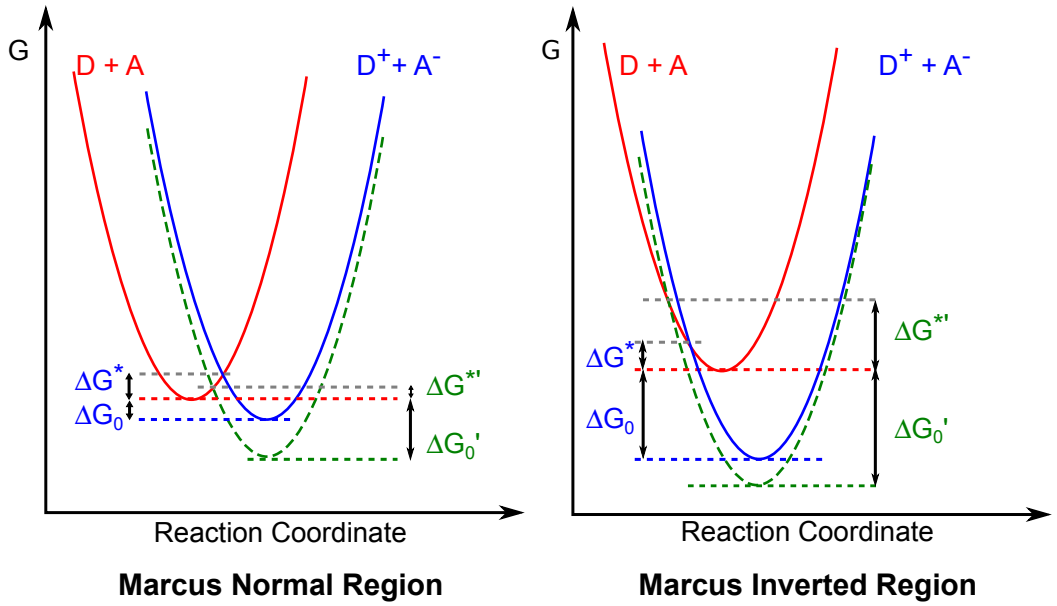

Figure 2.12.: Marcus normal (left) and inverted (right) region. In the normal region, increasing the energy difference ΔG_0 lowers the energy barrier ΔG^* and increases the electron transfer (ET) rate until $\Delta G^* = 0$. If ΔG_0 increases further, (inverted region, right), the energy barrier increases, lowering the ET rate.

The rate k_0 is estimated by a semiclassical model. Non-adiabatic Landau-Zener theory [Lan32, Zen32, Stü32] is used to calculate the electron transfer probability when passing through the intersection region. This gives the electron transfer rate k_{ET} (see for example[MS85]):

$$k_{ET} = \frac{2\pi}{\hbar}|H_{AB}|^2 \frac{2}{\sqrt{4\pi k_B T}} exp\left(-\frac{(\lambda + \Delta G_0)^2}{4\lambda k_B T}\right) \tag{2.6}$$

where H_{AB} is the electronic coupling between the initial state (A) and the final state (B).

More rigorous treatments of charge transfer processes approximate the electronic coupling more precisely by taking into account different vibronic levels [DKV72, KLJ74, UJ75, Jor76]. These mathematical models cannot be discussed in detail here, interested readers may read the cited literature.

2.4. DNA Photolesions

UV radiation can cause a multitude of DNA photolesions. The most common of them, the *cyclobutane pyrimidine dimers* (CPD) and the *(6–4) pyrimidine-pyrimidone adduct* ((6–4) lesion) (see Figure 2.13) [RDC01, Dou03] occur between two neighbouring pyrimidine bases [DC01].

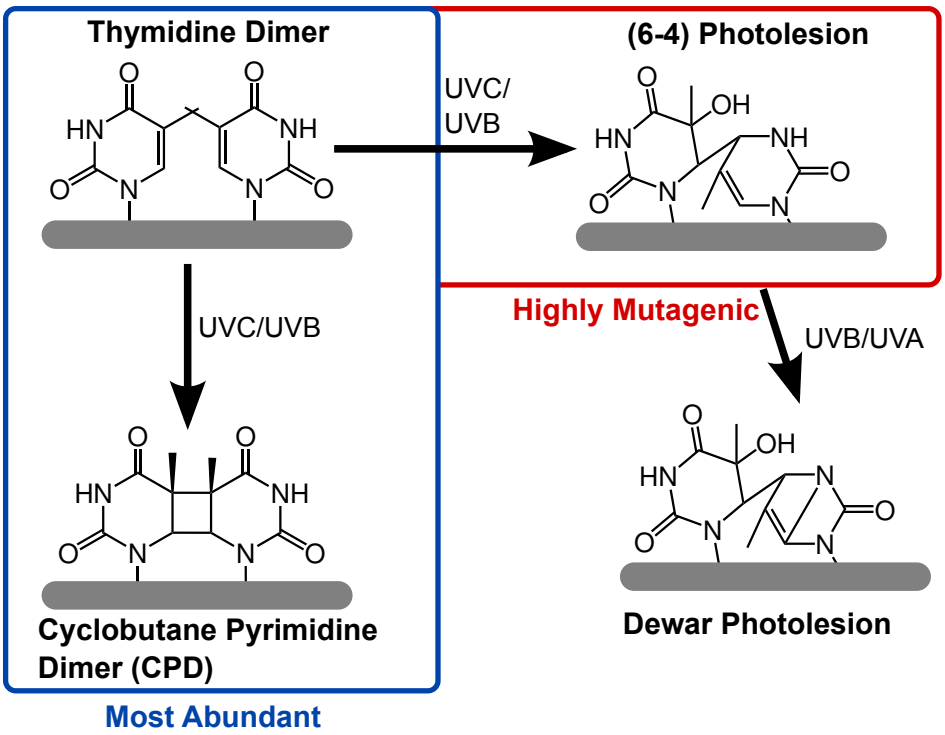

Figure 2.13.: The most important DNA photolesions at dipyrimidic sites. The most abundant lesions are the cyclobutane pyrimidine dimers (CPD, blue). These are formed by a cycloaddition of the C5 and C6 atoms of neighbouring pyrimidines. The (6–4) lesion is formed by linking the C6 atom of one base to the C4 of another. The (6–4) lesion is highly mutagenic, by absorbing UVA light it can form a Dewar lesion.

These are linked by one ((6–4) lesion) or two (CPD) covalent bonds (see Figure 2.13). These lesions are described in the following.

2.4.1. CPD

CPD Mutations

The most abundant DNA photolesion is the cyclobutane pyrimidine dimer (CPD) between two pyrimidines [VR01, DC01]. It is formed by a cycloaddition of the C5 and C6 atoms of two neighbouring pyrimidines, see Figure 2.13. CPD lesions are

formed in all combinations of thymine and cytosine, but in different amounts: TT > TC > CT > CC [DC01, Mou06]. TT CPD lesions are not mutagenic themselves, but they can hinder replication and transcription of DNA [TK93]. If they are not repaired, these lesions can lead to cell death (apoptosis) [KWC72, San03, Elm07]. In this emergency situation, there exists a bypass replication mechanism that allows replication without damage repair [Tay94, Wal95]. This mechanism is error-prone and can lead to point mutations during replication. This mutation hazard exists for all CPD lesions, but those that contain cytosine bear additional risks. There are two possible mechanisms by which a C→T point mutation (or CC→TT tandem mutations) can occur (see Figure 2.14).

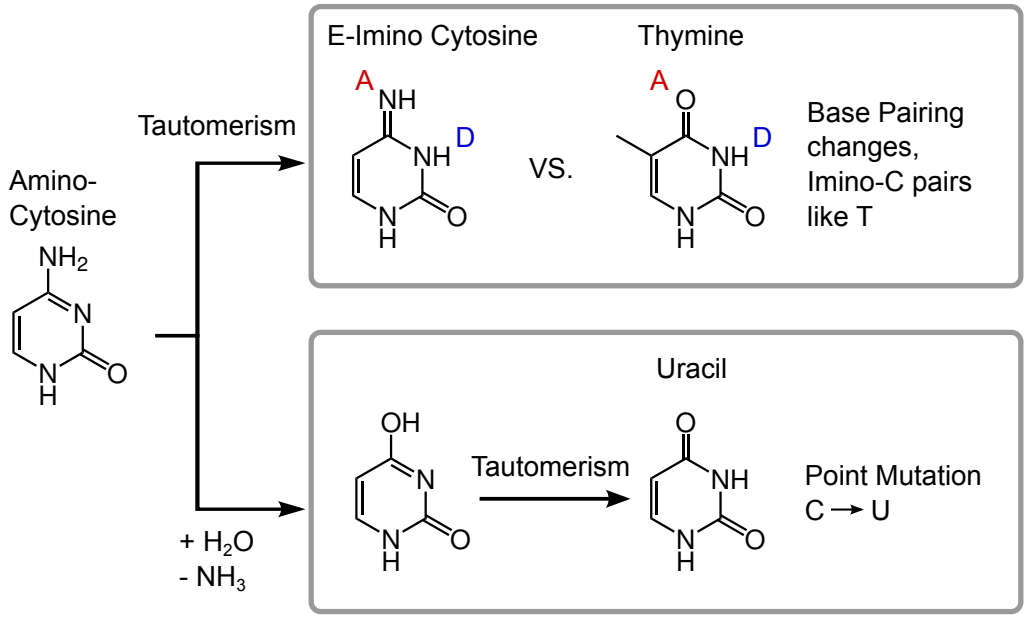

Figure 2.14.: Mutagenicity of cytosine: 1. Tautomerism of cytosine to the E-imino form changes the base pairing (D means H-bond donor, A acceptor) to a thymine-like pattern (upper panel). 2. Hydrolytic deamination of C leads to a tautomer of uracil (lower panel). If C is part of a CPD lesion, both processes are greatly increased.

1. Cytosine exists not only in the major amino-form, but also in a minor E-imino tautomer [JT93], where the amino group attached to the C4 atom is replaced by an imino group and the second hydrogen atom is attached to N3 (see Figure 2.14). In the CPD lesion, the C5=C6 bond is saturated, which makes aromatic stabilisation of the major amino form no longer possible. As a consequence, the fraction of the (otherwise minor) E-imino cytosines increases [BH68]. The base pairing pattern of the E-Imino cytosine is the same as that of uracil and thymine (see Figure 2.14) [JT93, BC73, Per74].

2. Cytosine is deaminated by a hydrolytic reaction and turns into a tautomer of uracil, resulting in a point mutation (see Figure 2.14). The rate of cytosine deamination is very low [FKS90], but it is substantially increased if cytosine is part of a CPD lesion [PS96]. A tautomeric regrouping of the deaminated cytosine then leads to a mutation C→U, the equivalent of thymine.

Each of those processes leads to a distorted base pairing. If the strands are replicated by a bypass mechanism without repairing the CPD lesion, mutations result. Figure 2.15 depicts the consequences of a bypass replication of unrepaired CPD containing strands.

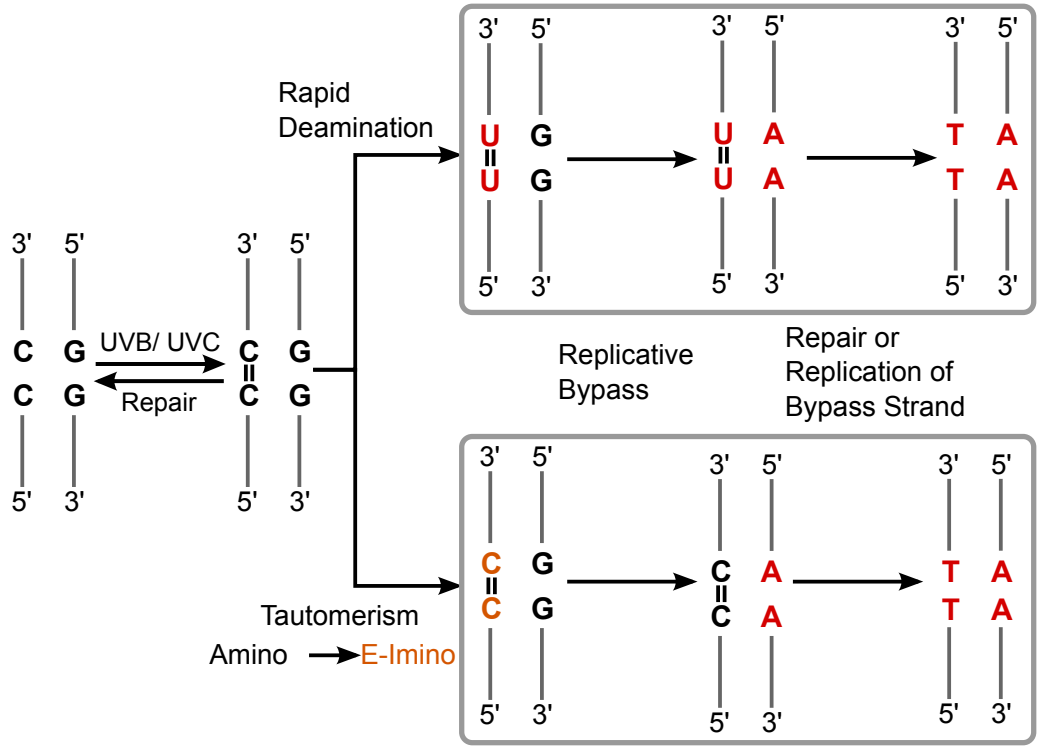

Figure 2.15.: Mechanisms of tandem mutations of C=C CPD lesions. By rapid deamination, (upper box) cytosine is replaced by uracil, leading to a point mutation after a bypass replication. The tautomerism of the CPD lesion (lower box) can lead to the E-imino form, which has a uracil/thymine-like base pairing pattern. This leads to a point or tandem mutation.

Starting from a CPD lesion formed out of two cytosines, damage repair, rapid deamination or tautomerism can take place. Rapid deamination replaces the C=C CPD by a U=U CPD lesion. Bypass replication replaces G by A in the opposite strand, then either bypass replication or replication after damage repair yields the mutated double strand. The tautomerism amino-C → imino-C changes the base pairing pattern; it becomes equivalent to that of thymine. If the damage is not

repaired, bypass replication can replace G by A in the opposite strand. Subsequently, if the opposite strand is used as the template for replication, C can be replaced by T. Both mechanisms lead to point- or tandem mutations, altering the genetic code. Note that the same processes also occur in TpC and CpT CPD lesions, leading to the same point mutations.

CPD Generation

The formation mechanism of the CPD lesion was controversial until recently. Most investigations were focussed on CPD lesions between thymines because of the relatively high quantum yield of 3 % to 5 % [Ban12]. The lowest triplet state of thymine ($^3\pi\pi^*$) was believed to be the main precursor for CPD formation, because sensitising experiments, i.e. the indirect population of the triplet state of thymine by triplet-triplet energy transfer (TTET) from another molecule in the triplet state (sensitiser), exclusively generates CPD lesions. However, recent studies have demonstrated the ultrafast CPD formation out of the excited $^1\pi\pi^*$ state between stacked thymine bases [Sch07]. A later study established this mechanism as the predominant one [Sch09]. This $^3\pi\pi^*$ reaction channel is relatively unimportant, if the $^1\pi\pi^*$ state is excited. This is in part because of the low intersystem crossing rate of 1.5 % (excitation wavelength 266 nm) [Ban12] that leads from the excited $^1\pi\pi^*$ state to the $^3\pi\pi^*$ state. However, the $^3\pi\pi^*$ state of thymine can be populated by sensitising. Because this process can be initiated by UVA radiation, which is much stronger than UVB radiation at sea level, this process may be very important. The details about the involvement of the triplet state in CPD formation will be addressed in chapter 5.

2.4.2. The (6–4) Lesion

Another important dimeric DNA photolesion is the (6–4) pyrimidine-pyrimidone adduct ((6–4) lesion). The 6-atom of a pyrimidine is bound to the 4-atom of a neighbouring pyrimidine (see 2.13).

The precise mechanism of (6–4) formation is still not known. It is assumed that an oxetane is formed via a Paternò–Büchi reaction, by which a cycloaddition between the C5=C6 bond of base 1 and the C4=O8 bond of base 2 takes place (see Figure 2.16). At temperatures above 80 K the oxetane is thermally unstable and forms a (6–4) lesion.

(6–4) Mutations

The (6–4) lesion is less ubiquitous than the CPD lesion, but more mutagenic. NMR spectroscopy shows that the (6–4) lesion distorts the DNA structure significantly [LHC99]. This leads to a highly erroneous replication, especially of T(6–4)T dimers [LBL91, HL94]. In a bypass replication, the 3' thymine can pair with a guanine,

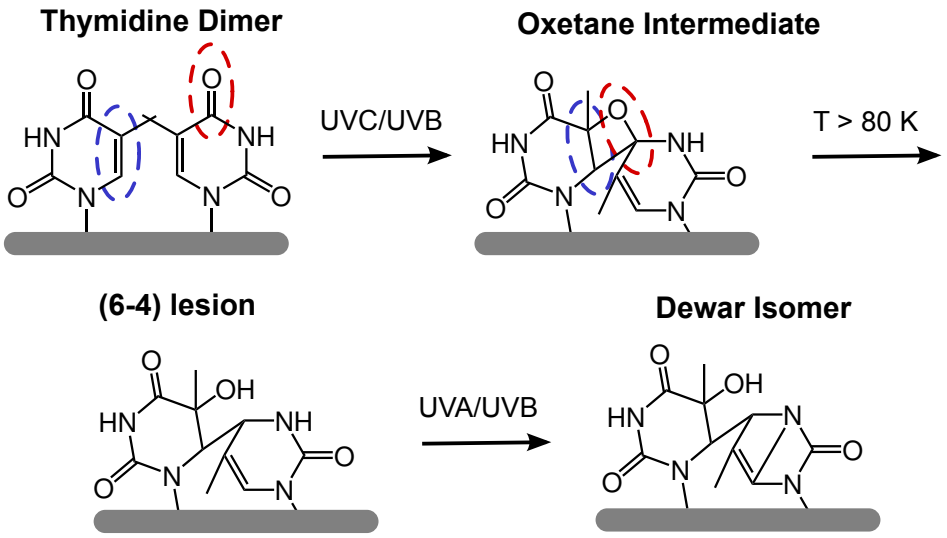

Figure 2.16.: Formation of the (6–4) lesion between two neighbouring thymines. In the first step, an oxetane intermediate is formed. The C6(1) is linked to the C4(2), and C5(1) to O4(2). At temperatures above 80 K, oxetane is thermally unstable. The C4(2)–O8(1) bond breaks, yielding the (6–4) lesion. Further irradiation with UVA/UVB light can yield the Dewar valence isomer.

while the 5' thymine correctly pairs with a adenine. So, the T(6–4)T lesion is likely to lead to a T→C point mutation [LHC99, Liv01] (see Figure 2.17).

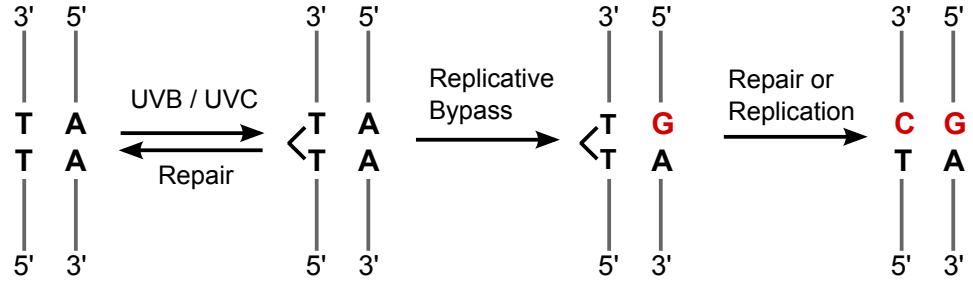

Figure 2.17.: UV-induced (6–4) lesions can be replicated by a bypass mechanism without being repaired. The 3' thymine pairs with guanine instead of adenine. Upon repair or replication of the complementary strand, the 3' thymine is replaced by cytosine.

In addition, cytosine in the (6–4) lesion can undergo deamination and thereby generate a C→T point mutation (the same mechanism of deamination and subsequent bypass replication as for deaminated C in CPD lesions applies, see section 2.4.1). Furthermore, after absorption of an UVA photon, the (6–4) lesion can form a Dewar valence isomer (see Figure 2.16), that can lead to further mutations. A Dewar lesion is not read correctly during replication. It is instead read as an abasic site, i.e. a

missing base [LBC00], so the base that is built in the complementary strand is not determined by the bases of the Dewar lesion.

Formation of the (6–4) Lesion

Due to its low quantum yield the time-resolved observation of the (6–4) formation was not achieved yet. It is therefore unclear from which electronic state the (6–4) formation starts. Theoretical investigations have led to different hypotheses. A $^3n\pi^*$ has been proposed as (6–4) precursor [Giu13], as well as the lowest triplet state $^3\pi\pi^*$ [YZE11]. A recent study suggested the existence of a charge separated state between neighbouring thymines, which leads in turn to the (6–4) formation [Imp12]. Experimental observations of $^3n\pi^*$ states of thymine and charge separated states between two thymines have not been reported yet. The TRIR measurements in this thesis were not able to observe the (6–4) formation due to the low quantum yield, but investigating the possible precursors can yield important information. The lowest triplet state will be addressed in chapter 5, the proposed charge transfer state in chapter 6.

3. Spectroscopy

The experimental data discussed in this thesis were obtained by *time-resolved infrared spectroscopy* (TRIR). TRIR is a version of pump-probe spectroscopy, which monitors dynamical changes of a photoexcited sample by measuring its absorbance changes with a temporal resolution of up to femtoseconds [Zew93, Zew00]. This temporal resolution is sufficient to observe even ultrafast transitions between different excited states that take place on a timescale of (sub)-picoseconds. In this chapter the spectroscopic techniques are introduced. A brief sketch of the setup is given, before the experimental setup is described in more detail. A discussion of typical signals obtained in TRIR measurements concludes this chapter.

3.1. Setup

3.1.1. Pump-Probe Spectroscopy

The pump-probe setup is schematically depicted in Figure 3.1. A sample is irradiated by UV pulses, which cause electronic transitions and thereby some time-dependent absorbance changes. At a delay time t_D the excited sample is irradiated by a MIR probe pulse. The transmitted part of the pulse is spectrally dispersed by an imaging spectrograph and then projected onto a detector. By blocking every other excitation pulse, signals proportional to the transmittance of the excited (T) and the unexcited (T_0) sample are obtained. The absorbance change $\Delta A(t_D, \lambda)$ induced by the excitation pulse is calculated according to:

$$\Delta A(t_D, \lambda) = -log\left(\frac{T(t_D, \lambda)}{T_0(\lambda)}\right) \tag{3.1}$$

The probe pulses are in the MIR range (5000 nm to 8000 nm), where the absorbance bands are due to vibrations. Compared to absorbance spectra in the ultraviolet and visible range, IR spectra offer much more detailed information, as they show various vibrational modes, which changes can be monitored individually. These informations can be used to identify excited states unequivocally. Moreover, IR spectra are highly sensitive not only to electronic changes, but also to conformational changes, which becomes important in the context of the DNA photolesions and the excited state physics of DNA single and double strands.

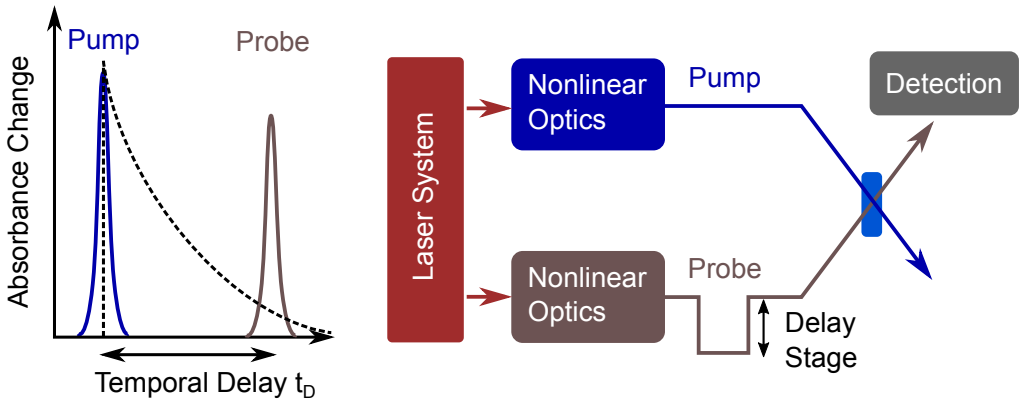

Figure 3.1.: Principle of pump-probe spectroscopy: An excitation pulse is absorbed by the sample and triggers some photophysical processes. A delayed probe pulse measures the transmittance of the excited sample volume. By blocking every other excitation pulse, the transmittances with and without prior excitation are obtained.

3.1.2. The Laser System

The TRIR setup is based on a titanium-sapphire (Ti:Sapph) femtosecond laser (Spitfire Pro, Spectra Physics), that provides near-infrared pulses with a central wavelength of 800 nm, a pulse duration of 100 fs and a pulse energy of 3 mJ (a maximum energy of 3.5 mJ is specified) at a repetition rate of 1 kHz. The setup is based on *Chirped Pulse Amplification* (CPA) [SM85, PMM87, Pes89]: Femtosecond pulses with low energy are generated by an oscillator and subsequently amplified in a Ti:Sapph resonator. The setup is schematically depicted in Figure 3.2.

A Kerr-lens mode-locked Ti:Sapph oscillator (Tsunami, Spectra Physics) generates short pulses (800 nm wavelength, spectral width > 30 nm, pulse energy ca. 5 nJ) at a repetition rate of ca. 82 MHz. These pulses are often referred to as 'seed pulses'. The energy for the oscillator is provided by a diode-pumped, frequency doubled Nd:YVO_4 laser (Millennia Pro, Spectra Physics, maximum output power 5 W, usually a power of 4 W is used).

With a rate of 1 kHz, seed pulses are trapped in a Ti:Sapph resonator, amplified and then coupled out with an energy exceeding 3 mJ (*regenerative amplification*). The amplifier is supplied with energy by a frequency doubled, pulsed Nd:YLF laser (Empower, λ=527 nm, output power 16 W). However, with pulse durations in the femtosecond range, the intensity of the amplified pulses would damage the amplification medium. To avoid this, the intensities of the seed pulses need to be limited during amplification. The pulses pass a 'pulse stretcher'to increase the pulse duration by four orders of magnitude before they are coupled into the amplifier. In the stretcher a combination of a diffraction grating and mirrors induces a large group

velocity dispersion (GVD) in the pulse [Tre69], thereby increasing its pulse duration and decreasing the intensity. The stretched pulses are suitable for amplification in a Ti:Sapph resonator. The amplified pulses then pass a pulse compressor that works like the stretcher, only with inverted group velocity dispersion. It compresses the pulse duration again to around 100 fs. Unlike the stretcher, the compressor is tunable. The position of a retroreflector in the compressor is electronically adjustable, so the user can tune the resulting pulse duration ($>$ 80 fs) and the (linear) chirp of the pulse.

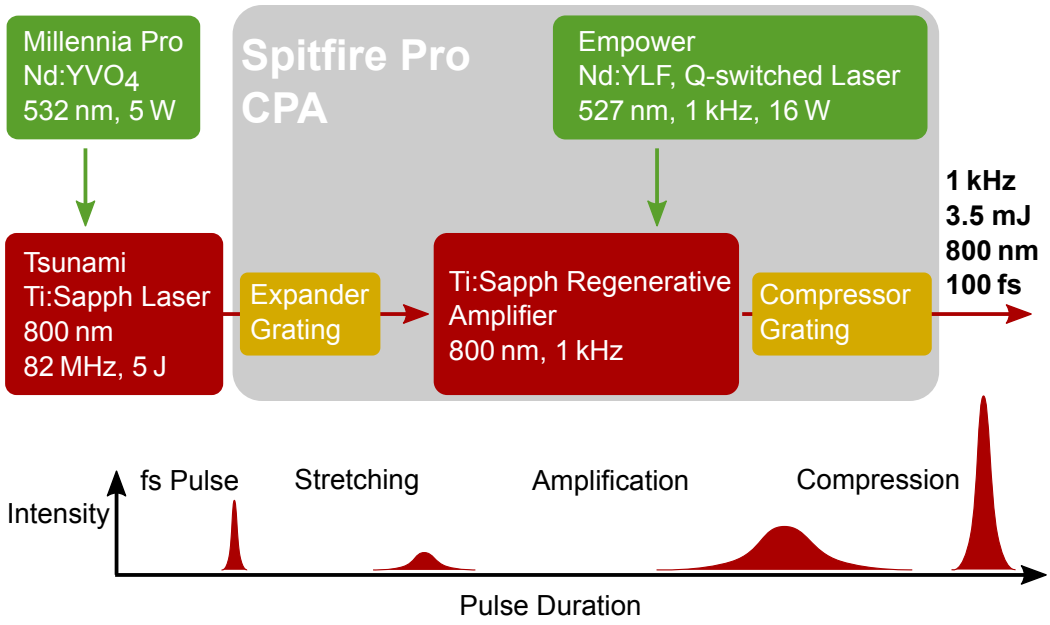

Figure 3.2.: CPA laser system Spitfire Pro: A Ti:Sapph Oscillator (Tsunami) provides 800 nm pulses with a pulse duration of circa 30 fs with a repetition rate of 82 MHz and a pulse energy of circa 5 nJ. By chirped pulse amplification (CPA), the pulse energy is increased by almost 6 orders of magnitude, while the repetition rate is reduced to 1 kHz.

3.1.3. The Experimental Setup

In this section a brief overview of the setup is given. Details will be provided in the following sections. The experimental setup is schematically displayed in Figure 3.3.

Probe Pulses

Synchronised pump and probe pulses are generated from the same 800 nm pulses that are provided by the Spitfire laser system. The probe pulses are generated in 3 steps of nonlinear conversion: The IR part (1400 nm, *signal*) of a supercontinuum is

amplified by a *noncollinear optical parametric amplifier* (NOPA) [WPR97, Rie00, CS03]. In a subsequent stage of *optical parametric amplification* (OPA) the energy of these pulses is further increased. The energy for the OPA is supplied by pulses at a wavelength of 800 nm. In the process of amplification, idler pulses are generated at a wavelength of 1800 nm, according to energy conservation:

$$\frac{1}{800\,\mathrm{nm}} = \frac{1}{1400\,\mathrm{nm}} + \frac{1}{1800\,\mathrm{nm}} \tag{3.2}$$

Signal and idler undergo *difference frequency mixing* (DFM) in an $AgGaS_2$ crystal to yield the MIR probe pulses. The MIR beam is split into a probe and a reference beam.

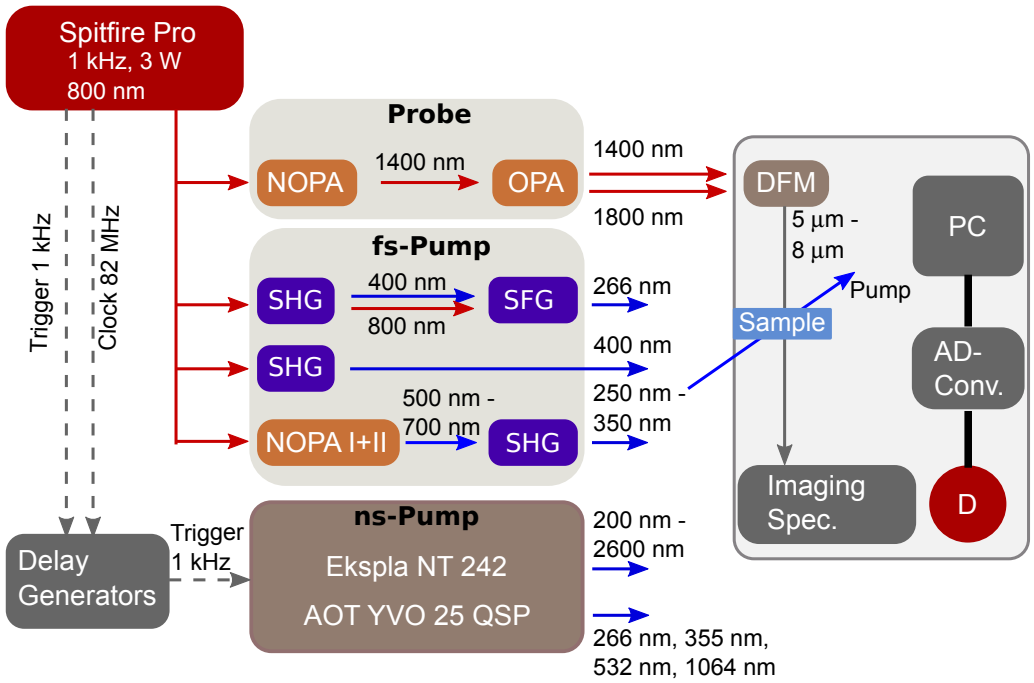

Figure 3.3.: Experimental setup: Probe pulses are generated by two steps of parametric conversion and subsequent difference frequency mixing (DFM). The generation of fs excitation pulses can be done by second harmonic generation (SHG), by SHG and subsequent sum frequency generation (SFG) or by parametric conversion (NOPA I+II) and subsequent frequency doubling. In the ns range, excitation pulses are provided by an electronically synchronised laser (AOT YVO 25 QSP or Ekspla NT 242).

Probe and reference beams irradiate different volumes of the sample. The probe beam overlaps with the pump beam inside the sample, whereas the reference beam passes through an unexcited volume of the sample above the probe beam. After

passing through the sample, the probe and the reference beams are projected by an imaging spectrometer onto two horizontal arrays of mercury cadmium telluride (MCT) MIR photoresistors of 64 elements each. The reference beam always probes the unexcited sample and does therefore not contain information about the photophysics of the sample. It is only used to correct the measured probe signals for the fluctuations of the MIR pulses to improve the signal-to-noise ratio. This makes detailed measurements of even very small effects possible.

Excitation Pulses

The excitation pulses (pump) can be generated in different ways, depending on the desired wavelength and the delay time range. Short excitation pulses can be generated by different techniques of frequency conversion and delayed by a mechanical stage (maximum delay 3.5 ns).

1. *Second harmonic generation* (SHG) yields excitation pulses at a wavelength of 400 nm. Maximum pulse energy exceeds 30 µJ.

2. *Second harmonic generation* (SHG) and subsequent *sum frequency generation* (SFG) of the first and second harmonic yield excitation pulses at a wavelength of 266 nm. Pulse energies up to 10 µJ are possible.

3. *Noncollinear optical parametric amplification* (NOPA) can generate tunable pulses in a wavelength range from 500 nm to 700 nm. Their second harmonic makes the spectral range from 250 nm to 350 nm accessible. Pulse energies of the second harmonic between 1 µJ and 2 µJ can be achieved.

If longer delay times than 3.5 ns are necessary, the excitation pulses are provided by another laser that is electronically synchronised with the Spitfire Pro. Two different systems are available:

1. A Nd:YVO_4 laser (AOT YVO 25 QSP/MOPA) can provide pulses at the fundamental wavelength of 1064 nm as well as the second, third and fourth harmonic (532 nm, 355 nm and 266 nm, respectively). The pulse duration is 0.7 ns, the pulse energies exceed 3 µJ at all wavelengths.

2. A tunable *optical parametric oscillator* (OPO) (Ekspla NT 242) covers the wavelength range from 200 nm to 2600 nm with pulse energies exceeding 10 µJ at every wavelength, but at a reduced temporal resolution due to its longer pulse duration of around 2 ns to 3 ns.

3.1.4. Sample Handling

For obvious biological reasons the DNA photophysics should be investigated in aqueous solution rather than in other solvents. However, the interesting vibrational bands are in the spectral region from 1250 cm^{-1} to 1800 cm^{-1} which is obscured by the very strong absorption of the O–H bending mode of water. This problem is circumvented by using D_2O instead of H_2O as the solvent. In D_2O the absorbance of the bending mode is shifted below 1250 cm^{-1}, making a measurement from 1250 cm^{-1} to 1800 cm^{-1} possible. In order to avoid pH-effects, a buffered solution of Na_2HPO_4 and KH_2PO_4 in D_2O is used with a concentration of 50 mM each. Unless otherwise stated, the measurements were performed with a sample concentration of 10 mM per DNA base in this buffered solution. All measurements were performed at room temperature (22 °C).

The handling of the sample is somewhat difficult, because the excited sample has to be exchanged between two consecutive shots, i.e. within 1 ms. Further, the available sample volume sometimes is limited to about 1 ml or less. Both requirements can be met by pumping the sample continuously through a flow cell (Figure 3.4).

A flow cell consists of two windows that are separated by a hollow Teflon spacer (thickness 100 µm) and two aluminium plates on the outside holding them together, as depicted in Figure 3.4. The sample solution enters and exits the flow cell via bores in the upper window and flows within the cavity of the Teflon spacer. Two types of Teflon spacers are used: for stationary absorbance measurements a circular cavity of 1 cm is used. For time-resolved measurements a canal of 1 mm to 2 mm thickness is used to increase the sample flow and thereby make it suitable for time-resolved measurements with a kHz repetition rate.

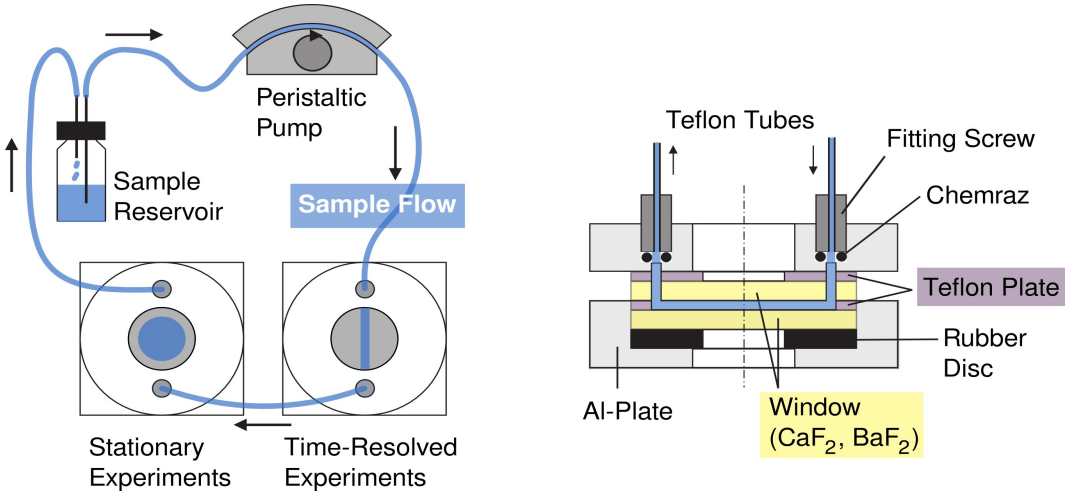

Figure 3.4.: The sample is pumped through a flow cell during measurements. The flow cell is comprised of a Teflon spacer with a thickness of 100 µm between two windows of BaF_2 or CaF_2. The sample flows through a thin channel in the Teflon spacer. Picture adapted from [Hai12a].

The window material has to be transparent in the UV and in the MIR spectral range. Test experiments [Kub09] showed that two materials are optimal under different conditions: CaF_2 is easy to handle and insoluble in water, but intense laser pulses generate artefacts by two-photon effects in it that last up to 100 ps [Kub09]. In the nanosecond to microsecond range, these effects are not observable. Therefore, a CaF_2 flow cell is used in these measurements. BaF_2 shows similar effects at the delay zeropoint, but they are smaller and last only for circa 1 ps, so BaF_2 is used in time-resolved measurements with fs- excitation. The drawback of BaF_2 windows is their solubility in a buffered solution we used. Thereby, the transparency of the window deteriorates within ca. 5 hours, making time-demanding measurements very difficult. This problem was solved recently by having the side of the window that is exposed to water covered with an anti-reflection coating, so the water is not in direct contact with the BaF_2 window. A detailed discussion of these effects and a characterisation of other materials can be found in [Kub09].

3.2. Probing and Detection in Detail

3.2.1. Generation of MIR Pulses

300 µJ of the Spitfire laser output (corresponding to an average power of 300 mW at the 1 kHz repetition rate) are used to generate MIR probe pulses. Frequency conversion to the MIR range is done in three steps (see Figure 3.5):

1. Noncollinear optical parametric amplification (NOPA) yields pulses at 1400 nm.

2. Optical parametric amplification (OPA) of these yields 1400 nm and 1800 nm pulses.

3. Difference frequency mixing (DFM) of those pulses yields MIR pulses.

The first two steps involve *parametric amplification*, which generates tunable pulses over a broad wavelength range. In parametric amplification, a strong (pump) beam (frequency ν_P) and a weak (frequency ν_S) (signal) beam are overlapped in a nonlinear crystal like a BBO. Difference frequency mixing (DFM) can convert a pump photon into a signal photon ν_S and an idler photon ν_I according to energy conservation $\nu_P = \nu_S + \nu_I$, if the phase-matching is suitable ([Boy08, She03]). Thereby, the pump beam is weakened, the signal is amplified and an idler beam is generated. This can be done with pump and signal propagating collinearly (OPA) or noncollinearly (NOPA). Explaining the detailed differences between a collinear (OPA) and a noncollinear (NOPA) configuration is beyond the scope of this thesis. For more details, see [WPR97, Rie00, CS03].

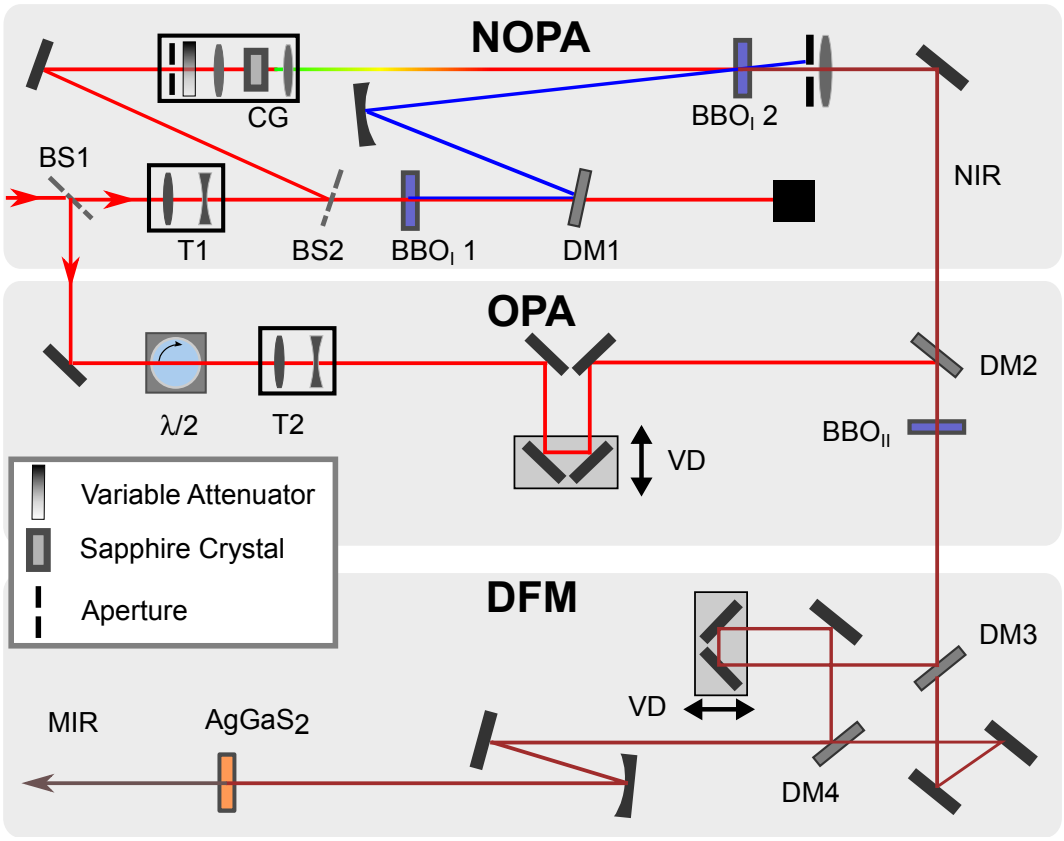

Figure 3.5.: Generation of MIR pulses in 3 steps: 1. The NIR part (around 1400 nm) of a supercontinuum (SC) is amplified in a NOPA (BBO type I crystal). The NOPA pump pulses are generated by frequency doubling of the 800 nm pulses. The supercontinuum is generated by focussing a small fraction of the 800 nm pulses onto a sapphire crystal. 2. The NOPA output pulses are amplified in an OPA (800 nm pump pulses, type II BBO crystal), with idler pulses at 1800 nm being generated in the process. 3. Difference frequency mixing (DFM) of signal and idler in an $AgGaS_2$ crystal (type I) yields MIR pulses.

First Stage: NOPA Generates NIR Pulses Around 1400 nm

The beamsplitter BS1 (top box of Figure 3.5) transmits 40 % of the incident beam energy (120 µJ) into the NOPA setup. The NOPA is depicted schematically in the top box of Figure 3.5. The laser pulses pass through a telescope (T1) that reduces their diameter to increase the intensity and the conversion efficiency. The beam is subsequently split into a strong (about 96 % of the energy) and a weak beam (4 % of the energy). The strong beam is frequency-doubled in a BBO crystal (type I, $\Theta = 29°$, thickness 500 µm) to yield pulses with a wavelength of 400 nm and an energy above 30 µJ. These are the pump pulses of the conversion process. The weak beam is focussed on a sapphire crystal to generate a white light continuum (signal) that contains all wavelengths from the visible to the near-infrared. It can be fine-tuned

by using an aperture (ID) and a variable attenuator (VA) in front of the sapphire crystal (Sa). The pump and the white light beams are spatially and temporally overlayed in a BBO crystal (type I, $\Theta = 32.5°$, thickness 2 mm). The intensities and diameters of both beams are adjusted by focussing them circa 5 cm before the BBO crystal. The pump beam path is tilted vertically about 3° to 4° with respect to the supercontinuum to compensate group velocity dispersion (GVD) between the pulses. At the right phase-matching angle of the BBO, signal pulses with a wavelength of 1400 nm are amplified and idler pulses (wavelength 560 nm) are generated. The signal pulses are subsequently converted further, while the simultaneously generated idler pulses are used to measure the stability and spectral quality of the generated pulses. The signal pulse energy after amplification should be 1 µJ, with a noise-to-signal ratio of 0.2 % to 0.3 %.

Second Stage: OPA Amplifies 1400 nm Pulses and Generates 1800 nm Pulses

BS1 reflects 60 % (180 µJ, OPA-pump) of the incident beam energy into the optical parametric amplifier setup. The OPA (see middle box of Figure 3.5) further increases the energy of the NOPA output pulses. To enable phase matching in the type II BBO ($\Theta = 27°$, thickness 3 mm), the polarisation of the pump pulses is rotated by a $\lambda/2$ plate. The beam diameter is adjusted to 1 mm by a telescope (T_2) to increase intensity and thereby conversion efficiency. Temporal overlap between the signal and the pump pulses is fine-tuned by a variable delay (VD). Amplifying the signal pulses yields corresponding idler pulses (1800 nm at a signal wavelength of 1400 nm).

NIR energies above 35 µJ can be achieved this way, but the energy should be kept below 30 µJ to avoid unwanted nonlinear effects in the subsequent conversion stages. The wavelengths of the signal and idler pulses can be varied from 1250 nm to 1550 nm and from 1650 nm to 2200 nm, respectively.

Third Stage: Difference Frequency Mixing

The MIR pulses are generated by difference frequency mixing (DFM) of the signal and idler pulses of the OPA (see lower box in Figure 3.5). To achieve a good signal-to-noise ratio the spatial and temporal overlap of the NIR pulses have to be optimised. For this purpose, signal and idler beams are separated and aligned individually. They are separated by a dichroic mirror (DM_3, type HR1400/HT1800), the delay between the two is adjusted by a variable delay (VD), then both beams are recombined by a second dichroic mirror (DM_4) and focussed onto a $AgGaS_2$ crystal (type I, $\Theta = 34°$, thickness 2 mm), where difference frequency mixing (DFM) takes place. The central wavelength of the MIR pulses can be varied from 4 µm to 10 µm (usually a range from 5 µm to 8 µm is used), depending on the wavelengths of the NIR pulses generated in the NOPA and OPA stages.

To avoid nonlinear effects in the $AgGaS_2$ crystal, especially self-focussing that distorts the beam quality, too high intensities in the $AgGaS_2$ crystal have to be

avoided. In order to achieve this, the NIR energy is adjusted below 30 µJ and the crystal is placed a few centimetres out of the focus of the NIR beams. The MIR pulses typically have an energy of 0.5 µJ to 1 µJ, a pulse duration from 100 fs to 200 fs and a spectral width of 150 cm^{-1}. Fluctuations of the MIR pulse energy of below 0.2 % can be achieved.

3.2.2. Probing and Detection Setup

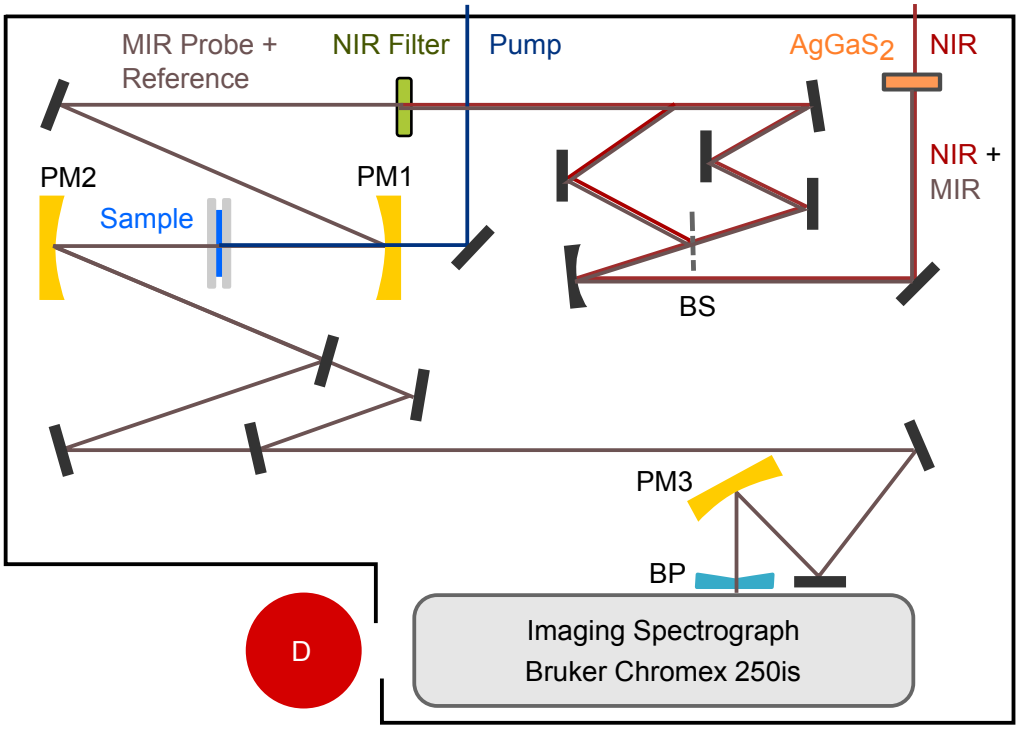

Figure 3.6.: Experimental setup: Difference frequency mixing in the $AgGaS_2$ crystal yields MIR pulses. The MIR beam is divided by a beam splitter (BS) into a probe and a reference beam. They are independently aligned and focussed onto the sample; the pump and the probe beams overlap in the sample. After passing through the sample, probe and reference beams are projected onto two horizontal arrays of 64 photoresistors each.

The detection setup is depicted in Figure 3.6. The MIR pulses that are generated in the $AgGaS_2$ crystal are divided into two parts, a probe and a reference beam, by a beam splitter (BS). Each of those beams is subsequently aligned separately. The NIR parts of the pulses are absorbed by two germanium (NIR filter) plates that only transmit the MIR pulses. The probe and the reference beams are focused by a parabolic mirror (PM1, f = 108 mm) and re-collimated by a second, identical parabolic mirror (PM2). The sample is placed in the focus of the probe beam. The

reference beam must be somewhat misaligned with respect to the parabolic mirror, because otherwise the probe and the reference beams would have a common focal point. The reference beam passes through the sample around 700 µm above the probe beam; therefore there is no overlap of the reference beam with the probe or the pump beams in the sample. After passing through the sample the beams are re-collimated by PM2 and then individually aligned. They are focussed by a parabolic mirror (PM3) onto the entrance slit of the spectrograph (Bruker Chromex 250is). After passing through the biprism (BP) probe and reference propagate parallel to each other with a vertical distance of 4 mm. The spectrograph uses a Czerny-Turner geometry [CT30, SMD64] to disperse the pulses and project them onto the two horizontal arrays of 64 MCT photoresistors. The spectral resolution and the spectral width depend on the grating used, see Table 3.1.

Grating	Spectral Resolution	Spectral Width
1	—	—
2	9.3 nm	595 nm
3	13 nm	830 nm

Table 3.1.: Spectral resolution and spectral width of the spectrograph gratings. Grating 1 is not suitable for wavelengths above 5600 nm and is therefore not used.

Grating 2 was used in all measurements in this dissertation. It combines a high resolution with a spectral width that is well suited for the MIR pulses. Grating 1 cannot be used, because its maximum wavelength is much too low. Grating 3 is a viable alternative to grating 2, but was not used in the measurements presented in this thesis. A detailed description of the spectrograph and the MCT detector can be found in [Pre09], the detection setup is explained in more detail in [Sch11].

3.3. Excitation Pulses

The excitation pulses are generated either by converting fs pulses to the desired wavelength or by an electronically synchronised ns laser. In the first case, the excitation pulses are delayed by a mechanical stage, yielding a maximum delay of 3.5 ns. In the second case, the delay range extends to 100 µs. This maximum delay is not a consequence of some electronic properties of the delay generators, but rather a limitation related to the handling of the sample. We use a flow cell to exchange the excited sample volume within two consecutive pulses (see subsection 3.1.4), i.e. within 1 ms. The probe pulse must illuminate the previously excited sample, i.e. within the maximum delay the sample must not be exchanged. This limits the maximum delay to about 100 µs.

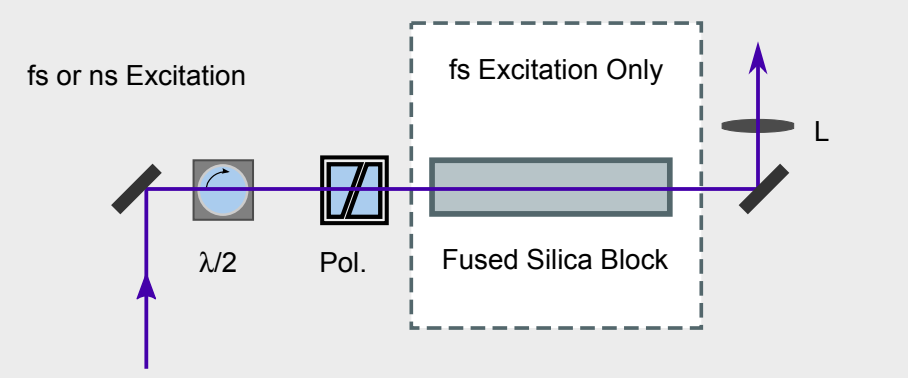

Figure 3.7.: Adjustment of energy and polarisation of the excitation pulses by a combination of a $\lambda/2$ plate and a polariser. The former rotates the polarisation of the transmitted beams and thereby defines the amount of energy that can pass through the polariser. The polarisation angle is chosen to be the magic angle relative to the probe pulses. If femtosecond excitation pulses are used, the pulse duration is increased by group velocity dispersion in a glass block to more than 1 ps.

The tuning of the pulse energy and the alignment of their polarisation is done in the same way for fs and ns excitation pulses, see Figure 3.7. The excitation pulses pass a combination of a $\lambda/2$ plate and a polariser. The former allows to rotate the polarisation of the pulses, the latter transmits only the part of the light that is polarised in a certain direction. Thereby the transmitted pulse energy as well as its polarisation can be freely chosen. To avoid measurement artefacts (see subsection 3.4.4), the polarisations of the probe and the excitation pulses must have an angle of circa 55° (the *magic angle*) relative to each other, so the polariser is adjusted accordingly. The resulting excitation pulses are focussed onto the sample, the beam diameter in the sample should be between 150 µm and 250 µm. The excitation energy and the polarisation are always tuned in this way, regardless what excitation source is used. If short sub-ps excitation pulses are used, the pulse duration is increased by group velocity dispersion in a glass block to more than 1 ps to avoid too high intensities (see subsection 3.4.5). The different methods of generating excitation pulses are described in the following subsections.

3.3.1. Ultrashort Excitation Pulses

Circa 750 µJ of the laser output energy are used to the generate excitation pulses. This beam is divided between the setup of harmonics generation (40 % = 300 µJ) and the setup of the parametric amplifiers (60 % = 450 µJ). Most of the measurements of this thesis were performed using the third harmonic (266 nm) of the CPA output. When other excitation wavelengths are needed, two stages of noncollinear optical parametric amplification and subsequent frequency doubling is used. Both setups

are described in the following. The second harmonic (400 nm) was not used in the measurements and is not described in detail.

UVC Pulses at a Wavelength of 266 nm

Circa 300 µJ of the output energy of the central laser system is used for frequency conversion to the UV range. The pulses are delayed by a variable mechanical stage before they are converted to the UV range. The third harmonic is generated in two steps:

1. Second harmonic generation (SHG) yields pulses with a wavelength of 400 nm.
2. Sum frequency generation of the 800 nm pulses and their second harmonic yields the third harmonic with a wavelength of 266 nm.

The details (see Figure 3.8): Before frequency conversion, the beam diameter of 4 mm is reduced by a factor of 3 by a telescope in order to increase the intensity and thereby the conversion efficiency.

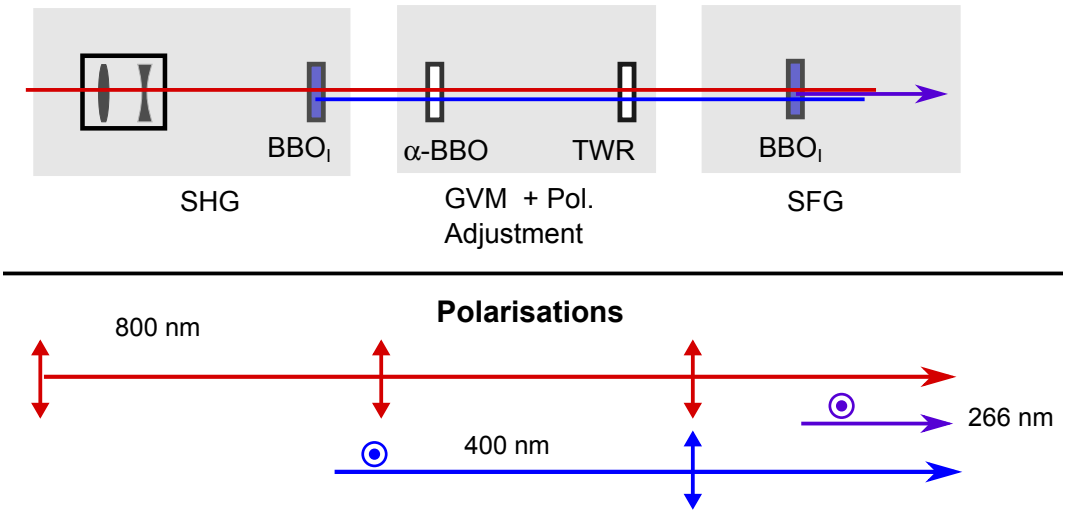

Figure 3.8.: The third harmonic is obtained by two steps of conversion: 1. SHG in a type I BBO yields the second harmonic ($\lambda = 400$ nm). Both beams pass an α-BBO that compensates for their group velocity mismatch and a two-wave retardation plate that rotates their polarisations by 90° (400 nm) and 180° (800 nm). 2. SFG of the fundamental and the second harmonic yields the third harmonic (wavelength: 266 nm).

The second harmonic is generated in a BBO (type I, $\Theta = 29°$, thickness 0.5 mm). It is polarised perpendicular to the 800 nm pulses. The sum frequency is generated in a type I BBO, because the conversion efficiency is higher than in a type II crystal. A type I SHG process requires both beams (fundamental and second harmonic) to have the same polarisation. To achieve this, they pass a two wavelengths retardation

waveplate (TWR). The TWR rotates the polarisation of the second harmonic by 90° and the polarisation of the fundamental by 180°, i.e. does not change it. To compensate the group velocity mismatch of the 800 nm and the 400 nm pulses in the BBOs and the TWR, an α-BBO (thickness 1.3 mm) is used. UV pulses with energies up to 10 µJ can be achieved (however, usually 2 µJ are suitable for most experiments). The pulse duration, measured by a UV autocorrelator [HKR11], is about 260 fs. To avoid two-photon effects that can be caused by short and intense pulses, the pulse duration is usually stretched to 1 ps to 2 ps by introducing a 20 cm block of fused silica into the beam path. The group velocity dispersion (GVD) [Sal07] of the pulse in the fused silica increases the pulse duration and decreases the intensity.

Parametric Amplification

450 µJ of the CPA output energy is used to generate tunable excitation pulses by two NOPAs and subsequent frequency doubling. Figure 3.9 depicts the two NOPAs. The first is virtually identical to the NOPA in the probe branch.

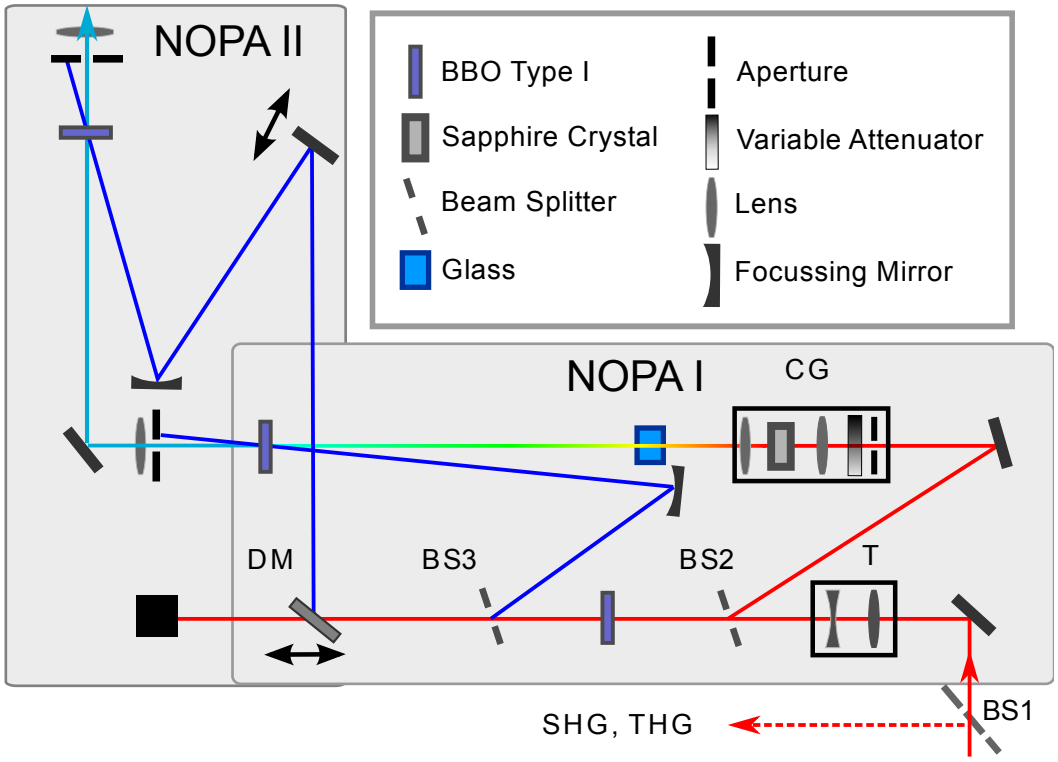

Figure 3.9.: Tunable pulses between 500 nm and 700 nm are generated by two stages of parametric amplification. The white light generated in a sapphire crystal (CG) is overlayed with the second harmonic of a BBO type I crystal, amplifying one component of the white light continuum. The NOPA output is amplified in the second NOPA stage. To increase the output energy, BS1 and the telescope T can be removed.

The beam splitter BS2 reflects a small fraction (circa 5 %) of the 800 nm beam energy into the continuum generation unit (CG). The CG consists of an aperture, a variable attenuator, two lenses and a sapphire crystal. After passing through a variable attenuator, the beam is focussed into a sapphire crystal (thickness 5 mm) to generate white light. The first aperture and the variable attenuator are used to fine-tune the energy in the sapphire crystal and thereby the generated continuum. The beam diameter of the white light is adjusted by focussing it circa 5 cm before the BBO crystal, where noncollinear amplification takes place. To improve the wavelength selectivity, an additional piece of fused silica is introduced into the white light beam path to increase its group velocity dispersion. Thereby, fine-tuning of the temporal overlap allows to choose the central frequency more precisely.

The 800 nm pulses that are transmitted by BS2 (circa 95 % of the incident energy) are frequency-doubled in a type I BBO crystal (thickness 2 mm) to provide 400 nm pump pulses. These are split 30:70 between the first and the second stage of the NOPA. Pump and signal beams are overlaid in the BBO crystal, generating pulses of about 1 µJ to 2 µJ in the first NOPA. In the second stage, these pulses are amplified to more than 10 µJ. The NOPA ouput pulses are collimated and delayed by the mechanical stage and subsequently frequency-doubled.

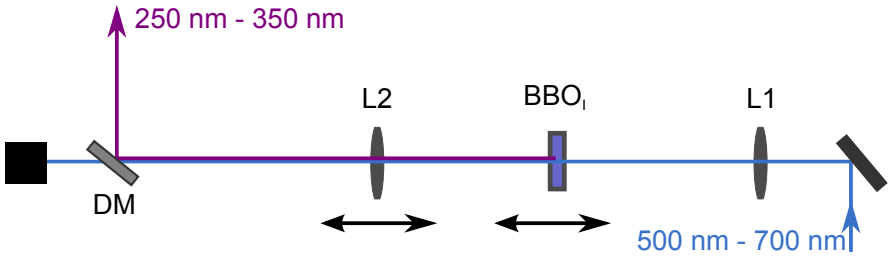

Figure 3.10.: Frequency doubling of the NOPA output. The pulses are focussed (L1, f = 75 mm) into a type I BBO (40° to 50°, depending on the desired wavelength, thickness 50 µm), where frequency doubling takes place, and re-collimated by L2.

SHG takes place in BBO crystals ($\Theta = 40°$ to 50°, depending on the desired wavelength, thickness 50 µm). Such thin crystals maximise the conversion efficiency, presumably because of their large amplification bandwidth and acceptance angle. The energy of the resulting UV pulses is 1 µJ or lower. After re-collimation by L2, the beam passes a combination of a $\lambda/2$ plate and a Glan-Taylor polariser [AT48, Lit05, Bas10]. The polarisation is usually fixed at the magic angle, then the $\lambda/2$ plate defines the energy (see Figure 3.8). Since this particular setup suffers from quite low pulse energy (about 1 µJ), often the $\lambda/2$ plate is optimised to magic angle and the measurement is then performed without a polariser to minimise losses.

Recently, the NOPA setup (see Figure 3.9) was amended to provide more output power. The first beam splitter BS1 in Figure 3.9 has been removed from the setup,

using the full 750 µJ of energy in the pump setup for parametric amplification. The beam diameter has been increased by removing the pump telescope T to avoid distortions of the beam profile by nonlinear effects. Beam diameters in the crystals are increased to limit the power density. With this setup, pulses with more than 30 µJ can be generated. The energy of the second harmonic of these pulses was 2 µJ to 3 µJ, three times the previous value. Test measurements on double-stranded DNA (not shown in this thesis) look very promising.

3.3.2. Nanosecond Excitation Pulses

The experimental observation of long-living excited states requires delay times up to microseconds. This can obviously not be achieved by a mechanical delay stage, since 1 µs corresponds to an optical path length of 300 m. A second laser is necessary to provide the excitation pulses.
This laser does not need to match the specifications of the femtosecond laser system. Thus much less expensive nanosecond lasers are sufficient, if they can be triggered externally with high precision at a kHz rate. In our setup two options are available:

1. A Nd:YVO_4 laser (AOT YVO QSP/MOPA) can be equipped with modules for second, third and fourth harmonic generation. The fourth harmonic (generated by two consecutive second harmonic generations) yields pulses with up to 5 µJ energy and a pulse duration of around 0.5 ns. If triggered appropriately, the temporal jitter is well below 1 ns, so fs- and ns measurements have a window of temporal overlap from 1 ns to 3 ns.

2. The laser system Ekspla NT 242, which is tunable from the deep UV (200 nm) to the IR (2600 nm), provides pulse energies well above 10 µJ at every wavelength and a pulse duration of about 3 ns. If the better temporal resolution of the AOT laser is not needed, then the Ekspla is used due to its superior specifications.

For both lasers, synchronisation is provided by two delay generators. The basic trigger signal (sync) is synchronous with the Spitfire output. Because the pump pulses must arrive up to 100 µs before the probe pulses at the sample, the AOT or Ekspla has to be delayed by 900 µs to 1000 µs.

The electronic synchronisation scheme is depicted in Figure 3.11. The sync pulses (electronic trigger output of the Spitfire laser system) are delayed by 900 µs to 1000 µs by two consecutive delay generators (DG1 and DG2 in Figure 3.11). A PCI delay card (Bergmann BME SG05p) (DG1 in Figure 3.11) receives a sync signal from the CPA and emits a trigger signal t_1 later. To increase the accuracy of the PCI card, an external 82 MHz clock signal is provided. This clock signal is generated by reflecting a small fraction of the oscillator light (Tsunami) onto a photodiode and then electronically transforming the resulting signal to a sine wave to make it suitable for the PCI card. The trigger output of the PCI card serves as trigger input

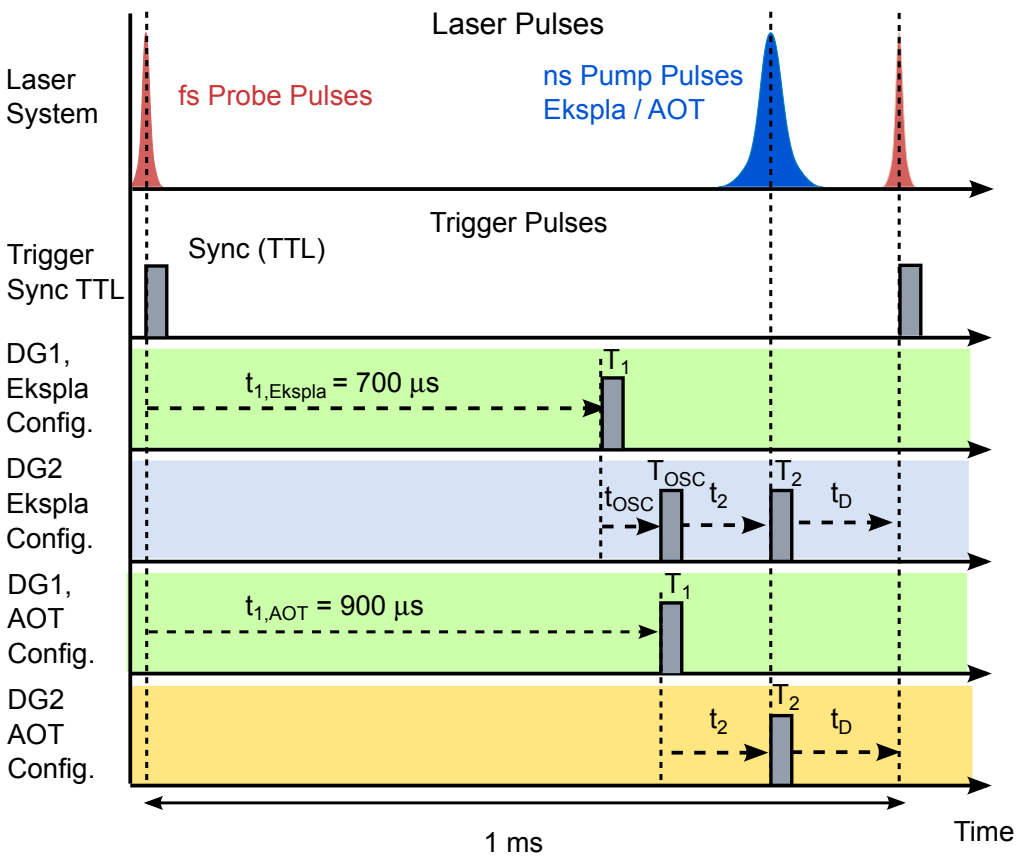

Figure 3.11.: Electronic synchronisation of the AOT or Ekspla laser to the fs laser system. The sync signal out of the CPA triggers all other delay generators. The delay of 900 µs to 1000 µs is achieved by using two delay generators, DG1 and DG2. DG1 generates a trigger T1 delayed by 700 µs (Ekspla configuration) or 900 µs (AOT configuration). DG2 subsequently triggers the excitation lasers. Details see text.

to the second delay generator DG2 (Stanford Research DG535). DG2 provides the trigger signals for the Ekspla or the AOT system. DG2 is controlled by the LabView program (MIST8.5) that runs the measurements.

As Figure 3.11 shows, the AOT and the Ekspla system require different configurations:

The Ekspla Triggering Scheme

The Ekspla NT 242 requires two trigger input signals for low-jitter operation. The first signal initiates the pumping of the oscillator, while the second (about 200 µs later) triggers a Pockels cell that couples out the pulse. This is realised in the following way: DG2 receives a trigger input from DG1 at a fixed time T_1 (700 µs

after sync). DG2 generates two trigger output signals. The first is generated at a delay time t_{OSC} after T_1, it triggers the pumping of the Ekspla Oscillator. t_{OSC} is a variable delay time that is controlled by the program MIST8.5 that runs the measurements. It is varied between 0 ns and 100 µs during a measurement. The second trigger output signal is generated at T_2, 200 µs after T_{OSC}. It triggers a Pockels cells that couples the laser pulse out of the oscillator. The experimentally observed delay time t_D is $t_D = 1000\,\mu s - t_1 - t_{OSC} - t_2 = 100\,\mu s - t_{OSC}$.

The AOT Triggering Scheme

The AOT configuration is simpler, because the AOT requires only 1 trigger input signal. The trigger timing of DG1 is fixed at 900 µs after the sync signal. DG2 triggers the AOT at a variable delay time t_2 after $T1$. t_2 is controlled by the measurement software and varied between 0 ns and 100 µs during the measurements. The experimentally observed delay time is $t_D = 1000\,\mu s - t_1 - t_2 = 100\,\mu s - t_2$.

From the descriptions above, the DG535 seems to be the only delay generator necessary, the PCI card (DG1) seems superfluous. However, the DG535 malfunctions if a trigger input is received while a trigger output signal from the preceding trigger event has to be produced. To avoid this, another delay generator is necessary, so the trigger input of the DG535 arrives at a different time.

3.4. Time-Resolved Spectroscopy

The details of TRIR spectroscopy are explained in this section. The first two subsections introduce the data acquisition and data analysis in more detail. This introduction is followed by a discussion of typical signals that are present in TRIR measurements.

3.4.1. Data Acquisition

Data acquisition from the MCT detector and controlling either the mechanical delay stage or the electronic delay generators are done by the LabVIEW program MIST8.5 (Mid-infrared Spectroscopy Tool). A measurement run consists of defining the delay points and recording data at every one of them. The MCT detector measures the energies of the transmitted pulses (probe (pr) and reference (rf)) at 64 different wavelengths and converts them into proportional output signals I_{pr}, $I_{pr,0}$, I_{rf} and $I_{rf,0}$, where the index '0'denotes pulses which have passed the sample while the excitation beam was blocked. The data are averaged over a number of shots (usually 2000) and then the relative transmittance is calculated according to $T_{pr} = \frac{I_{pr}}{I_{pr,0}}$ and $T_{rf} = \frac{I_{rf}}{I_{rf,0}}$. T_{pr} contains the information about the UV induced absorbance changes of the sample and the noise caused by the energy fluctuations between consecutive pulses, the noise of the detector etc. The paths of the reference beam and the excitation beam do not overlap, therefore T_{rf} contains only noise. The major part of the noise is due to the statistical energy fluctuations between consecutive pulses. Since the probe and the reference beams arise from simply splitting the MIR-beam, they contain the same fluctuations. The data can be corrected for this noise by calculating the referenced relative transmittance $T_{ref} = \frac{T_{pr}}{T_{rf}}$. This increases the accuracy of the measurements significantly. The absorbance changes are calculated from the relative transmittance according to:

$$\Delta A_{ref}(\lambda, t_D) = -log(T_{ref}) \tag{3.3}$$

The absorbance changes can be subsequently analysed to gain insight into the underlying photophysical processes.

3.4.2. Data Analysis

Data Modelling

One of the most important techniques of data analysis is fitting the data by a model function. The model function should reproduce the data and give some insights into the excited state decay mechanism, especially on the transient excited states

that are present and on their absorbance spectra. Routines to analyse data this way are implemented in the home-built data analysis program *Z20* [Spö01, Sat04]. The most important of these routines is used extensively throughout this thesis, so a short introduction is given in the following (for a more detailed discussion see [Sat04, Spö01]). To understand the data modelling procedure and how the model function is derived, a short description of the mathematical treatment of the excited state physics is necessary. Upon UV absorption, DNA bases undergo transitions between various excited states, ending either in the ground state or a photoproduct. Such processes are described by a system of rate equations:

$$\frac{d}{dt}c_i(t) = \sum_{j=1}^{n}(K)_{ij} \cdot c_j(t), \tag{3.4}$$

where $c_i(t)$ is the concentration of molecules in the state S_i, the matrix elements $(K)_{ij}$ are rate constants for the transition from S_i to the state S_j. These equations can be solved by a multiexponential ansatz. The resulting absorbance changes caused by these transitions are also described by a multiexponential model function, if thermal relaxation processes are neglected:

$$\Delta A(\lambda, t_D) = \sum_{i=1}^{n} \int_0^\infty a_i(\lambda, \tau_i) \cdot \exp^{-t/\tau_i} \cdot C(t_D - t)dt \tag{3.5}$$

The sum of exponential decay functions is convoluted with the cross-correlation function $C(t_D - t)$ of the excitation pulses and the probe pulses to take into account the effects of the pulse durations. Assuming Gaussian pulses with a cross-correlation width τ_{cc}, the equation can be re-written as:

$$\Delta A(\lambda, t_D) = \sum_{i=1}^{n} a_i(\lambda, \tau_i) \cdot \exp\left(\frac{\tau_{cc}^2}{4\tau_i^2} - \frac{t_D}{\tau_i}\right) \cdot \frac{1}{2}\left[1 + erf\left(\frac{t_D}{\tau_{cc}} - \frac{\tau_{cc}}{2\tau_i}\right)\right], \tag{3.6}$$

where $erf(X)$ is the error function $erf(X) = \frac{1}{2\pi}\int_0^X \exp(-X^2)$. The scaling factors $a_i(\lambda, \tau_i)$ describe the spectral changes associated with the time constants τ_i. At a given number of exponential decay components n, the $a_i(\lambda, \tau_i)$ and their time constants τ_i are varied until the best match with the experimental data is reached. The resulting optimum $a_i(\lambda, \tau_i)$ are the *Decay Associated Difference Spectra* (DADS); if τ_i is the time constant of a transition from one excited state to another, the corresponding DADS gives their difference in absorbance. The DADS themselves are in general not sufficient to determine the absorbance spectra of excited states, the *Species Associated Spectra* (SAS). They can be calculated from the DADS, if a particular decay scheme, i.e. a particular decay matrix K_{ij} is assumed [SLG04]. The absorbance spectra of the excited states can then be used to determine their

nature. The calculation of the SAS from the DADS by specific decay models is not implemented in the Z20 program. Fortunately, the DADS suffice for data analysis in most cases. If an excited state returns to the ground state with a time constant τ_i, then the DADS(τ_i) is proportional to the difference in absorption between the excited state and the ground state. This is the case for most of the excited state decays that are discussed in this thesis.

Limitations of the Modelling Procedure

The model function was derived from the assumption that thermal relaxation processes are negligible. Some discussion on this assumption is necessary to see in which cases it is applicable and what its limitations are. Figure 3.12 depicts a schematic representation of the transition from the state S_i to the state S_j. The base is in the state S_i and moves along its energy surface. At the surface crossing point (SCP), a transition to S_j occurs. The system then is in the state S_j, but not in its energy minimum. It moves along the energy surface of S_j and reaches its thermal equilibrium, dissipating the excess thermal energy ΔE_{therm} to the solvent.

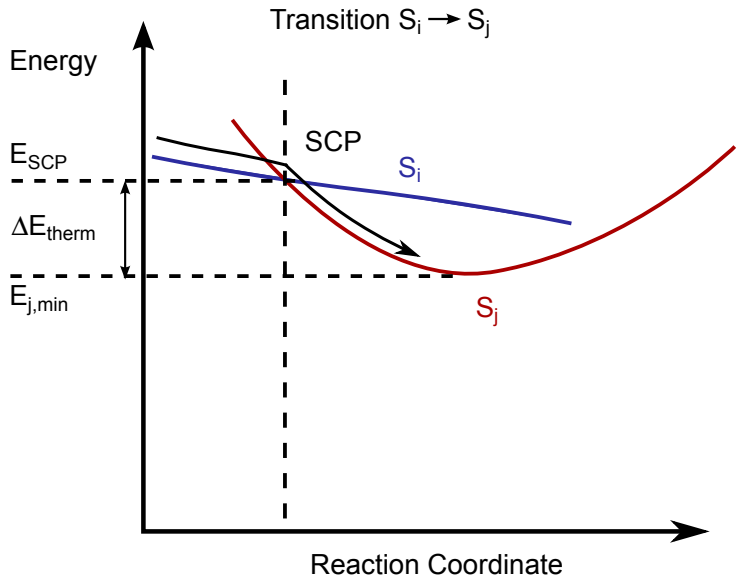

Figure 3.12.: Electronic transition between the states S_i and S_j and subsequent thermal relaxation to the minimum of the S_j potential energy surface. Thermal relaxation/ vibrational cooling dissipates the thermal energy ΔE_{therm} to the solvent.

The absorbance changes of thermal relaxation (= vibrational cooling) overlay those caused by the electronic transition and may distort the corresponding DADS. This effect depends on the thermal energy and the timescale of thermal relaxation compared to those of the electronic transition. Two extreme cases deserve attention:

1. Thermal relaxation is much faster than the electronic transition. Then the signals of the electronic transition will dominate the signal.

2. Thermal relaxation is much slower than the electronic transition. Then the absorbance changes will be dominated by the signals of thermal relaxation.

Thermal relaxation occurs on a timescale of a few picoseconds [Mid09]. Therefore, the DADS of long-living excited states with lifetimes of 100 ps or much more will not be affected significantly by the signals of thermal relaxation/vibrational cooling. However, the initially excited $^1\pi\pi^*$ state decays to the electronic ground state within less than 1 ps [PPK00], much faster than thermal relaxation/vibrational cooling. Therefore the absorbance changes in the first few picoseconds will be dominated by the signals of vibrational cooling.

3.4.3. Typical Signatures

The temporal resolution of the measurements is given by the cross-correlation between the excitation and the probe pulses. However, the absorbance changes are dominated by large signals that can obscure excited state kinetics in the first few picoseconds. Some of these effects are caused by two-photon effects in the window materials and in the sample (like two-photon ionisation of water or DNA bases [Kub09, Tsu02, Tan01]), some are due to the absorption of the hot ground state and vibrational cooling. These effects are described in the following.

Ultrafast Effects in the First Picosecond

The window materials used in the flow cell are transparent in both the MIR and the UV range. However, short and intense excitation pulses can undergo two-photon absorption (TPA) in the window materials (BaF_2 and CaF_2) [Tsu02, Tan01]. TPA subsequently leads to transient broadband absorption in the MIR range that decays on the timescale of 1 ps in BaF_2 and of 100 ps in CaF_2 [Kub09]. Measurements on the picosecond timescale therefore have to be performed using BaF_2 as window material. Then the additional MIR absorption after TPA occurs only in the first picosecond after the excitation. This effect does not disturb the measurements of long-living excited states that are discussed in this thesis. Another ultrafast nonlinear effect deserves some attention: Two-step ionisation of DNA bases yields solvated electrons and base cations [Nik90]. The precursors of the fully solvated electron have a broadband absorption in the MIR range that is observed by the TRIR measurements and overlays the interesting data. However, the fully solvated electron does not absorb in the MIR range, so these signals occur only before the electron is fully solvated, i.e. less than 1 ps after excitation [LRL00, LR01]. After that, the solvated electron only absorbs in the visible and NIR spectral range, but not in the MIR range. However, the generated cations cause a change in absorbance

over the entire delay time window from 1 ps to 3 ns that can easily be mistaken for a long-living excited state. These long-lasting effects are highly relevant for this thesis, they are discussed in subsection 3.4.5. As far as the ultrafast kinetics are concerned, the nonlinear effects in the window material and in the solvent only affect the measurements in the first picosecond after excitation, effectively reducing the temporal resolution to about 1 ps. Elongating the excitation pulse duration to 1 ps to reduce these effects insofar does not reduce the effective temporal resolution.

Vibrational Cooling

After UV excitation almost all single bases return to the hot ground state within 1 ps via a conical intersection [PPK00]. The excitation energy is then distributed over the vibrational modes. Energy redistribution between the vibrational modes is faster than the energy dissipation to the solvent, so the occupation of vibrational modes follows a Boltzmann distribution with a temperature of circa 1200 K [EK91, ORH94]. The IR spectra at different temperatures differ significantly, because thermal excitation changes vibrational frequencies via anharmonic coupling.

Figure 3.13 shows simulated vibrational spectra of benzene at different temperatures [Mas92, HOZ97]. The absorption maximum of hot molecules decreases and shifts to lower wavenumbers, while the spectral width increases. The difference in absorbance $\Delta A(\Delta T)$ is plotted in Figure 3.13, panel (B). As the molecule dissipates energy to the solvent, its temperature decreases, which leads to non-exponential changes in the absorbance spectrum. In DNA, almost all excited molecules return to the ground state in less than 1 ps [PPK00, PPK01], therefore the obtained transient spectra are completely dominated by these signatures. Other excited state kinetics that take place in the first few picoseconds can be obscured by the much larger signals of vibrational cooling. Furthermore, a global fit of the data will be inaccurate in the time window when vibrational cooling takes place because of its non-exponential nature, see subsection 3.4.2. In conclusion, the time window in which electronic transitions can be observed may not be defined by the cross-correlation between pump and probe, but by the duration of experimental artefacts as described in the previous paragraph and especially by the signals of vibrational cooling.

Heating of the Solvent

The hot bases in the ground state will dissipate their excessive vibrational energy to the surrounding solvent, thereby heating it. Within less than 10 ps, this process is complete and the IR data show the absorbance change caused by an increase of the solvent temperature. Figure 3.14, panel (A) shows the absorbance of D_2O at different temperatures. Increasing temperature leads ot a red-shift of the band and a slight decrease in amplitude.

The absorbance changes caused by temperature differences are depicted in panel (B) of Figure 3.14. The difference spectra have the same principle shape, an increased

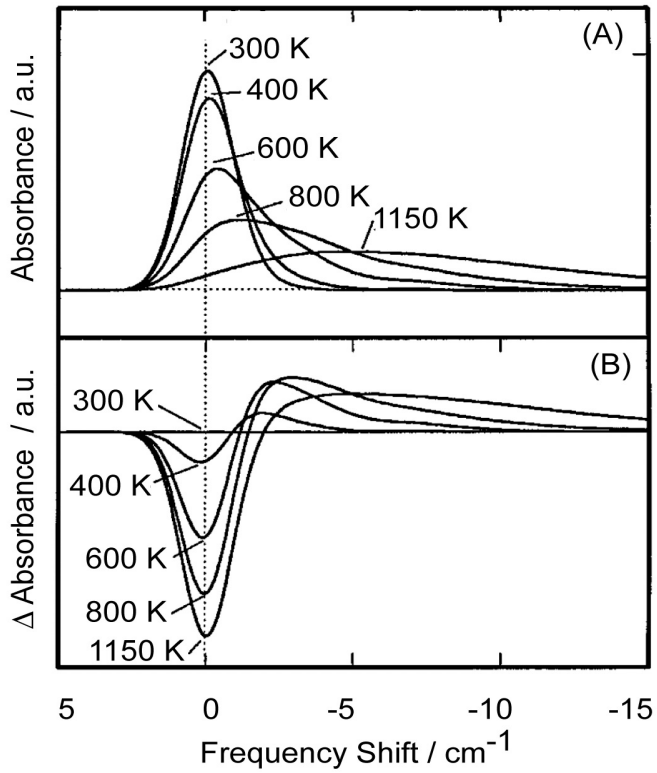

Figure 3.13.: Simulated spectra of the ground state of a vibration of benzene at different temperatures (A). (B) Absorbance difference between the hot and the cold ground state are observed in time-resolved measurements. The temporal evolution of the absorbance changes cannot be described by a multiexponential model function, the spectra ΔA ($\Delta T(t_D)$) are qualitatively different for different delay times t_D (and thereby different temperature differences ΔT). Figure taken from [HOZ97] and reprinted with permission (Copyright AIP Publishing LLC).

absorption between $1310\,\mathrm{cm}^{-1}$ and $1510\,\mathrm{cm}^{-1}$ and a decreased absorption above $1510\,\mathrm{cm}^{-1}$. Over a wide temperature range, the shapes of the difference spectra are constant and their amplitudes scale with the temperature difference [Sch08]. Therefore, it makes no difference if the sample is heated homogeneously or not, only the average temperature increase in the probed volume matters. This finding has an important implication for the temporal evolution of the TRIR spectra: The UV-excited bases predominantly return to the hot ground state within 1 ps. Then the excess energy is dissipated to the solvent by vibrational cooling. After 10 ps, the vibrational cooling is finished and the energy is deposited in the first solvation shells around the previously excited bases, increasing the temperatures of solvent molecules. From there, heat transport from the first solvation shell to the rest of the solvent takes place, but the average temperature of the sample stays constant. Therefore the temperature difference spectrum builds up in the first 10 ps and then

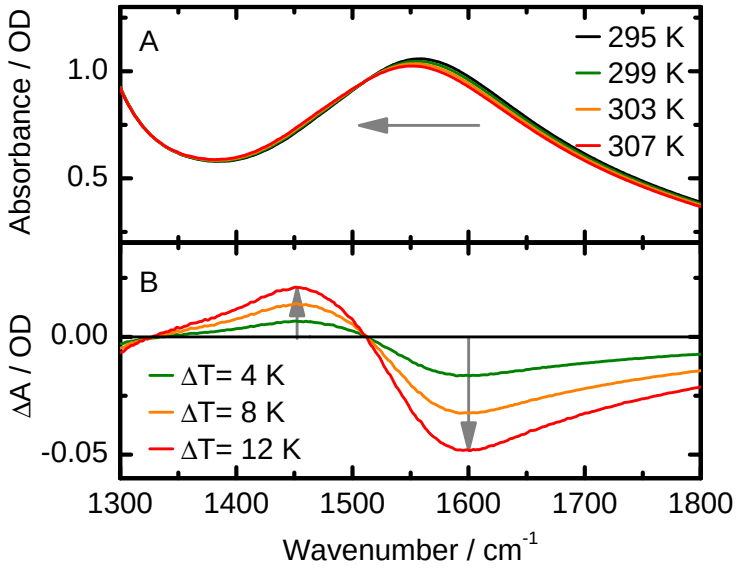

Figure 3.14.: (A) The absorbance of D_2O at different temperatures. As the temperature increases, the spectrum is shifted towards lower wavenumbers and decreased in amplitude. (B) The absorbance changes induced by heating of the solvent scales linearly with the temperature increase. Data taken from [Sch08].

stays constant at least until the maximum delay of 100 µs. To correct the TRIR data for the effects of solvent heating, the build-up of its signature needs to be modelled.

The model used in this thesis assumes that the heat transport from the base to the solvent is proportional to their temperature difference $\Delta T(t)$. Then $\Delta T(t)$ decays exponentially according to $\Delta T(t) = \Delta T_0 \cdot exp\left(-\frac{t}{\tau_{cool}}\right)$, where τ_{cool} is the time constant of vibrational cooling and ΔT_0 is the initial temperature difference between the hot base and the solvent. So the temperature of the solvent and thereby the signature of the heating of the solvent $A_{solv}(t)$ will build up according to $\Delta A_{solv}(t) = \Delta A_{solv,f} \cdot \left(1 - exp\left(\frac{-t}{\tau_{cool}}\right)\right)$, where the amplitude $\Delta A_{solv,f}$ is scaled to the TRIR data. Testing this model with time-resolved data confirms its applicability, if a time constant of circa 3 ps for τ_{cool} is used (see section A.1).

3.4.4. Measurement Artefacts: Rotational Effects

The effects discussed so far occur in all correctly performed TRIR measurements of DNA. However, some easily committed measurement errors can result in additional signals (artefacts) that can lead to misinterpretations. Of particular importance in the context of this thesis is the effect of the polarisations of pump and probe on

the measured signals. Because the excitation pulses are linearly polarised, they are predominantly absorbed by molecules whose dipole moments are parallel to their polarisation. Immediately after UV absorption, the sample is not isotropic any more, because the distribution of the excited molecules is not. This induced anisotropy translates into a polarisation dependence of the probe absorption by the excited bases, depending on the angles between the electronic and the vibrational dipole moments and the angle between the polarisations of the excitation and the probe pulses. As the excited molecules rotate randomly (*rotational diffusion*), the induced anisotropy decays exponentially with increasing delay time. Consequently, dynamical absorbance changes occur that are only caused by the reorientational motion of the molecules. These signals can easily be misinterpreted as stemming from excited state transitions. To avoid the signals of the reorientational motion, two possibilities exist:

1. Dichroic measurements with probe polarised perpendicular and parallel to pump. From both measurements, the isotropic absorbance change can be calculated according to:

$$\Delta A_{iso} = \frac{\Delta A_{par} + 2 \cdot \Delta A_{perp}}{3} \tag{3.7}$$

2. If the angle between pump and probe polarisations is the *magic angle* $= 54.7°$, the signal changes caused by reorientational motions vanish [MT86].

3.4.5. Two-Step Ionisation of DNA

If long excitation pulses (pulse duration in the nanosecond range) or cw irradiation are used, two-photon effects are negligible due to the low intensity. However, if short (sub-ps) and intense pulses are used, two processes can occur that depend quadratically on the intensity: two-photon absorption (TPA) and excited state absorption of another pump photon (two-step absorption, TSA). In the former case, two photons have to be absorbed at the same time to reach an excited state S_n, because the energy of one photon is not sufficient. Formally, one photon excites the system to a virtual level that absorbs another photon to reach the excited state. Two-step excitation proceeds via a real, not a virtual excited state; if a state exists that can be populated upon absorption of a single photon, then the excited state can absorb another photon. If TSA is possible, it should be much more probable than TPA. In the context of this thesis, the interesting two-photon or two-step processes are ionisations of DNA bases that yield cations and solvated electrons. The coefficient of two-photon absorption is very small [Göp09, Kle62], so very high excitation intensities are necessary. Such intensities can be achieved by lasers [KG61], so TPA may be relevant in this context. TPA by the solvent (water) can lead to the generation of solvated electrons [NOR83].

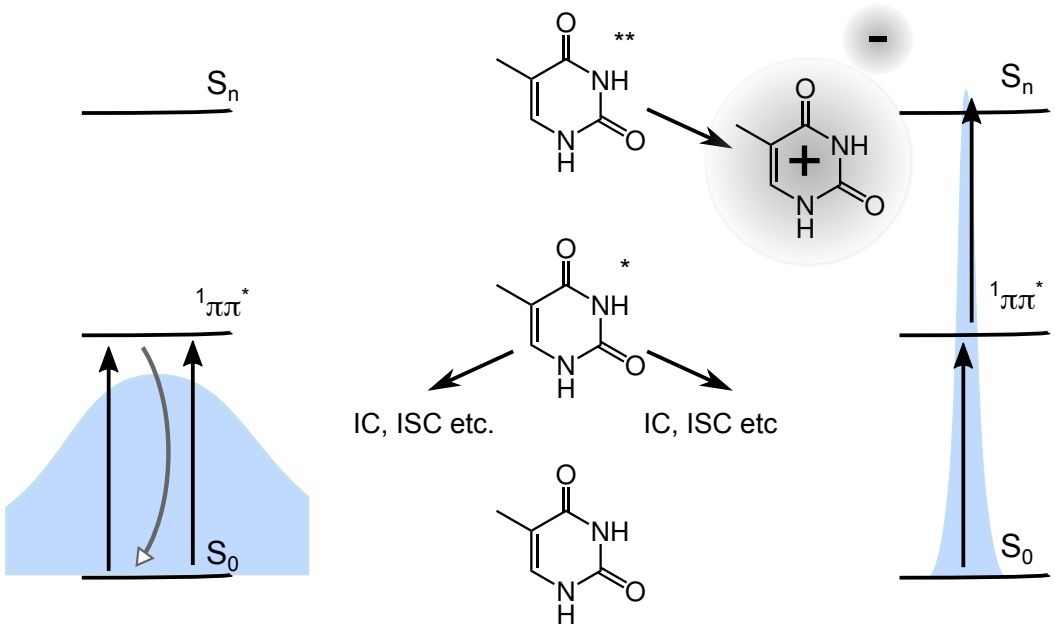

Figure 3.15.: Excitation of DNA bases with high-intensity pulses can result in excited state absorption, resulting in a cation and a solvated electron (right). If the pulse duration is much longer than the excited state lifetime, rapid excited state decay prevents excited state absorption (left).

The solvated electron has been studied extensively [NOR83, ALL98, RNL96, LRL00] by time-resolved spectroscopy (for a detailed discussion of the solvated electron, see [Abe11]). According to Laenen et al., after two-photon ionisation of D_2O, the solvated electron is formed via a few intermediate states until the electron is fully solvated [LRL00]. These short-living intermediates show NIR and MIR absorption within their respective lifetimes of a few 100 fs. Within less than 1 ps, the electron is fully solvated; in this state, it displays the well known broad absorbance that peaks at 720 nm [HMS71, JF77, JF79], but its MIR absorption is negligible. Time-resolved measurements of pure D_2O in the visible spectral range (data not shown) confirmed that under the experimental conditions, small amounts of solvated electrons are generated by two-photon ionisation of the solvent. Repeating these measurements with DNA in D_2O showed that the amount of solvated electrons was much higher, even though 90 % of the UV photons were absorbed by DNA.

The additional solvated electrons (in fact the vast majority) result from two-step photo-ionisation of DNA (see also [NL83]). This process can take place in the DNA samples within the excited state lifetime (< 1 ps). Because of the very short excited state lifetimes of DNA, two-step excitation can occur if short excitation pulses are used (shorter than a few picoseconds) (see Figure 3.15). Two-step ionisation of all

DNA bases was reported [Reu00], generating cations and solvated electrons. Their signals will overlie and potentially obscure the data. The generated DNA cations could easily be confused with long-living excited states.

To minimise these nonlinear effects in the presented studies, the pulse duration is increased from 200 fs to 1 ps to 2 ps by having the pulse travel through 20 cm of fused silica. This introduces a group velocity dispersion and thereby elongates the pulse duration. The lifetime of the solvated electron and thereby of the cations is much longer than the maximum delay of 3.5 ns [Abe11]. Therefore, its signature will overlay the residual absorbance change at the maximum delay. This must be taken into account when the time-resolved data are interpreted.

4. Steady State DNA Spectroscopy

This thesis deals with the excited state physics of thymidine mono- and oligomers as revealed by time-resolved infrared spectroscopy (TRIR). The samples are excited in the UVC spectral range, where the bases have very strong absorbance bands due to $^1\pi\pi^*$ transitions. The UV and IR spectra of thymine are presented in this chapter. The vibrational bands are identified and the influence of interactions between neighbouring thymine bases is briefly discussed. The IR signature of the main photoproduct between neighbouring thymine bases, the CPD lesion, is presented. In chapter 6 the charge separated states in $(dT)_{18}$ are discussed. They are identified by comparing the excited state physics of $(dT)_{18}$ and the dimer TpA, which was reported to undergo charge separation yielding $T^{\bullet-}pA^{\bullet+}$ [Doo13]. This makes a short discussion of adenine necessary.

4.1. TMP and $(dT)_{18}$

4.1.1. UV Spectra

The UV absorption of TMP and $(dT)_{18}$ is depicted in Figure 4.1. The left axis shows the absorbance at experimental conditions (concentration is 10 mM per base, sample thickness is 100 µm), the right axis shows the extinction coefficient per base in units of $1 \cdot 10^3\,\mathrm{M^{-1}cm^{-1}}$. Both samples show quite similar absorbance spectra from 230 nm to 300 nm, caused by the aforementioned $^1\pi\pi^*$ transitions. $^1n\pi^*$ states that might absorb in the vicinity [Gus06b, Cre04] do not alter the absorbance spectra significantly, because their oscillator strength is very low. The entire UV absorption can be attributed to the $^1\pi\pi^*$ state. Hence the excited state physics after UV excitation always starts from the $^1\pi\pi^*$ state. The shapes and amplitudes of the absorbance spectra of TMP and $(dT)_{18}$ differ somewhat, as interactions between neighbouring bases modify the absorbance spectrum of $(dT)_{18}$. A slight change in the spectra is observed by comparing the wavelengths of the absorption maxima (267 nm in TMP compared to 265 nm in $(dT)_{18}$). A more pronounced consequence of stacking interactions is the lowering of the absorbance of the thymine bases in the oligomer. This effect, called *hypochromicity*, occurs between stacked bases because of dipole-dipole interactions [Tin60] between their transition dipole moments. The hypochromicity of $(dT)_{18}$ relative to TMP is 10 %, much lower than that of $(dA)_{18}$ relative AMP (see section 4.2. The low hypochromicity reflects the weak interactions between the bases that result from a low amount of stacked thymine bases [MVH99,

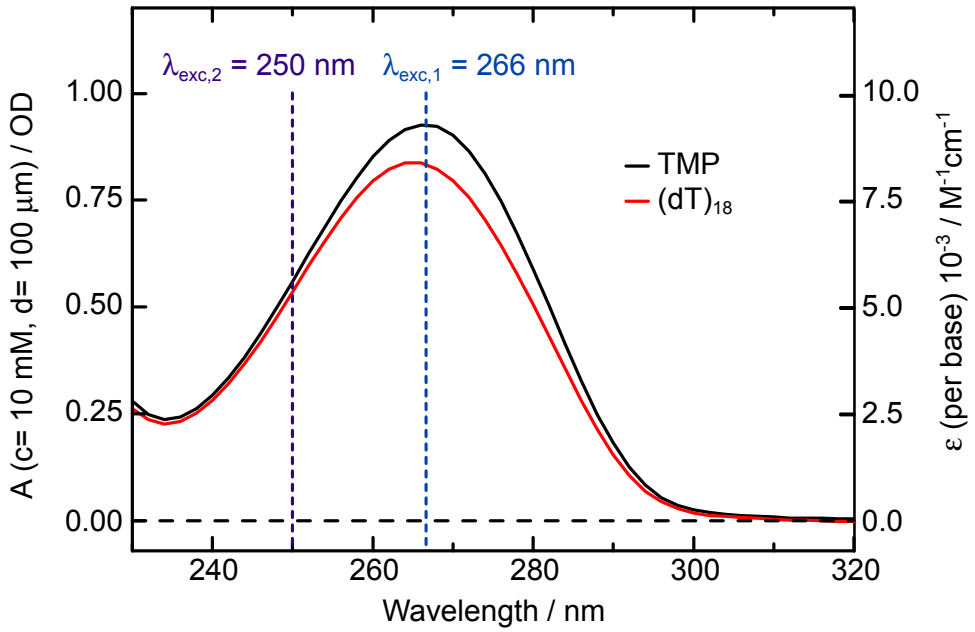

Figure 4.1.: Absorbance of TMP and $(dT)_{18}$ in a buffered solution of D_2O (c = 10 mM per base, d = 100 µm). The right axis depicts the molar extinction coefficients ε (per base). The dashed vertical lines mark the excitation wavelengths. Data taken from [Sch08] and adapted.

BH04, JW07a, MEK01]. A much more subtle change in the absorbance spectrum takes place in the UVA region. Stacked bases give rise to a small absorption in the UVA region [SG81, Mou10, Ban11], which may lead to UVA-induced photolesions [Roc03, Kap06]. The absorbance change in the UVA region is at least three orders of magnitude lower than the $^1\pi\pi^*$ absorbance. It is not visible in Figure 4.1 and is certainly not excited in a significant amount at wavelengths of 266 nm or 250 nm.

4.1.2. IR Spectra

The vibrational spectra of the thymidine monomer TMP and the oligomer $(dT)_{18}$ are depicted in Figure 4.2. They are much more structured and detailed than the UV spectra. Hence the vibrational spectra of excited states are much more characteristic than their UV spectra.

Table 4.1 shows the assignment of the vibrational modes of TMP and $(dT)_{18}$ [BSG03]. Starting from high wavenumbers, the first band of TMP/$(dT)_{18}$ at 1681 cm^{-1}/1693 cm^{-1} is due to a stretch vibration of the C2=O double bond. The C2=O vibration, the C4=O stretching vibration at 1661 cm^{-1}/1664 cm^{-1} and a ring vibration at 1630 cm^{-1}/1632 cm^{-1} dominate the spectrum. Below 1500 cm^{-1} there are four weaker bands. The assignment of at least three of these bands is controversial

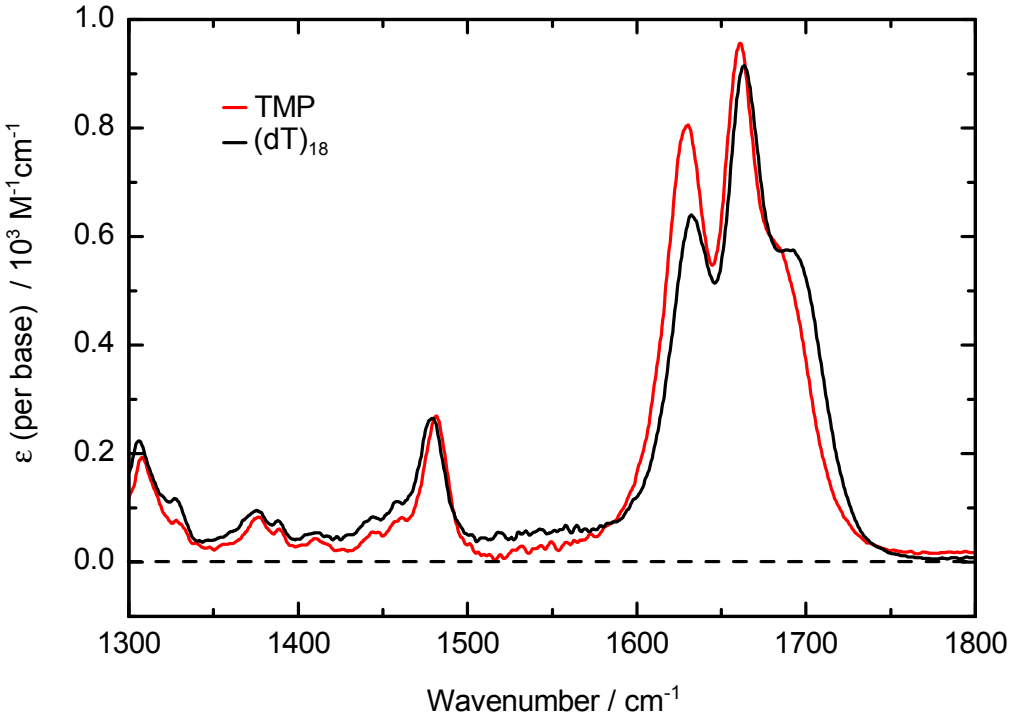

Figure 4.2.: Absorbance of TMP and $(dT)_{18}$ in a buffered solution of D_2O (c=10 mM per base, d=100 µm). Significant spectral differences are found between 1600 cm^{-1} and 1700 cm^{-1}. Data taken from [Sch08].

in the literature [Aam97, LGT87]. They are therefore marked with an asterisk. Importantly, the bands below 1330 cm^{-1} are partly due to sugar vibrations; hence they are sensitive to changes in the sugar conformation. The sensitivity to conformational changes makes these bands interesting for the identification of photoproducts like

TMP/cm^{-1}	$(dT)_{18}$/cm^{-1}	Band Assignment
1681	1693	C2=O
1661	1664	C4=O
1630	1632	In-Plane Ring Vibration,C5=C6
1481	1479	C4–C5, N1–C2, N3–C4*
1376	1376	CH_3 sym.
1327	1327	dT in C2'-endo/anti, C4'C5', C4'O1'*
1308	1306	CN3H bend.*

Table 4.1.: Assignment of the vibrational bands of TMP and $(dT)_{18}$ in a buffered solution of D_2O according to [BSG03].

the CPD lesion. In Table 4.1 the sugar atoms are written with an apostrophe. Comparing the vibrational spectra of TMP and $(dT)_{18}$ reveals significant differences in the spectral region from 1600 cm^{-1} to 1700 cm^{-1}. With respect to the monomer, the ring vibration mode at 1632 cm^{-1} is slightly blue-shifted and significantly decreased in absorption in the oligomer. The carbonyl vibration at 1681 cm^{-1} is blue-shifted about 12 cm^{-1}. The double bonds apparently are strongly influenced by the base stacking interactions.

4.1.3. CPD Signature

UV irradiation of $(dT)_{18}$ results in the formation of CPD lesions with a quantum yield of 5 % [Ban12]. Other photoproducts are formed in negligible amounts [Sch08]. Figure 4.3 shows the absorbance spectrum of $(dT)_{18}$ before (black) and after (red) UV illumination. The sample was irradiated for 1500 s with the fourth harmonic of a Nd:YAG laser (266 nm). The data are adapted from [Sch08].

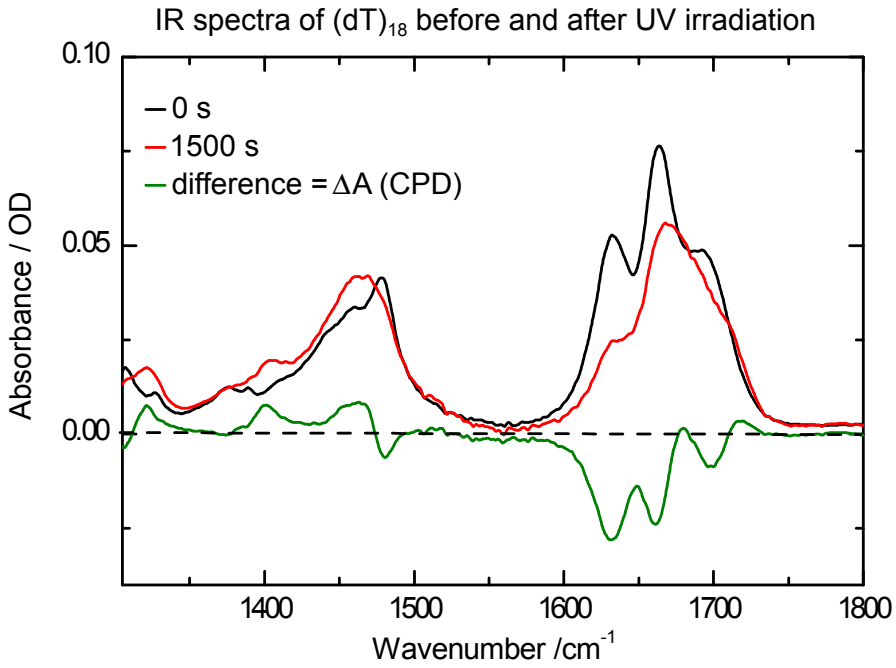

Figure 4.3.: IR spectra of $(dT)_{18}$ before (black) and after UV irradiation (red). After UV irradiation, the spectrum changes because of CPD formation. The difference between both spectra is ΔA(CPD) (green).

After illumination the absorbance decreases in the region of the C=O and C=C stretching vibrations (1620 cm^{-1} to 1720 cm^{-1}). The strongest absorbance change is observed at the position of the C5=C6 vibration at 1630 cm^{-1}, that disappears upon dimerisation. In the region from 1300 cm^{-1} to 1500 cm^{-1} three new bands appear at

1320 cm^{-1}, 1402 cm^{-1} and 1465 cm^{-1}. The vibrations in this region are influenced by the sugar backbone and therefore sensitive to conformational changes that result from CPD formation. A comparison of these bands to artificial model compounds has shown that these bands identify the cis-syn CPD unequivocally [Sch07, Sch08]. For this reason, this spectral region is sometimes referred to as 'fingerprint region'.

4.2. AMP and $(dA)_{18}$

4.2.1. UV Spectra

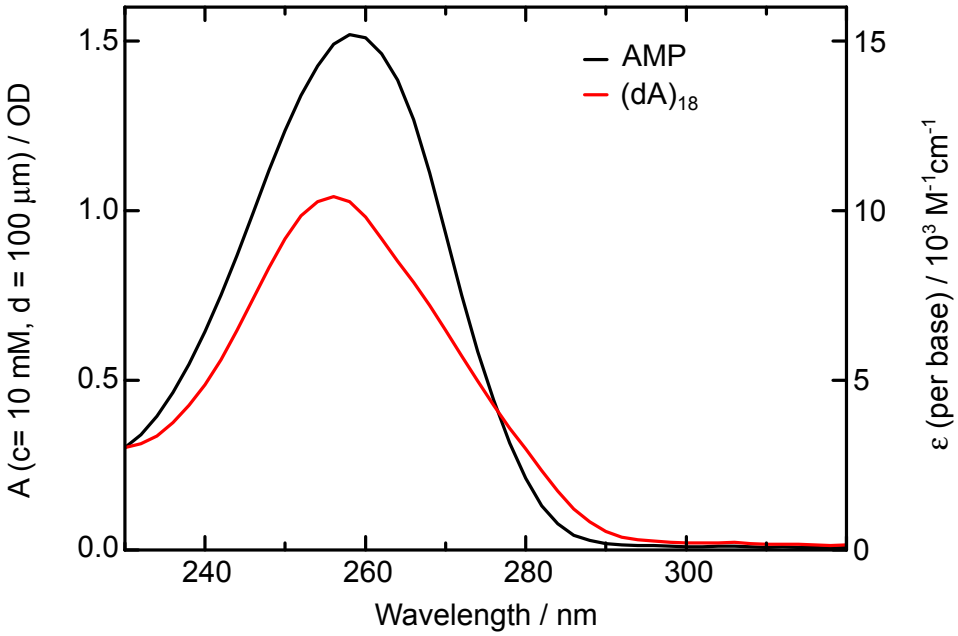

Figure 4.4.: Molar extinction coefficients ε(per base) of AMP and $(dA)_{18}$ in the UV range. $(dA)_{18}$ shows a drastic hypochromic effect and a red-shifted absorbance above 280 nm. The data are taken from [Sch08] and adapted.

Figure 4.4 shows the absorbance spectra of AMP and $(dA)_{18}$ in the UV range. Due to the high stacking probability (65 % stacked bases are reported in [DT79]), the interactions between neighbouring bases alter the spectrum significantly. Comparing $(dA)_{18}$ to the monomer AMP reveals the following changes:

1. A large hypochromic effect of 30 % in $(dA)_{18}$ around 260 nm.

2. An increased absorption of $(dA)_{18}$ at wavelengths above 280 nm.

3. A small blue-shift of the absorbance maximum from 259 nm (AMP) to 256 nm ($(dA)_{18}$).

These properties can be well understood in terms of dipole-dipole interactions. A theoretical study by Santoro et al. reproduced all three properties [SBI07]. Hypochromicity and band shifting occurs also in the mid-infrared (MIR) range, modifying the positions and the amplitudes of various absorbance bands.

4.2.2. IR Spectra

Figure 4.5 shows the IR absorbance of AMP and the oligomer $(dA)_{18}$. The spectral region of interest in the context of this thesis is from 1500 cm^{-1} to 1800 cm^{-1} (see chapter 6).

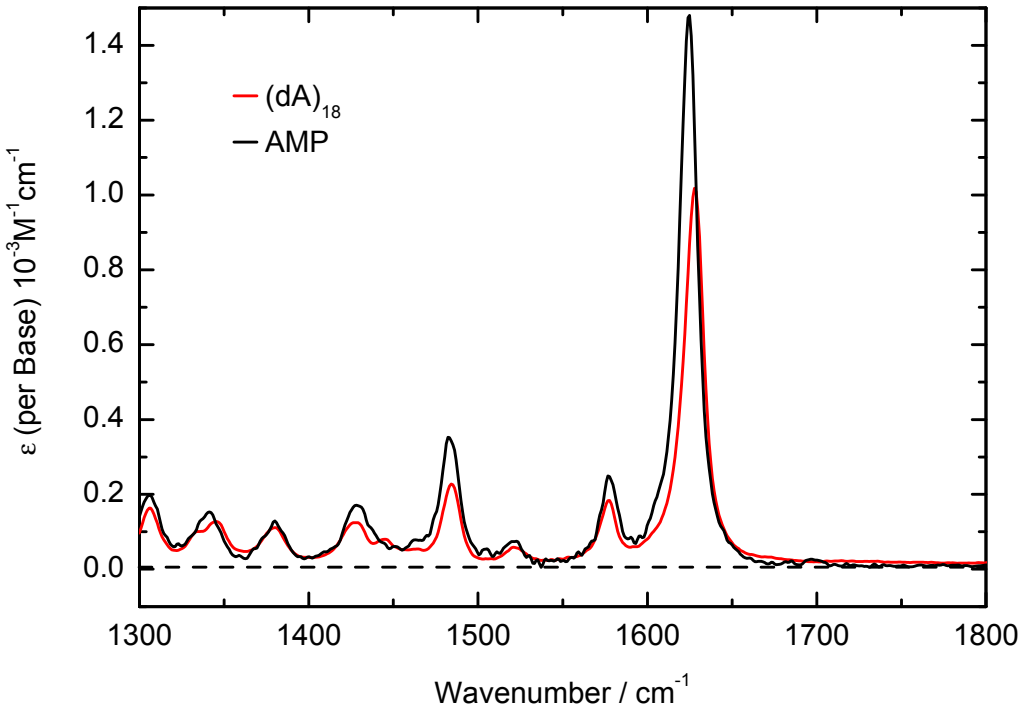

Figure 4.5.: Molar extinction coefficients ε(per base) of AMP and $(dA)_{18}$ in the MIR range. The spectra are dominated by absorption bands at 1624 cm^{-1} (AMP) and 1628 cm^{-1} ($(dA)_{18}$). Comparing both bands shows a blue-shift by 4 cm^{-1} and a drastic hypochromic effect of around 30 % for $(dA)_{18}$ compared to AMP.

The band assignment in Table 4.2 is therefore only given for the bands around 1624 cm^{-1} and 1577 cm^{-1}. For a more detailed discussion, see for example [BSG03, LGT87]. The IR spectrum of adenine is dominated by the maximum at 1624 cm^{-1},

AMP/cm^{-1}	$(dA)_{18}/cm^{-1}$	Band Assignment
1624	1628	C=N; C=C Ring Vib.
1577	1577	C4=C5, C5–C6 Ring Vib.

Table 4.2.: Assignment of the vibrational bands of AMP and $(dA)_{18}$ in a buffered solution of D_2O [BSG03] in the region from 1500 cm^{-1} to 1800 cm^{-1}. Only the bands in this spectral region are relevant in the context of this thesis.

which has a molar extinction coefficient of around 1500 $M^{-1}cm^{-1}$. The corresponding vibrations are C=N and C=C stretching vibrations [BSG03]. A much smaller vibrational band is located at 1577 cm^{-1}. It results from C4=C5 and C5–C6 vibrations. Both bands decrease in amplitude by circa 30 % in the oligomer $(dA)_{18}$. While the position of the minor absorbance band at 1577 cm^{-1} remains unchanged, the major band at 1624 cm^{-1} shifts to 1628 cm^{-1}.

5. The Lowest Triplet State of Thymine

The formation of CPD lesions between thymine bases has been investigated for decades (see for example [EL67]). Still, there is a substantial debate about the multiplicity of the CPD precursor. Two mechanisms have to be considered (see Figure 5.1):

1. Formation out of an excited $^1\pi\pi^*$ state.
2. Formation out of the lowest triplet state $^3\pi\pi^*$ (possibly via a reaction intermediate RI).

The Singlet Mechanism of CPD Formation

CPD formation out of the excited singlet state ($^1\pi\pi^*$) in frozen matrices was suggested in the late 1960s [EL67, LE68, FJ70]. However, it was not clear whether or not the results in frozen matrices, where the conformation of the bases is well-defined, could be transferred to CPD formation in aqueous solution, where the bases are flexible to arrange relative to each other. The lifetime of the $^1\pi\pi^*$ state is below 1 ps [PPK00], so excited bases in an arbitrary arrangement cannot reach a reactive conformation before they are deactivated to the ground state. Only the initially stacked bases could possibly form CPD lesions out of the $^1\pi\pi^*$ state. It was therefore questionable, whether significant amounts of CPD lesions are formed in this way. This question was answered in 2007, when the ultrafast CPD formation out of the $^1\pi\pi^*$ state was observed by TRIR spectroscopy [Sch07]. A subsequent study found that CPD lesions are predominantly formed by this mechanism [Sch09].

The Triplet Mechanism of CPD Formation

It has been known for decades that triplet sensitising of thymine leads to CPD formation [LY67, Cuq11, Epe11]. Since only the $^3\pi\pi^*$ state of thymine is populated by sensitising, it is certainly a CPD precursor. However, the aforementioned studies showed that after UV excitation of the bases the triplet mechanism only contributes in a minor way to CPD formation [Sch07, Sch09]. This is to a large degree due to the inefficient population of the $^3\pi\pi^*$ state out of the excited $^1\pi\pi^*$ state (the intersystem crossing quantum yield is only around 1 % to 2 % [Ban12]) and does by itself not exclude an efficient CPD formation out of the $^3\pi\pi^*$ state. The latter point is important for two reasons: 1. The $^3\pi\pi^*$ energy of thymine is the lowest of all DNA bases [GWR96, Cad92], so triplet-triplet energy transfer from other bases to thymine can lead to the localisation of triplet states on thymine bases, making thymine a

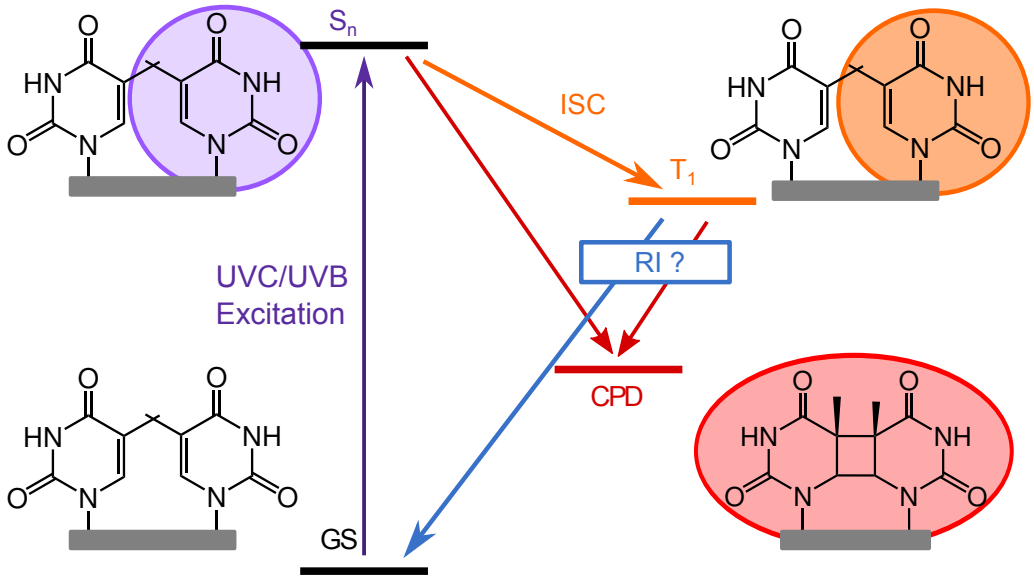

Figure 5.1.: CPD formation of the dinucleotide TpT after UV excitation of the $^1\pi\pi^*$ state. Stacked thymine dimers can form a CPD lesion directly out of the $^1\pi\pi^*$ state [Sch07]. Unstacked bases can form a CPD lesion out of the long-living triplet state. The triplet state is populated with a low quantum yield of circa 1 % to 2 % and subsequently either forms a CPD lesion or returns to the ground state, possibly via a reaction intermediate RI.

possible hotspot for mutations [Cuq11, Lam67]. 2. The low intersystem crossing (ISC) quantum yield Φ_{ISC} does not prevent efficient triplet population via sensitisers. Moreover, triplet sensitising of thymine is possible via UVA radiation [LY67]. The relative intensity of the solar radiation in the UVA range is much higher than in the UVB and UVC ranges, where DNA absorbs (see section 2.2).
For these reasons, triplet sensitisation of thymine by UVA radiation may be of major biological importance.

Despite decades of research, the mechanism of CPD formation out of the $^3\pi\pi^*$ state as well as its quantum yield are not known yet. CPD formation could occur directly out of the $^3\pi\pi^*$ state or via a transient intermediate state (reaction intermediate, RI in Figure 5.1). There has been considerable speculation about this question in the literature [WB68, WB70, ZE06], but since intermediates would be transient, time-resolved measurements are needed to determine which intermediates exist (if any) and what the exact mechanisms are.

The first time-resolved measurements of the $^3\pi\pi^*$ state of thymine were performed by laser flash photolysis [WJ72, SB75]. A more refined study [MM05] of TMP and $(dT)_{20}$ in water that used the same technique (temporal resolution: 200 ns) observed the $^3\pi\pi^*$ state only in TMP, not in $(dT)_{20}$. Two possible explanations were given:

1. Decay of the triplet state in $(dT)_{18}$ via CPD formation occurs much faster than triplet decay in TMP to the ground state.

2. Interactions of neighbouring bases reduce the triplet quantum yield by at least one order of magnitude, so it is below the experimental sensitivity.

In the first case, by comparing $(dT)_{20}$ to TMP, an additional decay corresponding to the transition $^3\pi\pi^* \rightarrow$ CPD should be expected; in the second case, no significant triplet signal should be observed at all. Such an additional decay component of $(dT)_{20}$ was reported by Kwok et al. [KMP08]. They discussed CPD formation out of the triplet state on a 100 ps timescale, but gave no direct evidence for this interpretation. In the light of other possibilities (like excimers/charge transfer states), it must be considered to be highly speculative. Consequently, the role of the triplet state in CPD formation is still unclear.

In this chapter, TRIR spectroscopy of the $^3\pi\pi^*$ state of thymine in monomers and oligonucleotides is reported. The triplet state of TMP is identified and the mechanisms of triplet quenching are discussed. The obtained data are then compared to the excited state kinetics of $(dT)_{18}$ on the same timescale. Finally, a model is presented that describes the triplet decay as well as its role in CPD formation.

5.1. Time-Resolved Spectroscopy of TMP

5.1.1. Characterisation of the $^3\pi\pi^*$ State

TRIR spectroscopy of the triplet state of TMP in water is challenging because of the low intersystem crossing (ISC) quantum yield $\Phi_{ISC} = 1.4\,\%$ according to [MM05, Ban12]. The ISC quantum yield of thymine is strongly solvent dependent [SB75, SBB79, WB70] and is much higher than 1.4 % in many other solvents. Hare et al. investigated thymine in acetonitrile (ACN) [Har08], where Φ_{ISC} is circa an order of magnitude higher than in water [WB70, SB75, SBB79]. They used TRIR spectroscopy in the delay range from 300 fs to 3 µs to monitor a long-living excited state that is formed within 10 ps and decays on the timescale of microseconds. Since it is quenched by oxygen, it was identified as a triplet state [Har08].

Table 5.1 shows the spectral positions of the C=O vibrations of thymine and deuterated thymine (i.e. the H-atoms at the N1 and N3 atom are replaced by D) in the ground state and in the observed triplet state. The C2=O7 vibration is somewhat red-shifted, so its absorption is obscured by the ground state bleach. The C4=O8 vibration is very strongly red-shifted by circa 80 cm^{-1}, so this band is spectrally isolated from the ground state bleach and is observed directly. To identify this state as the lowest triplet state ($^3\pi\pi^*$), the observed spectra were compared to theoretical calculations [Har08].

Molecule	Ground State/cm^{-1}		Lowest Triplet State/cm^{-1}	
	C2=O7	C4=O8	C2=O7	C4=O8
Thymine	1723	1683	1705	1603
Thymine-d_2	1715	1672	obscured	1590

Table 5.1.: Assignment of the C2=O7 and C4=O8 stretching vibrations of thymine and deuterated thymine (thymine-d_2) in the ground state and the lowest triplet state in deuterated acetonitrile [Har08]. The C2=O7 band of deuterated thymine is not shown because it is obscured by the ground state bleach.

Density functional theory calculations of thymine and thymidine (see Table 5.2) show a somewhat red-shifted C2=O7 band (by about $20\,cm^{-1}$ to $30\,cm^{-1}$) and a very strongly red-shifted C4=O8 band in the $^3\pi\pi^*$ state (compared to the ground state). This agrees very well with the obtained data, so the authors could identify the long-living state they observed as a $^3\pi\pi^*$ state [Har08].

Molecule	Basis Set	Ground State/cm^{-1}		Lowest Triplet State/cm^{-1}	
		C2=O7	C4=O8	C2=O7	C4=O8
Thymine	aug-cc-pVDZ	1786	1741	1759	1611
Thymine-d_2	aug-cc-pVDZ	1771	1730	1740	1591
Thymine	6-311++G**	1798	1751	1771	1619
Thymine-d_2	6-311++G**	1784	1751	1754	1604

Table 5.2.: Density functional theory calculations of the ground state and the $^3\pi\pi^*$ state of thymine and deuterated thymine by Hare et al. [Har08]. In the $^3\pi\pi^*$ state the C2=O7 band is weakly red-shifted, while the C4=O8 band is very strongly red-shifted. The calculated data agree well with the experimental data.

By this study, an important step towards monitoring the triplet decay and its involvement in the formation of photolesions was made. However, the excited state kinetics is profoundly modified by interactions with the solvent, as witnessed by the different ISC quantum yields in water and acetonitrile. The involvement of the triplet state in the formation of photolesions may also be influenced by the solvent. It is therefore important to take the next step and observe the triplet kinetics in the biologically relevant solvent, which is obviously water. The observations of the spectral characteristics of the $^3\pi\pi^*$ state in ACN serve as an important guideline for these measurements.

5.1.2. Experimental Conditions

The TRIR setup described in the introduction is capable of measuring absorbance changes in the range of 0.01 mOD, making measurements of excited states with quantum yields below 1 % possible. However, to identify excited states and monitor their kinetics, the temporal and spectral characteristics need to be obtained with high precision, i.e. a high signal-to-noise ratio, so a higher quantum yield is desirable.

At an excitation wavelength of 266 nm (fourth harmonic of the Nd:YVO_4 laser) the $^3\pi\pi^*$ state of TMP is clearly observable, as is the timescale of triplet decay. However, in the oligomer $(dT)_{18}$ the decay of the triplet state can in part result in CPD formation, in part in ground state recovery, both possibly via an intermediate state. Observing an intermediate state and determining the quantum yields of CPD formation and ground state recovery requires a very high experimental accuracy. Measurements with an excitation wavelength of 266 nm, where the triplet formation quantum yield is around 1 % [Ban12], proved insufficient to meet these challenging demands (these measurements are not shown to avoid redundancies). The triplet quantum yield needs to be increased without changing the solvent. An interesting possibility to achieve this with unmodified thymine in water was discovered recently by Banyasz et al.: They demonstrated by laser flash photolysis that the ISC quantum yield of TMP increases with decreasing excitation wavelength [Ban12]. At an excitation wavelength of 250 nm, the triplet quantum yield is between 3 % and 4 %.

The tunable ns-laser NT 242 allows to utilize this property by providing excitation pulses with a wavelength of 250 nm. All measurements described in this chapter were performed in a buffered solution of D_2O (see subsection 3.1.4). The excitation energy was 2 µJ, with a beam diameter of 180 µm to 220 µm. Unless stated otherwise, the concentration was always 10 mM per base.

5.1.3. The Triplet State of TMP

Figure 5.2 shows the results of a TRIR measurement of TMP on the timescale of nanoseconds to microseconds. The data have been corrected for the heating of the solvent. Transient absorbance changes are observed in the first microsecond after excitation (see panel (a)).

No absorbance changes persist at longer delay times, indicating that all nucleotides have returned to their ground states and no photoproducts have been formed. The absorbance changes in the first microsecond after excitation are caused by two processes that occur on different timescales. Immediately after UV excitation a relatively short-living state exists that decays on the timescale of 1 ns (this state is discussed in chapter 7). After this initial process the absorbance change is characterised by an absorption at 1598 cm^{-1} and three ground state bleach bands at 1628 cm^{-1}, 1660 cm^{-1} and 1700 cm^{-1}. In the region from 1300 cm^{-1} to 1500 cm^{-1} broad absorbance bands exist. Panel (b) shows the transient spectra at different

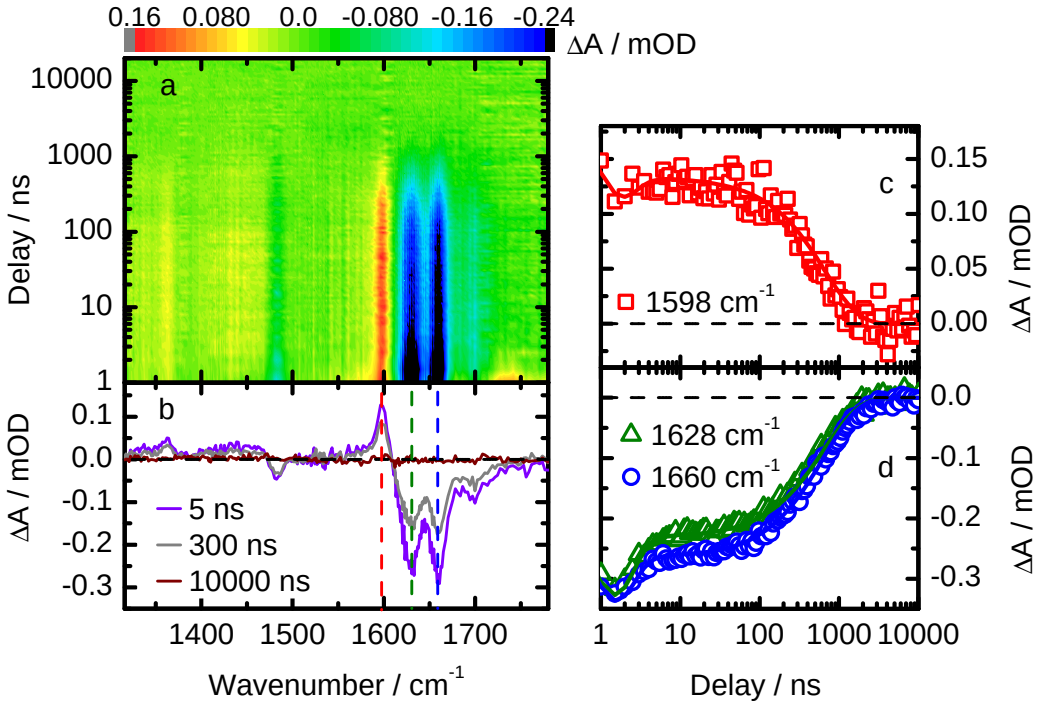

Figure 5.2.: TMP in a buffered D_2O solution on the ns timescale. After excitation, two excited states exist: A fast (circa 1 ns) decay and a long-living state that decays on a 650 ns timescale (panels (a) and (b)). Panels (c) and (d) show the decay of the indicated bands (symbols) and the multiexponential fit (lines) of the data.

delay times (note that the signature of solvent heating was subtracted). At different delay times (e.g. 5 ns and 300 ns) the transient spectra differ only by their respective amplitudes, indicating that only one excited state is present after a few nanoseconds, that decays to the ground state without forming intermediates or photoproducts. Monitoring the transient absorbance changes at different wavenumbers confirms this finding. Panels (c) and (d) show the transient absorbance changes at 1598 cm^{-1} (c), 1628 cm^{-1} (d) and 1660 cm^{-1} (d).

In both panels the symbols represent the data, while the straight lines are from a multiexponential fit. The data show an initial absorbance change in the first few nanoseconds and after that a uniform decay of the signals on a sub-µs timescale. The fit reproduces the data very accurately with 3 time constants. Panels (a)–(c) of Figure 5.3 show the decay associated difference spectra (DADS). As already stated, the short-living component (a) is not of interest in this context. The long-living component (red in panel (c)) is almost identical to the signal of solvent heating (black) (note that the data presented so far have been corrected for this component, so it is not visible in Figure 5.2). In the spectral range from 1600 cm^{-1} to 1700 cm^{-1},

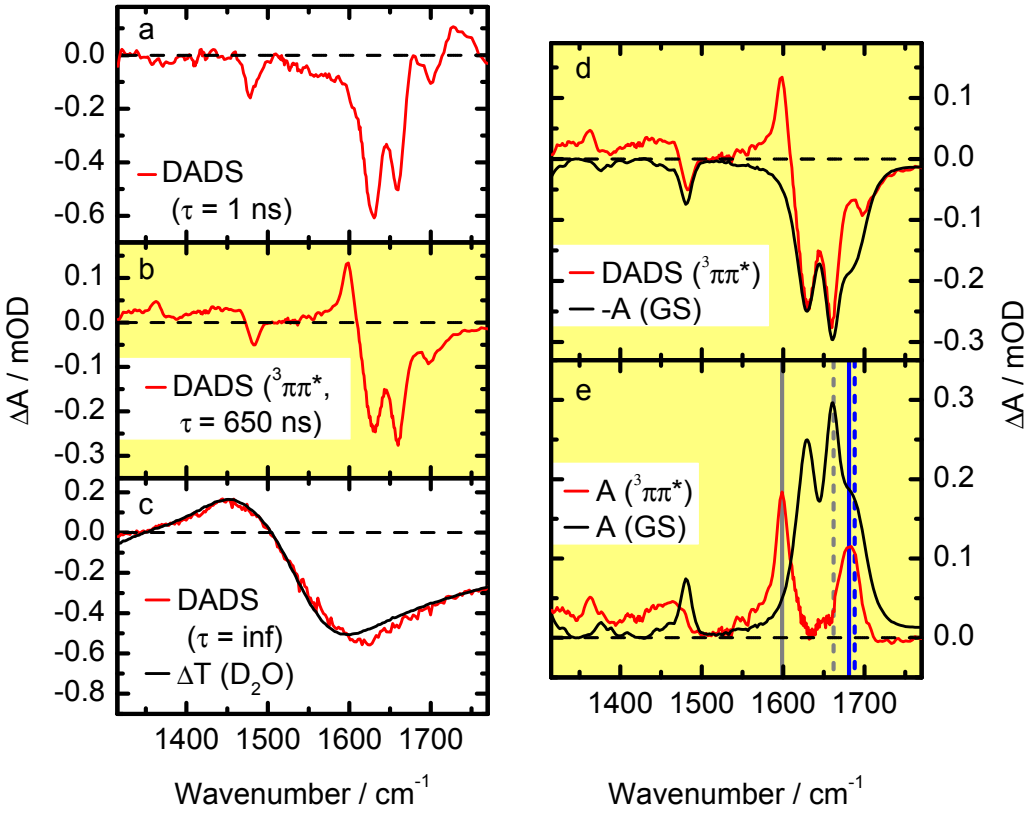

Figure 5.3.: Multiexponential fit of the excited state kinetics of TMP after UV excitation (λ_{exc} = 250 nm, E = 2 µJ). The fit describes the data accurately with 3 exponential time constants. The decay associated difference spectra (DADS) are depicted in panels (a)–(c). Panel (d) shows the DADS of the long-living state and the corresponding ground state bleach. The calculated absorbance spectra of the excited state and of the ground state are compared in panel (e).

the data somewhat deviate from the signature of solvent heating. Albeit small, these differences are too significant to dismiss them as experimental inaccuracy. They may point to the formation of some photoproduct like a CPD lesion. CPD lesions could be formed out of a long-living excited state when nucleotides meet by diffusion or out of the short-living $^1\pi\pi^*$ state, if some nucleotides just 'stick together', i.e. if some dimers are present in the solution. A small amount of CPD formation by either of these mechanisms might explain the data, but the signals are too small to make a precise analysis. The CPD formation and the possible role of the long-living triplet state in it are addressed in the second part of this chapter. In this section, the long-living excited state is investigated (panel (b) of Figure 5.3). Its DADS (panel

(b)) describes the absorbance changes caused by the decay of the excited state to the ground state, so it can be calculated as the difference in absorption:
$DADS(\tau = 650\,\text{ns}) = A(ES) - A(GS)$, where GS and ES refer to *ground state* and *excited state*, respectively. The absorbance of the excited state is $A(ES) = \Delta A + A(GS)$. Panel (d) shows how the calculation is done: $-A(GS)$ is obtained by scaling an inverted ground state spectrum of TMP to the DADS. Addition of the ground state spectrum to the DADS (= subtraction of the inverted ground state spectrum from the DADS) yields the absorbance spectrum of the excited state $A(ES)$. Panel (d) shows the DADS and the inverted ground state spectrum that was scaled to the ground state bleach. Panel (e) depicts $A(ES)$ and $A(GS)$. The excited state is characterised by two absorption bands at $1598\,\text{cm}^{-1}$ and $1680\,\text{cm}^{-1}$. It can be identified as the lowest triplet state $^3\pi\pi^*$ by a number of considerations:

1. Spectrally: Ground state bleach and a red-shifted absorption (triplet marker band at $1598\,\text{cm}^{-1}$) are characteristic of the $^3\pi\pi^*$ state [Har08].

2. Quenching: The lifetime depends on the oxygen concentration (see next section), therefore it has to be a triplet state. The energetically lowest triplet state is a $^3\pi\pi^*$ state [SBB79].

3. Quantum yields: The ISC quantum yield at an excitation wavelength of 250 nm is higher than at 266 nm. The same behaviour was reported for the $^3\pi\pi^*$ state [Ban12].

4. Lifetime: The lowest triplet state is expected to be the longest-living excited state.

1. Spectral characterisation: Compared to the ground state, the C5=C6 double bond disappears in the electronically excited state, so the band at $1628\,\text{cm}^{-1}$ vanishes (see Figure 5.3, panels (d) and (e)). The two bands between $1590\,\text{cm}^{-1}$ and $1700\,\text{cm}^{-1}$ can be assigned to C=O vibrations. The C2=O7 vibration (around $1681\,\text{cm}^{-1}$ in the ground state) is somewhat shifted, while the C4=O8 vibration is red-shifted from $1661\,\text{cm}^{-1}$ in the ground state to $1598\,\text{cm}^{-1}$ in the excited state. Both features agree very well with the data of thymine in acetonitrile (see previous section).

2. Measurements with different concentrations of oxygen (see next section) show that oxygen quenches this state; it is therefore a triplet state.

3. Test measurements (data not shown) have proved that the yield of the triplet state depends on the excitation wavelength as described by [Ban12] for the $^3\pi\pi^*$ state.

4. As the data clearly show, the obtained excited state has the longest lifetime. After its decay all bases are in the ground state again.

These findings demonstrate that the observed state is the lowest triplet state $^3\pi\pi^*$.

5.1.4. Quenching Mechanisms of the Triplet State

The intrinsic decay rate of the $^3\pi\pi^*$ state of thymine is between $4000\,s^{-1}$ [Son98] and $8000\,s^{-1}$ [JW71, WJ72] (in water), resulting in intrinsic lifetimes between 125 µs and 250 µs. The experimentally observed triplet lifetime is much shorter, because two mechanisms of triplet quenching occur:

1. Quenching by oxygen
2. Quenching by thymine molecules

Quenching by Oxygen

O_2 is a well-known triplet quencher. Its ground state is a triplet, therefore if it interacts with triplet thymine, the spin of the system $(^3O_2 +^3 T)$ can be 2, 1 or 0, depending on the orientation of the individual spins. If the spin is 0, the transition $(^3O_2,^3 T) \rightarrow (^1O_2,^1 T)$ is allowed because the overall spin is conserved. Thereby the triplet state is quenched and singlet oxygen is formed. This is a bimolecular reaction, but the experiments were performed at low TMP triplet concentrations where the reaction becomes pseudo-first order: The oxygen-dependent measurements were performed with a concentration of 5 mM per base; less than 10 % of them are excited by a UV pulse. The ISC quantum yield is below 4 % at an excitation wavelength of 250 nm [Ban12]. Therefore, in the illuminated volume, the triplet concentration is $c(^3TMP) \leq 5\,\text{mM} \cdot 10\,\% \cdot 4\,\% \leq 0.020\,\text{mM}$, which is less than 10 % of the oxygen concentration (around 0.240 mM). The reaction is therefore pseudo-first order according to:

$$k_{O_2} = k_2 \cdot c[O_2] \tag{5.1}$$

Quenching by Thymine

When a triplet state thymine collides with a ground state thymine, the triplet can be quenched by the reaction [WB68]:

$$(^3T +^1 T) \rightarrow (RI) \rightarrow (^1T^1T) \text{ or } (CPD) \tag{5.2}$$

The two thymines can form a reaction intermediate (RI) and subsequently return to their ground states or form a CPD lesion. The concentration of ground state TMP is more than two orders of magnitude higher than the concentration of thymine in the triplet state, so this reaction is also pseudo-first order:

$$k_T = k_3 \cdot c[T] \tag{5.3}$$

In principle, self-quenching of two triplet state thymines is possible under spin conservation, like oxygen quenching. This bimolecular reaction depends on the second order of the (very low) triplet concentration and is therefore very slow. Hence it is neglected in the following.

In conclusion, if k_1 denotes the spontaneous triplet decay rate, the total quenching rate k_{quench} can be written as follows:

$$k_{quench} = k_1 + k_2 \cdot c[O_2] + k_3 \cdot c[T] \tag{5.4}$$

5.1.5. Experimental Data on Triplet Quenching

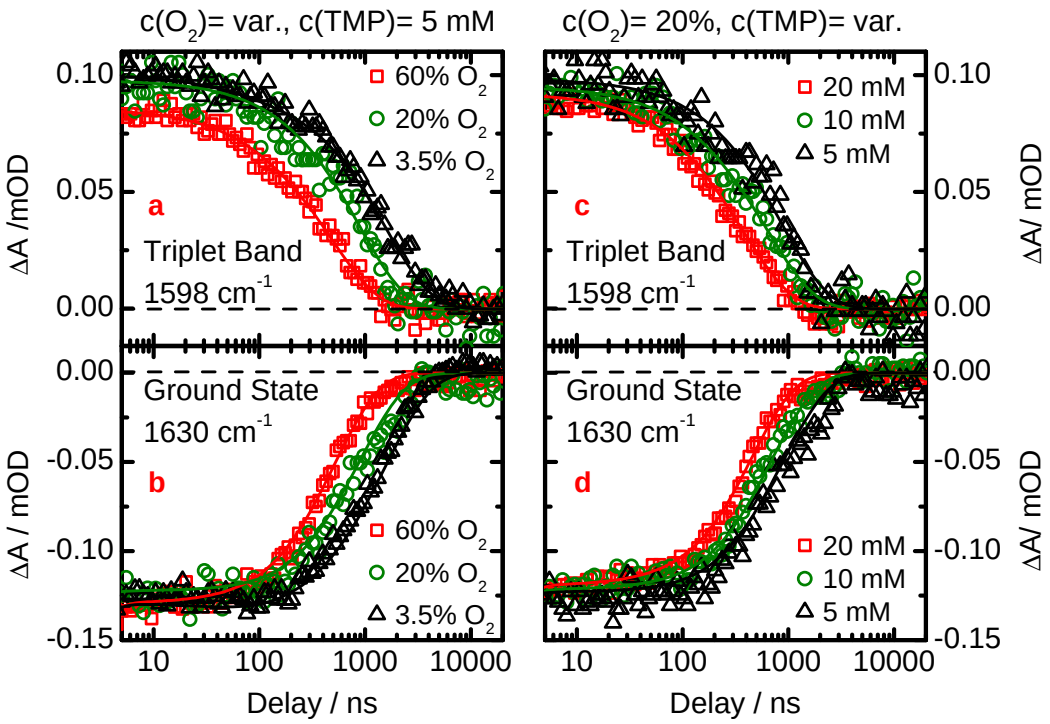

Figure 5.4.: TMP in a buffered D_2O solution on the ns timescale. On the left side, the decay of the triplet marker band at 1598 cm^{-1} (a) and the ground state recovery at 1630 cm^{-1} (b) with a TMP concentration of 5 mM and different concentrations of oxygen are depicted. On the right side the triplet decay (c) and ground state recovery (d) at normal oxygen concentration and different TMP concentrations are shown. Triplet decay and ground state recovery occur on the same timescale, therefore no intermediate state is visible. Oxygen and TMP concentrations clearly affect the triplet lifetime (see text).

TRIR measurements of TMP with different concentrations of TMP and O_2 were performed to investigate the triplet quenching processes. The triplet lifetimes were determined by multiexponential fits of the data.

The left panels (a) and (b) of Figure 5.4 depict the results of measurements with a constant TMP concentration of 5 mM, while the oxygen concentrations were 3.5 %, 20 % and 60 % of the saturation concentration, corresponding to concentrations of 0.050 mM, 0.28 mM and 0.850 mM, respectively. The value of 20 % represents normal conditions. The O_2 concentration of 60 % was generated by purging the sample with oxygen. Low oxygen concentrations were achieved by using a commercially available degasser (Knauer Online Degasser). The oxygen concentration was measured by using an oxygen sensor (NeoFox Sport, Ocean Optics).

The panels on the right side ((c) and (d)) of Figure 5.4 show the influence of the TMP concentration on the triplet lifetime, while the oxygen concentration was not regulated and therefore at the equilibrium value of about 20 % of its saturation value. The $^3\pi\pi^*$ lifetime is measured by the decay of the triplet marker band at 1598 cm^{-1} ((a) and (c)). The ground state recovery is measured at 1630 cm^{-1} ((b) and (d)) (monitoring the ground state bleach at 1660 cm^{-1} would give the same result).

The depicted data show that the $^3\pi\pi^*$ state lifetime is reduced by increasing concentrations of TMP and O_2, corresponding to increasing quenching rates. At all concentrations of TMP and oxygen, the triplet decay occurs at the same time constant as ground state recovery, no reaction intermediate is observed.

Rate Constants of Triplet Quenching

An estimation of the rate constants of the two quenching mechanisms can be derived from the data. To obtain more precise values for the quenching constants, more measurements with additional concentrations of oxygen and TMP are necessary; however, the order of magnitude of the rate constants can be derived. Figure 5.5 shows the decay rates of the $^3\pi\pi^*$ state depending on the concentrations of oxygen (a) and TMP (b).

Linear fits of the obtained $^3\pi\pi^*$ decay rates (= lifetimes^{-1}) yield rate constants of $k_3 = 8.7 \cdot 10^7\ M^{-1}s^{-1}$ for concentration quenching and of $k_2 = 1.7 \cdot 10^9\ M^{-1}s^{-1}$ for oxygen quenching. Concentration-dependent measurements of thymine self-quenching reported values between $0.3 \cdot 10^7\ M^{-1}s^{-1}$ [Son98, GWR96] and $1 \cdot 10^8\ M^{-1}s^{-1}$ [SBB79]. The obtained value of $k_3 = 8.7 \cdot 10^7\ M^{-1}s^{-1}$ is well within that range. The rate constant of quenching by oxygen differs by a factor of 2 from the value reported in the literature ($3.5 \cdot 10^9\ M^{-1}s^{-1}$ [JW71]). Even with these few measurements, both rates are in the same order of magnitude as the ones reported in the literature. The method of determining the rate constants used here differs from the one used in the cited studies [JW71, SBB79, GWR96, Son98]. By flash photolysis, using a

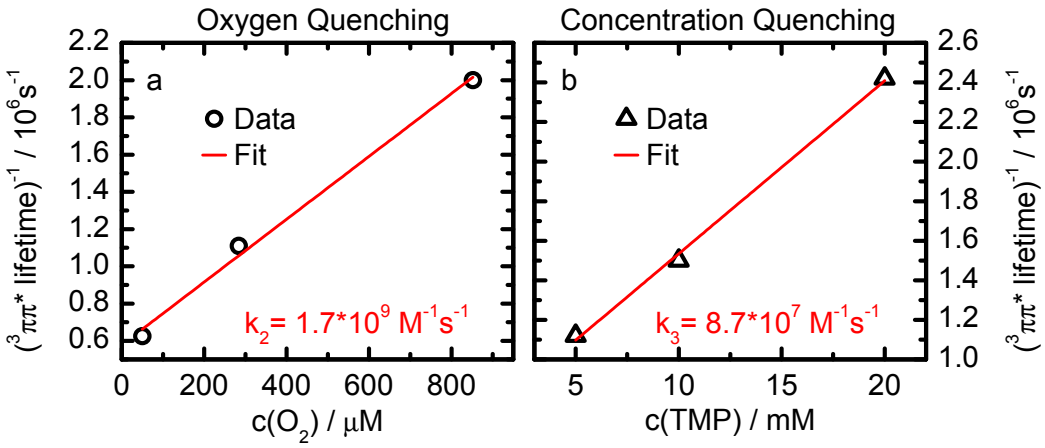

Figure 5.5.: Quenching of the triplet state of TMP by oxygen (a) and ground state TMP (b) at different concentrations. A linear fit determines the values of the rate constants k_2 and k_3.

triplet sensitiser to increase the triplet yield, they monitored the $^3\pi\pi^*$ state in the visible spectral range, where its absorbance is broad and not very specific. Due to this low specificity, it is not clear whether reaction intermediates, which might be formed during self-quenching, could be distinguished from the $^3\pi\pi^*$ state. Moreover, those measurements did not keep track of the ground state bleach of the sample, so they did not observe whether ground state recovery occurs simultaneously with triplet decay or not. For these reasons, a possible formation of reaction intermediates during self-quenching is not observable by these techniques. TRIR spectroscopy can monitor triplet decay, ground state recovery and the formation of photolesions at the same time, with superior specificity and temporal resolution. These advantages are particularly important in the more interesting case of the $^3\pi\pi^*$ state in thymidine oligomers.

5.2. The $^3\pi\pi^*$ State of Thymidine Oligonucleotides

The excited state kinetics of oligonucleotides are more complex than those of single nucleotides, because interactions between neighbouring bases give rise to additional excited states. On the timescale of a few picoseconds to a few hundred picoseconds, such delocalised states include excitons and excimers [Mid09] that are related to the initially excited singlet states. These relatively short-living states are not expected to be observable on a timescale of nanoseconds to microseconds.

Kinetics related to the $^3\pi\pi^*$ state, on the other hand, occur on that timescale in the monomer TMP. Though these monomers can only meet by diffusion, their interactions result in a quenching of the triplet-excited bases by ground state thymine. This quenching mechanism should be much more efficient in thymidine oligomers

like $(dT)_{18}$, where every base has at least one neighbouring base, resulting either in ground state recovery or CPD lesion formation.

The differences of triplet kinetics of TMP and $(dT)_{18}$ were already addressed by a previous study that used laser flash photolysis [MM05]. The $^3\pi\pi^*$ state of thymine was clearly observed and characterised, but within the temporal resolution of 200 ns no corresponding signals were found in $(dT)_{18}$. Different explanations have to be considered:

1. Interactions between neighbouring bases reduce Φ_{ISC} by at least one order of magnitude.
2. Triplet quenching by neighbouring bases results in ground state recovery within less than 200 ns.
3. The $^3\pi\pi^*$ state is quenched by CPD lesion formation within less than 200 ns.

The first possibility could be plausible because interactions between neighbouring bases can change the excited state dynamics and thereby the quantum yield of various states. In addition, they give rise to states that are not present in monomers, thereby reducing the quantum yield of other states. The second and third possibility are in line with the expectations, since self-quenching of the $^3\pi\pi^*$ state in $(dT)_{18}$ is not limited by diffusion and thereby relatively fast. Deciding whether or not triplet quenching results in significant CPD lesion formation requires a short discussion.

5.2.1. CPD Formation in Thymidine Oligonucleotides

After UV excitation of $(dT)_{18}$, CPD lesions can be formed in two different ways:

1. Ultrafast CPD formation out of the $^1\pi\pi^*$ state [Sch07].
2. CPD formation out of the $^3\pi\pi^*$ state, possibly via a reaction intermediate (RI).

These processes occur under different conditions on different timescales (see Figure 5.6). Ultrafast CPD formation within 1 ps out of the $^1\pi\pi^*$ state can only occur between suitably oriented (stacked) bases. During the $^1\pi\pi^*$ lifetime (less than 1 ps, see section 2.2), no reorientation of the bases can take place, so only the subset of stacked bases can produce CPD lesions out of the $^1\pi\pi^*$ state (Figure 5.6, (a)).

On the nanosecond timescale, CPD lesions can be formed out of the $^3\pi\pi^*$ state ((b) in Figure 5.6). This mechanism does not require initially stacked bases, because molecular rearrangements of unstacked bases into a stacked geometry can occur on this timescale. If a suitable conformation is reached, a CPD lesion can be formed out of the $^3\pi\pi^*$ state. Since the triplet quantum yield (3 % to 4 % at 250 nm excitation wavelength [Ban12]) is below the CPD quantum yield in $(dT)_{18}$ out of the $^1\pi\pi^*$ state (5 % [Ban12]), the increase of the CPD concentration on the slower timescale should be below the amount of initially formed CPD lesions.

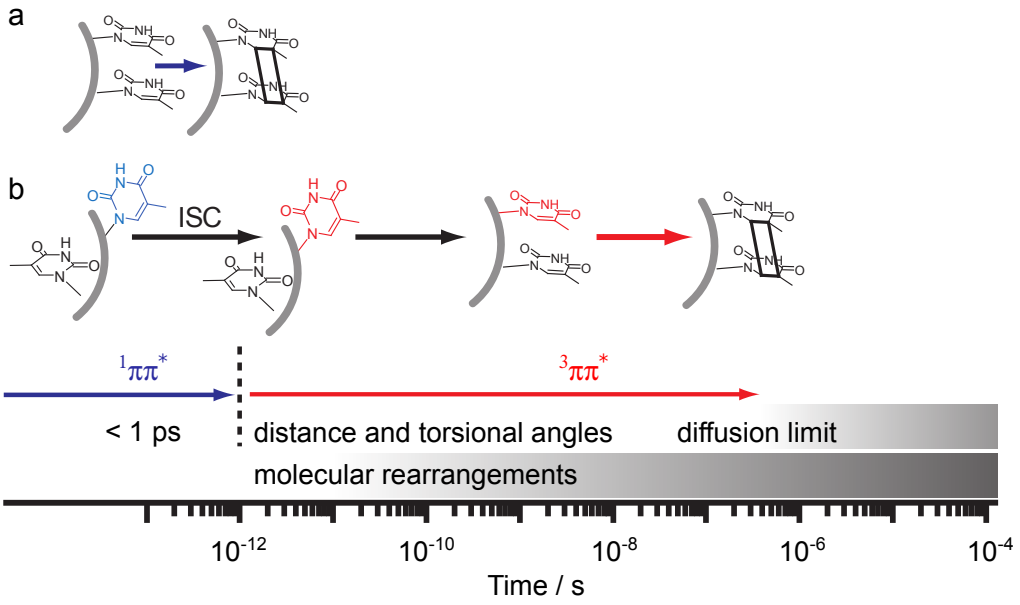

Figure 5.6.: CPD generation in thymidine strands. Pre-stacked bases can form a CPD lesion out of the excited singlet state within 1 ps. Unstacked bases in the triplet state can reorient within the triplet lifetime, reaching suitable conformations to produce CPD lesions on the ns timescale. Picture adapted from [Pil14a].

5.2.2. $^3\pi\pi^*$ Decay in Thymidine Oligonucleotides

Figure 5.7 shows the absorbance changes of $(dT)_{18}$ after UV excitation at a wavelength of 250 nm. The signature of solvent heating has been subtracted from the data. Panel (a) of Figure 5.7 depicts a contour plot of the data. It shows ground state bleach between 1600 cm^{-1} and 1700 cm^{-1} and induced absorption features at 1598 cm^{-1} and in the CPD fingerprint region between 1300 cm^{-1} and 1500 cm^{-1}. The feature at 1598 cm^{-1} decays relatively fast (between 10 ns and 20 ns), while the ground state recovery occurs on a longer timescale (100 ns), pointing to more than one excited state (see panel (c)). After more than 100 ns the signal remains constant. Panel (b) shows the transient absorbance changes around 10 µs and the signature of the CPD lesion. The latter was obtained by FTIR spectroscopy of $(dT)_{18}$ after UV illumination. The excellent agreement shows that only the CPD lesions persist at delay times above 100 ns. The CPD marker bands at 1320 cm^{-1}, 1402 cm^{-1} and 1465 cm^{-1} are clearly visible immediately after UV absorption. Their initial (i.e. in the first few nanoseconds) amplitudes represent the amount of CPD lesions that are formed out of the $^1\pi\pi^*$ state on a picosecond timescale. As the excited states decay within 100 ns, the amplitudes of these bands do not increase. To the contrary, the absorption in the fingerprint region decreases on that timescale. These decreasing

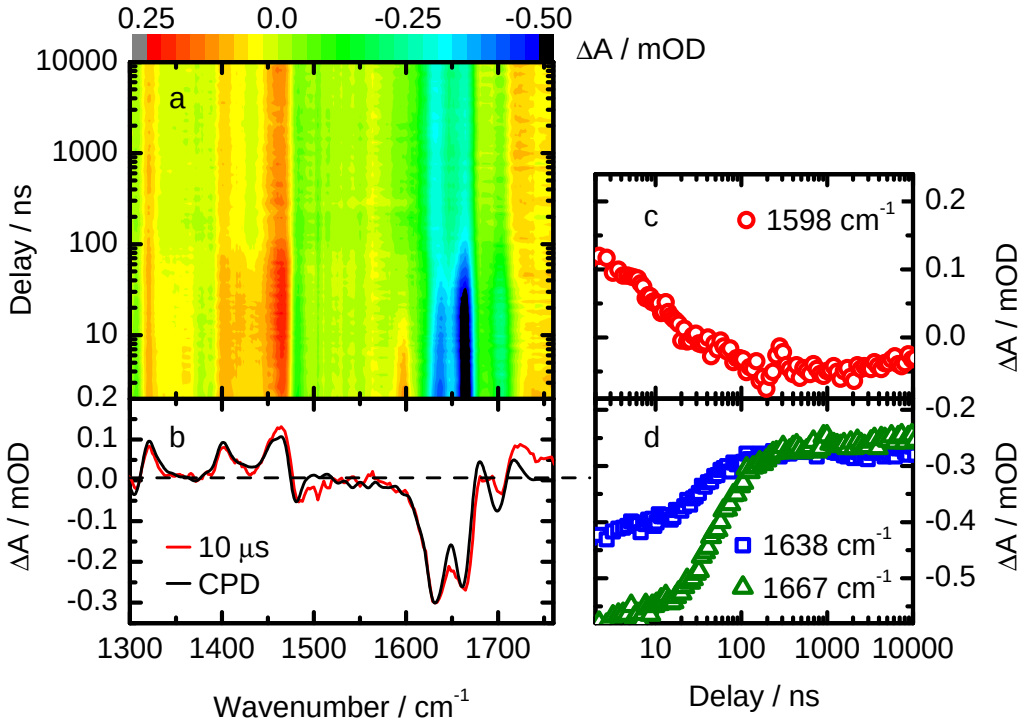

Figure 5.7.: $(dT)_{18}$ after UV excitation on the ns timescale. The excited state kinetics is finished after ca. 100 ns (see panels (a), (c), (d)). After that, the remaining absorbance change agrees very well with the signature of the CPD lesion (panel (b)). The marker bands of the CPD lesion at 1320 cm^{-1}, 1402 cm^{-1} and 1465 cm^{-1} are clearly visible from the beginning, indicating the ultrafast CPD formation out of the excited singlet state.

signals reflect the decay of an excited state that initially absorbs in that spectral range. Its absorption overlays the CPD bands at 1402 cm^{-1} and 1465 cm^{-1}, but the third CPD marker band at 1320 cm^{-1} is spectrally isolated from the excited state absorption. It does not change after more than 1 ns, so no significant amounts of CPD lesions are formed on the nanosecond timescale. The long-living excited states predominantly return to the ground state.

Excited State Kinetics in Detail

Since the CPD amount does not change noticeably on the nanosecond timescale, its signal (absorbance change after 10 µs) can be treated as a constant background and it can be subtracted from the data to monitor the excited state kinetics more closely. Figure 5.8 depicts the resulting data. The contour plot (panel (a)) shows two excited states: The first one decays on a 10 ns timescale. It is characterised by an absorption around 1598 cm^{-1}. As this state decays, another band appears around

1624 cm^{-1}. This band disappears on the same timescale as the ground state bleach (1620 cm^{-1} to 1700 cm^{-1}), i.e. within 100 ns.

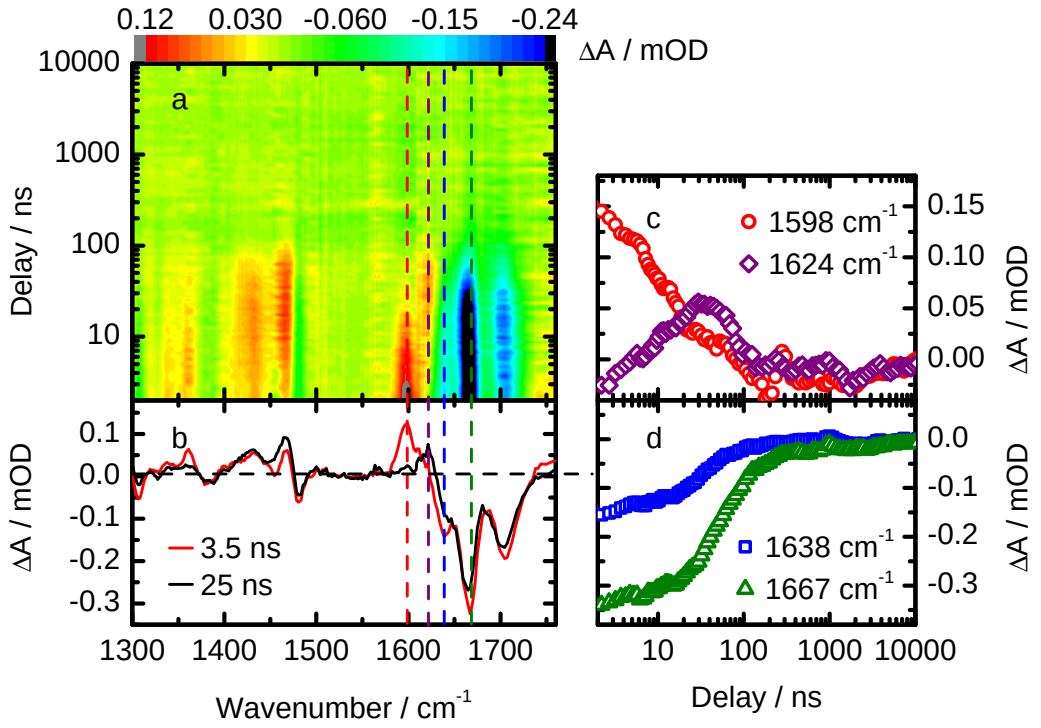

Figure 5.8.: UV-excited $(dT)_{18}$ after subtraction of the CPD absorbance $\Delta A(10\,\mu s)$. In the first 100 ns two excited states exist. A short-living excited state X1 decays on the 10 ns timescale, while another excited state X2 is formed. X1 and X2 are characterised by absorption bands at 1598 cm^{-1} and 1624 cm^{-1}, respectively (c). Ground state recovery takes place on the same timescale as the decay of X2 (d).

Based on the temporal features, a sequential model can be assumed: An excited state (here labelled X1) decays on a timescale of 10 ns to another excited state (here labelled X2). From X2 the bases return to the ground state within 100 ns.
The identification of the excited states X1 and X2 requires a spectral characterisation of them. The absorbance change caused by the relatively short-living state X1 can be calculated readily by comparing the signals at short and at long delay times.

Identification of X1

In the first few nanoseconds after excitation, the signal is comprised of the signature of X1 and of the CPD lesion. After 10 µs only the CPD lesion persists (see panel (a) of Figure 5.9). Since the amount of CPD does not increase significantly on the ns to µs timescale, the difference $\Delta A(3.5\,\text{ns}) - \Delta A(10\,\mu\text{s})$ yields the absorbance change $\Delta A(X1)$ caused by X1 (see panel (b) of Figure 5.9, red).

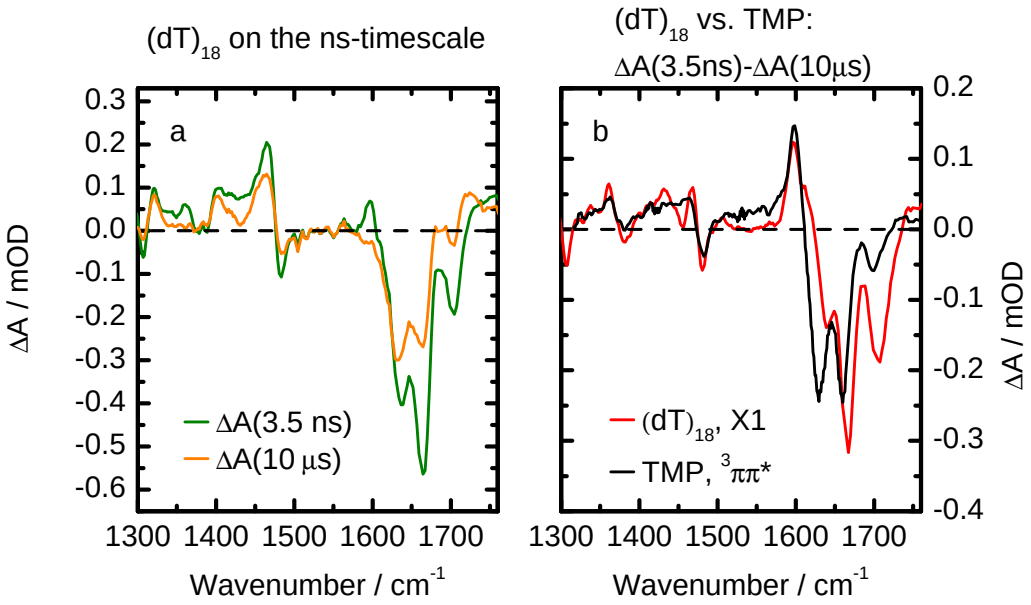

Figure 5.9.: Comparison of the absorbance changes by the triplet state $^3\pi\pi^*$ of TMP and X1 of $(dT)_{18}$ (panel (b)). The latter is obtained by subtracting the residual signal at 50 µs from the signal at 3.5 ns (panel (a)). The spectra are scaled to the same excitation energy. X1 is easily identified as the lowest triplet state by the absorption around 1600 cm^{-1}.

Performing the same calculation for TMP yields the DADS of the $^3\pi\pi^*$ state (see panel (b) of Figure 5.9, black). The comparison of the spectra of TMP and $(dT)_{18}$ in panel (b) of Figure 5.9 shows striking similarities; specifically, the marker band at 1598 cm^{-1} identifies X1 as the $^3\pi\pi^*$ state. The spectra in panel (b) were scaled to the same excitation energy. Therefore the amplitudes of the triplet states can be compared to determine the relative ISC quantum yields (see panel (b) of Figure 5.9). Within experimental accuracy, the triplet yield in $(dT)_{18}$ is the same as in TMP. The $^3\pi\pi^*$ state is quenched within less than 20 ns by the formation of the reaction intermediate X2, which subsequently returns to the ground state within 100 ns. These findings explain why earlier measurements in thymidine oligonucleotides with a temporal resolution of 200 ns [MM05] failed to observe the $^3\pi\pi^*$ state.

5.2.3. Multiexponential Modelling of the Data

A multiexponential fit reveals the excited state kinetics more precisely. The transition of the $^3\pi\pi^*$ state to X2 occurs with a time constant of 12 ns (see Figure 5.10, (a)). The corresponding DADS represents the difference in absorption between the $^3\pi\pi^*$ state and X2. Some of its features can be readily interpreted: The negative bands between 1400 cm^{-1} and 1500 cm^{-1} as well as at 1624 cm^{-1} are due to the increasing absorption at those wavenumbers during the transition $^3\pi\pi^* \rightarrow$ X2 that was observed

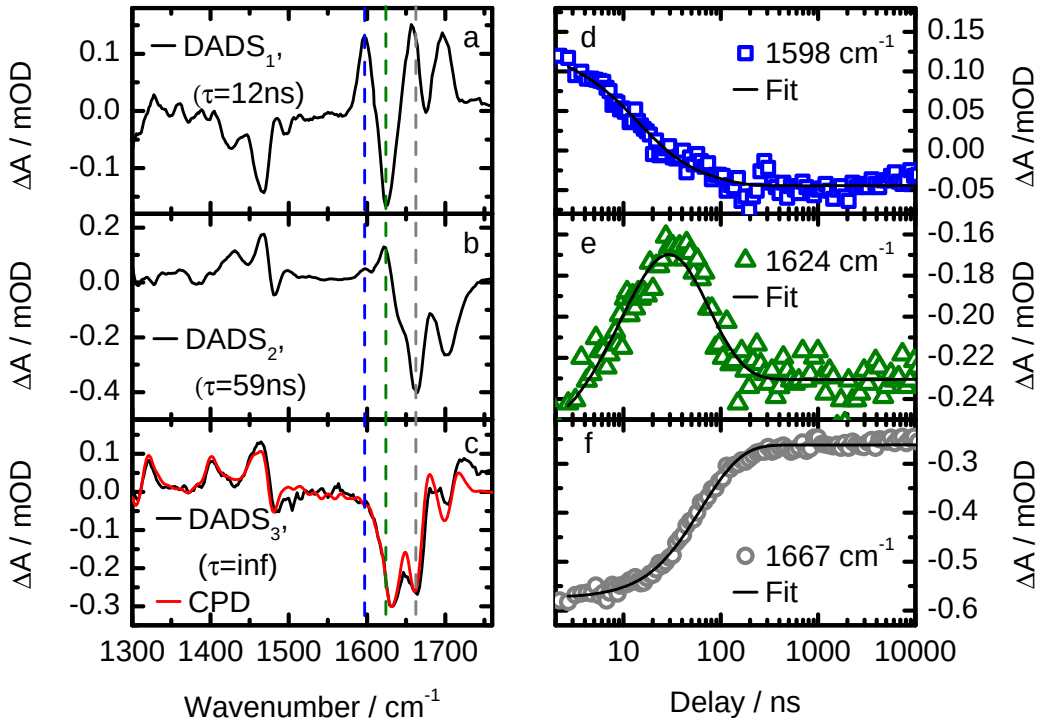

Figure 5.10.: DADS of $(dT)_{18}$ after UV excitation at 250 nm (left). The first two DADS describe the transitions $^3\pi\pi^*$ to X2 (a) and X2 to the ground state (b). The third DADS (c) is identical to the signature of the CPD lesion (red). The time dependence of the experimental data is compared to the global fit at the indicated wavenumbers on the right side. The triplet band at 1598 cm^{-1} (d) disappears as another absorbance band at 1624 cm^{-1} appears (e). This state decays on the same timescale as ground state recovery takes place (f). The time dependencies point to a transition of the triplet state to an intermediate state X2, that subsequently decays to the ground state.

in the data (see Figure 5.8). The positive band at 1598 cm^{-1} describes the decay of the triplet marker band. The features between 1650 cm^{-1} and 1700 cm^{-1} were obscured in the raw data by the ground state bleach and are only revealed by the multiexponential fit.

X2 returns to the ground state with a time constant of 59 ns. The corresponding DADS is depicted in panel (b) of Figure 5.10. The positive features between 1400 cm^{-1} and 1500 cm^{-1} and at 1624 cm^{-1} describe the decay of the absorbance of X2, the negative features between 1630 cm^{-1} and 1700 cm^{-1} indicate ground state recovery. After the decay of X2, no changes in the signals occur any more. The residual absorbance changes (after subtraction of the signals of solvent heating) agree very well with the CPD signature (Figure 5.10, panel (c)).

Figure 5.10, panels (d), (e) and (f) show the temporal evolution of the triplet marker band at 1598 cm^{-1}, the marker band of the intermediate state at 1624 cm^{-1} and the ground state bleach at 1667 cm^{-1}. The symbols show the data and the lines the multiexponential fit. The first two nanoseconds were excluded from the multiexponential fit to ignore short-living states directly after UV excitation. The excellent agreement of the fit with the data confirms the validity of the DADS presented in the panels (a)–(c).

5.2.4. The Intermediate State X2

Spectral Characterisation

The data presented so far show that the decay of the $^3\pi\pi^*$ state in $(dT)_{18}$ occurs via an intermediate state X2. This possibility has been discussed since the 1960s [WB68, WB70]. More specifically, a biradical (^{3}BR) has been suggested as an intermediate in triplet quenching many times in the literature [WB70, DE02, ZE06, Cli10]. In a biradical two neighbouring thymines are covalently linked by the C6 atoms, leaving an unpaired electron remaining on the C5 position of each base (see sketch in Figure 5.11). The biradical then can either return to the ground state or form a CPD lesion [WB70]. The presented data show for the first time that the $^3\pi\pi^*$ state is quenched by an intermediate and revealed its spectral characteristics [Pil14a]. The DADS obtained by the multiexponential fit of the data can be used to identify X2.

The DADS describe the transitions $^3\pi\pi^* \rightarrow$ X2 and X2 $\rightarrow$ GS. So, $DADS_1(\nu)$ gives $A_{^3pp^*}(\nu) - A_{X2}(\nu)$ and $DADS_2(\nu)$ gives $A_{X2}(\nu) - A_{GS}(\nu)$.

The IR spectra of the electronic ground state, of the $^3\pi\pi^*$ state and of the biradical are calculated using DFT (density functional theory) methods. Since the expected states involve only one (GS,$^3\pi\pi^*$) or two bases (^{3}BR), it is reasonable to assume that the spectra of the dimer TpT resemble closely those of the oligomer $(dT)_{18}$. The calculations are carried out for TpT to limit the computational complexity. The B3LYP density functional is used [Bec93, Ste94] with the 6-311G** basis set with the Gaussian 03 (Revision E.01) program [Fri03]. After geometry optimisations, calculations of harmonic vibrational wavenumbers, IR normal modes and intensities were carried out. The obtained IR spectra were convoluted with a Lorentzian (FWHM of 25 cm^{-1}). A detailed description of the calculations can be found in the supporting information of [Pil14a].

Figure 5.11 shows a comparison between the experimental and the theoretical data. On the left, the transition from the $^3\pi\pi^*$ state to the triplet biradical ^{3}BR is depicted. Panel (a) shows the experimental data, (b) the theoretical calculation. At high wavenumbers the DADS shows two positive bands between 1650 cm^{-1} and 1700 cm^{-1}, separated by a minimum at 1675 cm^{-1}. A bleach is found at 1624 cm^{-1} and a positive absorption at 1598 cm^{-1}. The same pattern is found in the calculated spectra. The

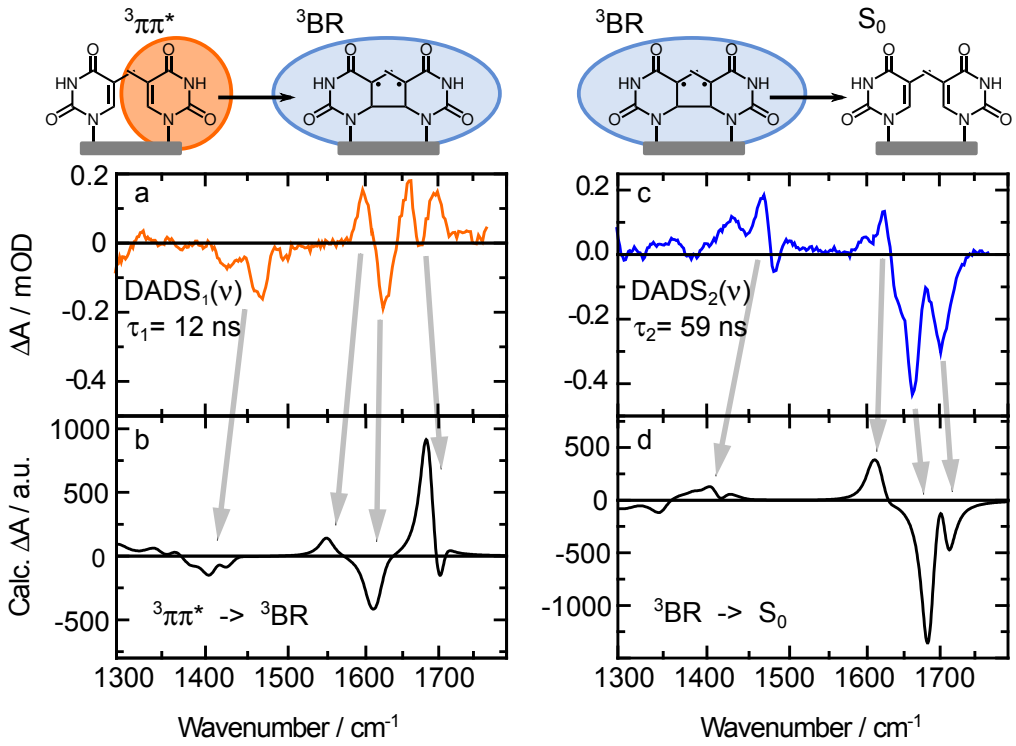

Figure 5.11.: $(dT)_{18}$ after UV excitation. DADS of the transitions of the local triplet state to the intermediate state (a) and from the intermediate state to the ground state (c). The lower panels show DFT calculations of the absorbance changes caused by transitions $^3\pi\pi^* \rightarrow {}^3$BR (b) and ^{3}BR$\rightarrow S_0$ (d). Picture taken from [Pil14a] and adapted.

positions of the calculated bands match the experimental data quite well, especially the C=O double bond region from 1650 cm^{-1} to 1750 cm^{-1}, with some differences in oscillator strength. The disappearing of the triplet marker band at 1598 cm^{-1} and the build-up of the absorption at 1624 cm^{-1} is modelled at somewhat lower wavenumbers. Still, the structural similarities between the calculated and the observed spectrum support the identification of X2 as a biradical. The transition of the intermediate state X2 to the ground state (Figure 5.11, (c)) is also well described by the theoretical calculations. Two strong negative bands between 1650 cm^{-1} and 1700 cm^{-1}, that indicate ground state recovery, are well modelled (panel (d) in Figure 5.11), as well as the positive absorption band at 1624 cm^{-1}. The small absorption changes below 1500 cm^{-1} are qualitatively described by the calculation, albeit at shifted wavenumbers.

Temporal Features of ^3BR

The spectral characteristics of the intermediate state are in line with the ^{3}BR assignment. But are the observed timescales consistent with it? Consider two

neighbouring thymine bases that have a random configuration. If one of them is excited to the $^3\pi\pi^*$ state, it can form a biradical with its neighbour only when a suitable conformation is reached. Until that time the excited base will remain in a $^3\pi\pi^*$ state. The experimentally observed time constant of biradical formation (12 ns) depends therefore not only on the rate of biradical formation between suitably oriented bases, but also on the timescale of reconfiguration of the bases.
The former rate was estimated by a recent theoretical study by Climent et al. [Cli10]. Assuming a 'proper' orientation of two thymines, they found a barrierless reaction path from the $^3\pi\pi^*$ state to the biradical. Such a barrierless transition should occur on a timescale of picoseconds rather than nanoseconds.
The conformational changes of bases in single strands take place on a timescale larger than 1 ns [Wu90, JH04]. These studies suggest that the timescale of biradical formation (12 ns) is related to the reorientation of the bases, and after a 'proper' configuration is reached, the formation of a biradical is fast. The timescale of biradical formation out of initially unstacked bases is therefore in line with the expectations.

Initially stacked bases could form a biradical on a sub-ns timescale, but no corresponding signals are observed in the experiments. However, only a small fraction of the thymine bases are stacked [MVH99, BH04, JW07b], and they presumably do not populate the $^3\pi\pi^*$ state efficiently, because they can either form CPD lesions or other delocalised states (see chapter 6). The kinetics of the triplet state of initially stacked bases would therefore not be observed in the experiments.

The return of the intermediate state X2 to the ground state occurs with a time constant around 60 ns. The transition of a biradical to the ground state requires a change of the multiplicity from triplet to singlet. Such transitions in organic radical pairs are driven by the hyperfine interaction [SU89, Rod09]. Experimentally, the lifetime of biradicals in some biological molecules was found to be in the 100 ns range [DTW89], in good agreement with the lifetime of X2. The observed time constants of the formation and of the decay of X2 therefore support the identification of X2 as a biradical.

In conclusion, the good agreement between the experimental and the theoretical spectra, the agreement between the kinetics and the expected kinetics of biradical formation and decay alongside with the massive theoretical support for a biradical mechanism [DE02, WB70, Cli10, ZE06], make the ^{3}BR assignment very convincing.

5.3. Conclusion and Outlook

TRIR measurements were reported that identified the $^3\pi\pi^*$ state of thymidine nucleotides and oligonucleotides (TMP and $(dT)_{18}$). The $^3\pi\pi^*$ state is populated in thymidine oligomers as well as monomers with approximately the same quantum yield (3 % to 4 % at an excitation wavelength of 250 nm [Ban12]) on a sub-ns timescale. The

$^3\pi\pi^*$ state of TMP is quenched by oxygen and ground state thymine alike, on a timescale that depends on the respective concentrations (under our conditions circa 600 ns).

Interactions with neighbouring bases in thymidine strands change the kinetics of triplet quenching. The mechanism of triplet quenching in thymidine oligomers was monitored for the first time (see [Pil14a]). A thymine base in the $^3\pi\pi^*$ state forms a biradical with a neighbouring base with a time constant of 12 ns. The biradical predominantly decays to the ground states of both bases (time constant: 60 ns). No CPD lesion formation out of the biradical is observed. Taking into account the finite experimental accuracy, the quantum yield of CPD lesion formation out of the biradical is estimated to be below 15 %. These findings correct some recent studies on the role of triplet state in CPD formation [MM05, KMP08] and confirm earlier speculations [WB68, WB70]:

Marguet et al. found a triplet state after a delay time of more than 200 ns only in TMP, not in $(dT)_{18}$ [MM05]. They proposed two alternative explanations: Either the CPD formation out of the $^3\pi\pi^*$ state in $(dT)_{18}$ or a much lower ISC quantum yield in $(dT)_{18}$. Both alternatives do not apply, the triplet signal of $(dT)_{18}$ is absent after 200 ns, because it decays to the ground state via a biradical on a much faster timescale.
Kwok et al. suggested that the CPD lesion is formed in $(dT)_{18}$ within 140 ps out of the $^3\pi\pi^*$ state [KMP08]. This is clearly not the case as witnessed by the triplet decay on the ns timescale (the nature of this 140 ps decay will be addressed in the next chapter).
Unlike these relatively recent studies, Wagner and coworkers reported a small dimerisation quantum yield out of the $^3\pi\pi^*$ state and postulated an intermediate state in triplet quenching that predominantly returns to the ground state [WB68, WB70]. These studies are confirmed by the presented work [Pil14a].

Regarding the biological relevance of the $^3\pi\pi^*$ state as a hazard to the genetic code, the present work shows that it is quenched to the ground state with a quantum yield of at least 85 % without forming CPD lesions. Combined with the low intersystem crossing quantum yield of only 0 % to 4 % (depending on the excitation wavelength [Ban12]), CPD formation out of the triplet state after direct UV excitation of thymine is almost negligible. However, the triplet state can be reached via sensitising [Lam67]. Sensitizers of suitable energy absorb in the UVA range, where the sun's radiation at sea level is much stronger than in the UVB and UVC ranges. They subsequently undergo ISC to a triplet state. By triplet-triplet energy transfer (TTET), they can excite a ground state thymine to the triplet state. Depending on which sensitisers exist in organisms, this could easily be of major importance.

The role of the triplet states in more complex strands is another interesting topic for research. According to calculations, thymine has the lowest triplet energy of all DNA bases [GWR96, Cad92]. So, triplet migration along the strand to thymine is possible. Moreover, it is not clear whether or not triplet thymines also form biradicals with other bases like cytosine, thereby activating them. By such a mechanism, cytosine could be damaged simply by being located next to a triplet state thymine. TRIR spectroscopy is well-suited to investigate this question by performing measurements of (5'–3')T–C or (5'–3')C–T dimers in the nanosecond to microseconds time range.

6. Charge Separation in Thymidine Oligonucleotides

Base stacking can give rise to delocalised states like excitons and exciplexes [CCK05, Vay10, Vay12]. It has been speculated for a long time that long-living excited states of oligonucleotides are exciplexes with partial charge transfer character, albeit only on indirect evidence [Eis66, SBI07, Mid09]. Such excited states might be reactive and thereby pose a hazard to the integrity of DNA. This potential problem is amplified if full charges are transferred between DNA bases, generating reactive radical cations and anions. An extensive theoretical study suggests that the (6–4) lesion between two thymines originates from a charge transfer between neighbouring pyrimidines [Imp12]. By such mechanisms, charge transfer could be a great hazard to DNA. However, lacking evidence for this mechanism, it is possible that the opposite might be true: Rapid charge transfer, followed by charge recombination to the ground state, could deactivate excited stacked bases that could otherwise dimerise into lesions like CPDs. Beyond preventing dimerisation, electron transfer onto a CPD lesion may even repair it in a photolyase-like fashion [Pan11]. Taking into account the relatively high yield of those presumed exciplexes/charge separated states [Tak08], those questions gain relevance. Though they are not answered yet, several important steps have been taken in the last few years. TRIR spectroscopy of the dimer ApT identified a charge separated state of UV-excited stacked bases by comparing its spectrum to calculated spectra of adenine cations and thymine anions [Doo13]. Recently, in dimers composed of two different bases, Bucher et al. identified charge separated states by a comparison of their IR signature with that of the cations and anions of the nucleotides [Buc14a]. This study focusses on dimers composed of different bases, where their difference in oxidation potential determines the direction of charge transfer. It did not address the possibility of charge transfer between two identical bases. This case however is particularly important concerning the role of dipyrimidines like TpT and CpC in DNA photo dimerisation (yielding CPDs and (6–4) lesions) and the possible involvement of charge transfer processes in them. Even though the pyrimidine strands $(dT)_n$ and $(dC)_n$ have been studied extensively, no experimental evidence was reported for photo-induced charge transfer yet. On the contrary, long-living excited states that were observed in those strands were interpreted differently. In the case of cytosine, one long-living state was observed in CMP and $(dC)_n$. It was identified as a localised state, presumably of $^1n\pi^*$ character [Qui07, Kea12].

A similar assignment has been made for thymine, where Hare et al. observed a 100 ps decay in nucleotides and thymidine strands [HCK07]. However, measurements

by other groups found a 100 ps decay only in the oligomers $(dT)_{18}$ [Sch08, KMP08]. Kwok et al. hypothesised that the formation of CPD lesions out of the $^3\pi\pi^*$ state takes place on that timescale [KMP08]. Both of these interpretations are quite speculative. Lacking evidence, they cannot exclude the possibility of charge transfer in thymidine strands.

In this chapter, the excited state physics of $(dT)_{18}$ is discussed as it is revealed by TRIR spectroscopy. The aforementioned state that decays on the 100 ps timescale is observed and characterised. The discussion about its nature begins with reviewing the literature about it. The previous assignments of this state are critically evaluated and rejected in the face of conflicting evidence. Instead, it is identified as a charge separated state (CSS) that is formed directly out of the excited $^1\pi\pi^*$ or exciton state. This assignment is substantiated by comparing the decay associated difference spectra (DADS) to the expected absorbance changes caused by thymidine radical anions and cations. The method can be summarised as follows:

1. TRIR measurement of the 100 ps decay of $(dT)_{18}$
2. TRIR measurement of the DADS of the CSS of TpA ($T^{\bullet-}pA^{\bullet+}$)
3. TRIR measurement of the spectra of the cations of thymine $T^{\bullet+}$ and adenine $A^{\bullet+}$
4. Calculation of the extinction coefficients ε of the cations and the $T^{\bullet-}pA^{\bullet+}$ state
5. Calculation of $T^{\bullet+}pT^{\bullet-}$ and comparison to the DADS of $(dT)_{18}$

The cation difference spectrum is obtained directly by using two-step ionisation of the bases [Buc14b]. The spectrum of the thymine anion is calculated from the spectrum of a CSS of TpA ($T^{\bullet-}pA^{\bullet+}$), that is formed upon UV absorption (see [Doo13]). To calculate the spectrum of the charge separated state in thymidine oligomers, the spectra and extinction coefficients of thymine cations and anions are derived. The calculation of the DADS of the hypothetical $T^{\bullet+}pT^{\bullet-}$ state is then done according to the following equation:

$$T^{\bullet+}pT^{\bullet-} = T^{\bullet+} + (T^{\bullet-}pA^{\bullet+} - A^{\bullet+}) \tag{6.1}$$

The calculated DADS of $T^{\bullet+}pT^{\bullet-}$ is finally compared to that of the excited state of $(dT)_{18}$ in question. A discussion of charge transfer in oligonucleotides concludes this chapter.

6.1. Time-Resolved Measurements of $(dT)_{18}$

6.1.1. Time-Resolved Data in the First 500 ps

The excited state physics of the thymidine oligomer $(dT)_{18}$ in a buffered solution of D_2O was observed by TRIR spectroscopy on the picosecond timescale. The sample was excited by UV pulses (wavelength 266 nm, excitation energy 2 µJ, beam diameter 160 µm), whose pulse duration was increased by group velocity dispersion in a fused silica block (path length 20 cm) to almost 2 ps. By stretching the pulse duration, the pulse intensity is decreased, reducing effects like two-step ionisation of the sample.

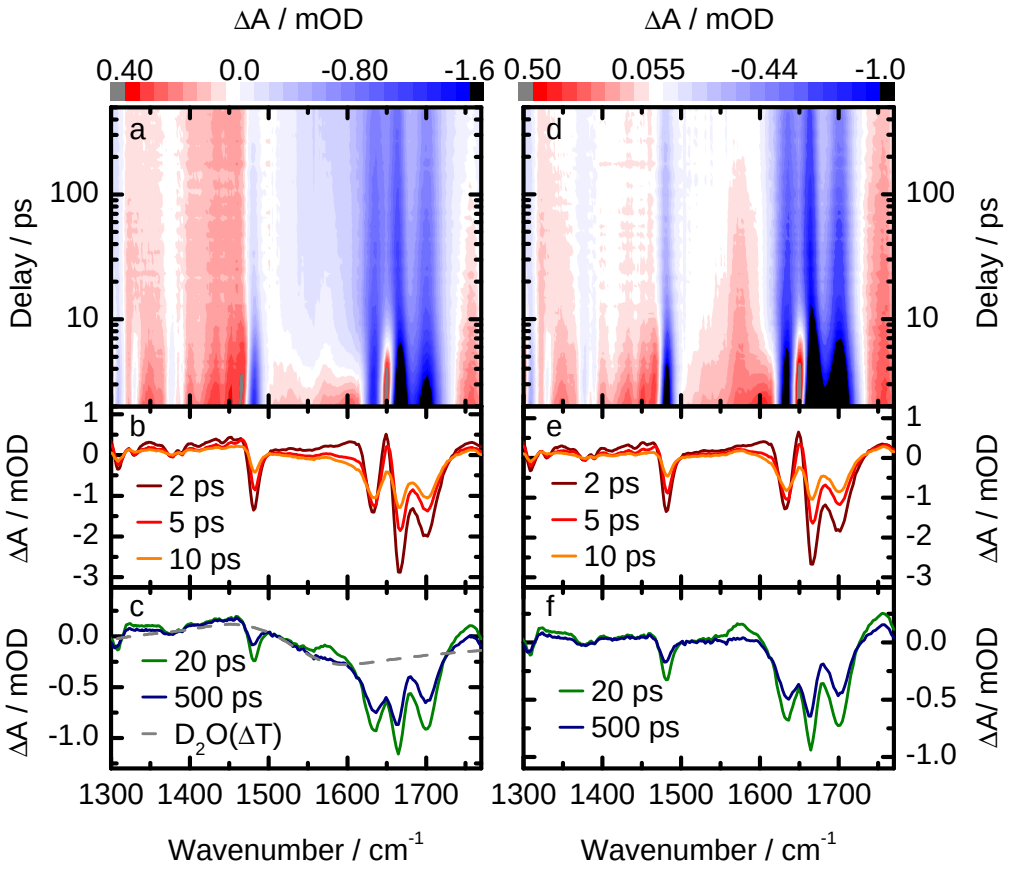

Figure 6.1.: Excited state physics of $(dT)_{18}$ in D_2O. The panels on the left show the raw data, the panels on the right the data after correction for the time-dependent absorbance change caused by the heating of the solvent (see section A.1). In the first few ps, the signal is dominated by the signature of vibrational cooling (panels (b) and (e)). Between 20 ps and 500 ps an excited state decays that is characterised by an absorption at 1570 cm^{-1} (panels (d) and (e)). After its decay, the remaining absorbance changes are due to the CPD lesions, the lowest triplet state and potentially other long-living states (panel (f)).

The data have been recorded in a temporal window from 0 ps to 2 ns. If excimers/charge separated states exist in thymidine oligonucleotides, they should be formed immediately out of the excited $^1\pi\pi^*$ or exciton state and decay on a timescale that is similar to that of excimer decay in other dimers or oligonucleotides. In different DNA dimers, the lifetime of charge separated states varies between 20 ps and 300 ps [Buc14a]. The analysis of the excited state physics of $(dT)_{18}$ is therefore focussed on a similar time window. Figure 6.1 depicts the absorbance changes within the first 500 ps. The panels on the left side ((a),(b),(c)) show the raw data. After UV absorption most of the excited bases return to a vibrationally excited ('hot') ground state by a conical intersection with a sub-picosecond time constant [PPK00]. The corresponding absorbance changes are the difference in absorption of the vibrationally excited ('hot') and the relaxed ground state. The hot ground state exhibits broad, red-shifted absorptions, giving rise to difference spectra like the ones in section 3.4 (see panel (b)). The excess vibrational energy is dissipated to the solvent within circa 10 ps, thereby heating the solvent. At delay times higher than 10 ps, vibrational cooling is finished. Then, the absorbance changes are due to the heating of D_2O (dashed grey in panel (c)), the CPD lesion and long-living excited states (see panel (c)). Between 20 ps and 500 ps the signal changes significantly, indicating the decay of at least one excited state.

Since the signature of the solvent somewhat obscures the data, the time-dependent signals of solvent heating are subtracted from the data. The subtraction of the solvent signal was explained in more detail in subsection 3.4.3, it is also demonstrated in section A.1. The right side of Figure 6.1 shows the resulting data (see panels (d)–(f)). After the correction, the excited state kinetics are more clearly visible. There is a clear absorption band at 1570 cm^{-1} that decays on the 100 ps timescale. The ground state bleach between 1600 cm^{-1} and 1700 cm^{-1} partially recovers on the same timescale (see panels (c) and (f)). After its decay, the residual absorbance changes are due to the CPD lesion and long-living states like the $^3\pi\pi^*$ state (see chapter chapter 5) and possibly others (see chapter 7).

6.1.2. Multiexponential Modelling of the Data

A global fit of the data reveals the decay associated difference spectra (DADS) of the excited states (see Figure 6.2). Since absorbance changes shortly after UV excitation are dominated by vibrational cooling (VC), the first 10 ps are excluded from the fit. Then, the small remainders of VC after 10 ps can be approximated by a single exponential decay with a time constant around 10 ps. The corresponding DADS contains only information on vibrational cooling. It is therefore not shown in Figure 6.2. The right side of Figure 6.2 depicts the temporal evolution of the absorbance changes and the global fit at 1570 cm^{-1}, 1664 cm^{-1} and 1700 cm^{-1}. The data is apparently well described by the multiexponential fit, validating the obtained DADS (see panels (d)–(f)). Three DADS characterise the excited state decay of

$(dT)_{18}$. As already stated, the remaining absorbance changes after 2 ns (panel (c)) are comprised of the signatures of solvent heating, of the CPD lesion (see the CPD marker bands in the fingerprint region from 1300 cm^{-1} to 1500 cm^{-1}) and of the $^3\pi\pi^*$ state (see section 5.2). Another excited state decays with a time constant of 1000 ps (panel (b)). Its characteristic feature is a blue-shifted absorption around 1740 cm^{-1}. This state is also observed in TMP, it is therefore localised on one base. This state is addressed in chapter 7.

The absorbance changes in the first few hundred picoseconds are dominated by an excited state decay on the 100 ps timescale. The corresponding DADS is depicted in Figure 6.2, panel (a).

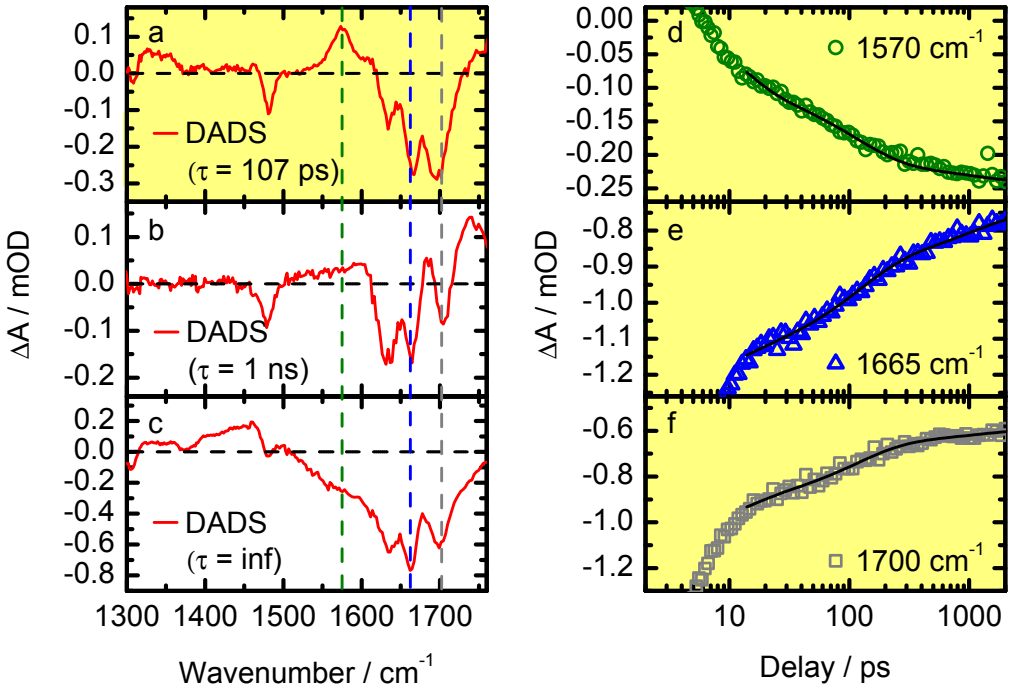

Figure 6.2.: Global multiexponential fit of $(dT)_{18}$ after UV excitation in the time window from 15 ps to 2000 ps. The fit describes the data accurately (right panels) with 4 time constants. One of them (10 ps) approximates the residual signals of vibrational cooling. Its DADS is therefore not shown. Two excited state decays exist in the time window from 15 ps to 2 ns: a 100 ps decay that is only observed in $(dT)_{18}$ and a 1000 ps decay that also exists in TMP. The residual absorbance change (panel (c)) can be attributed to the heating of the solvent, the CPD lesion and the triplet state $^3\pi\pi^*$.

It is characterised by a ground state bleach between 1600 cm^{-1} and 1700 cm^{-1} and a red-shifted absorption around 1570 cm^{-1} (see panel (a) of Figure 6.2). This marker band is visible immediately after UV excitation (see panel (d) of Figure 6.1), so the

state (denoted as X in the following) is formed directly out of the excited singlet or exciton state within less than 1 ps.

6.1.3. Quantum Yield of X

The quantum yield of X can be estimated by comparing its DADS to that of a state or photoproduct of $(dT)_{18}$ with known quantum yield. Such a photoproduct is the CPD lesion, because the quantum yield can be measured precisely by steady-state spectroscopy. Banyasz et al. determined it to be 5 % [Ban12]. Since UV irradiation of $(dT)_{18}$ yields X and the CPD lesion alike, the corresponding DADS can be compared.

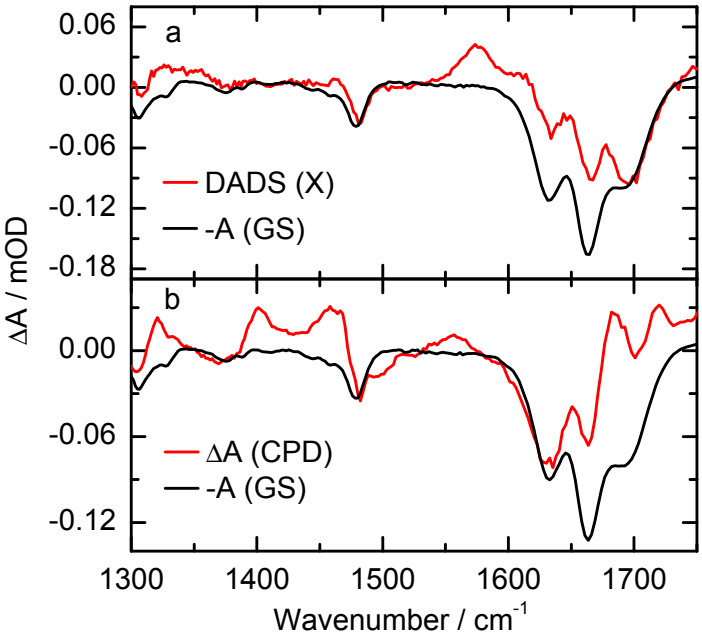

Figure 6.3.: Comparison of the amplitudes of the DADS of X (a) and the absorbance difference spectrum of the CPD lesion (b) to estimate the quantum yield of the former. To improve the precision, not the absorbance changes themselves but rather the corresponding ground state bleach spectra are compared. From the CPD quantum yield of 5 % [Ban12], a quantum yield of circa 7 % for X is calculated.

However, comparing the amplitudes of some absorbance bands of the two DADS is potentially misleading: The amplitudes of the absorbance changes depend not only on the amount of the formed state, but also on the extinction changes between excited state (ES) and ground state (GS): $\Delta\epsilon(\lambda) = \epsilon_{ES}(\lambda) - \epsilon_{GS}(\lambda)$. Different absorbance change amplitudes of X and the CPD lesion can therefore be partly due to different amounts of the states and partly due to different extinction changes. So, rather than using the absorbance changes themselves, the corresponding ground state bleaches

are calculated and compared in amplitude. Figure 6.3 shows the DADS of X (panel (a)) and the CPD lesion (panel (b)) in red and the inverted corresponding ground state absorbance spectra (black). When scaling the ground state spectra, one point has to be considered: each of the CPD lesions is caused by one photon, but its DADS is caused by the two bases involved in the CPD lesion. If X is localised on one base, this factor of two has to be included in the calculations, resulting in a quantum yield from 12 % to 14 %. If X also involves two bases, like a charge separated state would, the quantum yield is from 6 % to 7 %.

6.2. Hypotheses about X in the Literature

An excited state decay of $(dT)_{18}$ on the timescale of 100 ps was already reported by other groups [HCK07, KMP08]. Several interpretations were considered:

1. Long-living localised states like $^1n\pi^*$ [HCK07].
2. The formation of a photoproduct like a CPD lesion out of a long-lived state like $^3\pi\pi^*$ [KMP08].
3. A delocalised state like an excimer/charge separated state. Such states were discussed in other dimers or oligonucleotides [Tak08, Buc14a], but not in thymidine strands.

The first two possibilities are discussed in the following, before evidence for the third possibility is given.

6.2.1. A Localised State?

Hare et al. reported a 100 ps decay of photoexcited TMP and $(dT)_{18}$, which they identified as a $^1n\pi^*$ state [HCK07]. The existence of $^1n\pi^*$ states is supported by numerous theoretical studies (see for example [EFM09, Ser07, Gon10a] and many more). However, the 100 ps decay in TMP was not found by other authors [KMP08, Sch08]. To resolve this contradiction, TRIR spectroscopy of TMP was performed (identical conditions as in the $(dT)_{18}$ measurements) for comparison.
Figure 6.4 depicts the excited state kinetics of $(dT)_{18}$ (left) and TMP (right). The contour plots show the data after time-dependent subtraction of the signature of solvent heating (see section A.1) and subsequent subtraction of the respective absorbance changes after 500 ps. Both contour plots show absorbance changes on the timescale of hundreds of picoseconds. However, the marker band of X at 1570 cm^{-1} is clearly visible in $(dT)_{18}$ and equally clearly absent in TMP. Comparing the transient spectra of both samples at a delay time of 30 ps, $(dT)_{18}$ shows a stronger ground state bleach between 1600 cm^{-1} and 1700 cm^{-1} and the additional 1570 cm^{-1} band. At a delay time of 200 ps after excitation the absorbance changes of TMP and $(dT)_{18}$

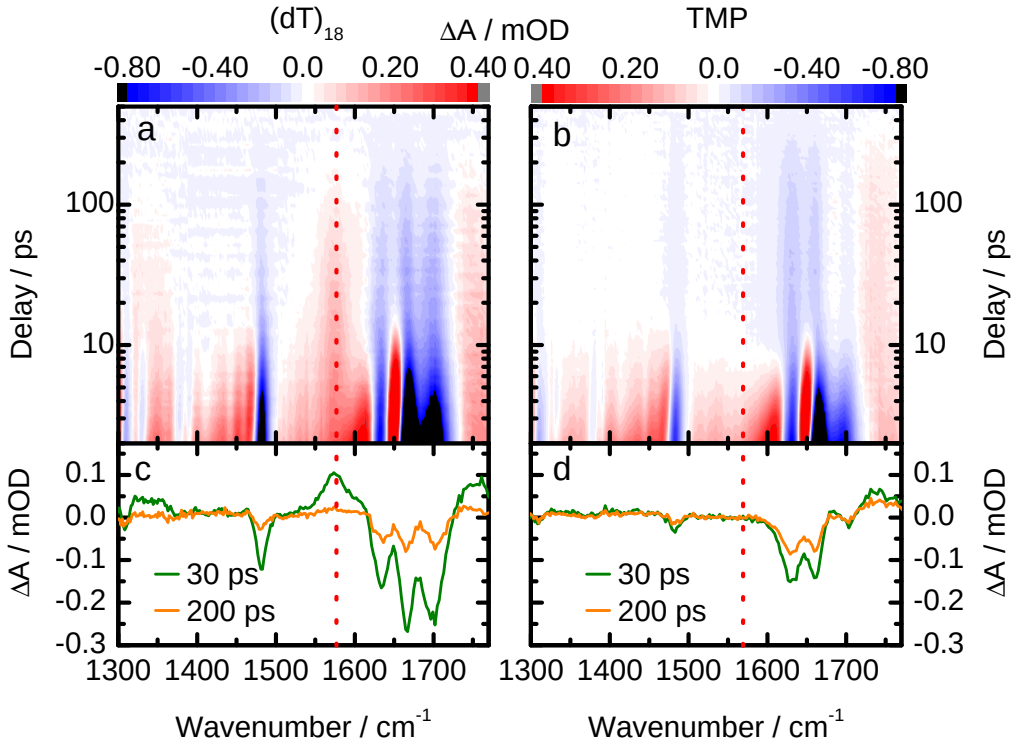

Figure 6.4.: $(dT)_{18}$ (left panel) versus TMP (right panel) after UV irradiation. The absorbance changes caused by X are only observed in $(dT)_{18}$, but not in TMP.

are quite similar (see panels (c) and (d)). These are in both cases caused by the longer-living state that decays on the 1000 ps timescale. The data show clearly that X is only present in the strand $(dT)_{18}$ and not in the nucleotide TMP. TMP does not show an excited state decay on the 100 ps timescale, nor an excited state decay that is characterised by an absorption around 1570 cm^{-1} on any timescale.

In conclusion, X is present only in thymidine strands, not in nucleotides. It is therefore not a $^1n\pi^*$ state that would be localised on a single base. Still, the question remains how Hare et al. found an excited state decay of TMP on the 100 ps timescale. An answer is given by dichroic measurements, i.e. such that use differently polarised excitation pulses. If the magic angle polarisations are not applied, the reorientational motion of TMP is observed in addition to the excited state kinetics. These signals can easily be confused with excited state kinetics. The reorientational time of TMP happens accidentally to be 100 ps (see chapter 7), the same as the decay time of X in $(dT)_{18}$. In conclusion, a 100 ps decay is only observed in thymidine oligomers, not monomers. The hypothesis that this excited state is of $n\pi^*$ nature can therefore be excluded from the discussion.

6.2.2. CPD Formation Out of the Triplet State?

An excited state decay in thymidine oligomers with a time constant around 100 ps was already reported and (tentatively) assigned to the formation of CPD lesions out of the $^3\pi\pi^*$ state [KMP08]. This interpretation is highly unlikely in view of other findings: the CPD lesions are predominantly formed out of the excited singlet state within 1 ps [Sch07, Sch09]. No CPD increase on the 100 ps timescale was reported in these studies. Moreover, the triplet decay of single-stranded thymidine was observed on the nanosecond timescale [Pil14a]. In thymidine oligomers the triplet state decays via a biradical intermediate to the ground state (see chapter 5).

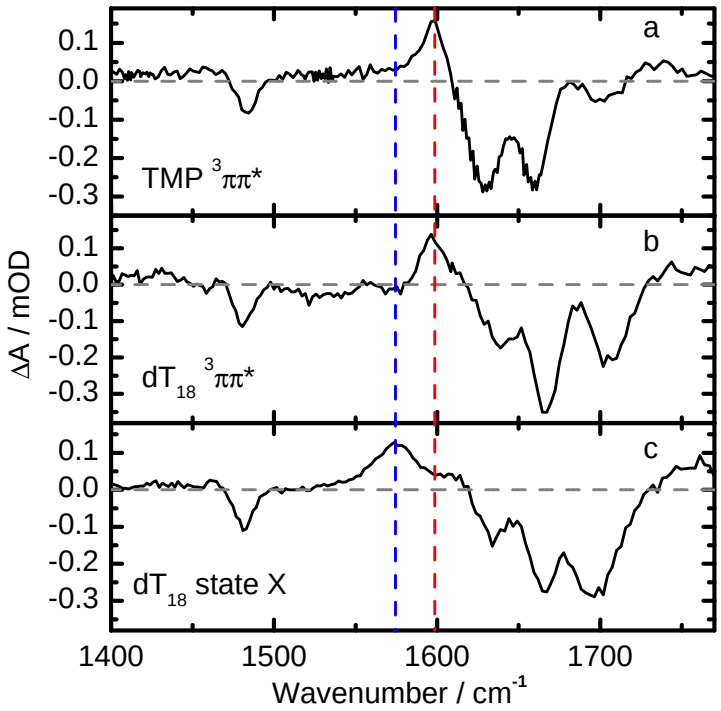

Figure 6.5.: DADS of the $^3\pi\pi^*$ state of TMP (a) and $(dT)_{18}$ (b) and of X (c). Clearly, the latter is not a triplet decay, since it lacks the triplet marker band around 1600 cm^{-1} and exhibits instead a marker band at 1570 cm^{-1}.

The timescale of biradical formation (12 ns, see chapter 5) is determined by the time it takes for unstacked bases to reach a suitable conformation [Pil14a]. So, there could be a faster triplet decay between stacked bases, possibly on a sub-ns timescale. However, only a small fraction of the thymine bases are stacked [GS78, JW07a], so only a small fraction of the triplet states could decay by this mechanism. The expected amplitudes would be barely observable, if at all. Additional evidence against the proposed mechanism can be gained by evaluating the absorbance spectra

more closely. If the triplet state decayed to a CPD lesion, to the ground state or to some other photoproduct on the 100 ps timescale, the corresponding DADS would show the absorption difference between the $^3\pi\pi^*$ state and the ground state or CPD lesion or other photoproduct, respectively. Consequently, the triplet marker band around 1600 cm^{-1} would be present. Figure 6.5 shows a comparison of the absorbance changes caused by the triplet state of TMP and $(dT)_{18}$ (panels (a) and (b)) and DADS of X (panel (c)). Unlike the former, the latter clearly does not absorb at the triplet marker position; it therefore does not describe a transition out of the triplet state.

The observed state is likely to be a delocalised state like an exciton, excimer or a fully charge separated state. Excitons should be present on the timescale of only few picoseconds [Vay10, Vay12]. Exciplexes have been reported in many dimers and in adenine oligonucleotides [Tak08]. Bucher et al. provided direct spectroscopic evidence for charge separated states [Buc14a] by measuring the spectra of DNA cations and comparing them to the DADS of long-living states in oligonucleotides. Cations can be generated by two-step ionisation of the sample [Nik90, Buc14b] (see also subsection 3.4.5). The DADS of the thymine cation can be determined in the same way. It is, however, insufficient to decide whether X is an excimer/charge separated state or not. The spectral characterisation of the thymine anion is additionally required to calculate reliably the absorbance change caused by a hypothetical charge separated state.

6.3. Charged States in Model Systems

UV excitation of thymidine can yield its cations, but not its anions. However, there are charge separated states in dimers that contain thymine, in which an electron is transferred onto it. The IR signature of such a state was firstly reported by Doorley et al. [Doo13]: upon UV excitation, stacked ApT dimers undergo charge transfer to yield $A^{\bullet+}pT^{\bullet-}$. This state has a lifetime of 75 ps, similar to other charge separated states reported by Bucher and coworkers [Buc14a]. By measuring the DADS of this charge separated state and of the adenosine radical cation $A^{\bullet+}$, the DADS of $T^{\bullet-}$ can be derived. Together with the spectrum of the thymidine radical cation, the spectrum of a hypothetical charge separated state in $(dT)_{18}$ can be calculated. In this section, the decay associated difference spectra of the thymidine radical anion and cation are derived, to compare the resulting hypothetical charge separated state of $(dT)_{18}$ to X.

6.3.1. Charge Transfer in TpA

Based on the aforementioned study, TRIR spectroscopy of TpA and ApT was performed to obtain the absorption difference spectra of the charge separated states. Both samples undergo charge separation, only the amplitudes and the charge recombination time constants differ somewhat. To avoid redundancies, the discussion in the following will be limited to TpA.

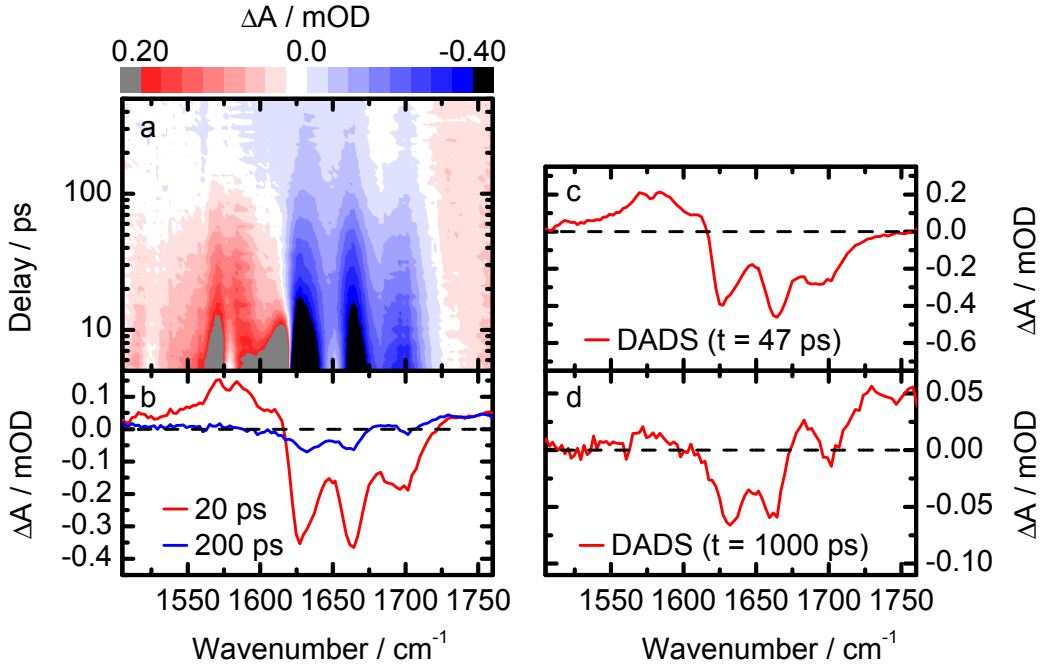

Figure 6.6.: (a) Absorbance changes of TpA after UV excitation. The data were corrected for heating of the solvent and the remaining absorbance change after 1500 ps. Panel (b) shows the transient spectra 20 ps and 200 ps after UV absorption. The right panels show the DADS of the excite states that decay within 2 ns. After vibrational cooling (after circa 10 ps), the absorbance changes are dominated by the charge separated state that was already reported by Doorley et al. [Doo13]. The long-living state (panel (d)) is also observed in TMP and $(dT)_{18}$ (see section 6.1 and chapter 7).

TRIR spectroscopy of TpA was performed in a temporal range between 0 ps and 1500 ps. Charge transfer occurs directly after UV excitation out of the $^1\pi\pi^*$/exciton state, charge recombination happens within 100 ps [Doo13]. The corresponding absorbance changes are overlayed by the signals of solvent heating and of long-living excited states. These excited states are the $^3\pi\pi^*$ of thymine (see chapter 5) and the cations of adenine and thymine that have been generated by two-step photo-ionisation of the respective base (for a discussion of long-living states, see for example [Mid09]). The lifetimes of those states are orders of magnitude higher than the maximum delay of 1.5 ns [Pil14a, Reu00], so their amplitudes do not change in the investigated time

window. In the following, the absorbance change at the maximum delay time of 1500 ps is therefore treated as a constant background and subtracted from the data.

Figure 6.6 depicts the resulting data after the background subtraction. The contour plot in panel (a) of Figure 6.6 shows the data in the temporal window from 5 ps to 500 ps. In the first 10 ps, vibrational cooling (VC) dominates the absorbance change. After VC is finished, two excited states can be distinguished. One of them decays to the ground state within 100 ps. It is characterised by ground state bleaches around 1624 cm^{-1}, 1660 cm^{-1} and 1700 cm^{-1} and an absorption increase around 1570 cm^{-1}. After the decay of this state, absorbance changes persist (see panel (b)). The characteristic feature is a blue-shifted absorption at 1740 cm^{-1}. This state decays with a time constant of 1000 ps (see panel (c)). It is also observed in TMP and $(dT)_{18}$ (see section 6.1 and chapter 7), so it is localised on thymidine (for a discussion of this state see chapter 7).

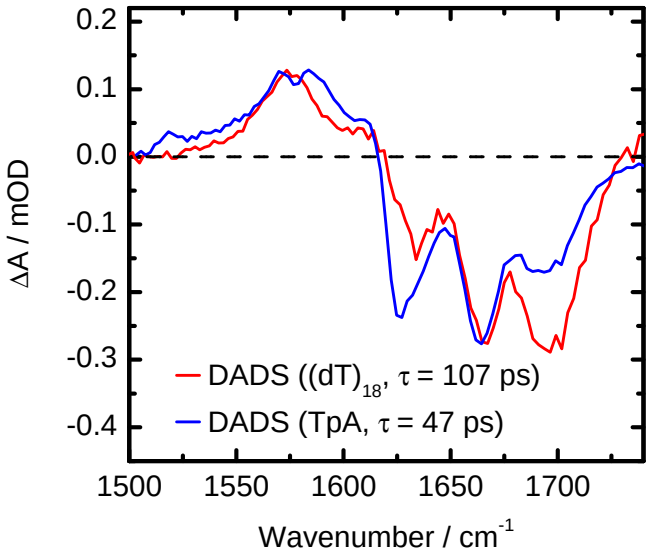

Figure 6.7.: Comparison of the DADS of the supposed charge separated states of $(dT)_{18}$ (red) and TpA (blue). The spectra were scaled to the same amplitude. If the DADS of $(dT)_{18}$ represents charge transfer, both states would have the same anion, but different cations, possibly explaining the similarities and the differences between both spectra. This assumption will be further examined in the following sections.

The DADS of the relatively short-living state (lifetime 47 ps, see panel (c) of Figure 6.6) agrees well with the charge separated state of ApT that was reported by Doorley et al. [Doo13]. Following the discussion of this study, a fraction of the dimers are stacked (38 % stacked bases were reported for ApT, a similar number is expected in TpA). They undergo charge transfer, while the unstacked bases behave like monomers, i.e. decay via localised states. The data indeed show a very significant

charge transfer signature, reflecting the relatively high stacking probability, along with a long-living localised state of thymidine that probably occurs only in unstacked dimers.

The DADS of the charge separated state of TpA is an important guideline to the investigation of charge transfer in thymidine oligomers. In TpA and $(dT)_{18}$, charge transfer would result in the same radical anion ($T^{\bullet-}$), with different radical cations ($T^{\bullet+}$ and $A^{\bullet+}$, respectively). The DADS of both charge separated states should therefore show some similar anion features and different cation features. Figure 6.7 gives a comparison of both spectra. They were scaled to the same amplitude to make the comparison easier. Strikingly, both spectra show an absorption around $1570\,cm^{-1}$. A slight dip at $1577\,cm^{-1}$ is present in TpA, that is likely related to a ground state bleach of adenine (see section 4.2) upon charge transfer. The same explanation can be given for the stronger ground state bleach of TpA at $1624\,cm^{-1}$. Around $1690\,cm^{-1}$, the DADS of $(dT)_{18}$ shows a stronger ground state bleach, that is possibly related to the absorbance changes of the thymidine radical cation which is not present in TpA. This preliminary analysis suggests that the spectrum of the hypothetical charge separated state of $(dT)_{18}$ can be calculated according to Equation 6.1:

$$T^{\bullet+}pT^{\bullet-} = T^{\bullet+} + (T^{\bullet-}pA^{\bullet+} - A^{\bullet+}) \tag{6.2}$$

Having obtained the DADS of the charge separated state $T^{\bullet-}pA^{\bullet+}$, the DADS of the cations $T^{\bullet+}$ and $A^{\bullet+}$ are needed.

6.3.2. Photoinduced Cations: Sample Selection

Short and intense UV pulses can ionise DNA bases (see section 3.4), leading to radical cations and solvated electrons [Reu00]. Solvated electrons do not absorb in the MIR [HMS71, JF77, JF79], therefore the resulting absorbance changes are due to the cations only. To obtain the difference spectra of the cations, two measurements of the same sample are performed, using the same excitation energy, but different pulse durations. This is easily achieved by using fs and ns excitation pulses, respectively (see section 3.3). The differences of the resulting data can be attributed to the absorbance changes due to the cations (see subsection 3.4.5).

To calculate the absorbance change caused by a hypothetical charge separated state of $(dT)_{18}$ according to Equation 6.1, the spectra of the cations of T and A are needed. They can be gained by investigating either nucleotides or oligomers of A and T. Determining whether nucleotides or oligonucleotides should be investigated requires some considerations: In the oligomers the bases are partially stacked. The IR spectra are affected by base stacking, as seen by the comparison of the absorption spectra of TMP and $(dT)_{18}$ and of AMP and $(dA)_{18}$ (see Figure 6.8). The left panel of Figure 6.8 shows the extinction coefficients per base of AMP and $(dA)_{18}$. Obviously, these spectra differ significantly. The absorbance band at $1624\,cm^{-1}$ of

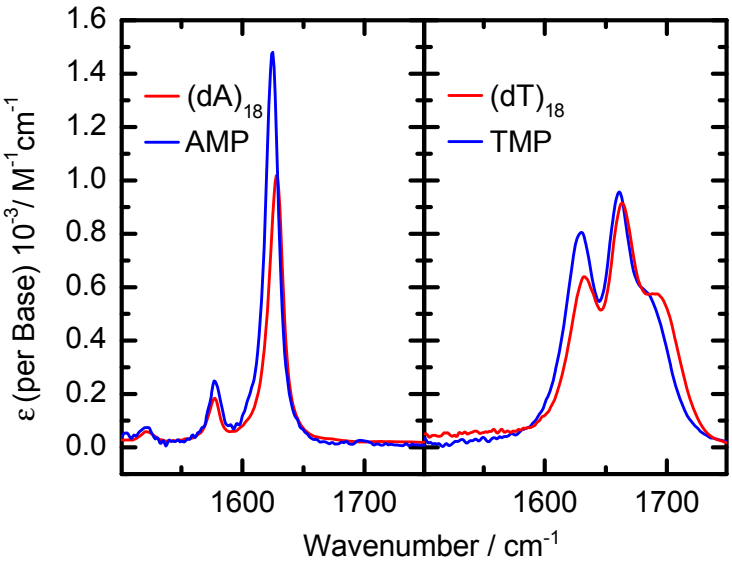

Figure 6.8.: Comparison of the extinction coefficients of AMP to $(dA)_{18}$ (left) and TMP to $(dT)_{18}$ (right). Base stacking in the oligomers affects the spectra profoundly, resulting in frequency shifts and amplitude changes of various bands. Especially $(dA)_{18}$ shows a very strong hypochromic effect.

AMP (assigned to C=N and C=C double bonds, see [BSG03]) is shifted to 1628 cm^{-1} in $(dA)_{18}$, while the extinction shows a hypochromicity of 30 % (see Figure 6.8, right panel)[1]. The minor absorption band at 1575 cm^{-1} also decreases in amplitude by about 30 %, while the position is unchanged. The thymine vibrational spectra (right panel of Figure 6.8) change less drastically, but still significantly due to base stacking: the C5=C6 vibration around 1630 cm^{-1} is reduced due to base stacking, the C2=O mode at 1664 cm^{-1} is basically unchanged, and the C2=O vibration at 1675 cm^{-1} is blue-shifted to around 1685 cm^{-1}.

Spectral modifications by base stacking like those in the ground state can also be expected to occur in excited states and 'photoproducts'like cations. If charge transfer occurs in dimers or oligonucleotides, it requires properly stacked bases [Tak08, LRH08]. Therefore, the charge separated state of TpA consists of stacked cations and anions. The cations of $(dT)_{18}$ and $(dA)_{18}$ are affected by the partial base stacking of the strand. It is therefore plausible to assume, that their IR spectra resembles that of the charge separated states more closely than those of the cations of TMP and AMP. In the case of adenine, this assumption can be directly validated by reviewing the data published by Doorley et al. [Doo13]. The authors of this study report a hypochromic effect of adenine in stacked TpA dimers similar to that of $(dA)_{18}$. Consequently, the oligomers $(dT)_{18}$ and $(dA)_{18}$ were investigated.

[1]For a discussion of hypochromicity see [Tin60, Rho61, FH65, LF66, MGL75].

6.3.3. Photoinduced Cations $(dA)_{18}^{\bullet+}$ and $(dT)_{18}^{\bullet+}$: Results

Two TRIR measurements of the photophysics of $(dT)_{18}$ were performed using excitation pulses with pulse durations of 1 ps and of 0.7 ns. The sub-picosecond pulses were provided by the third harmonic of the fs-laser (excitation wavelength 266 nm, pulse energy 2 µJ). The pulse duration of the third harmonic is around 250 fs.

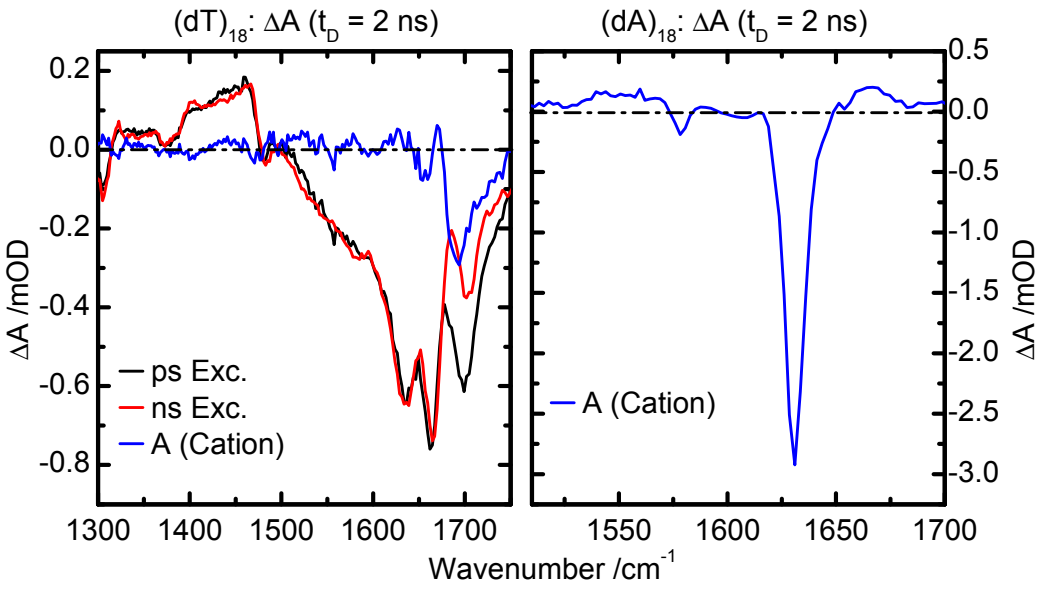

Figure 6.9.: Left: $\Delta A((dT)_{18}, t_D$=2 ns) after excitation by short (1 ps duration) (black) and long (0.7 ns duration) pulses at a wavelength of 266 nm (energy 2 µJ). The difference is due to the cation formation (blue). Right: $(dA)_{18}$ 2 ns after UV excitation with a sub-ps pulse (4 µJ pulse energy). The absorbance changes are due to the generated cation. The spectrum has been corrected for the heating of the solvent.

For this measurement, it is increased to almost 1 ps by transmitting the pulses through a block of fused silica. This limits the amount of generated cations, but it also keeps the distortion of the 'one-step' photophysics, i.e. the excited state physics triggered by absorption of one photon, small. Then the obtained data differs from that of the one-step photophysics only because of the signals of the cations. The one-step photophysics is probed by using excitation pulses with a duration of almost nanoseconds, which reduces the intensity by three orders of magnitude and therefore prevents two-step ionisations of the bases. These pulses (wavelength 266 nm, pulse energy 2 µJ) are provided by the fourth harmonic of the AOT ns-laser. Picosecond and nanosecond excitation make the delay ranges from (sub-)ps to 3 ns and from 0.7 ns to 100 µs accessible, respectively. The resulting data of both measurements have to be compared in the temporal overlap region between 1 ns and 3 ns. The data are therefore evaluated at 2 ns, well after excitation even with the longer (0.7 ns)

pulses. A higher delay value is not chosen, because the adjustment of the mechanical delay stage with very high precision is troublesome over the entire delay range.

After 2 ns the absorbance changes are due to heating of the solvent, the signatures of the UV-induced CPD lesions, the long-living $^3\pi\pi^*$ state (see chapter 5) and additional cations only in the measurement that used the short excitation pulses. The relatively minor ionisation consumes only a small fraction of the excitation energy. Therefore, the same percentage of the excitation energy is converted to heating of the solvent by vibrational cooling with short and long excitation pulses. This allows to scale both spectra very precisely to the same excitation energy by using the signature of the solvent heating. The resulting spectra are shown in the left panel of Figure 6.9. The difference in absorbance yields the absorbance change caused by the cations. It consists predominantly of a ground state bleach around 1700 cm^{-1}. The other absorbance changes in the range between 1600 cm^{-1} and 1700 cm^{-1} are negligible in comparison.

In the case of $(dA)_{18}$, no excited states exist 2 ns after UV absorption [KMP06, Mid09]. Hence a measurement using the ns-laser is not necessary; besides the signature of heating of the solvent, the entire absorbance change after 2 ns is due to the cations. Since it does not have to be compared to pure excited state physics triggered by one photon, the yield needs not to be limited by increasing the pulse duration or reducing the energy. Therefore, the pulse duration is not increased from circa 250 fs to 1 ps and the pulse energy is 4 µJ to obtain a larger amplitude and a better accuracy. The resulting difference spectrum is depicted in the right panel of Figure 6.9. They are characterised by ground state bleach at 1628 cm^{-1} and 1577 cm^{-1} and small positive absorption bands at 1660 cm^{-1} and around 1550 cm^{-1}.

6.4. Identification of the Charge Separated State $T^{\bullet+}pT^{\bullet-}$

In the previous section the decay associated difference spectra of the charge separated state of TpA and the cations of $(dA)_{18}$ and $(dT)_{18}$ were presented. These spectra are analysed further in this section . To be able to quantify the amount of those states/photoproducts by the amplitude of the absorbance change they induce, the extinction changes associated with their formation are determined. Being able to scale the various difference spectra to each other, the DADS of the hypothetical $T^{\bullet+}pT^{\bullet-}$ is calculated from the spectra of $(dA)_{18}{}^{\bullet+}$, $(dT)_{18}{}^{\bullet+}$ and $T^{\bullet-}pA^{\bullet+}$ according to Equation 6.1. The $T^{\bullet+}pT^{\bullet-}$ state is then compared to X.

6.4.1. Scaling of the Spectra

The absorbance difference spectrum of a hypothetical charge separated state $T^{\bullet+}pT^{\bullet-}$ can be calculated from the spectra of the cation and the anion that comprise it. The cation can be observed after two-step photoionisation of $(dT)_{18}$, whereas the anion

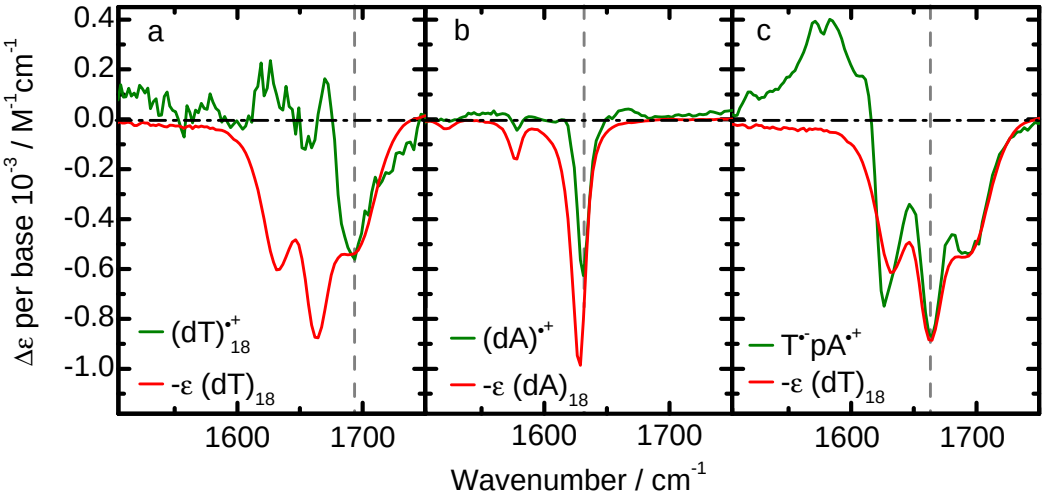

Figure 6.10.: The extinction coefficients of the cations and of the $T^{-}pA^{+}$ state are estimated by calculating the corresponding ground state bleaches. The extinction of the T containing species is compared to the ground state extinction of $(dT)_{18}$ (panels (a) and (c)), the A cation is scaled to the $(dA)_{18}$ extinction (b) to determine its extinction change.

has to be derived from the data of $T^{\bullet-}pA^{\bullet+}$ and $(dA)_{18}{}^{\bullet+}$. The resulting spectra need to be scaled so their amplitudes represent the same concentration of cations and anions. The well-known law of Lambert-Beer can be used to calculate the absorbance change caused by a photoproduct:

$$\Delta A = \Delta\epsilon \cdot c_{PR} \cdot d, \tag{6.3}$$

where c_{PR} denotes the concentration of the photoproduct, d the sample thickness and $\Delta\epsilon$ the change of extinction between the photoproduct and the ground state. Scaling the difference spectra to the same concentration and the same sample thickness therefore requires knowledge of the extinction changes $\Delta\epsilon$. The ground state extinction can easily be determined by conventional IR spectroscopy (this was done in [Sch08]). Figure 6.10 shows how the ground state extinctions are used to calculate the extinction differences of $(dA)_{18}{}^{\bullet+}$, $(dT)_{18}{}^{\bullet+}$ and $T^{\bullet-}pA^{\bullet+}$. The cations of $(dT)_{18}$ and $(dA)_{18}$ were scaled to their ground state absorbance spectra (panels (a) and (b)). In the case of $T^{\bullet-}pA^{\bullet+}$, the DADS would ideally be scaled to the ground state extinction of the stacked TpA dimers, since only stacked bases undergo charge transfer [CCK05, Tak08, Doo13]. These data are not easily available, as the TpA ground state absorbance represents both stacked and unstacked dimers. The IR-spectra of stacked and unstacked TpA differ substantially [Doo13], mainly because of the strong hypochromic effect of adenine (see the comparison of TMP to $(dT)_{18}$ and AMP to $(dA)_{18}$ in subsection 6.3.2). Since adenine does not absorb in the

Species	Wavenumber ν/cm^{-1}	$\Delta\epsilon(\nu)$ (per Base)/$\mathrm{M}^{-1}\mathrm{cm}^{-1}$
$(\mathrm{dA})_{18}^{\bullet+}$	1631	630
$(\mathrm{dT})_{18}^{\bullet+}$	1693	560
$\mathrm{T}^{\bullet-}\mathrm{pA}^{\bullet+}$	1664	880

Table 6.1.: Molar extinction changes of $(\mathrm{dA})_{18}^{\bullet+}$, $(\mathrm{dT})_{18}^{\bullet+}$ and $\mathrm{T}^{\bullet-}\mathrm{pA}^{\bullet+}$ per base at selected wavenumbers.

region from $1640\,\mathrm{cm}^{-1}$ to $1700\,\mathrm{cm}^{-1}$, that part of the DADS of $\mathrm{T}^{\bullet-}\mathrm{pA}^{\bullet+}$ is entirely due to thymine. It can therefore be scaled to the inverted ground state of $(\mathrm{dT})_{18}$. Table 6.1 shows the molar extinction changes $\Delta\epsilon$ (per base) at the wavenumbers (see dashed lines in Figure 6.10) where they are largest.

6.4.2. Calculation of the Spectra

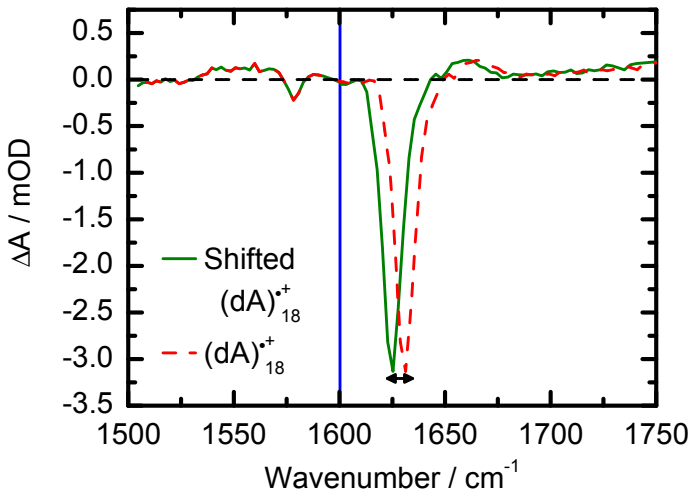

Figure 6.11.: The adenine absorption is profoundly modified by stacking interactions. It results in a strong hypochromic effect as well as a shifting of the absorbance band. T–A and A–A stacking result in comparable hypochromic effects, but in different spectral shifts [Doo13]. To account for this effect, the spectrum of $(\mathrm{dA})_{18}^{\bullet+}$ above $1600\,\mathrm{cm}^{-1}$ is red-shifted by $6\,\mathrm{cm}^{-1}$ to model the expected spectrum of the cation in $\mathrm{T}^{\bullet-}\mathrm{pA}^{\bullet+}$.

The analysis presented so far determined the spectra and the extinction changes of the cations $(\mathrm{dA})_{18}^{\bullet+}$ and $(\mathrm{dT})_{18}^{\bullet+}$. This is not sufficient to calculate the DADS of the thymidine anion in $\mathrm{T}^{\bullet-}\mathrm{pA}^{\bullet+}$ and the hypothetical charge separated state of $(\mathrm{dT})_{18}$, because base stacking affects adenine in TpA and $(\mathrm{dA})_{18}$ differently. While the magnitude of the hypochromic effects are similar, A–A stacking leads to a blue-shift

of the main absorbance band, while T–A stacking shifts it to the red [Doo13]. To deal with this effect, the obtained $(dA)_{18}^{\bullet+}$ spectrum has to be red-shifted from $1631\,cm^{-1}$ to $1625\,cm^{-1}$, while the minor absorption at $1577\,cm^{-1}$, that is not shifted by base stacking [Doo13], remains at the same spectral position. Figure 6.11 depicts how this adjustment is done. The DADS of $(dA)_{18}^{\bullet+}$ (dashed red) is divided into two parts, one above and one below $1600\,cm^{-1}$. The part below $1600\,cm^{-1}$ is not modified at all, the part above $1600\,cm^{-1}$ is red-shifted by $6\,cm^{-1}$. The resulting spectrum (green) should describe the adenine cation in $T^{\bullet-}pA^{\bullet+}$ quite well, since the hypochromic effect and the spectral shift have been taken into account.

6.4.3. DADS of the Charge Separated State $T^{\bullet+}pT^{\bullet-}$

Figure 6.12 depicts the stepwise determination of the DADS of the hypothetical charge separated state of UV-excited $(dT)_{18}$. Panel (a) shows the comparison of the DADS of the charge separated state of TpA (green) and the modified DADS (see previous subsection) of $(dA)_{18}^{\bullet+}$ (black), scaled to the same concentration. The difference between them yields the DADS of the thymidine anion. Panel (b) shows the DADS of thymidine cation (black) and anion (red). Adding these difference spectra yields the signature of the hypothetical charge separated state of $(dT)_{18}$. Panel (c) compares it (black) to the DADS of X (blue). Both spectra are virtually identical: They are both characterised by the absorption around $1570\,cm^{-1}$ and ground state bleaches around $1630\,cm^{-1}$, $1665\,cm^{-1}$ and $1690\,cm^{-1}$. It is apparent, that X is a charge separated state. Hence the excited state lifetime of around 100 ps is the timescale of charge recombination.

The time-resolved data of $(dT)_{18}$ show no evidence for the formation of a photoproduct out of the charge separated state. This conclusion is based on the signals of the ground state recovery between $1600\,cm^{-1}$ and $1700\,cm^{-1}$ without any discernible build-up of a photoproduct marker band. To substantiate this conclusion further, the data is reviewed more closely in the following section.

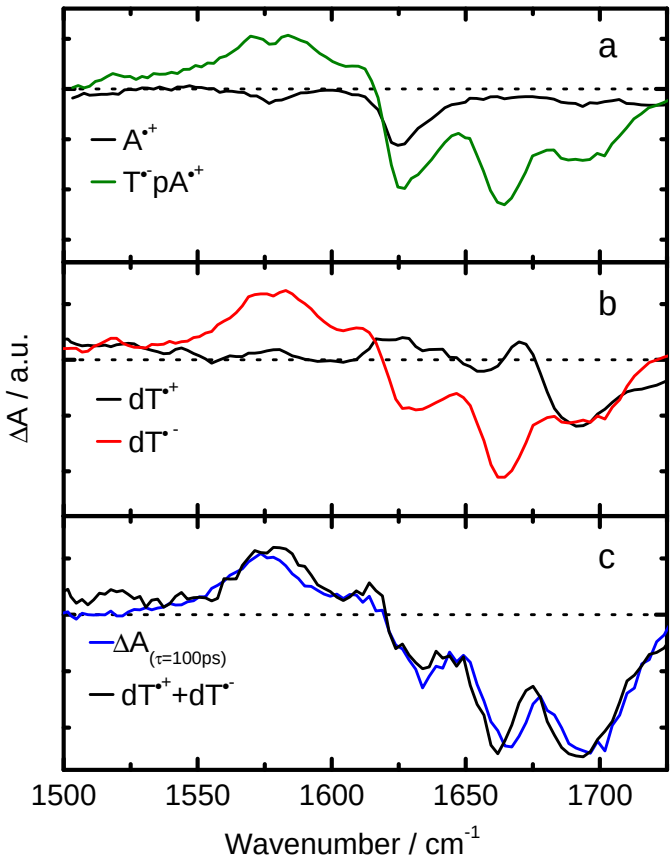

Figure 6.12.: (a) DADS of the charge separated state of TpA and of the cation of $(dA)_{18}$, scaled to the same concentration. Their difference yields the thymidine anion (red in panel (b)). Adding the DADS of the thymidine cation (black in panel (b)) and anion yields the DADS of the hypothetical charge separated state state (black in panel (c)). Comparing it to the DADS of X (blue in panel (c)) shows high agreement. Picture adapted from [Pil14b].

6.5. Discussion

6.5.1. Charge Recombination or Photoproduct?

The charge separated state can decay to the ground state by charge recombination or form a photoproduct.

Figure 6.13 shows the data of $(dT)_{18}$ after the time-dependent correction for the heating of the solvent and subsequent subtraction of the absorbance changes at a delay time of 500 ps. This eliminates the signals of all photoproducts and long-living states that do not change significantly in this time window. The resulting absorbance changes are then caused by vibrational cooling in the first 10 ps, the charge separated state and a minor contribution of the long-living state that decays with a 1000 ps

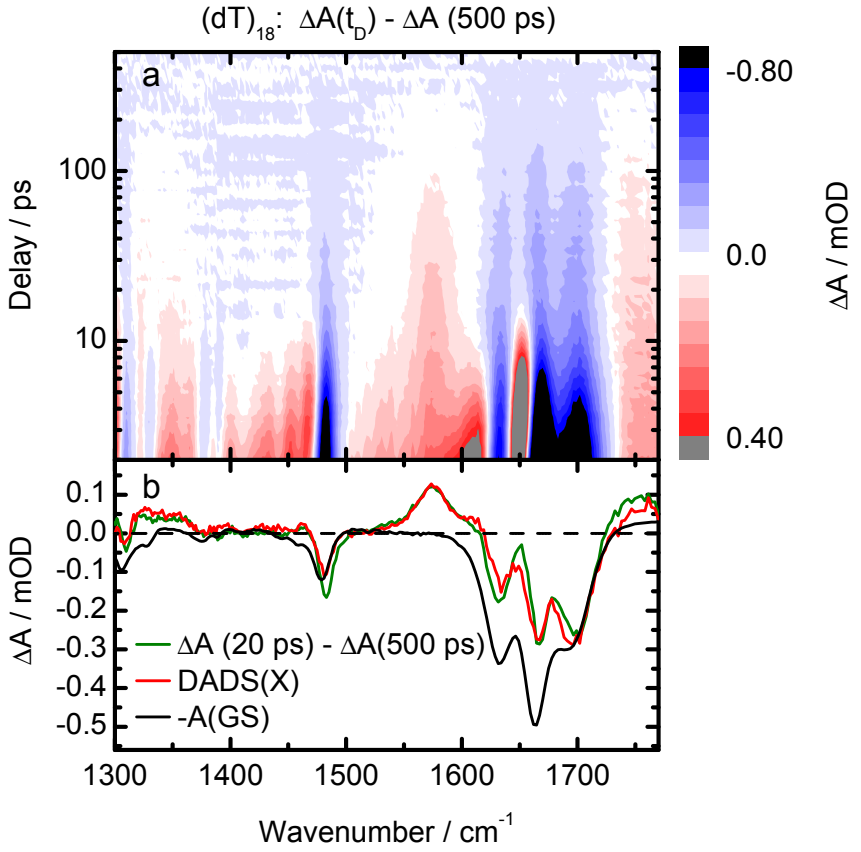

Figure 6.13.: (a) Double difference spectra $\Delta(\Delta A(t_D)) = \Delta A(t_D) - \Delta A(t = 500\,\text{ps})$ of UV-excited $(dT)_{18}$ after subtraction of the absorbance change at a delay time of 500 ps. After vibrational cooling is finished, the residual absorbance change in the first 200 ps is almost entirely due to charge transfer (see the comparison of the DADS of the charge separated state to the absorbance change at 20 ps in panel (b)). The decay of the CSS results in ground state recovery, not a photoproduct.

time constant. In the time window from 10 ps to 200 ps, the absorbance changes are almost entirely due to the decay of the charge separated state to the ground state/photoproduct. The latter possibility should result in the build up of some marker band absorption of the photoproduct on the 100 ps timescale. It furthermore should not result in a ground state recovery, but a persistent ground state bleach between 1600 cm^{-1} and 1700 cm^{-1} (see DADS of the charge separated state and the inverted ground state absorption in panel (b)). The only ground state bleach that is observed after the decay of the charge separated state is due to the decay of the long-living state. No trace of a photoproduct is observed at all. Taking into account the limitations of experimental accuracy, it cannot be excluded that less than 10 %

of the charge separated states decay by forming a photoproduct, but at least 90 % undergo charge recombination to the ground state.

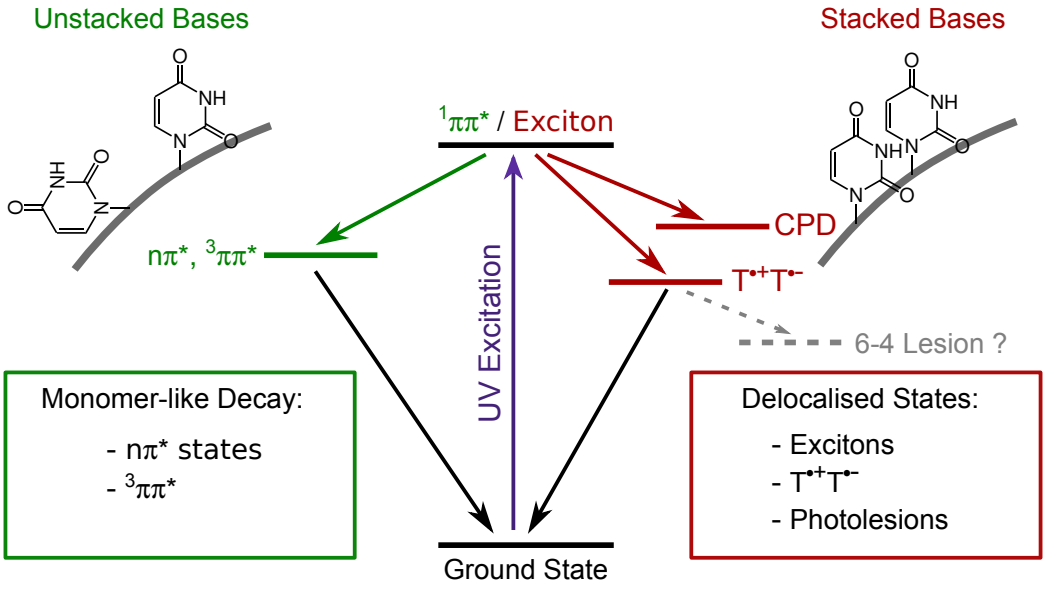

Figure 6.14.: Schematic illustration of the excited state decay of $(dT)_{18}$. Unstacked bases have the same excited states as the monomer TMP, while stacked bases are excited to an exciton, that can give rise to CPD lesions and charge transfer. The charge separated state decays predominantly to the ground state, but a small fraction might form oxetane intermediates that subsequently yield (6–4) lesions.

Even though charge recombination is by far the dominant decay mechanism of the charge separated state, there might be some photoproduct that cannot be detected due to its low yield. Recent computational studies suggest the formation of the precursor of the (6–4) lesion, the oxetane, out of charge separated states of thymidine dimers [Imp12, Ban12]. This transition is hampered by an energy barrier of almost 1 eV between the equilibrated CSS (i.e. the dipoles of the solvent have adapted to the charge distribution) and the oxetane. Then it seems plausible that charge recombination is more likely than oxetane formation, explaining the low quantum yield of the latter. These computational studies were published before direct evidence for charge transfer in $(dT)_{18}$ was reported. The identification of a CSS in $(dT)_{18}$ [Pil14b] insofar at least partly validates them. Concerning the formation of the oxetane and subsequently the (6–4) lesion, the experimental observation is hindered by the very low quantum yield of 0.4 %: Assuming the quantum yield for oxetane formation is the same, this overall quantum yield would imply that only 6 % of the charge separated states have to form oxetane intermediates. This small percentage is possibly consistent with the aforementioned energy barrier of 1 eV between the equilibrated CSS and the oxetane [Ban12]. However, so small an effect would be

below the experimental sensitivity. The observation of the CSS alone does not validate the proposed mechanism of (6–4) formation, because alternatives have been proposed by other theorists (like (6–4) formation out of a $^3n\pi^*$ state [Giu13]).

In conclusion, the photophysics of $(dT)_{18}$ can be summarized as depicted in Figure 6.14. The bases of $(dT)_{18}$ can be grouped into stacked and unstacked bases. Unstacked thymines behave just like the monomer TMP. The vast majority of photoexcited bases decay to the electronic ground state via a conical intersection [PPK00, PPK01]. The only long-living excited states that exist are localised on one base (like $^1n\pi^*$ states and the $^3\pi\pi^*$ state). They decay to the ground state on different timescales. The decay mechanisms are not shown in detail (for the decay of the $^3\pi\pi^*$ state see chapter 5). Stacked bases behave very differently: they can be excited to delocalised excitons that promote CPD formation [Sch07, Sch09, Ban12]. Another fraction of those excited states can undergo charge transfer. According to the already quoted study by Improta [Imp12], charge transfer can result in (6–4) lesions. This suggestion is depicted in dashed grey lines in Figure 6.14 to show its uncertainty. The vast majority of the charge separated states decay to the ground state with a time constant of 100 ps.

6.5.2. Electron Transfer Theory

UV-induced charge transfer can in principle start from other excited states than the $^1\pi\pi^*$ or exciton state. In this chapter the excited $^1\pi\pi^*$ or exciton state was identified as a precursor of charge transfer. Charge transfer was demonstrated to occur on the timescale of less than 1 ps and decay monoexponentially to the ground state with a time constant around 100 ps. No charge transfer was observed on any other timescale, other long-living excited states like the lowest triplet state $^3\pi\pi^*$ decay differently (see chapter 5). In the following, charge transfer rates out of the excited $^1\pi\pi^*$ and $^3\pi\pi^*$ states and the charge recombination rate to the ground state that were calculated by non-adiabatic electron transfer theory are given and compared to the experimental values. These rates were calculated using many assumptions, so they should be accurate only by an order of magnitude. The details of the calculation are provided in the supporting information of [Pil14b]. Only the results will be discussed in this section. The obtained rates are given in Table 6.2. The experimental values can be derived from the measured data: charge transfer (CT) out of the excited state depends on the excited state (ES) lifetime (τ_{ES}) and the CT quantum yield out of this state ($\Phi_{CT,ES}$):

$$k_{CT,ES} = \frac{\Phi_{CT,ES}}{\tau_{ES}} \tag{6.4}$$

Given the $^1\pi\pi^*$ lifetime around 0.5 ps [PPK01] and the CT quantum yield of 6 % to 7 %, a CT rate of around $1 \cdot 10^{11}\,s^{-1}$ is calculated. This rate is based on the assumption that all excited $^1\pi\pi^*$ states can undergo charge separation. In fact,

Transfer Process	Theoretical Value	Experimental Value
$^1\pi\pi^*$ → CS state	$6.7 \cdot 10^9\,s^{-1}$	$> 1 \cdot 10^{11}\,s^{-1}$
$^3\pi\pi^*$ → CS state	$5.2 \cdot 10^3\,s^{-1}$	$< 1 \cdot 10^7\,s^{-1}$
CS state → GS	$6.8 \cdot 10^9\,s^{-1}$	$1 \cdot 10^{10}\,s^{-1}$

Table 6.2.: Comparison of experimentally observed rates of charge transfer processes and the calculated rates. Details see text.

however, only suitably oriented bases can (for a discussion of reactive conformations, see for example [Imp12]). These are only a small fraction of the excited bases [GS78, JW07a], and no rearrangement of the bases can occur within the $^1\pi\pi^*$ lifetime. The effective quantum yield of charge transfer out of this subset of the bases is therefore expected to be higher, perhaps by an order of magnitude. Then, the rate of charge transfer could exceed $1 \cdot 10^{12}\,s^{-1}$.

Concerning the triplet state $^3\pi\pi^*$, its lifetime in $(dT)_{18}$ is in the range of 10 ns, while no charge transfer is observed (see chapter 5). The quantum yield of charge transfer out of the $^3\pi\pi^*$ state must therefore be below 10 %. Consequently, the CT rate out of the $^3\pi\pi^*$ state must be below $1 \cdot 10^7\,s^{-1}$. Charge recombination occurs with a time constant of 100 ps, so the recombination rate is $1 \cdot 10^{10}\,s^{-1}$.

The comparison of the experimental and theoretical values yields only partial agreement. The charge recombination rate constants agree within an order of magnitude. The rate of charge transfer out of the $^3\pi\pi^*$ state ($k_{CT,^3pp^*}$), was found to be $5.3 \cdot 10^3\,s^{-1}$, well below the experimental maximum value of $1 \cdot 10^7\,s^{-1}$. This low rate explains why no charge transfer out of the triplet state is observed at all. Only in the case of charge transfer out of the $^1\pi\pi^*$ state the theoretical and the experimental values differ by more than one order of magnitude, perhaps by more than two. Since the rates depend very sensitively on the parameters, a deviation of one order of magnitude might be just a result of inaccuracies of the parameters of the calculation. A deviation by two orders of magnitude is possibly more than an inaccuracy, it may be indicative of a slightly different mechanism of charge transfer: the calculations assume a localised $^1\pi\pi^*$ as starting point of charge transfer. Studies by other groups assume that charge separated states are formed out of excitons (see for example [Mid09, Vay12]). Since excitons are delocalised over more than one base, charge transfer out of an exciton would be more efficient than out of the $^1\pi\pi^*$ state. Insofar, the calculated rate would be a lower boundary for the real charge transfer rate. Therefore, the calculated rates are fully consistent with the assumption that charge separation originates from delocalised exciton states.

6.6. Outlook

Bucher et al. showed that exciplexes in photoexcited DNA are fully charge separated states [Buc14a]. Excimers were reported for adenine strands, but not for pyrimidines. In this thesis, spectroscopic evidence for charge separated states in all-thymidine strands was presented. A number of questions arise from this finding:

1. Do all π-stacked strands undergo charge separation?
2. Do charge separated states contribute to the formation of photolesions like the (6–4) adduct?
3. Does charge separation between stacked bases compete with CPD formation?
4. Can the transfer of an electron onto a CPD lesion repair it?
5. Does base pairing affect charge transfer?

1. Do All π-Stacked Strands Undergo Charge Separation?

The presented data identified charge transfer in UV-excited $(dT)_{18}$ for the first time [Pil14b]. No such charge transfer was reported in cytidine strands yet. On the contrary, Keane et al. reported an excited state decay in the time range from 40 ps to 100 ps in CMP and poly-dC [Kea12], which they identified as a $^1n\pi^*$ state. No sign of an excimer was observed. They do however note a difference between CMP and poly-dC: The excited state lifetimes were different (40 ps in CMP compared to 80 ps in poly-dC). This difference may possibly be due to a misinterpretation of the data: In addition to a $^1n\pi^*$ state, there may be a charge separated state in poly-dC with a similar lifetime. In this case, two different states would be mistaken for just one. The data analysis presented by Keane et al. does not suffice to exclude that possibility. Since it seems implausible that stacked thymines can undergo charge separation, but stacked cytosines cannot, this possibility seems likely. Furthermore, theoretical studies support the existence of cytosine excimers [Dan94, Ola06, Gon10b, Yua11]. TRIR measurements and a more detailed analysis that takes advantage of the published spectra of cations and anions of DNA nucleotides [Buc14a, Buc14b] should be able to answer this question.

2. Do Charge Separated States Contribute to the Formation of Photolesions Like the (6–4) Adduct?

The quantum yield of charge separation is much higher than that of (6–4) formation. The data clearly establish charge recombination to the ground state as the dominant mechanism of the decay of the $T^{\bullet+}pT^{\bullet-}$ state. According to Improta, charge separated states can form an oxetane, a precursor to the (6–4) lesion [Imp12]. The reaction path from a CSS to an oxetane has to overcome a substantial energy barrier. Such a

barrier would decrease the rate and thereby the quantum yield of (6–4) formation. This could be in agreement with the experimental fact that (at least) almost all CSS decay by charge recombination without forming oxetane intermediates. Presently, a quantitative analysis of barrier heights and expected oxetane formation rates is not possible. The observed formation and decay rates of charge separated states may yet provide some guidance for further theoretical work on the subject of (6–4) formation. Experimentally, the direct observation of (6–4) formation is seriously hampered by the low (6–4) quantum yield. Therefore, direct measurements of the (6–4) formation by time-resolved spectroscopy seem not feasible. To progress further, the possible connection between charge transfer and (6–4) formation [Imp12] can be investigated indirectly: the formation of (6–4) lesions is governed by the sugar conformation [Des08]. A particular sugar conformation (*C2'-endo*) seems to be necessary for it. The same conformation, according to Improta, leads to charge transfer [Imp12]. Modifications of the sugar that change the amount of bases in these conformations should therefore affect the (6–4) quantum yield and the charge transfer quantum yield alike. Since sugar modification should not affect the intrinsic properties of the bases profoundly, a strong positive correlation between both quantum yields should exist. The same approach has been successfully applied to thymidine dimers with respect to the so-called *C3'-endo* conformation that promotes CPD formation, drastically increasing the CPD quantum yield [Ost03, Sch09]. The (6–4) quantum yield can be measured by steady-state spectroscopy, while TRIR spectroscopy can determine the CT yield. Testing different modified thymidine dimers for such a correlation can shed further light on the formation of the (6–4) lesions.

3. Does Charge Separation Between Stacked Bases Compete with CPD Formation?

CPD formation and charge transfer both require stacked bases. However, the exact sugar conformations that promote either state are presumably different [Imp12]. If that is true, CPD formation and charge transfer would be independent of each other. If not, charge transfer could deactivate potentially damage-prone stacked bases and reduce CPD yield. Since the conformational requirements for charge transfer are not known experimentally, this question cannot be decided yet. Again, measurements of differently modified thymidine dimers and determination of the CPD and CT quantum yields could elucidate this question.

4. Can the Transfer of an Electron Onto a CPD Lesion Repair It?

Many bacteria, among other organisms, use specialised molecules called *photolyases* to repair DNA lesions [San03, Kim94, Web05, Web02]. The repair mechanism involves a light-triggered transfer of an electron onto a CPD lesion. The electron opens the cyclobutane ring and restores the pyrimidines, before the electron is transferred back to the photolyase. Therefore, charge transfer onto a CPD lesion might repair it.

Attempts to repair a DNA lesion by inducing a charge transfer from a neighbouring base B to a CPD ($B - CPD \rightarrow B^+(CPD)^-$) were unsuccessful [Pan11], but this may be due to poor stacking between the base and the CPD lesion. Damage repair might be possible by inducing charge separation between two bases B_1 and B_2 next to a CPD lesion and subsequent electron transfer from the anion to the CPD lesion $B_1 - B_2 - CPD \rightarrow B_1^+ - B_2^- - CPD \rightarrow B_1^+ - B_2 - (CPD)^-$. The transferred electron could repair the CPD lesion and return the intact pyrimidines. Measurements that address this questions are currently in progress.

5. Does Base Pairing Affect Charge Transfer?

In single-stranded DNA the excited state physics of the bases is modified by base stacking. Base stacking can give rise to states like excitons, charge separated states and others. In double-stranded DNA there are additionally the effects of base pairing. Several studies aimed at the excited state physics of DNA double-strands. Time-resolved spectroscopy on DNA double strands led to the conclusion that the excited state physics is governed by base stacking, not base pairing [CCK05, Tak08, Mid09]. However, TRIR experiments by Bucher et al. on natural DNA showed a simultaneous excited state decay of complementary bases in the double strand [Buc14a]. An interstrand proton transfer between complementary bases was proposed by the authors to explain the observed data. They suggest that interstrand proton transfer may deactivate harmful charge separated states. Based on the published data, it is not possible yet to decide whether or not CS states of thymidine are quenched or prevented by such a mechanism. Further investigations on this questions are currently in progress.

7. $n\pi^*$ States and Intersystem Crossing

Even without the additional complexity of base stacking and base pairing, the task of understanding the excited state physics of DNA bases and nucleotides is challenging both theoretically and experimentally. There is an intense ongoing discussion about the excited states that are populated during the decay of the $^1\pi\pi^*$ state [Mar06, Cre04]. Among the DNA bases, pyrimidines are most vulnerable insofar as they form the most common photolesions (CPDs and (6–4) adducts), so their long-living excited states receive special attention. This thesis focusses on thymine, so it will be at the centre of the discussion, but comparisons to C and U will be drawn when it seems necessary. In this chapter, TRIR measurements of thymine and TMP in different solvents are presented in the temporal window from (sub-)picoseconds to circa 2 nanoseconds. The discussion will focus on the possible role of $n\pi^*$ states in the $^1\pi\pi^*$ decay and their involvement in the intersystem crossing (ISC) process to the $^3\pi\pi^*$ state. This chapter begins with a review of previous studies of the excited state physics of pyrimidines, especially thymine. Then, solvent dependent measurements of TMP and thymine are presented. A long-living excited state that was not reported before is observed and characterised. The intersystem crossing process is monitored and the involvement of long-living excited states in it is discussed. A widely used model for the excited state decay of pyrimidines [HCK07, Mid09] has to be revised in view of the findings presented here. A discussion of different possible models of the excited state physics of thymine concludes this chapter.

7.1. $n\pi^*$ States of Pyrimidines

Quantum chemical calculations of thymine in the gas phase identify 3 excited states that are energetically below the excited $^1\pi\pi^*$ state. These are, in descending order $^1n_{O8}\pi^*$, $^3n_{O8}\pi^*$ and $^3\pi\pi^*$ states [FKH07]. As the name of the $n\pi^*$ states suggests, the non-bonding electron is located on the O8 atom. The O7 atom can also provide non-bonding electrons for $^1n_{O7}\pi^*$ and $^3n_{O7}\pi^*$ states, but they are energetically above the $^1\pi\pi^*$ state and therefore not accessible [FKH07, Ser07, Che13]. The $^1n_{O8}\pi^*$ and $^3n_{O8}\pi^*$ states will in the following be simply referred to as $^1n\pi^*$ and $^3n\pi^*$ states, respectively. $n\pi^*$ states of pyrimidines are interesting for two reasons:
First, they can be reactive themselves and mediate the formation of some photoproducts via Paternò–Büchi reactions. In particular, they are discussed (along with charge transfer states) as precursors to the formation of (6–4) lesions [Giu13]. According to this study, after UV excitation, an ultrafast ISC to a $^3n\pi^*$ state occurs,

from where the formation of oxetane, the precursor of the (6–4) lesion, takes place via a Paternò–Büchi reaction.
Second, $^1n\pi^*$ states are likely precursors to $^3\pi\pi^*$ states [ElS63, SB75], which in turn can form CPD lesions (see chapter 5) [LY67].

The involvement of $n\pi^*$ states in the excited state physics of pyrimidines was studied extensively with various methods. These studies resulted in different models:

1. Indirect approach by measuring ISC quantum yields: solvent dependent $^1n\pi^*$ accessibility

2. Indirect approach by fluorescence spectroscopy: short-living $^1n\pi^*$ states in protic and aprotic solvents

3. Direct approach by TA spectroscopy: long-living $^1n\pi^*$ states in protic and aprotic solvents

7.1.1. ISC in Different Solvents: Solvent-Dependent $n\pi^*$ Accessibility?

The first approach to investigating the role of $^1n\pi^*$ states in the photophysics of thymine was an indirect one that measured not $^1n\pi^*$ states themselves, but the intersystem crossing quantum yield Φ_{ISC} in different solvents [SB75, SBB79]. It was found that Φ_{ISC} of thymine depends sensitively on the solvent, ranging from 1 % in water to 6 % to 20 % in acetonitrile (different values were reported in [SB75] and [WB70]).

Despite the disagreements in the exact numbers, there is consensus that a low proticity (tendency to form H-bonds) tends to increase Φ_{ISC}. Interestingly, the proticity of a solvent destabilizes $n\pi^*$ states [McC52, BK55], increasing their energy and thereby potentially making them inaccessible from the $^1\pi\pi^*$ state (see subsection 7.1.2). Since $n\pi^*$ states are likely precursors to $^3\pi\pi^*$ states [ElS63], Salet et al. [SBB79] proposed a model that explains the solvent dependence of Φ_{ISC} (see Figure 7.1). It assumes that the triplet precursor is a $n\pi^*$ state, either $^1n\pi^*$ or $^3n\pi^*$. This state is energetically below the $^1\pi\pi^*$ state in the gas phase and in aprotic solvents, but it is above the $^1\pi\pi^*$ state in protic solvents like water. In protic solvents the $n\pi^*$ state is not populated in significant amounts. ISC has to occur from the $^1\pi\pi^*$ state to the $^3\pi\pi^*$ state, a process which is inefficient [ElS63]. Thus Φ_{ISC} is low. In aprotic solvents the $n\pi^*$ state is accessible. If it is a $^1n\pi^*$ state, then the conversion $^1\pi\pi^* \rightarrow {}^1n\pi^*$ is spin-allowed and ISC $^1n\pi^* \rightarrow {}^3\pi\pi^*$ is in line with the rule of El-Sayed and therefore quite efficient. If it is a $^3n\pi^*$ state, then the ISC $^1\pi\pi^* \rightarrow {}^3n\pi^*$ is in line with the rule of El-Sayed and the conversion $^3n\pi^* \rightarrow {}^3\pi\pi^*$ is spin-allowed, so both processes may be efficient. Both possibilities can explain the high intersystem crossing quantum yield in aprotic solvents like acetonitrile.

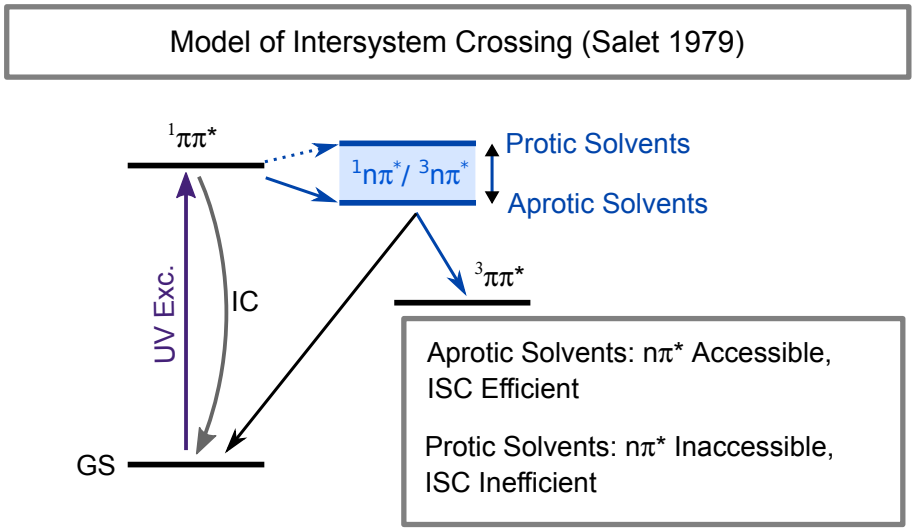

Figure 7.1.: Scheme of intersystem crossing to the $^3\pi\pi^*$ state of thymine in different solvents as it was proposed by Salet et al. [SB75]. Either a singlet or a triplet $n\pi^*$ state is hypothesised as the triplet precursor. The $n\pi^*$ state is below the $^1\pi\pi^*$ state in the gas phase and aprotic solvents (high Φ_{ISC}), but is shifted above the $^1\pi\pi^*$ state in protic solvents like water (low Φ_{ISC}).

The experiments by Salet et al. could not observe the process of ISC due to insufficient temporal resolution. They measured only the resulting triplet yield. Their model was in line with the known empirical facts and plausible, but lacked direct evidence.

Theoretical Studies of ISC

Theoretical studies of thymine in the gas phase indicate that $n\pi^*$ states are involved in the excited state decay [Can05, Bla07, ZH14]. Quantum chemical calculations identified conical intersections between the $^1n\pi^*$ and the $^1\pi\pi^*$ energy surfaces, promoting an efficient conversion to the $^1n\pi^*$ state [Gon10a]. From there, either ISC to the $^3\pi\pi^*$ state or decay to the ground state may take place. Despite the similar energetics of $^1n\pi^*$ and $^3n\pi^*$, the population of the $^3n\pi^*$ state is quite different. It requires intersystem crossing ($^1\pi\pi^* \rightarrow {}^3n\pi^*$) and there is doubt that the ISC rate can be high enough to compete with the ultrafast $^1\pi\pi^*$ decay [EFM09]. Consequently, the $^3n\pi^*$ is expected to play only a minor role in the decay of the $^1\pi\pi^*$ state.

In solution the energetics are modified by the solvent. The most pronounced effect in this regard is the destabilisation of $n\pi^*$ states by H-bonds in protic solvents [BK55]. In protic solvents like water, this effect may be strong enough to increase the $^1n\pi^*$ state energy above that of the $^1\pi\pi^*$ state [EM10, Nak13]. Then the $^1n\pi^*$ state would not be populated during the $^1\pi\pi^*$ decay in water, but in less protic solvents like acetonitrile or methanol. These recent studies are directly supporting the model of ISC presented in the previous section. However, it is unclear how reliable these

studies are. Most theoretical studies are done in the gas phase, and still there are disagreements about the energies of excited states (see for example [LFR95, PSD06, FKH07, Ser07] and the supporting information of [FKH07]). Calculations on DNA photophysics in solution have to take into account interactions with the solvent, which further increases the difficulty and further decreases the accuracy. Insofar, the participation of the $^1n\pi^*$ state in the $^1\pi\pi^*$ decay in water is doubtful, but it cannot be excluded.

7.1.2. Indirect Approach by Fluorescence Spectroscopy: Short-Living $n\pi^*$ States in All Solvents?

Time-Resolved Fluorescence Data of Thymine

Time-resolved fluorescence spectroscopy can be applied to monitor the $^1\pi\pi^*$ decay, which may give some indirect hints towards the underlying mechanisms and the potential involvement of dark (non-fluorescent) states. The fluorescence of the $^1\pi\pi^*$ state of thymine in water decays biexponentially, with time constants around 0.2 ps and 0.6 ps [Oni02, GSM02]. A later study showed that the appearance of the slower component is solvent dependent [Gus07, Gus08]. The slow component was strongest in protic solvents like water, where the $^1n\pi^*$ energy is highest. The authors explained this finding by assuming that the $^1n\pi^*$ state is energetically below the $^1\pi\pi^*$ state in aprotic solvents, and iso-energetic with the $^1\pi\pi^*$ state in protic solvents like water. Then a part of the $^1\pi\pi^*$ population can undergo internal conversion (IC) to the dark $^1n\pi^*$ state in all solvents. In protic solvents, where $^1n\pi^*$ and $^1\pi\pi^*$ states are iso-energetic, a back-conversion from the $^1n\pi^*$ to the $^1\pi\pi^*$ state is possible, giving rise to *delayed fluorescence*. The slow fluorescence component is interpreted as delayed fluorescence after a back-transfer of population from the $^1n\pi^*$ to the $^1\pi\pi^*$ state. If this model is correct, the $^1n\pi^*$ state is accessible from the $^1\pi\pi^*$ state in all solvents and its lifetime then corresponds to the slower sub-picosecond decay component.

Alternative Explanation of the Fluorescence Data

The involvement of the $^1n\pi^*$ states in the fluorescence decay is not directly deducible from the data, because $^1n\pi^*$ states themselves are not fluorescent. Other explanations for the biexponential decay of the fluorescence and its solvent dependence are possible. Such an alternative explanation was proposed recently: Nakayma et al. suggested that two major excited state pathways of the $^1\pi\pi^*$ state exist that lead to internal conversion to the ground state via different conical intersections on different timescales [Nak13]. The slower of these pathways encounters a solvent dependent energy barrier, so it would be more or less important in different solvents. This model could also explain the cited fluorescence data without assuming the presence of a dark $^1n\pi^*$ state. In view of this study, the fluorescence data cannot be considered as conclusive evidence for the participation of $^1n\pi^*$ states in the $^1\pi\pi^*$ decay.

7.1.3. Direct Approach by TA Spectroscopy: Long-Living $n\pi^*$ States and ISC

TA Spectroscopy: Long-Living $n\pi^*$ States?

Time-resolved absorption spectroscopy can observe dark states that are populated from the $^1\pi\pi^*$ state directly. Different groups have investigated the excited state physics of pyrimidines and observed long-living excited states [HCK07, Kea11, Kea12].

Hare et al. performed measurements of all pyrimidine bases and their nucleotides and found long-living excited states in all of them (see Table 7.1). These states were efficiently populated from the $^1\pi\pi^*$ state and decayed to the ground state on timescales between 30 ps and 150 ps. Hare et al. interpreted these states as $^1n\pi^*$ states, based on theoretical considerations about the involvement of $^1n\pi^*$ states in the $^1\pi\pi^*$ decay [Ser07, Gon10a, Ast09, Imp09]. Remarkably, the lifetimes of the nucleotides were much shorter than that of the bases, but this effect has not been explained yet.

TA Spectroscopy of ISC to the $^3\pi\pi^*$ State

Hare et al. observed ISC of thymine in acetonitrile by TRIR spectroscopy [Har08].

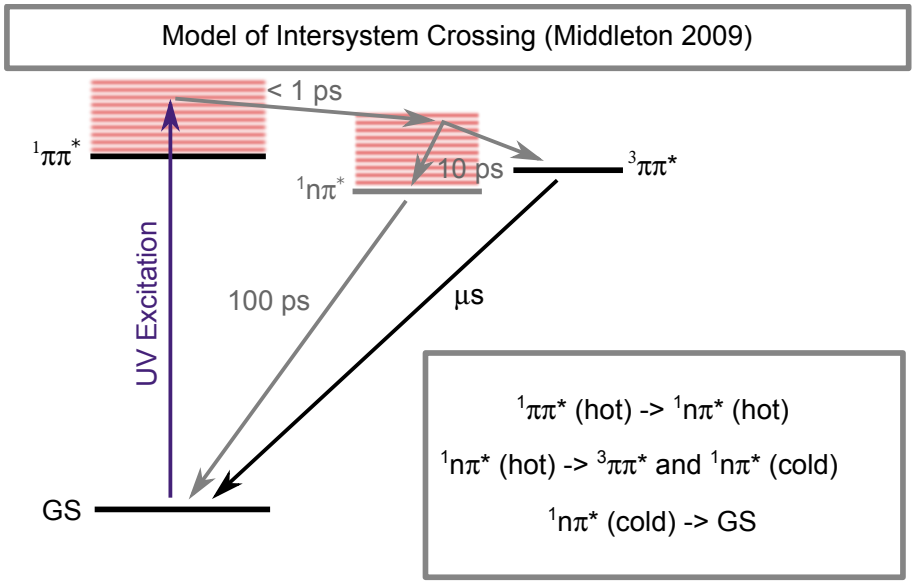

Figure 7.2.: The model of excited state physics of TMP as proposed in [Mid09]. Depending on the excitation wavelength, more or less excess energy is stored in the vibrational modes. A fraction of the excited bases undergo a transition to a vibrationally excited $^1n\pi^*$ state, that subsequently either dissipates the excess energy to the solvent or undergoes ISC to the $^3\pi\pi^*$ state in 10 ps. The relaxed $^1n\pi^*$ state cannot undergo ISC, but only decays to the ground state on a 100 ps timescale. The parts of this model that are disputed in this thesis are depicted in grey.

ISC to the $^3\pi\pi^*$ state takes place within 10 ps. In a previous study, they already observed a longer-living excited state that they identified as a $^1n\pi^*$ state [HCK07] (see Table 7.1 and the discussion in subsection 7.1.2). Middleton et al. combined the findings of both studies in a model that describes the ISC process [Har08, Mid09]. It is depicted schematically in Figure 7.2. It assumes that the $^1\pi\pi^*$ populates a $^1n\pi^*$ state within less than 1 ps. Depending on the excitation wavelength, the $^1\pi\pi^*$ state and subsequently the $^1n\pi^*$ state have more or less excess vibrational energy. To explain why the triplet is formed out of the $^1n\pi^*$ state, but much faster than the $^1n\pi^*$ state decays, the model proposes that the vibrationally excited (hot) $^1n\pi^*$ state can either undergo intersystem crossing (ISC) to the $^3\pi\pi^*$ or dissipate the vibrational energy to the solvent. The thermally relaxed $^1n\pi^*$ state then cannot reach the triplet state any more, but returns to the ground state on a timescale of 100 ps [HCK07, Mid09]. The model proposed by Salet et al. [SBB79] identified the energetic accessibility of the $^1n\pi^*$ state as the 'bottleneck' that limits the triplet yield. In the model by Middleton, Hare and coworkers the $^1n\pi^*$ state is accessible in all solvents, but the ISC process from the $^1n\pi^*$ state to the $^3\pi\pi^*$ state requires excess vibrational energy, limiting the triplet quantum yield.

Conflicting Data by Other Groups

Several theoretical and experimental objections can be raised against this model: Quantum chemical calculations indicate that excess vibrational energy should not be necessary to undergo intersystem crossing from the $^1n\pi^*$ to the $^3\pi\pi^*$ state [Ser07, Gon10a], since the $^3\pi\pi^*$ is energetically far below the $^1n\pi^*$ state.

Molecule	Lifetime/ps	Amount/%
CMP	34[a]; 39[b]	41[a]; 16[b]
Cyt	12[a]; –[b]	9[a]; –[b]
TMP	137[a]; –[d]	14[a] ; 0[c,d]
Thy	30[a]; –[d]	11[a]; 0[d]
UMP	147[a]	42[a]
Ura	24[a]	28[a]

Table 7.1.: Lifetimes and relative amplitudes of excited states identified as $^1n\pi^*$ states in pyrimidines (bases and nucleotides) reported by (a) Hare et al. [HCK07], (b) Keane et al. [Kea11], (c) Kwok et al. [KMP08], and (d) Pilles et al. [Pil14b]. Hare et al. report excited states of all pyrimidine bases and nucleotides with a quantum yield of 10 % or more. For CMP other values were reported by Keane et al., in TMP no state that decays on the 100 ps timescale is reported by other groups [KMP08, Pil14b].

Substantial energy barriers on the way to intersystem crossing that would require excess energy to overcome were not reported in any of these studies. Furthermore, vibrational energy does not increase spin-orbit coupling or the ISC probability

according to a quantum chemical study by Etinski [Eti13]. The presented model is therefore conflicting with theoretical studies. Moreover, the experimental findings that motivated this model are controversial. Other groups have investigated the excited state physics of thymine, cytosine and their nucleotides, but obtained different results. As Table 7.1 shows, only the excited state of CMP was also observed by other groups, but with a different quantum yield (16 % compared to 41 %), while the excited states of C, T and TMP were not observed at all [Qui07, Kea11, KMP08, Kea12, Pil14b].

Focussing on the data of thymine, even the existence of a long-living excited state (other than the $^3\pi\pi^*$ state) is uncertain, given the conflicting findings of Hare et al. [HCK07] and other groups [KMP08, Pil14b].

Resolving the Conflicting Claims by Dichroic Measurements

As was described in subsection 7.1.2, the supposed $^1n\pi^*$ state of thymine that Hare et al. reported was not observed by other groups [KMP08, Sch08, Pil14b]. Such a discrepancy can point towards measurement errors and artefacts. A measurement error that may explain an 'additional' excited state decay that is not found by other groups is the accidental observation of the reorientational motion of the molecules, if pump and probe pulses are not polarised properly (see subsection 3.4.4).

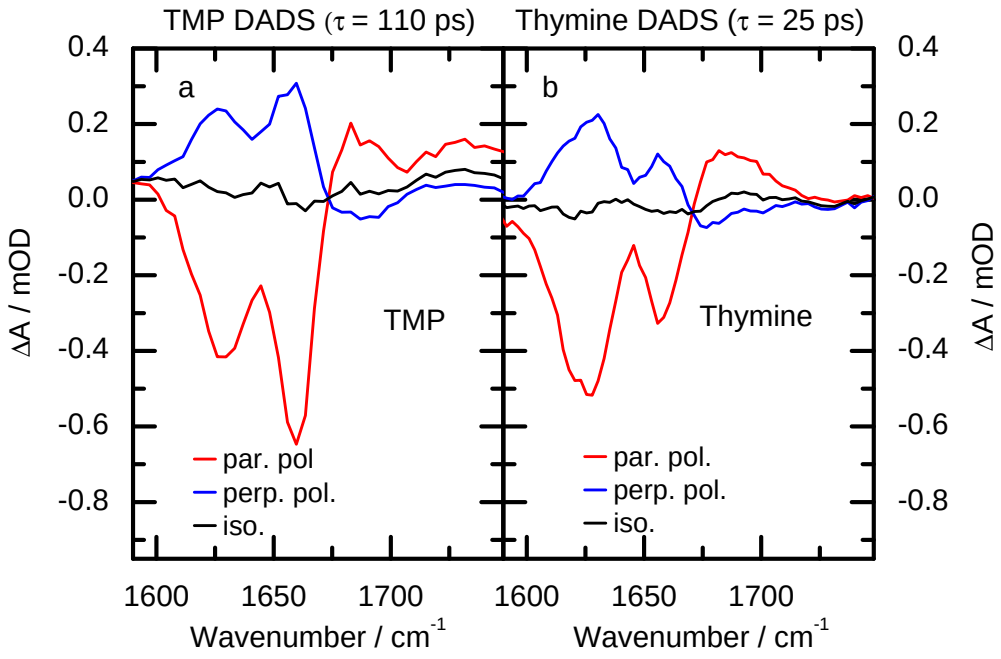

Figure 7.3.: DADS of the reorientational motion of TMP (a) and thymine (b) using excitation polarisations parallel (red) and perpendicular (blue) to the probe polarisation. If the isotropic signals are calculated, the DADS cancel out.

To test for this possibility, dichroic measurements of TMP and thymine were performed using excitation polarisations parallel, perpendicular and in magic angle to the probe pulses. The isotropic signal ΔA_{ISO} is calculated according to:

$$\Delta A_{ISO} = \frac{\Delta A_{\parallel} + 2 \cdot \Delta A_{\perp}}{3} \tag{7.1}$$

The isotropic signal as well as the magic angle measurements observe the excited state physics. Measurements that used parallel and perpendicular polarisation observe additional kinetics that are due to the reorientational motion of the sample. These kinetics would appear as an additional exponential decay in a multiexponential fit and can easily be mistaken for an excited state decay. The data measured in a magic angle configuration showed no 100 ps decay for TMP and no 25 ps decay of thymine. However, if parallel or perpendicular polarisation is used, there are substantial signals that decay with time constants of 110 ps (TMP) or 25 ps (thymine). Figure 7.3 shows those DADS of TMP (left) and thymine (right). The calculated isotropic signal is a baseline (within experimental accuracy), indicating that there is no excited state decay corresponding to those time constants. The same result is obtained by using a magic angle configuration. The different time scales (around 110 ps for TMP and 25 ps for thymine) simply result from the faster rotation of the smaller molecule thymine. These findings conclusively demonstrate that these signals are only due to reorientational motion, not to excited state physics. Therefore, the features reported as '$^1n\pi^*$-states' of TMP and thymine were due to measurement errors. This implies, that the model that was proposed for the excited state physics of TMP [HCK07, Mid09] (see Figure 7.2) is not supported by the experimental results.

7.1.4. Conclusion

In conclusion, neither fluorescence nor absorption spectroscopy have yet provided conclusive evidence for the involvement of $^1n\pi^*$ states in the $^1\pi\pi^*$ decay of thymine. It is not clear if the $^1n\pi^*$ state is energetically accessible in all solvents, particularly in water. The solvent dependence of the triplet quantum yield hints toward a solvent dependent $^1n\pi^*$ accessibility, but does not proof it. A re-investigation of the excited state physics of thymine is necessary to shed light onto these open questions. TRIR measurements of thymine and TMP in different solvents (water, methanol and acetonitrile, all fully deuterated) were performed to address the open questions about long-living excited states and the mechanism of intersystem crossing.

7.2. Long-Living States of TMP in D_2O

7.2.1. Time-Resolved Measurements of TMP in Water

The excited state physics of TMP in a buffered solution of D_2O is monitored by TRIR spectroscopy. The sample was excited by UV pulses (wavelength 266 nm, energy 2 µJ, pulse duration 1 ps to 2 ps). Figure 7.4 shows the resulting data after the signature

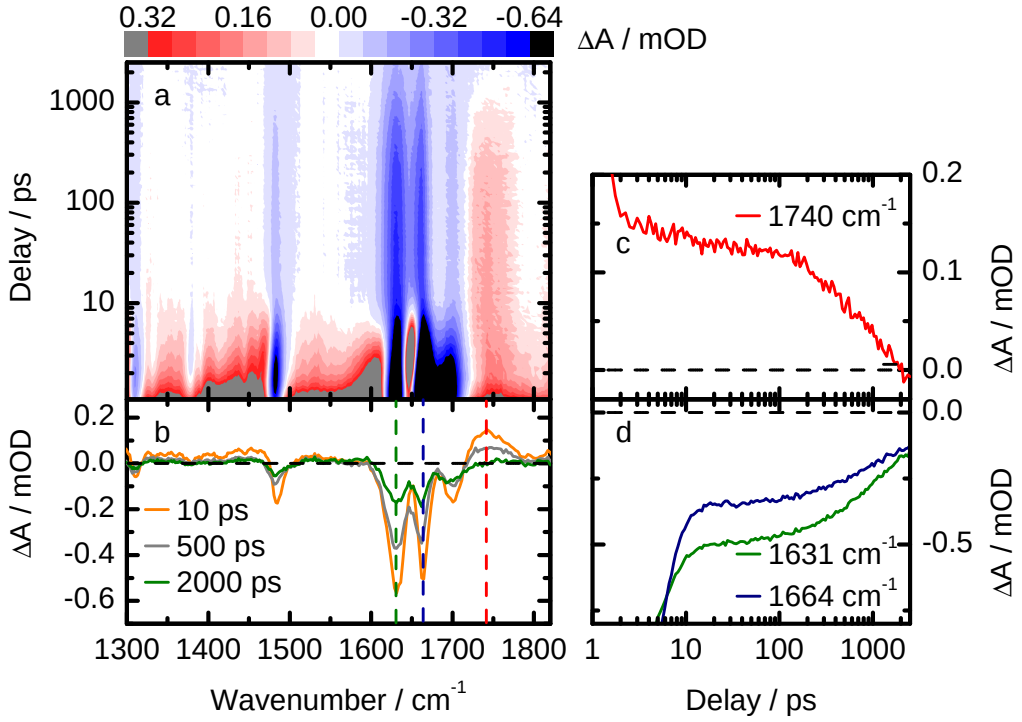

Figure 7.4.: (a) Excited state dynamics of TMP in a buffered solution of D_2O. Absorbance changes after VC are due to long-living excited states (b). Panels (c) and (d) show the absorbance changes at the indicated wavelengths. There appears to be a monoexponential decay with a time constant around 1000 ps.

of solvent heating was subtracted (see section A.1). After UV excitation, 80 % to 90 % of the excited bases decay from the $^1\pi\pi^*$ state to the vibrationally excited (hot) ground state.

The resulting absorbance changes are due to the difference in absorption between the hot and the cold ground state until the vibrational energy is dissipated to the solvent (vibrational cooling, VC). The 'hot' vibrations are typically red-shifted and broadened (see subsection 3.4.3), so the absorbance difference spectra are characterised by a bleach of the ground state bands (between 1600 cm^{-1} and 1700 cm^{-1} and at 1480 cm^{-1}) and broad absorbance bands at lower wavenumbers. Vibrational cooling

is finished after a little more than 10 ps. After that, persisting absorbance changes are caused by long-living excited states. Figure 7.4, panel (b) shows the transient spectra at 10 ps, 500 ps and 2000 ps. The spectra are characterised by ground state bleaches at 1480 cm^{-1}, 1631 cm^{-1}, 1665 cm^{-1} and around 1700 cm^{-1} and an excited state absorption around 1740 cm^{-1}. Panels (c) and (d) show the temporal evolution of ΔA at the indicated wavenumbers. As the absorption at 1740 cm^{-1} decays, the ground state partially recovers. The remaining signal after more than 2 ns can be investigated by TRIR spectroscopy on the nanoseconds to microseconds timescale. As was shown in chapter 5, the only remaining excited state after more than 2 ns is the lowest triplet state $^3\pi\pi^*$. It decays on the timescale of around 600 ns (see chapter 5) under the experimental conditions and therefore does not change in amplitude significantly in the first 2 ns. At least one other excited state must exist that causes the absorbance changes between 10 ps and 2 ns. The uniform recovery of the absorption bands between 1600 cm^{-1} and 1700 cm^{-1} on that timescale suggests that an excited state decays to the ground state.

7.2.2. Multiexponential Modelling of the Data

A more precise characterisation of the excited state physics is obtained by performing a multiexponential fit to the data. The data have been corrected for the heating of the solvent before data modelling (see section A.1). To avoid the non-exponential signals of vibrational cooling, the first 10 ps are excluded from the fit. Then the data can be reproduced with 3 exponential decay components. The resulting DADS are depicted in the left panels of Figure 7.5, while the right panels shows a comparison of the data (circles) and the model (lines) at the indicated wavenumbers. The good agreement validates the fit and consequently the obtained DADS. Panel (a) shows the DADS that describes the residual absorbance changes caused by vibrational cooling after more than 10 ps. The non-exponential evolution of the absorbance changes caused by VC involves a shifting of absorbance bands. These shifts result in large amplitudes of the corresponding DADS (see for example the band at 1650 cm^{-1} of the DADS in panel (a) Figure 7.5), even if the data in the first 10 ps are excluded from the fit. If electronic transitions occur in the same temporal window, their DADS will be overlayed and obscured by such spectra. As a result, DADS of electronic transitions cannot be obtained in the first 15 ps to 20 ps after excitation. These residual signals of vibrational cooling are not related to excited state physics and are therefore not discussed further.

After more than 20 ps, the absorbance changes are caused by electronic transitions. Two exponential decay components describe the data after more than 20 ps. They are depicted in panels (b) and (c) of Figure 7.5.

The decay of absorption band at 1740 cm^{-1} as well as the ground state recovery at 1631 cm^{-1} and 1661 cm^{-1} in the time window from 20 ps to 2000 ps are described by a single decay with a time constant of 1000 ps. It describes the decay of an excited

state to the ground state. The excited state will be called 'X1' for the remainder of this chapter. The corresponding DADS is depicted in panel (b) of Figure 7.5. It reveals that in addition to the blue-shifted excited state absorption around 1740 cm^{-1}, another absorbance band exists around 1700 cm^{-1}, that is partly obscured by the ground state bleach. After the decay of X1, the residual absorbance change in panel (c) is composed of the signals of long-living excited states or photoproducts of TMP that decay on longer timescales than a few nanoseconds. The TRIR measurements on the nanosecond to microsecond timescale (see chapter 5) show that the only excited state that decays in that time window is the $^3\pi\pi^*$ state. The only photoproducts that are expected are thymidine cations generated by two-step ionisation by picosecond UV pulses (see chapter 6). Despite the elongation of the excitation pulses in a fused silica block (path length = 20 cm), small amounts of cations are generated.

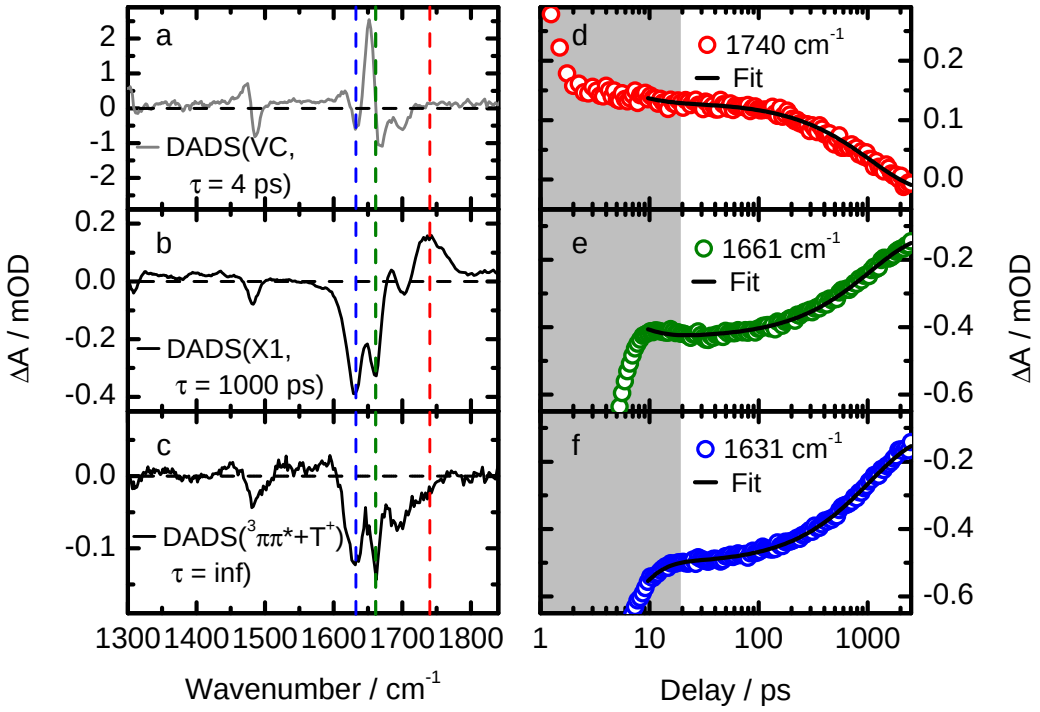

Figure 7.5.: Multiexponential fit of the excited state physics of TMP in the time window from 10 ps to 2.5 ns after UV excitation. The data have been corrected for the heating of the solvent. Three decay components are sufficient to model the data. One of them describes the residual signals of vibrational cooling after more than 10 ps (panel (a)). Cooling features are visible in the first 20 ps (grey area in panels (d)–(f)). A long-living state X1 decays to the ground state with a time constant of 1000 ps (panel (b)). The residual absorbance change after more than 2.5 ns is caused by the $^3\pi\pi^*$ state and to some extent by thymine cations. The right panels depict the observed data (circles) and the model curves (lines) at the indicated wavenumbers.

7.2.3. Spectral Characterisation of the Excited State X1

The obtained DADS are used to characterise the excited states spectrally and determine their respective quantum yields. Since the $^3\pi\pi^*$ state was already discussed in chapter 5, only X1 will be characterised here.

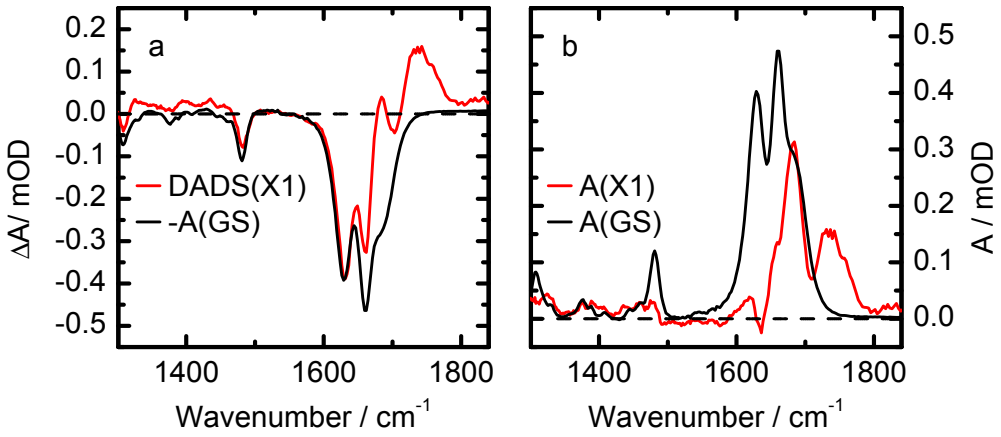

Figure 7.6.: (a): By scaling the DADS of state X1 to the (inverted) ground state absorbance (black), the absorbance of X1 is calculated. (b): The absorbance of X1 (A(X1), red) is compared to that of the ground state of TMP (black). A(X1) is characterised by two absorbance bands at 1685 cm^{-1} and 1740 cm^{-1}.

The decay of X1 results in a recovery of the absorption at all ground state absorption bands. The vast majority ($> 90\,\%$) of the bases in X1 consequently return to the ground state, not a photoproduct or another excited state. Hence the DADS of X1 essentially is the difference in absorption between X1 and the ground state. The absorbance of X1 can be calculated using the DADS of X1 and the ground state absorbance spectrum (as demonstrated in chapter 6). Figure 7.6 shows how the calculation is done. The ground state absorbance (black) is scaled to the DADS of state X1 (red) (left panel). The difference between the DADS and the inverted ground state spectrum is the absorbance of X1. It is compared to the ground state absorbance of TMP in the right panel of Figure 7.6. In the ground state, the absorbance between 1600 cm^{-1} and 1700 cm^{-1} consists of bands from the three vibrational modes C5=C6, C4=O8 and C2=O7 (see section 4.1). In the excited state X1, two absorbance bands at 1685 cm^{-1} and 1740 cm^{-1} are observed. There seems to be another feature around 1618 cm^{-1}, but given its small amplitude, this feature might only be due to experimental inaccuracy. This absorbance spectrum will be compared to calculated IR spectra of the $^1n\pi^*$ state when the experimental results are discussed in subsection 7.5.1.

Quantum Yields

X1 and the $^3\pi\pi^*$ state are populated from the excited $^1\pi\pi^*$ state, possibly via intermediate states. The quantum yields of formation of both states (Φ_{X1} and Φ_{ISC}, respectively) can be calculated from the data.

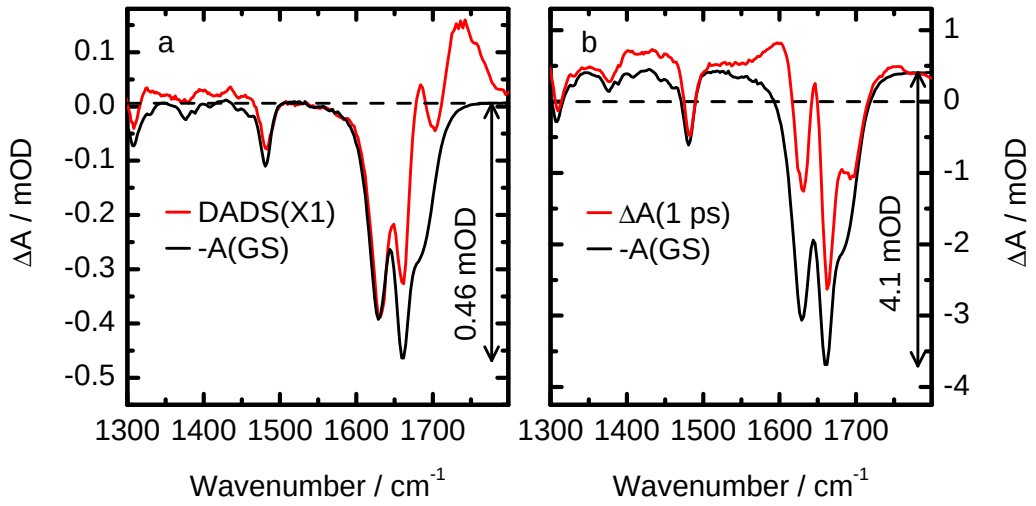

Figure 7.7.: Calculation of the quantum yield of the formation of X1. The ground state bleach (GSB) caused by X1 (a) is compared to the GSB directly after UV excitation (b). The resulting quantum yield of X1 is 11 %.

The discussion will be restricted to the unknown state X1, because the triplet quantum yield was already determined in other studies [Ban12] (see also chapter 5). The quantum yield of X1 is calculated by comparing the ground state depletion caused by X1 to that caused by the $^1\pi\pi^*$ state. The method was already introduced in section 6.1 and will not be explained in great detail in this section, but a few remarks about the DADS of the $^1\pi\pi^*$ state are necessary.

The DADS of the $^1\pi\pi^*$ state cannot be obtained with our picosecond temporal resolution, since it decays to the (hot) ground state with a sub-picosecond time constant [PPK00]. However, ground state absorption recovers only after the dissipation of the excess vibrational energy to the solvent (VC) on the timescale of several picoseconds [Mid09]. At a delay time of 1 ps, the ground state bleach is still the same as immediately after UV absorption. Consequently it can be used instead of the ground state bleach caused by the $^1\pi\pi^*$ state. Figure 7.7 depicts the DADS of X1 (red in left panel) and the absorbance change 1 ps after excitation (red in right panel). The inverted ground state spectra (black) are fitted to the data. Comparing their amplitudes yields a X1 quantum yield Φ_{X1} of 11 % (see section 6.1).

7.2.4. Population of the Excited States

Population of X1

The data reveal two long-living excited states, the lowest triplet state $^3\pi\pi^*$ and the yet unidentified state X1. How are these states populated? The blue-shifted absorbance at 1740 cm^{-1} makes it possible to monitor the formation and decay of X1 even at early delay times, where the signals are dominated by hot ground state absorption/vibrational cooling.

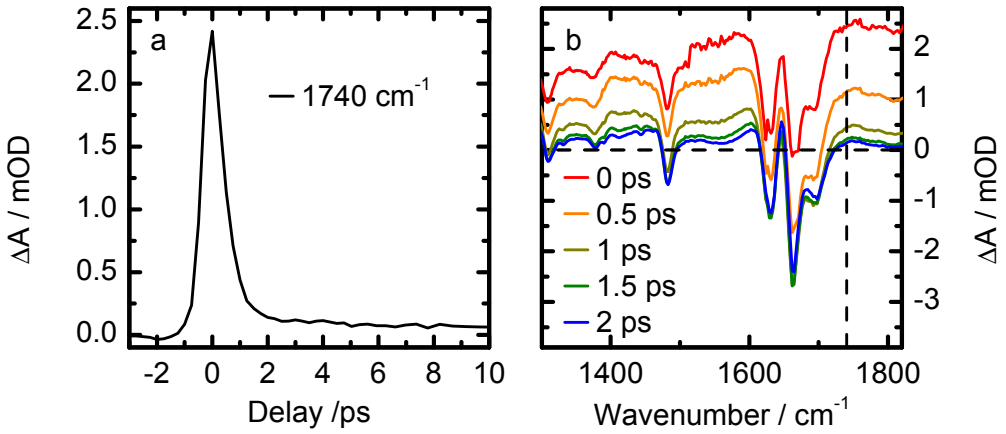

Figure 7.8.: The absorption at 1740 cm^{-1} decreases in the first 2 ps after excitation (a). This is not related to any real decay of X1, but is merely an artefact at the temporal zeropoint: In the first picosecond an artificial increase of the absorption is observed all over the spectrum (b) (see subsection 3.4.3).

After more than two picoseconds, the marker band is clearly present in the data (see Figure 7.4). However, a direct population out of the $^1\pi\pi^*$ state has to occur within the $^1\pi\pi^*$ lifetime of less than 1 ps. A slower population time would require an intermediate state. A closer look at the data in the first picosecond after excitation is necessary to decide this alternative. Panel (a) of Figure 7.8 shows the transient absorbance changes at the marker position of 1740 cm^{-1} during the first 10 ps after excitation. At the temporal zeropoint a large absorption is visible that decays within less than 2 ps. Looking at the signals at other wavelengths shows that this absorption is not related to the excited states of TMP: Panel (b) of Figure 7.8 shows the absorbance changes in the first 2 ps. The absorption at the delay zeropoint extends over the entire spectrum. It is an experimental artefact, caused by two-photon effects in the window material (BaF_2) and the solvent (see subsection 3.1.4). Despite these effects, the absorbance band at 1740 cm^{-1} is clearly visible at a delay time of 0.5 ps, so X1 is populated within the $^1\pi\pi^*$ lifetime.

ISC in D_2O

The $^3\pi\pi^*$ state of TMP was only observed after the decay of all other excited states. The intersystem crossing process by which the $^3\pi\pi^*$ state is populated was not observed directly. To achieve this, the ISC quantum yield Φ_{ISC} needs to be increased. As was already demonstrated in chapter 5, tuning the excitation wavelength to 250 nm increases Φ_{X1} by a factor of 2 to 3 [Ban12].

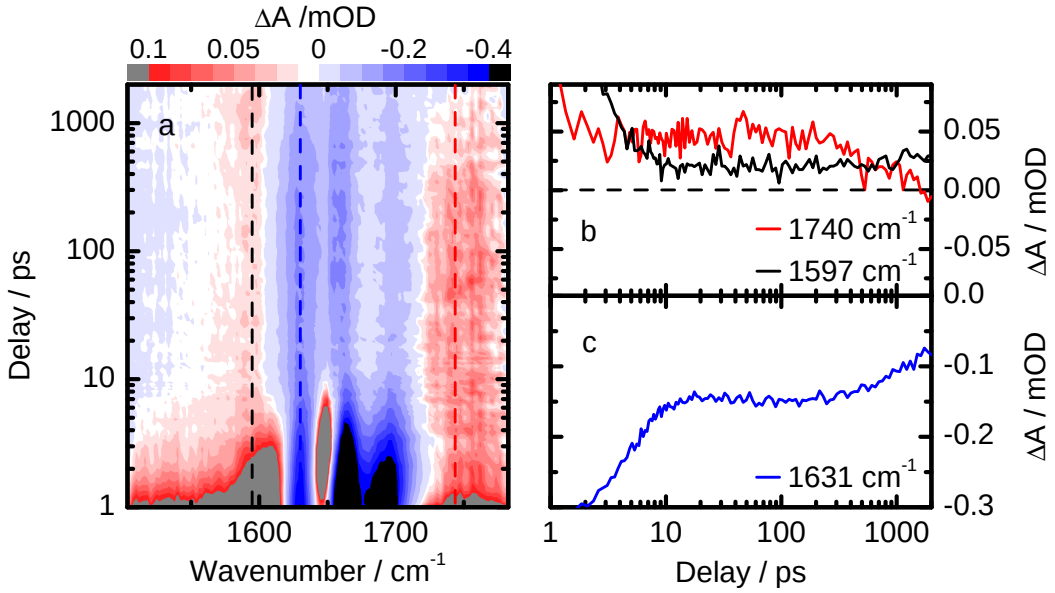

Figure 7.9.: (a) TMP in D_2O after UV irradiation at 250 nm. The data have been corrected for the heating of the solvent. The triplet marker band around 1600 cm^{-1} is visible after 10 ps. The amount of triplet is unaffected by the decay of X1 on the timescale of 1000 ps (see marker band 1740 cm^{-1} in panel (b)). Panel (c) shows the ground state recovery as X1 decays.

Using parametric amplification and subsequent frequency doubling (see Figure 3.9), excitation pulses at a wavelength of 250 nm with an energy of 0.8 µJ were generated. Figure 7.9 depicts the result of a TRIR measurement of TMP in D_2O using these excitation pulses. The data have been corrected for the heating of the solvent. The contour plot in panel (a) clearly shows the triplet marker band below 1600 cm^{-1} after vibrational cooling is finished. The exact time constant of ISC is not observed. However, the triplet absorption is visible after 10 ps, much faster than the decay of X1. X1 might still be a precursor of the $^3\pi\pi^*$ state, if the transition X1 $\rightarrow$ $^3\pi\pi^*$ requires excess vibrational energy. Then the triplet state would be populated on the timescale of thermal relaxation (within 10 ps), partly quenching X1. A closer look at the data nearly excludes this possibility: Panels (b) and (c) show the temporal evolution of the marker bands of the $^3\pi\pi^*$ state (black in (b)), X1 (red in (b)) and the ground state bleach (blue in (c)). The absorbance at 1740 cm^{-1} is not quenched in the time window from 1.5 ps to 10 ps after excitation, when thermal relaxation of X1

should take place (note that the decrease of absorption at 1740 cm^{-1} that occurs 1 ps to 2 ps after excitation is again due to non-linear effects at the temporal zeropoint).

In conclusion, X1 is very unlikely to be a significant triplet precursor. The details of the ISC process cannot be resolved, because the small triplet signals are obscured by the larger signals of vibrational cooling in the first 10 ps. ISC into the $^3\pi\pi^*$ state can therefore proceed in two different ways:

1. There could be an additional short-living state X2 that is quenched by triplet formation within 10 ps. This characteristic could be met by either a $^1n\pi^*$ or a $^3n\pi^*$ state.

2. Intersystem crossing proceeds directly out of the $^1\pi\pi^*$ state, despite the rule of El-Sayed. In this case, the triplet would have to be formed within the $^1\pi\pi^*$ lifetime.

Additional spectroscopic evidence is necessary to decide this alternative.

7.3. TMP in Methanol

The excited state physics of TMP in deuterated methanol (CD_4O) was measured under the same conditions that were applied to the measurement of TMP in water. The results are therefore directly comparable.

7.3.1. Time-Resolved Measurements of TMP in Methanol

Figure 7.10 shows the result of the measurements. As in water, the first few picoseconds are dominated by the signals of vibrational cooling. After the end of vibrational cooling, two excited states persist.

One of them is characterised by a blue-shifted absorption around 1750 cm^{-1}. It is formed within 1 ps and decays within 2 ns. Both features easily identify this state as X1 (this will be further substantiated when the absorbance spectrum of X1 is calculated). The second long-living state is characterised by a red-shifted absorption around 1596 cm^{-1}. It is populated within 20 ps and does not decay until 2.5 ns. This long-living state is identified by the marker band around 1596 cm^{-1} as the $^3\pi\pi^*$ state, that is formed in methanol with a higher quantum yield than in water [SBB79]. Since the triplet marker band is more pronounced and spectrally more isolated than in water, it is possible to monitor triplet formation and its possible relation to X1 more precisely.

The right panels of Figure 7.10 depict the absorbance changes at the marker positions of X1 (blue), the triplet state (red) and the ground state absorbance at 1664 cm^{-1} (green). The absorbance at 1596 cm^{-1} in the first 10 ps is dominated by the signals of vibrational cooling. The increase in absorbance after more than 10 ps

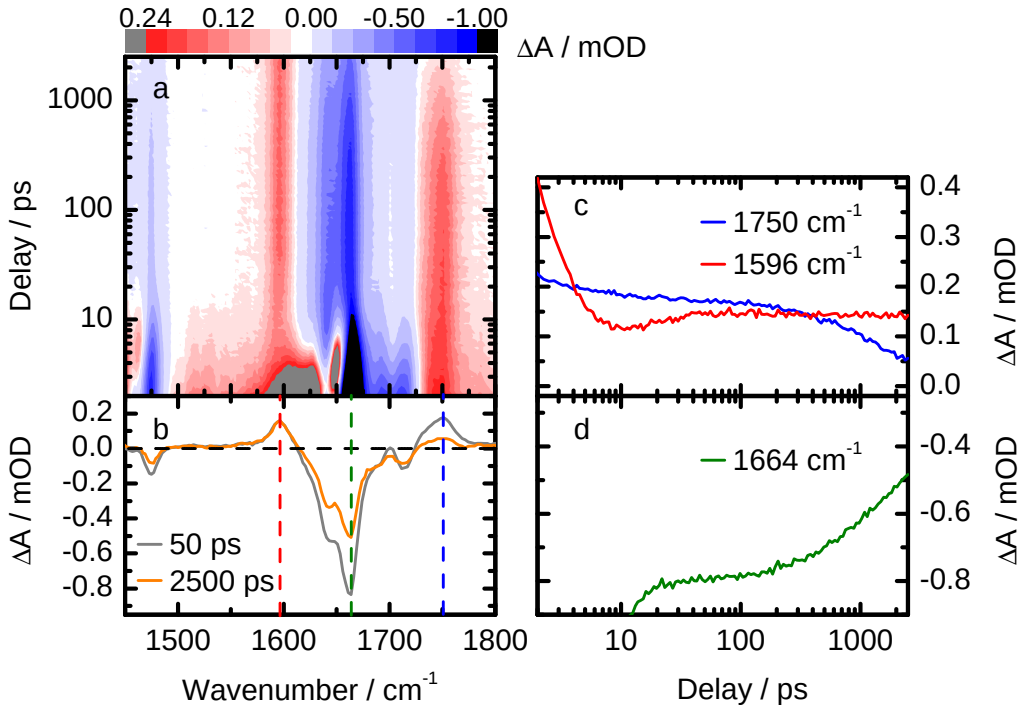

Figure 7.10.: Excited state physics of TMP in methanol (CD_4O). After VC, two long-living excited states exist. State X1 is identified by the absorbance around 1740 cm^{-1}. It decays to the ground state within 2 ns. The triplet state (identified by the marker band around 1600 cm^{-1}) is formed within a few ps. The right panels show the absorbance changes at the marker positions of X1 (1740 cm^{-1}), of the triplet state (1596 cm^{-1}) and the ground state (1664 cm^{-1}). The triplet band rises with a time constant around 10 ps. X1 is unaffected by the intersystem crossing to the $^3\pi\pi^*$ state and the $^3\pi\pi^*$ state is unaffected by the decay of X1 to the ground state.

is caused by the build-up of the $^3\pi\pi^*$ absorption. The X1 marker band absorption is not diminished in the first 20 ps, except by a small amount due to the decay of the broadband signatures of vibrational cooling. This finding confirms that X1 is not a triplet precursor. The decay of X1 occurs on the timescale of 1 ns to 2 ns, similar to the kinetics in water.

7.3.2. Multiexponential Data Modelling and Further Analysis

Multiexponential modelling of the data is done in the same way as previously for the measurements of TMP in water. The obtained DADS of X1 and the $^3\pi\pi^*$ state are depicted in panels (a) and (b) of Figure 7.11, together with the inverted ground state absorbance (black) and the calculated absorbance spectra of the excited states (green). The DADS that describe vibrational cooling are not depicted. The panels on

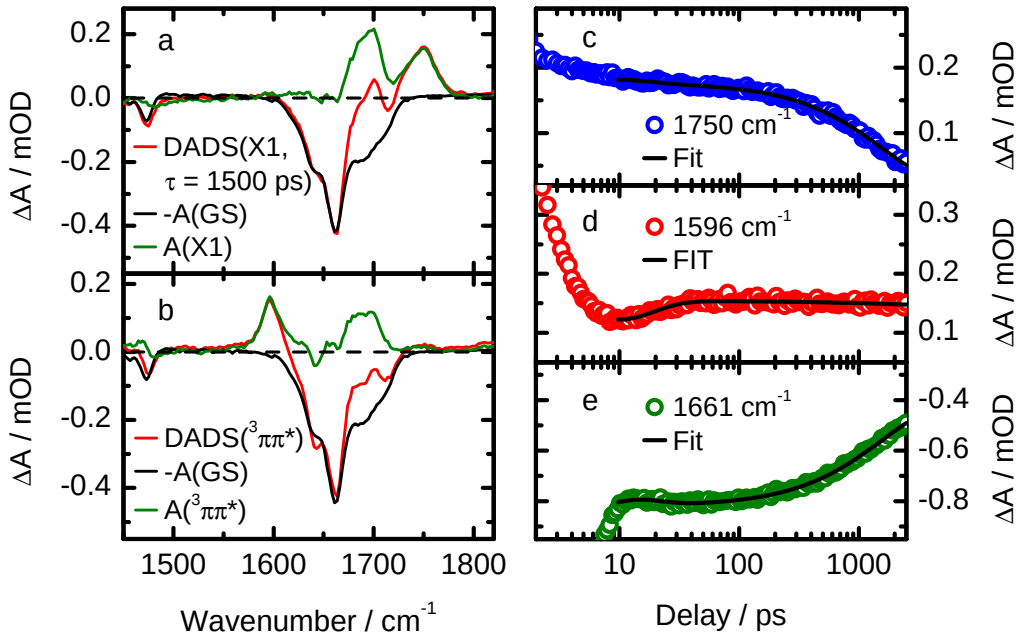

Figure 7.11.: DADS of the excited states X1 (red in (a)) and $^3\pi\pi^*$ (red in (b)) compared to the ground state absorbance (black in (a) and (b)) and the calculated absorbance spectra of both states (green in (a) and (b)). The right panels (c)–(e) depict the data (circles) and the modelled data (lines) at the indicated wavenumbers. The good agreement validates the fit.

the right ((c),(d),(e)) compare the data (circles) and the model function (black lines) at the indicated wavenumbers. The good agreement validates the model and the DADS. As in water, X1 is characterised by two absorption bands around 1700 cm^{-1} and 1750 cm^{-1} and decays to the ground state with a time constant in the nanosecond range (1.5 ns in methanol compared to 1 ns in water).

The $^3\pi\pi^*$ state is characterised by a red-shifted marker band around 1600 cm^{-1} and an absorption band around 1700 cm^{-1} that is obscured by the ground state bleach in the DADS.

Quantum Yields of X1 and $^3\pi\pi^*$

While the spectral features of both states are very similar in water and methanol, the quantum yield Φ_{ISC} is drastically modified by the solvent. The quantum yields are calculated as demonstrated in subsection 7.2.2. Figure 7.12 shows the absorbance change (red) and the inverted ground state absorbance spectra (black) of X1 (left), the $^1\pi\pi^*$ state/hot ground state (middle) and the triplet state (right). Table 7.2 shows the resulting numbers. The quantum yields of X1 and the $^3\pi\pi^*$ state are in the 10 % range.

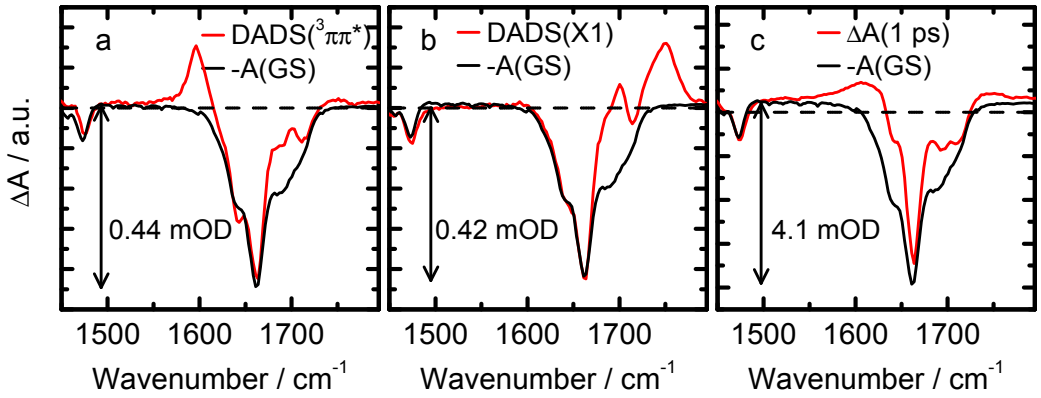

Figure 7.12.: Determination of the quantum yields the $^3\pi\pi^*$ state (a) and X1 (b) of TMP in deuterated methanol (CD_4O). The ground state absorbances of those states are compared to the initial absorbance change after 1 ps. The resulting quantum yields are Φ_{ISC} =11 % and Φ_{X1} = 10 %.

Changing the solvent from water to methanol increases the $^3\pi\pi^*$ quantum yield 8-fold, while it does not change the quantum yield of X1 significantly.

7.3.3. Population of the Excited States

The population of X1 occurs in methanol and water on the same timescale with about the same quantum yield. A discussion of the mechanism is therefore not necessary, it was already given in the corresponding section for TMP in water. The intersystem crossing process on the other hand needs some discussion. ISC to the $^3\pi\pi^*$ state occurs during vibrational cooling and is therefore obscured by it. Even though the spectra of excited states cannot be observed in this temporal window, spectrally isolated features and their temporal evolution may still be observable during VC. The $^3\pi\pi^*$ marker band around 1596 cm^{-1} is red-shifted compared to all major ground state bands and thereby may be such a feature. The absorbance at 1596 cm^{-1} is the sum of the absorptions of the triplet marker band and the hot ground state during vibrational cooling. The amplitude of the triplet absorption band can be calculated if the absorbance of the hot ground state at 1596 cm^{-1} can be approximated and subtracted from the data. This calculation is depicted in the left panel of Figure 7.13. The absorbance change caused by vibrational cooling $\Delta A_{VC}(1596\,\mathrm{cm}^{-1}, t_D)$ at the triplet marker position is approximated by a linear interpolation between 1580 cm^{-1} and 1612 cm^{-1}:

$$\Delta A_{VC}(1596\,\mathrm{cm}^{-1}, t_D) = \frac{\Delta A(1580\,\mathrm{cm}^{-1}, t_D) + \Delta A(1612\,\mathrm{cm}^{-1}, t_D)}{2} \tag{7.2}$$

The right panel of Figure 7.13 shows the transient absorbance change at 1596 cm^{-1} (red), the interpolated absorbance change of VC (grey) and the difference that is

Excited State	$\Delta A(1661\,cm^{-1})/mOD$	Amount/%
$^1\pi\pi^*$	−4.1	100
X1	−0.42	10
$^3\pi\pi^*$	−0.44	11

Table 7.2.: Amplitudes of the ground state bleach of the indicated excited states at 1661 cm^{-1}. Comparing the amplitudes of the $^3\pi\pi^*$ state and X1 to that of the $^1\pi\pi^*$ state determines their quantum yields.

identical to the $^3\pi\pi^*$ absorbance. The triplet absorption starts at zero and builds up in the first 20 ps. An exponential fit reveals that the triplet state is formed with a time constant of around 9 ps.

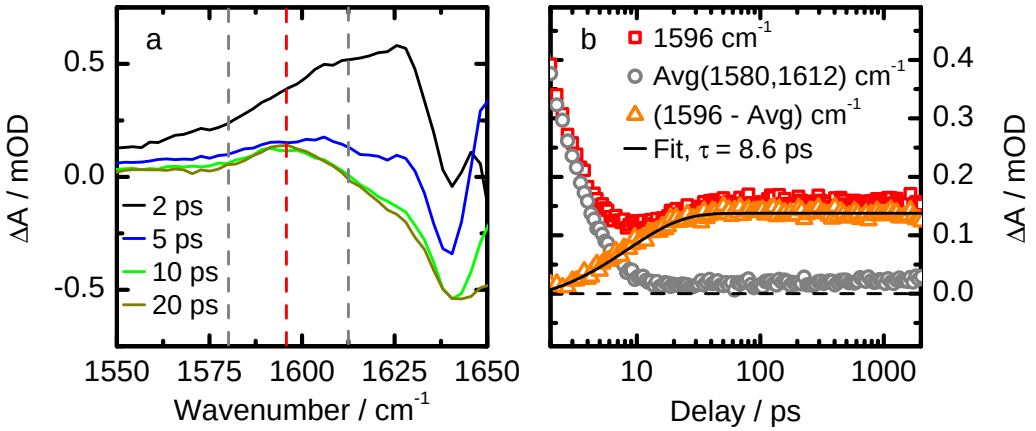

Figure 7.13.: ISC of TMP in CD_4O. The $^3\pi\pi^*$ absorption at 1596 cm^{-1} is overlayed by the hot ground state absorption (a). The latter is approximately the average value of the absorption at 1580 cm^{-1} and 1612 cm^{-1}. Panel (b) shows the absorption at 1596 cm^{-1}, the signal of vibrational cooling and the calculated triplet absorption. An exponential fit of the data reveals that ISC takes place with a time constant of 9 ps.

The excited $^1\pi\pi^*$ state has a lifetime below 1 ps [PPK01, PPK01], therefore the $^1\pi\pi^*$ state can be excluded as the triplet precursor.

The data of TMP in water already provided evidence that a $^3\pi\pi^*$ state is populated within a few picoseconds after excitation, much faster than the decay of X1. The thermally relaxed state X1 was ruled out as the triplet precursor. However, it is possible that only a thermally excited state X1 can undergo ISC to the $^3\pi\pi^*$ state (such an idea was proposed for a thermally excited $^1n\pi^*$ state [HCK07, Mid09], see section 7.1). The data of TMP in methanol confirm that X1 is not quenched on the timescale of triplet population, so X1 can be conclusively ruled out as a triplet precursor.

An additional excited state X2 must exist that is populated from the initially excited $^1\pi\pi^*$ state and then undergoes a transition to the $^3\pi\pi^*$ state. It is probably strongly affected by the solvent, explaining the solvent dependence of the triplet quantum yield. However, without its spectral signature, a definitive identification is not possible. The DADS of the transition X2 $\rightarrow$ $^3\pi\pi^*$ could provide an adequate spectral characterisation, but it is not accessible: The time constant of the transition X2 $\rightarrow$ $^3\pi\pi^*$ is circa 9 ps. Its DADS is not obtainable via a multiexponential fit, because it is obscured by the non-exponential signals of vibrational cooling (see the discussion in subsection 7.2.2). More data in solvents with high ISC yields may provide further insight into this question.

7.4. Thymine in Water and Acetonitrile

The ISC quantum yields of thymine in acetonitrile is reported to be between 6 % [SB75] and 18 % [WB70]. Acetonitrile is aprotic, therefore the $n\pi^*$ states, the supposed triplet precursors [ElS63, EFM09, Gon10a], should be energetically below the $^1\pi\pi^*$ state and may be populated in significant amounts [Nak13]. Moreover, the measurements that led Hare et al. to propose ISC from vibrationally excited $^1n\pi^*$ states [Har08] were performed in acetonitrile. It is therefore worthwhile trying to reproduce these measurements and compare the obtained data. In this section, TRIR measurements of thymine in deuterated acetonitrile (CD_3CN) and D_2O are presented. Thymine is chosen as the sample instead of TMP, because the latter is nearly insoluble in CD_3CN.

7.4.1. Thymine in Water: Excited State Decay

Figure 7.14 shows the excited state physics of thymine (left panels) and TMP (right panels) in D_2O. To focus on X1, the residual absorbance changes after the maximum delay (1.5 ns for thymine, 2.5 ns for TMP) were subtracted from the data, correcting the data for the signals of solvent heating, the lowest triplet state and thymine cations. The lower panels show the DADS of X1 (red), the ground state absorbance (black) and the calculated absorbance spectra of X1 (green). As in TMP, the absorbance spectra of X1 in thymine is characterised by two absorbance bands, one of them blue-shifted with respect to all the ground state bands. The X1 marker bands of thymine are red-shifted by circa 20 cm^{-1} compared to the equivalent bands of TMP. The excited state lifetimes are drastically different in the samples. X1 of thymine decays to the ground state with a time constant of 280 ps, compared to a lifetime of 1000 ps in TMP. The glycosidic bond (bond between N1 and the sugar) of TMP apparently has a profound influence on the lifetime of X1.

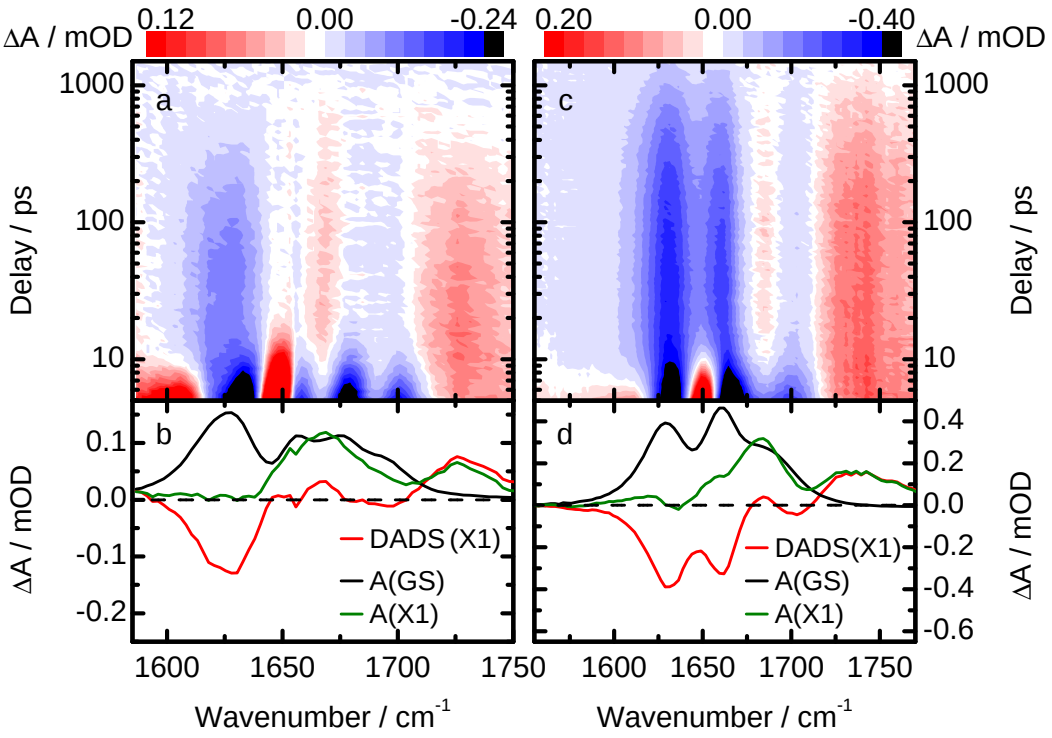

Figure 7.14.: Comparison of the excited state physics of thymine (left) and TMP (right) in D_2O after UV excitation. To focus on the long-living state, the residual absorbance changes after 1.5 ns (thymine) and 2 ns (TMP) have been subtracted from the data. Panels (a) and (c) show the contour plots of the absorbance changes, panels (b) and (d) show the DADS of X1 (red), the ground state absorbance (black) and the absorbance spectra (green). The decay of X1 in both cases is quite different: The excited state decay of thymine proceeds with a time constant of 280 ps, about a fourth of the value obtained for TMP (1000 ps).

7.4.2. Thymine in Water: Quantum Yields

The presence or absence of the deoxyribose affects the lifetime and may as well influence the quantum yields of X1. The quantum yield of X1 is determined by comparing the ground state bleach amplitudes associated with X1 (panel (a) in Figure 7.15) and the initially populated $^1\pi\pi^*$ state/hot ground state (panel (b) in Figure 7.15). The quantum yield of X1 in thymine is determined to be 7 %, lower than the X1 quantum yield of TMP (10 %).

The difference between 7 % and 10 % is well within the achievable accuracy of the quantum yield measurements. The N-glycosidic bond affects the lifetime as well as the quantum yield of X1.

A discussion of the $^3\pi\pi^*$ state of thymine in water is not given at this point, because the low ISC quantum yield hampers the investigation.

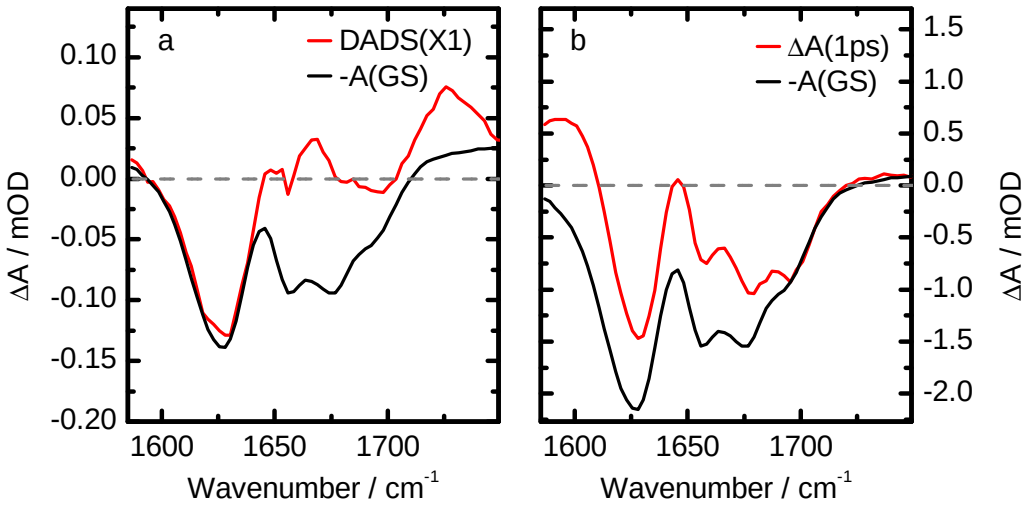

Figure 7.15.: Determination of the quantum yield of X1 of thymine in water by comparing the ground state bleach of X1 (a) to the initial ground state bleach (b). The quantum yield Φ_{ISC} is determined to be 7 %.

7.4.3. Thymine in Acetonitrile

The excited state physics of thymine (concentration circa 3 mM) in deuterated acetonitrile (CD_3CN) is probed by TRIR spectroscopy. Figure 7.16 depicts the resulting data. Panel (a) shows the contour plot of the transient absorbance changes after UV excitation.

The signatures of vibrational cooling dominate the absorbance changes in the first 20 ps after excitation. This comparatively long timescale results from the slow dissipation of energy to the solvent (compared to water). Panel (b) shows the transient spectra at delay times of 10 ps, 500 ps and 2000 ps. The excited state signatures can only be identified after VC is finished. After circa 20 ps, the spectrum is characterised by an induced absorption around 1590 cm^{-1}, ground state bleaches at 1670 cm^{-1} and at 1720 cm^{-1} and an induced absorption around 1745 cm^{-1}. As the 1745 cm^{-1} band disappears, the ground state partially recovers, while the absorption at 1590 cm^{-1} remains unchanged. Again, two long-living states X1 and $^3\pi\pi^*$ exist: X1 is identified by a blue-shifted absorption at 1745 cm^{-1}, the $^3\pi\pi^*$ state (Figure 7.16, panel (c)) by the marker band around 1590 cm^{-1} (the identification of these states as X1 and $^3\pi\pi^*$ will be validated by the calculation of the absorbance spectra of both states, see Figure 7.17).

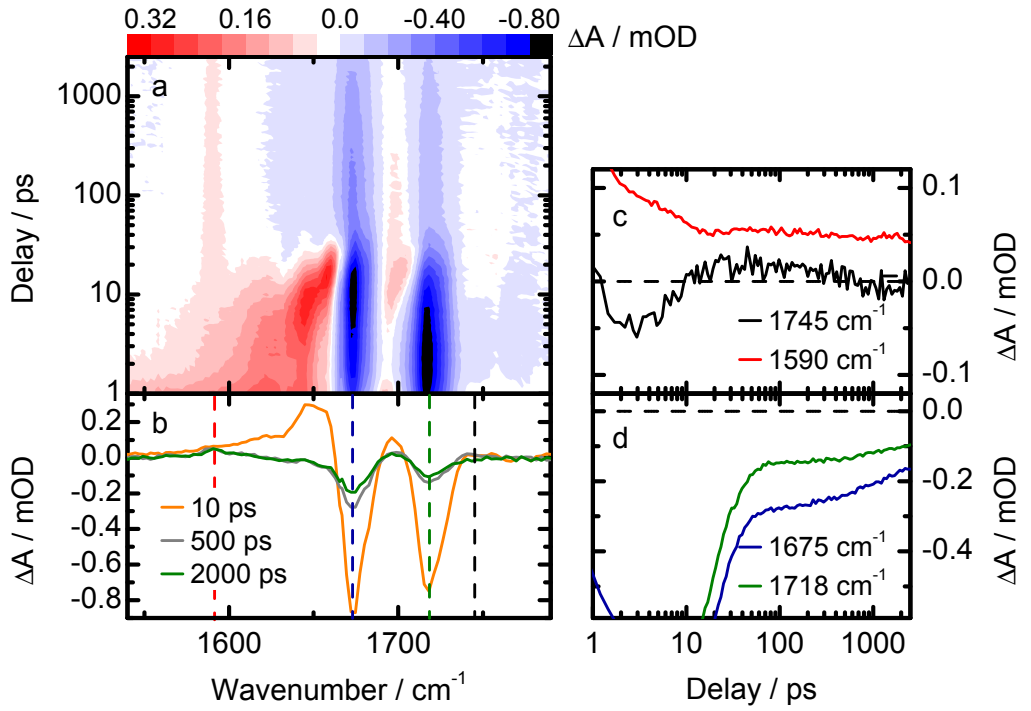

Figure 7.16.: Excited state physics of thymine in acetonitrile. In the first 20 ps vibrational cooling dominates the excited state physics. Two long-living states exist, X1 and $^3\pi\pi^*$. X1 is identified by the absorption around 1745 cm^{-1}, the $^3\pi\pi^*$ state by the marker band around 1590 cm^{-1}.

7.4.4. Spectral Characterisation and Quantum Yields

A multiexponential fit reveals the DADS of both states (panels (a) and (b) of Figure 7.17). The corresponding absorbance spectra are calculated in panels (c) and (d). X1 is characterised by two absorbance bands at 1700 cm^{-1} and 1750 cm^{-1}, the $^3\pi\pi^*$ state by two bands at 1695 cm^{-1} and 1590 cm^{-1}, in agreement with the data in other solvents. The lifetime of state X1 is around 1000 ps, a circa 4-fold increase compared to the X1 lifetime of thymine in water. A small solvent dependence of the X1 lifetime was also observed comparing the data of TMP in water and methanol, but this time the effect is stronger.

The solvent is also expected to affect the quantum yields of the states X1 and $^3\pi\pi^*$. The determination of those yields is done the same way as with the previous samples (see subsection A.2.2). The quantum yield of X1, Φ_{X1}, is 12 %, comparable to the values for TMP in water and methanol, but higher than the value for thymine in water. The ISC quantum yield Φ_{ISC} is 13 %, almost in the middle between the reported values of 6 % [SB75] and 18 % [WB70].

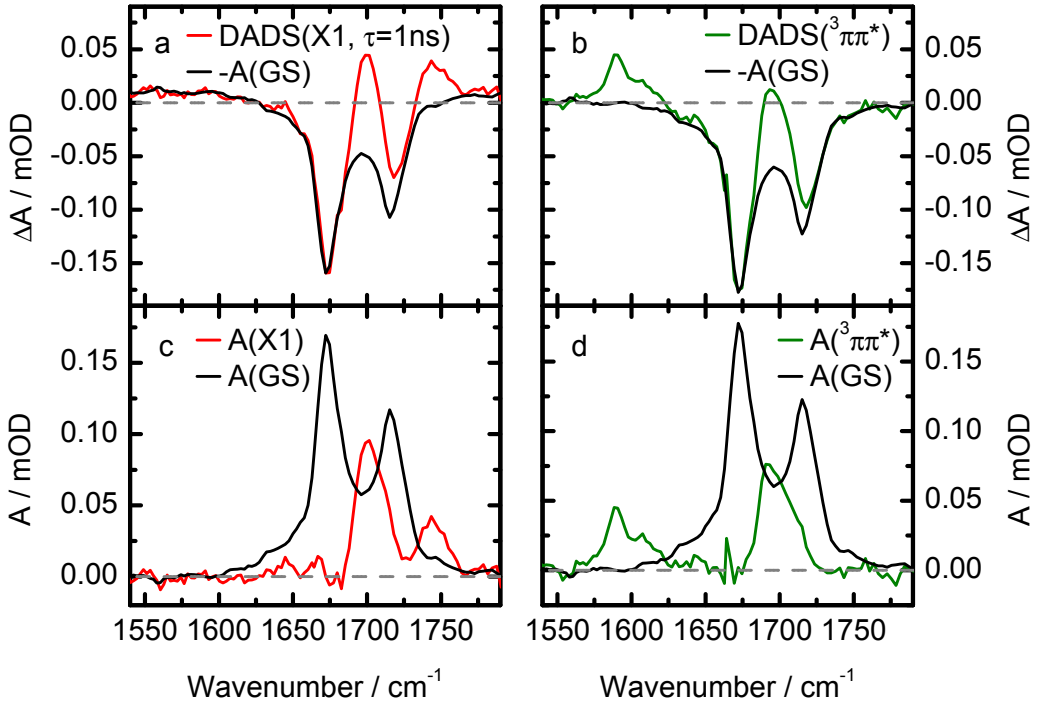

Figure 7.17.: The DADS and the calculated absorbance spectra of X1 (left panels) and the $^3\pi\pi^*$ state (right panels). The results agree well with the previously determined spectra of X1 and the $^3\pi\pi^*$ state in different solvents.

7.4.5. Population of the Excited States X1 and $^3\pi\pi^*$

Population of X1

The temporal evolution of the absorbance bands is depicted in the right panels of Figure 7.16. The X1 marker band at 1745 cm^{-1} builds up in the first 20 ps, not in the first picosecond as it did in the other solvents. However, upon closer inspection, the increasing absorption at 1745 cm^{-1} in the first 20 ps is due to a recovery of the ground state absorption by vibrational cooling, not due to a delayed population of X1: Ground state thymine has a small absorption band at 1745 cm^{-1} (see panel (c) in Figure 7.17). The absorbance of the X1 marker band is therefore overlaid by the ground state bleach during vibrational cooling. In section A.1 the absorbance of the excited state at 1745 cm^{-1} is calculated. The increase of absorption turns out to be entirely due to the vanishing of the ground state bleach, not a slow build-up of the X1 marker band. The X1 absorption is present within 1 ps, just as in the other samples.

Population of the $^3\pi\pi^*$ State

The triplet marker band at 1590 cm^{-1} is quite small, so its build-up is obscured by the signals of vibrational cooling in the first 20 ps.

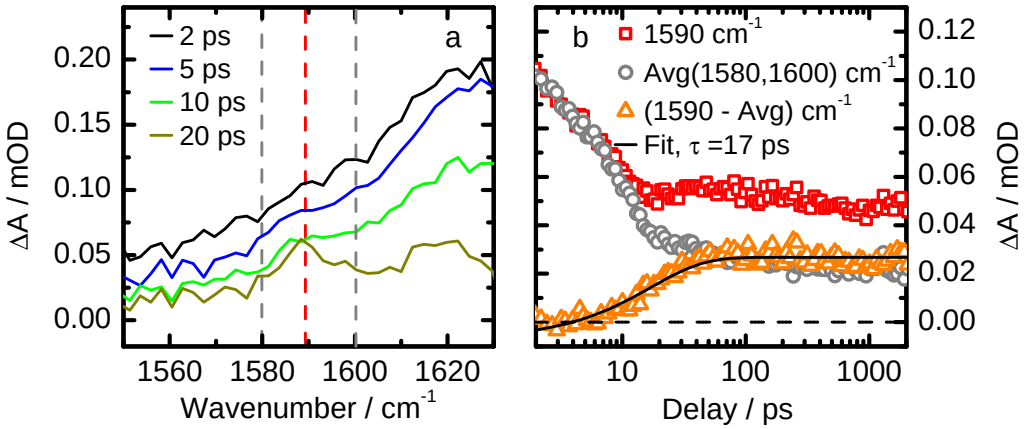

Figure 7.18.: Transient spectra in the first 20 ps after excitation in the spectral region around the triplet marker band (a). The triplet band is overlayed by the absorption of the hot ground state during VC (red in (b)). The hot ground state absorption at 1590 cm^{-1} is approximated as the average signal at 1580 cm^{-1} and 1600 cm^{-1} (grey). Subtracting the latter from the data at 1590 cm^{-1} yields the signal of the triplet marker band (orange). The triplet signal apparently builds up with a time constant around 20 ps.

The data can be corrected for these effects the same way it was done for TMP in methanol: The hot ground state signature is approximately linear around 1590 cm^{-1} (see the left panel of Figure 7.18). Consequently, the expected absorbance at 1590 cm^{-1} caused by the hot ground state, $\Delta A_{VC}(1590cm^{-1}, t_D)$, can be calculated:

$$\Delta A_{VC}(1590\,\mathrm{cm}^{-1}, t_D) = \frac{\Delta A(1580\,\mathrm{cm}^{-1}, t_D) + \Delta A(1600\,\mathrm{cm}^{-1}, t_D)}{2} \tag{7.3}$$

The time-dependent absorbance change of the triplet marker band is then calculated by subtracting this value from $\Delta A(1590\,\mathrm{cm}^{-1}, t_D)$. The right panel of Figure 7.18 depicts the resulting triplet absorption around 1590 cm^{-1}. The triplet marker band builds up with an exponential time constant of 17 ps. As was already seen for TMP in methanol, the $^3\pi\pi^*$ state is populated predominantly via an intermediate state long after the decay of the excited $^1\pi\pi^*$ state. Again, the signatures of vibrational cooling make the DADS of the transition X2 $\rightarrow$ $^3\pi\pi^*$ inaccessible.

In conclusion, efficient ISC to the $^3\pi\pi^*$ state requires an intermediate state. Since the ISC yield is very low in water, it is tempting to assume that the triplet precursor is not populated in water, maybe because it is energetically not accessible from the $^1\pi\pi^*$ state. These descriptions match the theoretical expectations of a $^1n\pi^*$ state: The $^1n\pi^*$ state is predicted by theoretical studies to be an efficient triplet precursor [ElS63,

Ser07, EFM09, Gon10a], if it is populated in significant amounts. The population of the $^1n\pi^*$ state depends on the energetic accessibility, and some studies suggest that the $^1n\pi^*$ state is not accessible in water [Nak13, EM10], where Φ_{ISC} is low.

7.5. Discussion: Nature of X1 and X2

Two excited states X1 and X2 that are populated out of the $^1\pi\pi^*$ state were reported in the previous section. X1 is populated in protic and aprotic solvents with similar quantum yields and shows similar kinetics. Table 7.3 depicts an overview of the quantum yields of X1 and $^3\pi\pi^*$ in different solvents that were determined in the previous sections. While the quantum yield of X1 is only weakly affected by the solvent, the ISC quantum yield varies drastically with changing solvents. There appears to be no correlation between the quantum yields of X1 and of the $^3\pi\pi^*$ state, and the TRIR data presented in the previous sections directly showed that X1 does not contribute to triplet formation. It returns to the electronic ground state on a timescale of 280 ps to 1.5 ns.

Sample	$\Phi_{X1}/\%$	τ_{X1}/ps	$\Phi_{ISC}/\%$
TMP in D_2O	11	1000	—
TMP in CD_4O	10	1500	11
Thy in D_2O	7	280	—
Thy in CD_3CN	12	1000	13

Table 7.3.: Quantum yields of X1 (Φ_{X1}) and $^3\pi\pi^*$ (Φ_{ISC}) and X1 lifetime of thymine and TMP in different solvents as determined in this thesis. Φ_{ISC} of TMP and thymine in D_2O were determined by other studies to be in the 1 % to 2 % range [Ban12].

The other excited state X2 was not observed directly, because it is obscured by the signals of vibrational cooling. Its existence was only derived from the observation that neither the excited $^1\pi\pi^*$ state nor X1 are the major $^3\pi\pi^*$ precursors. The drastically varying ISC quantum yields in different solvents suggest that X2 is highly solvent dependent.

Theoretical studies of thymine in the gas phase predict that three excited states are energetically below the $^1\pi\pi^*$ state. These are, in descending order, $^1n\pi^*$, $^3n\pi^*$ and $^3\pi\pi^*$ states (see for example [FKH07, Ast09]). If these are the only accessible excited states, X1 and X2 have to be identified as the $^1n\pi^*$ and $^3n\pi^*$ states, otherwise other excited states have to be postulated. These possibilities are discussed in this section. It suggests itself to start this discussion by comparing the observed features of X1 to the expected features of the $n\pi^*$ states.

7.5.1. Spectral Characterisation of $n\pi^*$ States

The absorbance spectrum of X1 that was obtained experimentally can be compared to calculated absorbance spectra of $n\pi^*$ states. Such calculations can partly be found in the literature [Ser07, Ast09, FKH07], but in addition state-of-the-art quantum chemical calculations were performed by Dr. Benjamin Fingerhut (Max Born Institute Berlin). The details of the calculations will be described in a manuscript that is to be published.

Figure 7.19 depicts the thymine molecule and the bond lengths of the C5=C6, the C2=O7 and the C4=O8 bonds that cause the IR absorption between 1600 cm^{-1} and 1700 cm^{-1}. The right side of Figure 7.19 shows the bond lengths of the three bonds in the ground state (left) and the $n\pi^*$ state (right) ($^1n\pi^*$ and $^3n\pi^*$ state exhibit nearly the same geometries and vibrational spectra, see also [Ser07]).

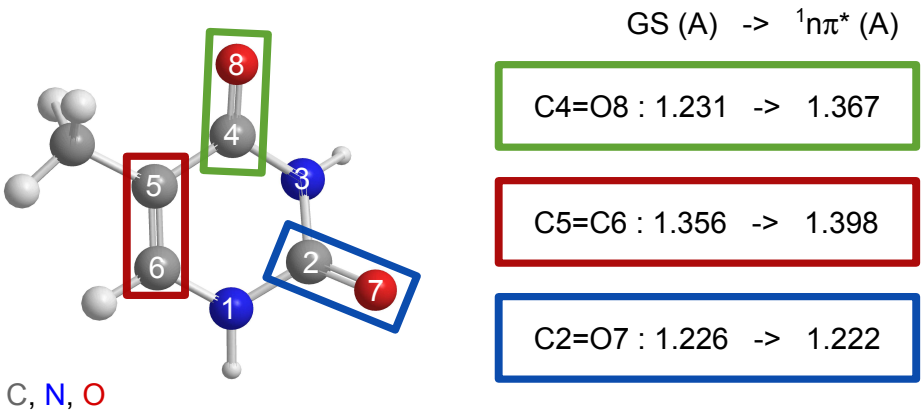

Figure 7.19.: CASPT2 calculation of the bond lengths of thymine in the ground state and in the $^1n\pi^*$ state. The MIR absorbance of thymine is dominated by vibrations of the C2=O7, C5=C6 and C4=O8 bonds. The C5=C6 and the C4=O8 bond are elongated in the $^1n\pi^*$ state, red-shifting the IR bands. The C2=O7 is slightly shortened, blue-shifting the corresponding vibration.

The C4=O8 band in the $n\pi^*$ state has single-bond character, therefore its vibration is red-shifted by more than 100 cm^{-1}. The C5=C6 bond is elongated compared to the ground state, so the absorbance band is also red-shifted. Only the C2=O7 bond is slightly shortened, blue-shifting the absorbance band.

Since the ground state absorbance between 1600 cm^{-1} and 1700 cm^{-1} is caused by vibrations of those three bonds [BSG03], the $n\pi^*$ state should only show one blue-shifted absorbance band, and two red-shifted bands at wavenumbers below 1600 cm^{-1} with strongly decreased amplitudes. Figure 7.20 depicts the absorbance of TMP in methanol (left) and water (right) in the ground state (black) and X1 (red) compared to the C=O bands of the $^1n\pi^*$ state calculated using CASPT2. The calculated vibrations are blue-shifted compared to the experimentally observed ones

by around 150 cm^{-1}, but the relative spectral positions are correct. In the $^1n\pi^*$ state the absorbance band of the C2=O7 vibration is blue-shifted by around 50 cm^{-1} and increased in amplitude. This band agrees reasonably well with the blue-shifted absorbance band. The absorbance bands of the C4=O8 and C5=C6 vibrations are red-shifted by more than 100 cm^{-1} (see the elongations of the bonds in Figure 7.19) and decreased in amplitudes. These bands would be present below 1500 cm^{-1} and overlay the absorbance bands in this spectral region. No fundamental vibration is found that can account for the absorbance band around 1690 cm^{-1}.

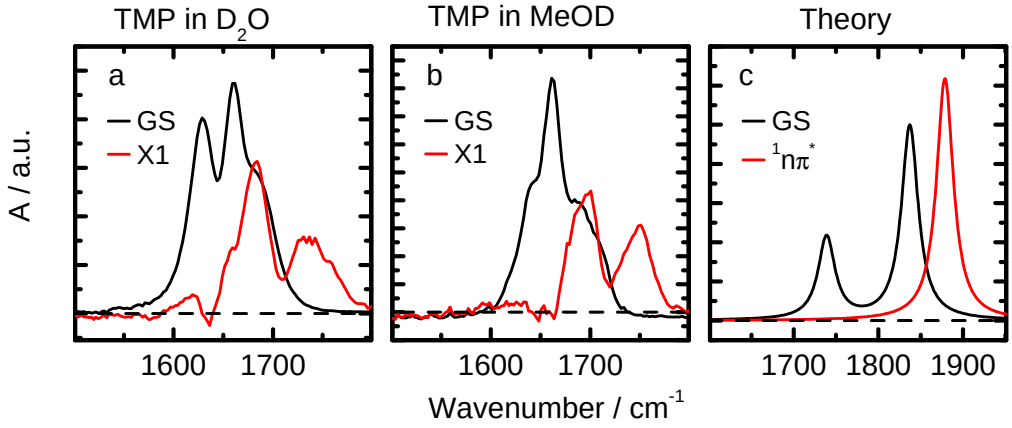

Figure 7.20.: Comparison of the experimentally observed absorption spectra of X1 and the ground state in D_2O (a) and CD_4O (b) to the calculated spectra of the ground state and the $^1n\pi^*$ state (c). The experimental data for X1 show two strong absorbance bands around 1700 cm^{-1}, while only one band is predicted by the calculation for the $^1n\pi^*$ state.

An explanation for this disagreement between these experimentally observed and the calculated spectra could be a Fermi resonance [GG12] of the C2=O7 vibration with overtones or combination tones of lower-frequency vibrations that causes a splitting of the C2=O7 absorbance band, resulting in two absorbance peaks instead of one. This explanation is at this point purely speculative and not yet supported by evidence. Such evidence can in principle be provided experimentally, if the coincidental match between the frequencies of the C2=O7 vibrations and overtones of other vibrations are eliminated by shifting the vibrational frequencies.

7.5.2. Models That Involve Only $n\pi^*$ States

The comparison of the experimental data of X1 to the theoretical data of $n\pi^*$ states does not give strong support for the identification of X1 as a $n\pi^*$ state. However, it also does not rule it out, since the mismatch of the spectra may be caused by a Fermi resonance.

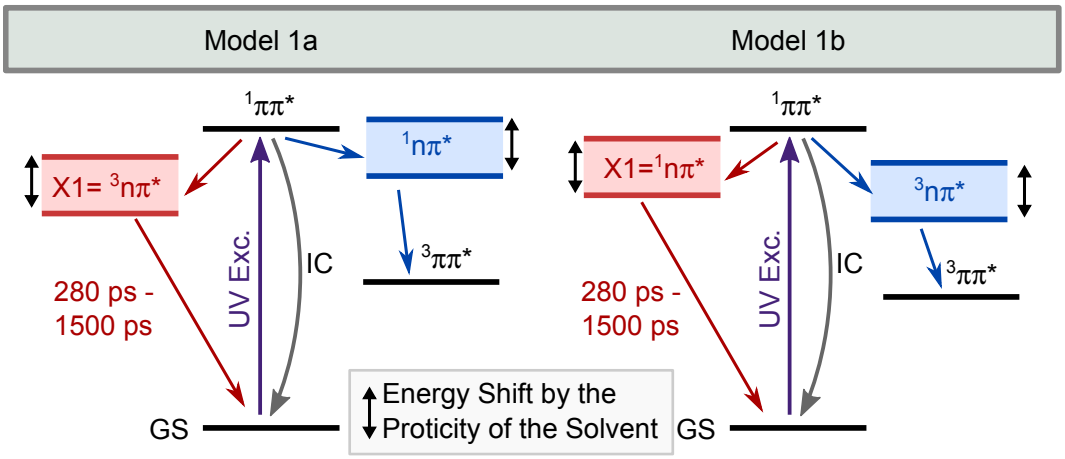

Figure 7.21.: Excited state physics of thymine. The models assume that either the singlet (1a) or the triplet (1b) $n\pi^*$ state is the $^3\pi\pi^*$ precursor X2, while the other is the long-living state X1. The energy levels of the $n\pi^*$ states are shifted by the proticity of the solvent, as indicated by the black arrows.

A more detailed discussion of the different possible models is necessary. Obviously, two possibilities exist to identify X1 and X2 as the $n\pi^*$ states. They are depicted in Figure 7.21.

Is X1 a $^3n\pi^*$ State? Model 1a assumes that the triplet precursor X2 is a $^1n\pi^*$ state and the long-living state X1 is of $^3n\pi^*$ nature. This model could describe the solvent dependence of the ISC yield and the relative solvent independence of X2, because the $^1n\pi^*$ state becomes inaccessible in water, whereas the lower-energy $^3n\pi^*$ state is accessible in protic and aprotic solvents alike. This energy ordering of the excited states agrees with recent theoretical studies [Nak13, Buc15b]. However, this model assumes that the $^3n\pi^*$ state may be populated quite efficiently (circa 10 %) from the $^1\pi\pi^*$ state and then returns to the ground state. This is highly implausible, since internal conversion from the $^3n\pi^*$ state to the $^3\pi\pi^*$ state does not require a change in multiplicity and is not hindered by substantial energy barriers [Gon10a]. The $^3n\pi^*$ should therefore predominantly decay to the $^3\pi\pi^*$ state, not return to the ground state. X1, however, is not a $^3\pi\pi^*$ precursor, but decays to the ground state. It is therefore most likely not a $^3n\pi^*$ state, so model 1a is not satisfactory.

Is X1 a $^1n\pi^*$ State? Even though theoretical studies predict relatively efficient ISC from the $^1n\pi^*$ state to the $^3\pi\pi^*$ state, the $^1n\pi^*$ state may still predominantly return to the ground state. Then, the $^1n\pi^*$ state may be X1 and the $^3n\pi^*$ state would have to be the major $^3\pi\pi^*$ precursor X2. Since X1 is found with about the same quantum yields in protic and aprotic solvents, the $^1n\pi^*$ state and the lower-energy $^3n\pi^*$ state would both have to be energetically accessible in protic and aprotic solvents. However,

if the triplet precursor was accessible in water and acetonitrile, it is unclear why the triplet yields differ drastically in both solvents.

7.5.3. A Model That Involves More Than $n\pi^*$ States

The models discussed so far assumed that both states X1 and X2 are of $n\pi^*$ nature. Both of those models did contain implausibilities and were insofar unsatisfactory.

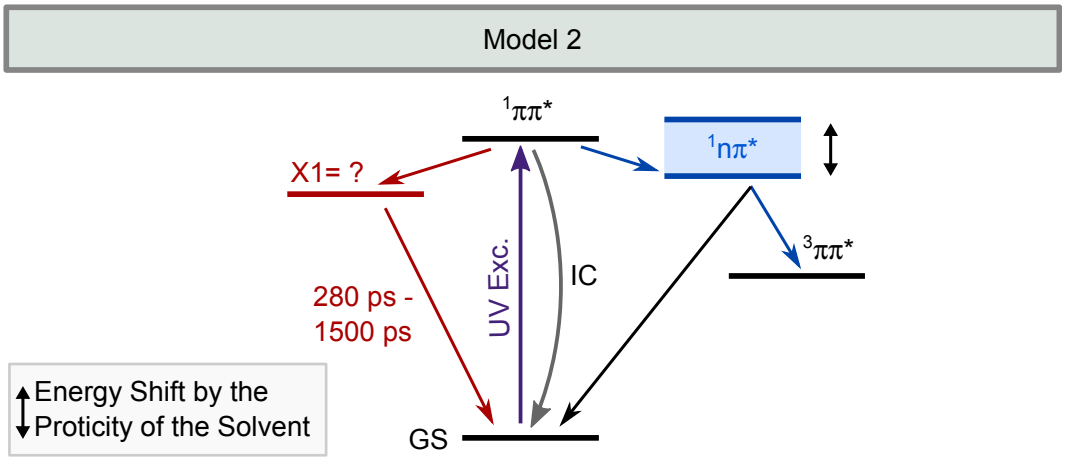

Figure 7.22.: Excited state physics of thymine. Model 2 identifies X2 as a $^1n\pi^*$ state. The energetic accessibility of X2 is solvent dependent, explaining the solvent dependence of Φ_{ISC}. X1 is not identified, but it is not a $n\pi^*$ state.

An alternative interpretation of the data assumes that only the triplet precursor X2 is a $n\pi^*$ state, either $^1n\pi^*$ or $^3n\pi^*$. Both $n\pi^*$ states could be efficient precursors to the $^3\pi\pi^*$ state, because the intersystem crossing also changes the orbital type: In one case, ISC occurs from the $^1\pi\pi^*$ to the $^3n\pi^*$ state, that subsequently undergoes IC to the $^3\pi\pi^*$ state. In the other case, internal conversion from the $^1\pi\pi^*$ to the $^1n\pi^*$ state precedes ISC from $^1n\pi^*$ to $^3\pi\pi^*$. Both ISC processes are 'allowed' by the rule of El-Sayed [ElS63] and therefore should be relatively efficient. However, ISC from the $^1\pi\pi^*$ state to the $^3n\pi^*$ state might not be efficient enough to compete with the sub-picosecond decay of the $^1\pi\pi^*$ state to the ground state: A theoretical study suggested that the $^3n\pi^*$ state is not populated in significant amounts [EFM09], while the $^1n\pi^*$ state is populated efficiently after $^1\pi\pi^*$ excitation and subsequently acts as the major triplet precursor. Moreover, some studies suggest that the $^1n\pi^*$ state is energetically below the $^1\pi\pi^*$ state in the gas phase and aprotic solvents, but is above it in water [FKH07, Nak13, Buc15b]. These hypotheses about the role of $n\pi^*$ states can be easily reconciled with the solvent dependent triplet quantum yield in a simple model (Model 2 in Figure 7.21): It assumes that the $^1n\pi^*$ state is accessible in methanol and acetonitrile, but not in water, while the $^3n\pi^*$ is not significantly populated in all solvents. The $^1n\pi^*$ state then undergoes ISC to the $^3\pi\pi^*$ state (and

possibly partly returns to the ground state) on the timescale of triplet formation, i.e. within less than 20 ps. This model agrees well with theoretical studies, but it leaves open the question about the nature of X1. Then, X1 must be an additional excited state of thymine that was not yet reported and discussed in the literature (see for example [Ser07, Che13, FKH07, Mid09]).

This model is explored further by discussing a few possibilities to identify X1.

7.5.4. Is X1 the Result of Two-Step Excitation?

One possibility is that the observed absorbance changes of X1 are not caused by a decay cascade of the $^1\pi\pi^*$ state at all.

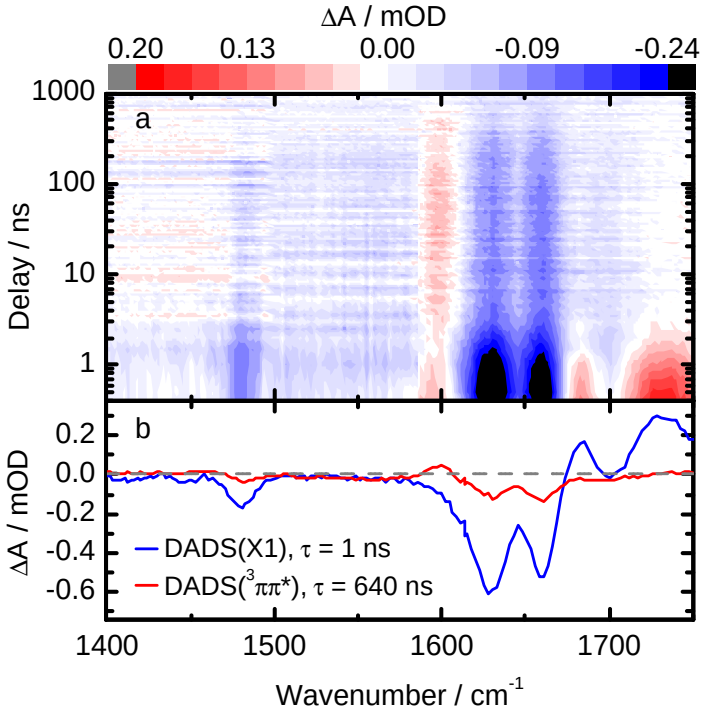

Figure 7.23.: Absorbance changes of TMP after UV excitation on the ns timescale, corrected for the signal of solvent heating (a). In the first nanosecond the signal is dominated by the absorbance changes of X1, easily identified by the absorption around 1740 cm^{-1}. A multiexponential fit reveals the DADS of X1 and the $^3\pi\pi^*$ state (b).

Since short and thereby intense pulses are used, the excitation of a higher excited state by two photons seems possible. Two-step ionisation of bases, yielding cations and solvated electrons, was already demonstrated [Nik90, Reu00]. While it can be excluded that the observed state is the cation, as it does not match either the spectrum, nor the amplitude, nor the lifetime of the cation (see chapter 6), it

still might be a state populated by a decay of a higher excited state than $^1\pi\pi^*$. That possibility can be addressed by using longer excitation pulse durations to suppress two-step excitations. Using the Nd:YVO_4 ns-laser (pulse duration around 0.5 ns), excitation pulses can be provided that are long enough to suppress two-step excitations, but also short enough to have a sufficient temporal resolution to observe an excited state with a lifetime of 1 ns.

Figure 7.23 shows the result of a TRIR measurement of TMP on the ns timescale. The data have been corrected for the signals of solvent heating. As was already shown in chapter 5, the lowest triplet state decays to the ground state within 1000 ns. In the first 2 ns after excitation, another excited state decay is observed. To identify it, a multiexponential fit of the data is performed. Panel (b) of Figure 7.23 shows the DADS. The excited state that decays with a time constant of 1 ns is obviously X1. Apparently, increasing the pulse duration by three orders of magnitude and thereby decreasing the intensity by the same factor does not diminish the amplitude of X1. X1 therefore cannot be the result of a two-step excitation of the sample.

7.5.5. A Long-Living $^1\pi\pi^*$ State?

The $^1\pi\pi^*$ decays to the ground state within less than 1 ps [PPK00, PPK01] via a conical intersection between the $^1\pi\pi^*$ state and the ground state. The CI to the ground state is characterised by a twisting of the C5=C6 double bond [PSD06, Mer06, ZB08, YT11]. However, a fraction of the excited thymine bases may take another pathway on the potential energy surface (PES) of the $^1\pi\pi^*$ state. A recent quantum chemical study found another pathway on the $^1\pi\pi^*$ PES to another conical intersection to the ground state [Nak13]. This new CI is characterised by an out-of-plane displacement of the C4 carbonyl group. This study is an example that different pathways on the PES of the $^1\pi\pi^*$ state can play a role. Additional pathways on the $^1\pi\pi^*$ PES might lead to a local minimum, not a conical intersection with the ground state. If no barrierless path from this minimum to a conical intersection with the ground state exists, the lifetime may be in the 1000 ps range. Could X1 represent such a local minimum of the $^1\pi\pi^*$ PES? If that were the case, the long-living fraction of the $^1\pi\pi^*$ state should decay radiatively to the ground state: Cohen et al. estimate the radiative lifetimes of thymidine to be 5 ns. If the radiative lifetime of a $^1\pi\pi^*$ state in such a hypothetical minimum is of the same order of magnitude, then the corresponding fluorescence quantum yield $\Phi_{rad,min}$ would be around 20 %. The total fluorescence quantum yield caused by this long-living minimum is then $\Phi_{rad} = \Phi_{X1} \cdot \Phi_{rad,min} = 10\,\% \cdot 20\,\% = 2\,\%$ and the fluorescence lifetime is the lifetime of X1. This estimation is directly contradicted by all fluorescence measurements: The fluorescence quantum yield of thymine is in the order of magnitude of 0.01 % [Gus11, Gus06a], and no long-living component of the fluorescence is observed. The radiative lifetime of the hypothetical $^1\pi\pi^*$ minimum would have to be orders of magnitude higher than the aforementioned 5 ns to be consistent with the fluorescence data. This

possibility cannot be excluded definitely, but seems unlikely and is furthermore not supported by any theoretical or experimental evidence published so far. X1 therefore does probably not represent a local minimum of the $^1\pi\pi^*$ state.

7.5.6. Tautomers

The chemical structure of the thymine molecule depicted in chapter 2 represents the canonical, i.e. the major thymine tautomer. The tautomers that can be formed out of TMP are depicted in Figure 7.24 (see also [SH84, Gon09, SS15]). Panel (a) shows the canonical tautomer T1, (b) the other two possible tautomers T2 and T3. The difference between them is seen at the N3 site and the C=O bonds. The canonical diketo form is characterised by C=O bonds with a strong double-bond character, a N3–H bond and two C–N3 single bonds. In each of the tautomers, the hydrogen is bound to one of the oxygen atoms. Then, this oxygen is connected to the carbon atom (C2 or C4, respectively) by a single bond and the C=N3 bond gains double-bond character.

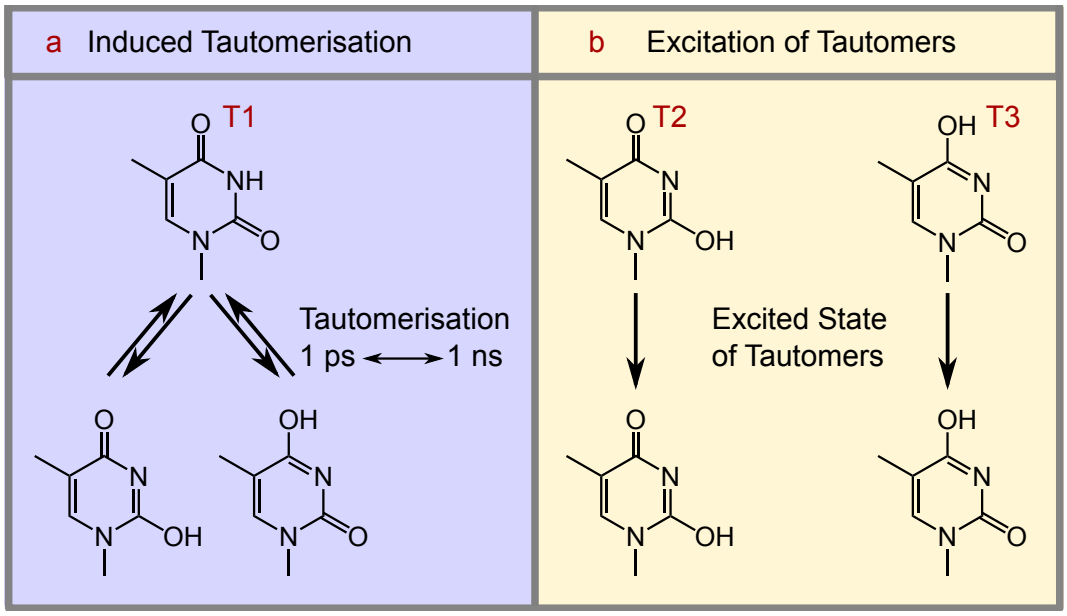

Figure 7.24.: The transitions between the thymine tautomers T1 (major), T2 (minor) and T3 (minor) may play a role in the excited state physics of TMP via two different mechanisms: (a) The major tautomer T1 is excited and may undergo tautomerisation into the ground state or excited states of T2 or T3. (b) T2 and T3 may be present in the sample in significant amounts, then they can be excited and may display different excited state kinetics.

There are two possibilities that tautomers can be involved in the excited state physics of thymine:

1. Non-canonical tautomers are present in significant amounts in the ground state. They are excited and decay slowly to the ground state.

2. The canonical tautomer is excited to the $^1\pi\pi^*$ state and subsequently undergoes tautomerisation.

1. If the tautomers T2 and T3 are present in significant amounts in the sample, the observed absorbance changes would be comprised of the excited state physics of each tautomer. Then the signals of X1 might be related to the excited state physics of T2 and T3, not of the canonical tautomer T1. This model might explain the lack of agreement between the observed DADS of X1 and the calculated spectra of $n\pi^*$ states, but it has to assume that T2 and T3 are present in amounts of circa 10 % or more of the thymine bases to explain the amplitudes of the state X1. Consequently, the ground state energies of T2 and T3 have to be only slightly above the energy of T1, so T2 and T3 can be present in significant amounts at room temperature. However, all calculations of the energies of different tautomers of thymine agree that the energy difference is circa 0.5 eV [Fan10, Gon09, SSK14], so T2 and T3 should be present only in trace amounts. Moreover, the amount of tautomers should vary drastically with different solvents, because the solvents affect the tautomer energies [Fan10]. In water, acetonitrile and methanol the yield of X1 is the same, in contrast to the expected behaviour of tautomers. These arguments strongly indicate that X1 is not caused by the excitation of non-canonical tautomers of TMP.

2. Even if all ground state thymines are in the T1 tautomer, excited state tautomerisation into T2 or T3 might be possible. Thereby an excited state of the tautomers would be reached. Decay of this excited state and re-tautomerisation would return the ground state of T1. The observed lifetime of 1000 ps may therefore be related to either the ground state or an excited state of T2 or T3. For the ground state of T2 and T3 the positions of the C=O bands have been calculated by Dr. Fingerhut. The transfer of a proton from N3 to either oxygen atom results in a drastic red-shift of the C=O vibration, but the other C=O vibration is also red-shifted compared to the ground state of T1. No spectra of the excited states are available at this point in time, so the excited state spectra of the tautomers T2 and T3 cannot be compared to the observed data.

In addition, the insensitivity of X1 to a change of the solvent makes this explanation unlikely. The solvent affects the energy levels of tautomers quite strongly [Fan10], so the similar amount of X1 in different solvents is hard to reconcile with a tautomerisation. It is not clear yet, if suitable excited states of T2 or T3 exist, to which the tautomerisation can occur. A theoretical study that has been undertaken to address this question has calculated energy levels of tautomers and their excited states only at the optimised ground state geometry of T1 [Gon09]. No tautomerisation pathways were discovered under these conditions, but more extensive studies at different excited state geometries would be necessary to decide this question. So far

no studies support the idea of excited state tautomerisation of thymine, but such studies do exist for the other pyrimidines cytosine and uracil. Kosma et al. reported a long-living excited state of gas phase cytosine that they tentatively identified as an excited state tautomerisation into a $n\pi^*$ state of the keto–imino tautomer [Kos09]. In the case of uracil a quantum chemical study by Shukla and coworkers predicts a photoinduced keto–enol tautomerisation in the $^1\pi\pi^*$ state [SL02]. It is not clear which quantum yields of photo-induced tautomerisations can be expected or if these results are relevant to the photophysics of thymine as well. Lacking experimental evidence, this questions has to remain open at this point.

7.6. Conclusion and Outlook

7.6.1. The Excited State X1

The measurements presented in this chapter showed and characterised a long-living excited state of thymine that is populated with a substantial quantum yield of 10 % in different solvents. This state has not been reported before in the literature. Several hypotheses were discussed about the nature of X1.

Some of the possibilities that were raised in the previous discussion could be discarded as at least highly unlikely. If no other excited states than the $n\pi^*$ states and the $^3\pi\pi^*$ are populated out of the $^1\pi\pi^*$ state, X1 must be identified as one of the $n\pi^*$ states. In this case a Fermi resonance is necessary to explain the spectral characteristics of the excited state. Furthermore, a part of the literature about the $n\pi^*$ states and their role in ISC to the lowest triplet state has to be revised.

The other possibility is that the observed excited state X1 is not a $n\pi^*$ state. Alternatively it might be the product of a photo-induced tautomerisation of thymine in an excited state. This possibility has not been systematically explored yet, so it is not clear whether the IR signature of X1 and its quantum yield are consistent with it. The $^1n\pi^*$ state is then most likely the major precursor to ISC, and its energetic accessibility in different solvents explains the solvent dependence of Φ_{ISC}.

This alternative cannot be decided with the data available. The very sophisticated quantum chemical studies that are necessary to gain insight into photoinduced tautomerisation processes have to be undertaken. Experimentally, the pH value of the solvent may be critical in making tautomers accessible or inaccessible, so pH-dependent measurements could shed some light onto such mechanisms (see [MAS99]).

If X1 is a $^1n\pi^*$ state, then the existence of the two absorbance bands at 1685 cm^{-1} and 1740 cm^{-1} (TMP in water) can only be explained by a Fermi resonance. It would be caused by a coincidental degeneracy of a high-frequency vibration and an overtone of low-frequency vibrations. Such a degeneracy could be eliminated by changing the vibrational frequencies without changing the electronic structure. This could be

done by investigating the excited state physics of isotope-labelled samples. If the absorbance band at 1690 cm^{-1} is caused by a Fermi resonance, it should vanish in those samples. However, such samples are not easily available and highly expensive, so no measurements of these samples have been performed yet.

7.6.2. The ISC Process

The intersystem crossing process of TMP to the $^3\pi\pi^*$ state was monitored in different solvents. It proceeds within 20 ps, probably via a $^1n\pi^*$ intermediate. The spectral characteristics of the intermediate state could not be observed, because they are obscured by vibrational cooling. The solvent dependence of the ISC quantum yield is consistent with a model proposed by Salet et al. [SBB79], that assumes a solvent dependent accessibility of a $n\pi^*$ triplet precursor (see subsection 7.1.1). An alternative model that was proposed by Hare et al. suggested intersystem crossing out of vibrationally excited, long-living $^1n\pi^*$ states (see subsection 7.1.3). This model was demonstrated to be inconsistent with the experimental data presented in this chapter. Attempts to identify the triplet precursor by indirect means could proceed further if it can be decided whether X1 is of $n\pi^*$ nature or not.

7.6.3. Long-Living States of Other Pyrimidines

The excited state physics of other pyrimidines like uracil and cytosine were investigated by other groups [Qui07, Kea11, HCK07]. Long-living excited states were reported and tentatively identified as $^1n\pi^*$ states. So far, no absorbance spectra of the supposed $^1n\pi^*$ states were published, so it is not possible to compare the measured absorbance spectra to the calculated spectra. It would be important to re-investigate the excited state physics of CMP and UMP. This is especially interesting in the case of cytosine, where gas phase calculations suggest that the $n\pi^*$ states are energetically above the $^1\pi\pi^*$ state [Bla07, FKH07, TTM05]. Then, in protic solvents like water, the $^1n\pi^*$ states should be inaccessible from the $^1\pi\pi^*$ state.

8. Summary and Outlook

The excited state physics of TMP and $(dT)_{18}$ were investigated by TRIR spectroscopy in the delay time window from sub-picoseconds to microseconds. Several excited states were monitored and identified.

A Long-living Localised State

A long-living localised state of TMP was observed that was not reported before in the literature. It is populated directly out of the excited $^1\pi\pi^*$ state with a quantum yield of circa 10 % and returns to the ground state with a time constant of circa 1 ns. It is tempting to interpret this state as a $^1n\pi^*$ or $^3n\pi^*$ state, especially since previous reports of $^1n\pi^*$ states [HCK07] were based on measurement errors. However, the observed state does not meet the expectations about $^1n\pi^*$ states, because it is only weakly affected by the solvent, it is not involved in the intersystem crossing to the $^3\pi\pi^*$ state and its absorbance spectrum only partially agrees with a calculated spectrum of the $n\pi^*$ state. Several alternative interpretations were discussed and some of them could be excluded as highly unlikely. An interesting hypothesis is an excited state tautomerisation of thymine, but in this case the weak solvent effect on the quantum yields and lifetimes would be surprising. Further investigations are necessary to decide how plausible this hypothesis is or to develop alternatives. At present, the nature of the long-living excited state cannot be identified unequivocally.

The $^3\pi\pi^*$ State

The $^3\pi\pi^*$ state is populated within 20 ps after UV absorption out of a transient intermediate state. This state is obscured by the signature of vibrational cooling, so its IR signature cannot be compared to the calculated $n\pi^*$ spectra. A definitive assignment based on the spectral characteristics is not possible, but the triplet precursor is universally believed to be a $n\pi^*$ state [EFM09, Gon10a, Ser07].

The decay of the $^3\pi\pi^*$ state was observed by TRIR spectroscopy on the ns to µs timescale. Measurements were performed with varying concentrations of oxygen and TMP to monitor the triplet quenching mechanisms. Rate constants for the triplet quenching by oxygen and by other thymine molecules were derived from the observed $^3\pi\pi^*$ lifetimes.
In thymidine oligomers the quenching of triplet-excited thymine by ground state thymine is not limited by diffusion and hence much more efficient. Moreover, CPD

formation out of the $^3\pi\pi^*$ state may occur. Earlier studies have speculated about a relatively fast CPD formation out of the $^3\pi\pi^*$ state (time constants < 200 ns [MM05] and of 140 ps [KMP08] were reported) in $(dT)_{18}$. The TRIR measurements discussed in this thesis clarified this issue: Within experimental accuracy the triplet quantum yields are the same in TMP and $(dT)_{18}$, but the quenching mechanisms are different in $(dT)_{18}$; the excited base forms a biradical ^{3}BR with a neighbouring base on a timescale of 10 ns. Subsequently, the biradical decays to the ground state with a time constant of 60 ns, without a detectable CPD increase. Taking into account the limitations of experimental accuracy, the quantum yield of CPD formation out of the biradical can be estimated to be below 15 %.

Charge Transfer

UV-induced charge transfer in thymidine oligomers was observed and identified by the spectral characteristics for the first time [Pil14a] (see chapter 6). Stacked thymine bases can undergo charge transfer upon UV excitation within less than 1 ps. The resulting charge separated states do not seem to be very reactive. Within experimental accuracy all of them undergo charge recombination to the respective ground states of the thymine bases with a time constant of 100 ps.

While it cannot be excluded that a small fraction of the bases form a photoproduct (like an oxetane, the precursor of the (6–4) lesion [Imp12]), charge transfer appears to be mainly a deactivation mechanism for potentially reactive stacked bases that could otherwise form CPD lesions. In addition to such a photoprotective effect, charge transfer might even be able to repair existing CPD lesions: An electron transfer out of a charge separated state onto a neighbouring CPD lesion could lead to damage repair in a photolyase-like fashion.

Concerning the general understanding of DNA photophysics, these measurements, along with the ones in [Buc14a], indicate that UV-induced charge transfer processes take place between stacked bases, as was hypothesised earlier [Mid09]. They furthermore clear up some misunderstandings about a 100 ps decay in UV-excited thymidine oligomers that was assigned to $^1n\pi^*$ states [HCK07] or CPD formation out of the $^3\pi\pi^*$ state [KMP08].

Outlook

New discoveries about the photophysics of the DNA base thymine were reported and discussed in this thesis. In addition to them, long-living excited states that were already observed by other groups and led to conflicting interpretations (see for example [HCK07, KMP08]) could be identified on solid spectroscopic evidence. This was achieved by a combination of TRIR spectroscopy, multiexponential data analysis and theoretical modelling of the excited states' absorbance spectra. The comparisons of theoretically calculated IR spectra and the experimentally obtained

DADS makes use of the main advantage of TRIR spectroscopy over many other techniques: While an electronic transition often results in only one broad, unspecific excited state absorption band in the UV/VIS spectral range, the same transition changes many bond lengths, vibrational frequencies and oscillator strengths. The resulting changes in the IR spectra are highly characteristic of the excited states, which can often be identified unequivocally by specific marker bands. This property of IR spectra is especially useful for time-resolved spectroscopy: TRIR spectroscopy allows to monitor transitions between excited states that ultimately may result in photochemical reactions. The ability to identify the excited states is obviously of pivotal importance to the understanding of the reaction mechanisms. The combination of TRIR spectroscopy and theoretical modelling has contributed in a major fashion to the understanding of the photophysics of DNA and of photophysics and photochemistry in general. It is beyond the scope of this thesis to enumerate even a fraction of the possible applications of this technique in future research. Concerning only the field of DNA photophysics, some questions that can by addressed by TRIR spectroscopy in the near future were raised in the concluding remarks of chapters 5–7. The most important of them are certainly the ones related to the influence of the base pairing interactions on the photophysics of the DNA double strand. This topic is currently investigated by several groups. Based on the studies that are already published one can expect that the combination of TRIR spectroscopy and theoretical quantum chemistry will yield interesting and important new discoveries.

A. Appendix

A.1. Solvent Corrections

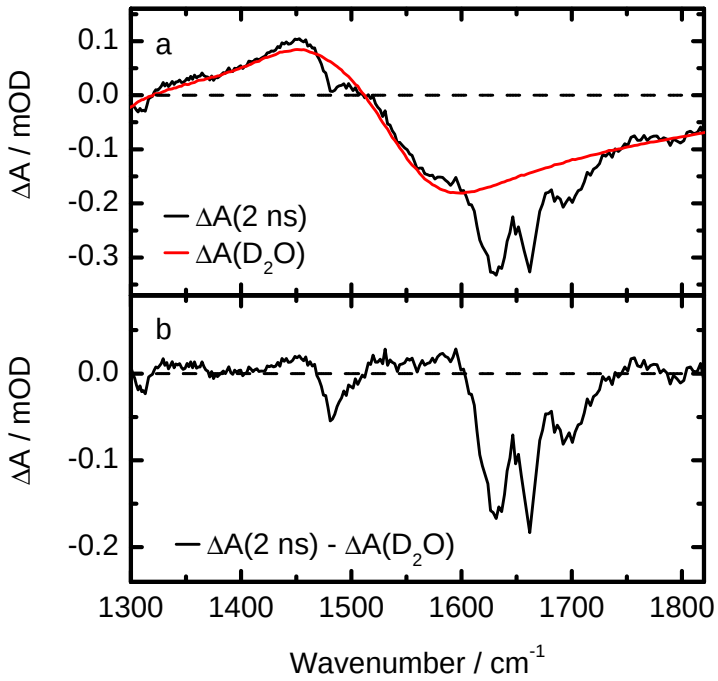

Figure A.1.: The spectrum of solvent heating is scaled to the transient spectra of TMP at the maximum delay time, when almost all excited states have returned to the ground state (a). After subtraction of the signature of solvent heating, the resulting absorbance changes are only due to the excited states and photoproducts of TMP (b).

The signals of solvent (D_2O) heating were subtracted from the data presented in this thesis. It was already briefly described how this subtraction is done in chapter 3. A more detailed description is given in this section. The signature of solvent heating builds up in the first 10 ps, when the vibrational energy of the excited thymine

bases is dissipated to the solvent, and then remains constant. The time-dependent amplitudes of the signature of solvent heating are modelled by the following equation:

$$A_{D2O}(t_D) = A_\infty \left(1 - exp\left(-\frac{t_D}{3.3\,\mathrm{ps}}\right)\right) \tag{A.1}$$

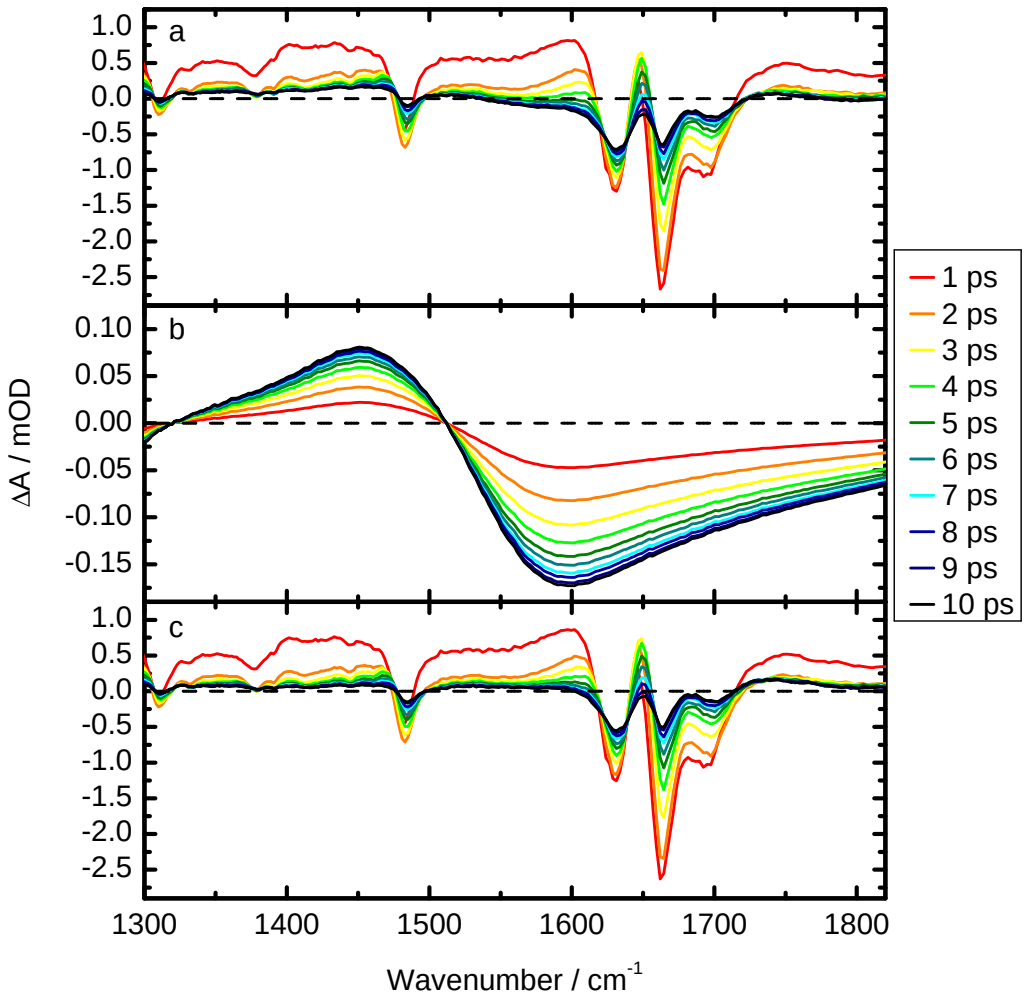

Figure A.2.: (a) Transient spectra of TMP after excitation with 266 nm pulses (pulse energy 2 µJ). In the first few ps the spectra are dominated by vibrational cooling (VC). VC results in heating of the solvent (b). The spectra of heating of the solvent are subtracted from the data to obtain the absorbance changes caused only by the bases (c).

The amplitude A_∞ is determined by manually fitting the signature of solvent heating to the transient spectra at late delay times when most excited states have returned to the ground state (see Figure A.1). Then the time-dependent amplitudes

are calculated according to Equation A.1. Figure A.2 shows how the calculation is done. Panel (a) shows the raw data of TMP in the first 10 ps after excitation. The signature of solvent heating that builds up in the first 10 ps is underlying the absorbance changes caused by TMP. The modelled solvent spectra are depicted in panel (b) of Figure A.2. They are subtracted from the raw data (panel (c)) to yield the corrected transient spectra of TMP (see panel (c)). Comparing the spectra in panels (a) and (c) shows that the correction for the signatures of solvent heating works quite well. The data of $(dT)_{18}$ that were presented in chapter 6 are corrected in the same way.

A.2. Long-Living States of Thymine

A.2.1. Population of X1 of Thymine in Acetonitrile

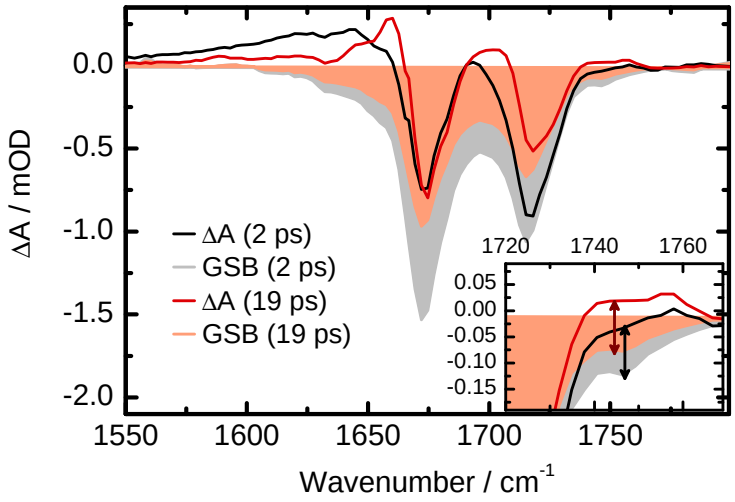

Figure A.3.: Transient absorbance changes at delay times of 2 ps (black) and 19 ps (red) and the corresponding inverted ground state spectra. The absorbance at 1745 cm^{-1} is the sum of the X1 marker band and the ground state bleach. The absorption of X1 is the difference between $\Delta A(t_D)(1745\,cm^{-1})$ and the ground state bleach at 1745 cm^{-1}.

The excited state physics of thymine in acetonitrile (CD_3CN) was discussed in subsection 7.4.3. The blue-shifted marker band of X1 was observed only a few picoseconds after the decay of the $^1\pi\pi^*$ state. The delayed increase of the absorption at 1745 cm^{-1} seems to indicate that X1 is not populated directly from the $^1\pi\pi^*$ state (see Figure 7.16). This would be contrary to the observed kinetics of TMP in D_2O and CD_4O as well as thymine in D_2O. A closer look at the data is necessary to clarify this issue. Figure A.3 depicts the absorbance changes at delay times of 2 ps (black)

and at 19 ps (red) and the inverted ground state spectra corresponding to the ground state bleach at those delay times (filled areas in grey and red, respectively).

The ground state spectrum of thymine in CD_3CN exhibits a small absorbance band around 1745 cm^{-1}, so the X1 marker band is not spectrally isolated from the ground state bands. Consequently, the ground state bleach overlays the X1 absorption at 1745 cm^{-1} during vibrational cooling. Taking this effect into account explains why the absorption at the marker position increases after more than 1 ps. The inset in Figure A.3 illustrates that the absorption at 1745 cm^{-1} is well above the ground state bleach even at early delay times. This additional absorption at 1745 cm^{-1} is caused by the marker band of X1. To be sure about this, the difference $\Delta A(1745\,cm^{-1}) - GSB(1745\,cm^{-1})$ is calculated at different delay times in the first 20 ps (see Figure A.4). Panel (a) depicts transient spectra at different delay times in the first 20 ps. The ground state bleach is subtracted from these spectra in the right panel. The resulting spectra represent the absorptions of all excited states and the hot ground state. The absorbance at 1745 cm^{-1} is the X1 marker band. It is present at early delay times and does not increase or diminish in the first 20 ps. X1 is therefore populated directly out of the $^1\pi\pi^*$ state within 1 ps, just like in other solvents.

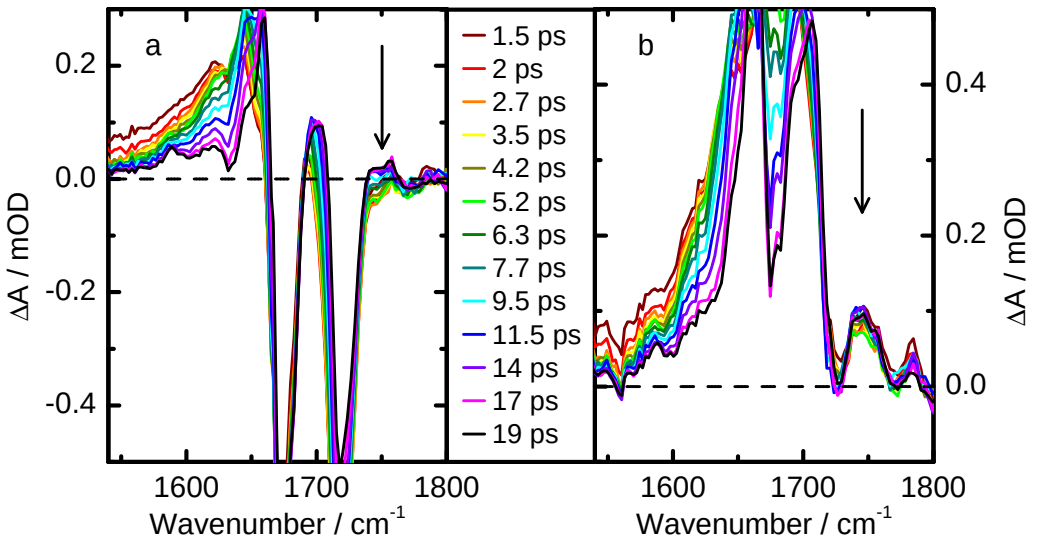

Figure A.4.: Excited state physics of thymine in acetonitrile in the first few picoseconds. The blue-shifted marker band for state X is partly overlayed by the ground state, resulting in an increase in absorption at 1745 cm^{-1} in the first few ps. This might create the misapprehension that state X1 is populated within a few picoseconds, so the excited $^1\pi\pi^*$ state would not be a precursor (a). However, after taking into account the ground state bleach during VC, it becomes clear that the marker band and therefore X1 is present within 1 ps (b).

A.2.2. Quantum Yields of Thymine in Acetonitrile

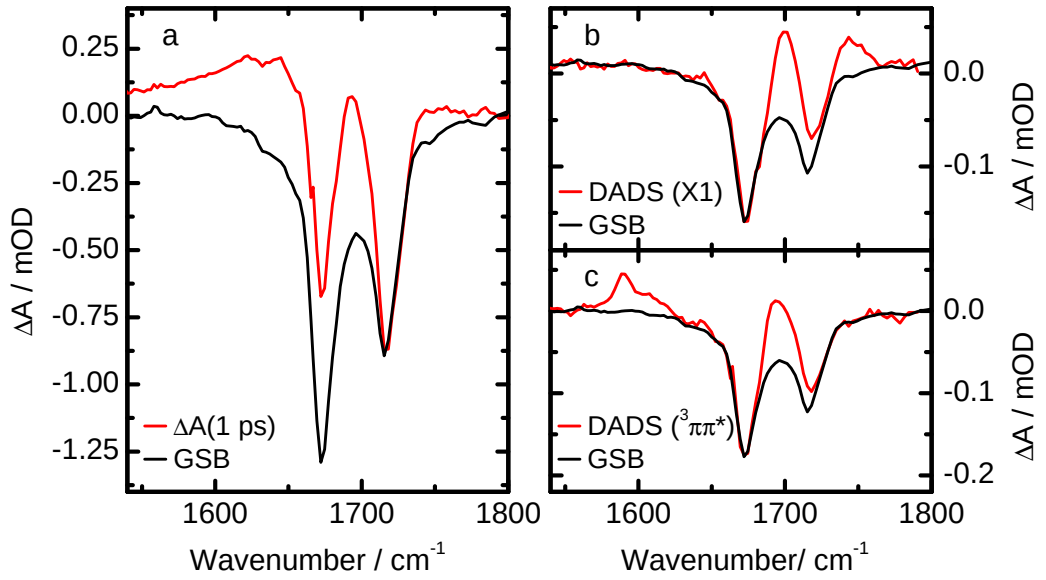

Figure A.5.: Determination of the quantum yields of X1 (b) and the $^3\pi\pi^*$ state (c). The ground state bleach associated with these states is compared to that caused by the initially excited $^1\pi\pi^*$ state (a) to determine the quantum yields. The resulting quantum yields are Φ_{X1} = 12 % and Φ_{ISC} = 13 %.

The quantum yields of thymine in acetonitrile are determined by comparing the ground state bleach associated with the DADS of the excited states to that of the $^1\pi\pi^*$ state 1 ps after excitation. The method has been described in detail in chapter 6. The resulting quantum yields are $\Phi_{X1} = 12\,\%$ and $\Phi_{ISC} = 13\,\%$.

List of Abbreviations

$(dA)_{18}$	18-mer Adenosine Oligonucleotide
$(dT)_{18}$	18-mer Thymidine Oligonucleotide
A	Adenine
$AgGaS_2$	Silver Thiogallate
AMP	Adenosine 5'-Monophosphate
ApT	Adenylyl-(3'–5')-Thymidine
BaF_2	Barium Fluoride
BBO	Beta Barium Borate
BR	Biradical
C	Cytosine
CaF_2	Calcium Fluoride
CG	Continuum Generation
CMP	Cytidine 5'-Monophosphate
CPA	Chirped Pulse Amplification
CpC	Cytidylyl-(3'–5')-Cytidine
CPD	Cyclobutane Pyrimidine Dimer
CpT	Cytidylyl-(3'–5')-Thymidine
CSS	Charge Separated State
CT	Charge Transfer
DFM	Difference Frequency Mixing
DM	Dichroic Mirror
DNA	Deoxyribonucleic Acid
ES	Excited State
FTIR	Fourier Transform Infrared Spectroscopy
G	Guanine

GS	Ground State
IC	Internal Conversion
IR	Infrared
ISC	Intersystem Crossing
MIR	Middle Infrared
NIR	Near Infrared
NOPA	Noncollinear Optical Parametric Amplifier
OPA	Optical Parametric Amplifier
OPO	Optical Parametric Oscillator
QY	Quantum Yield
RNA	Ribonucleic Acid
SFG	Sum Frequency Generation
SHG	Second Harmonic Generation
T	Thymine
TA	Transient Absorption
THG	Third Harmonic Generation
TMP	Thymidine 5'-Monophosphate
TpA	Thymidylyl-(3'–5')-Adenosine
TpC	Thymidylyl-(3'–5')-Cytidine
TpT	Thymidylyl-(3'–5')-Thymidine
TRIR	Time-Resolved Infrared
TTET	Triplet-Triplet Energy Transfer
U	Uracil
UV	Ultraviolet
VC	Vibrational Cooling
VIS	Visible

List of Figures

List of Tables

Bibliography

[Aam97] A. Aamouche, M. Ghomi, C. Coulombeau, L. Grajcar, M. H. Baron, H. Jobic and G. Berthier. *Neutron Inelastic Scattering, Optical Spectroscopies, and Scaled Quantum Mechanical Force Fields for Analyzing the Vibrational Dynamics of Pyrimidine Nucleic Acid Bases. 2. Thymine.* The Journal of Physical Chemistry A 101(10) (Mar. 1997), pp. 1808–1817.

[Abe11] B. Abel, U. Buck, A. L. Sobolewski and W. Domcke. *On the nature and signatures of the solvated electron in water.* Physical Chemistry Chemical Physics 14(1) (Dec. 2011), pp. 22–34.

[Alb11] B. Alberts, U. Schäfer, B. Häcker and Alberts-Johnson-Lewis-Raff-Roberts-Walter, eds. *Molekularbiologie der Zelle.* 5. Aufl. Weinheim: Wiley-VCH, 2011.

[ALL98] M. Assel, R. Laenen and A. Laubereau. *Dynamics of Excited Solvated Electrons in Aqueous Solution Monitored with Femtosecond-Time and Polarization Resolution.* The Journal of Physical Chemistry A 102(13) (Mar. 1998), pp. 2256–2262.

[And05] A. Andrady, P. J. Aucamp, A. F. Bais, C. L. Ballaré et al. *Environmental effects of ozone depletion and its interactions with climate change: progress report, 2004.* Photochemical & Photobiological Sciences: Official Journal of the European Photochemistry Association and the European Society for Photobiology 4(2) (Feb. 2005), pp. 177–184.

[Arn80] S. Arnott, R. Chandrasekaran, D. L. Birdsall, A. G. W. Leslie and R. L. Ratliff. *Left-handed DNA helices.* Nature 283 (Feb. 1980), pp. 743–745.

[Ast09] D. Asturiol, B. Lasorne, M. A. Robb and L. Blancafort. *Photophysics of the π,π* and n,π* States of Thymine: MS-CASPT2 Minimum-Energy Paths and CASSCF on-the-Fly Dynamics.* The Journal of Physical Chemistry A 113(38) (Sept. 2009), pp. 10211–10218.

[AT48] J. F. Archard and A. M. Taylor. *Improved Glan-Foucault Prism.* Journal of Scientific Instruments 25(12) (Dec. 1948), pp. 407–409.

[Ban11] A. Banyasz, I. Vayá, P. Changenet-Barret, T. Gustavsson, T. Douki and D. Markovitsi. *Base Pairing Enhances Fluorescence and Favors Cyclobutane Dimer Formation Induced upon Absorption of UVA Radiation by DNA*. Journal of the American Chemical Society 133(14) (Apr. 2011), pp. 5163–5165.

[Ban12] A. Banyasz, T. Douki, R. Improta, T. Gustavsson, D. Onidas, I. Vayá, M. Perron and D. Markovitsi. *Electronic Excited States Responsible for Dimer Formation upon UV Absorption Directly by Thymine Strands: Joint Experimental and Theoretical Study*. Journal of the American Chemical Society 134(36) (Sept. 2012), pp. 14834–14845.

[Bar10] M. Barbatti, A. J. A. Aquino, J. J. Szymczak, D. Nachtigallová, P. Hobza, H. Lischka and J. Michl. *Relaxation mechanisms of UV-photoexcited DNA and RNA nucleobases*. Proceedings of the National Academy of Sciences of the United States of America 107(50) (Dec. 2010), pp. 21453–21458.

[Bas10] M. Bass, C. DeCusatis, G. Li, C. A. MacDonald, E. W. Van Stryland and Optical Society of America. *Handbook of optics*. New York: McGraw-Hill., 2010.

[BC69] B. W. Bangerter and S. I. Chan. *Proton magnetic resonance studies of ribose dinucleoside monophosphates in aqueous solution. II. Nature of the base-stacking interaction in adenylyl-(3' → 5')-cytidine and cytidylyl-(3' → 5')adenosine*. Journal of the American Chemical Society 91(14) (July 1969), pp. 3910–3921.

[BC73] R. Bockrath and M. K. Cheung. *The role of nutrient broth supplementation in UV mutagenesis of E. coli*. Mutation Research/Fundamental and Molecular Mechanisms of Mutagenesis 19(1) (July 1973), pp. 23–32.

[Bec93] A. D. Becke. *Density-functional thermochemistry. III. The role of exact exchange*. The Journal of Chemical Physics 98(7) (Apr. 1993), pp. 5648–5652.

[Ber11] J. M. Berg, J. L. Tymoczko, L. Stryer and B. Häcker. *Biochemie*. Korr. Nachdr. der 6. Aufl. Heidelberg: Spektrum Akad. Verl, 2011.

[Ber14] J. M. Berg, J. L. Tymoczko, L. Stryer and G. J. Gatto. *Biochemie*. 7. Aufl., korr. Nachdr. Lehrbuch. Berlin: Springer Spektrum, 2014.

[Ber97] H. M. Berman. *Crystal studies of B-DNA: the answers and the questions*. Biopolymers 44(1) (1997), pp. 23–44.

[BH04] A. Buhot and A. Halperin. *Effects of stacking on the configurations and elasticity of single-stranded nucleic acids*. Physical Review E 70(2) (Aug. 2004), p. 020902.

[BH68] D. M. Brown and M. J. E. Hewlins. *Dihydrocytosine and related compounds.* Journal of the Chemical Society C: Organic (Jan. 1968), pp. 2050–2055.

[Bir67] J. B. Birks. *Excimers and Exciplexes.* Nature 214(5094) (June 1967), pp. 1187–1190.

[BK55] G. J. Brealey and M. Kasha. *The Role of Hydrogen Bonding in the n $\rightarrow \pi^*$ Blue-shift Phenomenon.* Journal of the American Chemical Society 77(17) (Sept. 1955), pp. 4462–4468.

[Bla07] L. Blancafort. *Energetics of Cytosine Singlet Excited-State Decay Paths-A Difficult Case for CASSCF and CASPT2.* Photochemistry and Photobiology 83(3) (May 2007), pp. 603–610.

[Blo00] V. A. Bloomfield. *Nucleic acids: structures, properties, and functions.* Sausalito, Calif: University Science Books, 2000.

[Bou02] B. Bouvier, T. Gustavsson, D. Markovitsi and P. Millié. *Dipolar coupling between electronic transitions of the DNA bases and its relevance to exciton states in double helices.* Chemical Physics. Photoprocesses in Multichromophoric Molecular Assemblies 275(1–3) (Jan. 2002), pp. 75–92.

[Bou03] B. Bouvier, J.-P. Dognon, R. Lavery, D. Markovitsi, P. Millié, D. Onidas and K. Zakrzewska. *Influence of Conformational Dynamics on the Exciton States of DNA Oligomers.* The Journal of Physical Chemistry B 107(48) (Dec. 2003), pp. 13512–13522.

[Boy08] R. W. Boyd. *Nonlinear optics.* 3rd ed. Amsterdam ; Boston: Academic Press, 2008.

[BSG03] M. Banyay, M. Sarkar and A. Gräslund. *A library of IR bands of nucleic acids in solution.* Biophysical Chemistry 104(2) (June 2003), pp. 477–488.

[Buc07] I. Buchvarov, Q. Wang, M. Raytchev, A. Trifonov and T. Fiebig. *Electronic energy delocalization and dissipation in single- and double-stranded DNA.* Proceedings of the National Academy of Sciences 104(12) (Mar. 2007), pp. 4794–4797.

[Buc14a] D. B. Bucher, B. M. Pilles, T. Carell and W. Zinth. *Charge separation and charge delocalization identified in long-living states of photoexcited DNA.* Proceedings of the National Academy of Sciences 111(12) (Mar. 2014), pp. 4369–4374.

[Buc14b] D. B. Bucher, B. M. Pilles, T. Pfaffeneder, T. Carell and W. Zinth. *Fingerprinting DNA Oxidation Processes: IR Characterization of the 5-Methyl-2'-Deoxycytidine Radical Cation.* ChemPhysChem 15(3) (Feb. 2014), pp. 420–423.

[Buc15a] D. B. Bucher, B. M. Pilles, T. Carell and W. Zinth. *Dewar Lesion Formation in Single- and Double-Stranded DNA is Quenched by Neighboring Bases.* The Journal of Physical Chemistry B 119(28) (July 2015), pp. 8685–8692.

[Buc15b] F. Buchner, A. Nakayama, S. Yamazaki, H.-H. Ritze and A. Lübcke. *Excited-State Relaxation of Hydrated Thymine and Thymidine Measured by Liquid-Jet Photoelectron Spectroscopy: Experiment and Simulation.* Journal of the American Chemical Society 137(8) (Mar. 2015), pp. 2931–2938.

[BW04] A. Bacolla and R. D. Wells. *Non-B DNA Conformations, Genomic Rearrangements, and Human Disease.* Journal of Biological Chemistry 279(46) (Nov. 2004), pp. 47411–47414.

[Cad12] J. Cadet, S. Mouret, J.-L. Ravanat and T. Douki. *Photoinduced Damage to Cellular DNA: Direct and Photosensitized Reactions Photoinduced Damage to Cellular DNA: Direct and Photosensitized Reactions.* Photochemistry & Photobiology 88(5) (Oct. 2012), pp. 1048–1065.

[Cad86] J. Cadet, M. Berger, C. Decarroz, J. R. Wagner, J. E. Van Lier, Y. M. Ginot and P. Vigny. *Photosensitized reactions of nucleic acids.* Biochimie. Molecular, Cellular and Medical Aspects of Photosensitization 68(6) (June 1986), pp. 813–834.

[Cad92] J. Cadet, C. Anselmino, T. Douki and L. Voituriez. *New trends in photobiology: Photochemistry of nucleic acids in cells.* Journal of Photochemistry and Photobiology B: Biology 15(4) (Sept. 1992), pp. 277–298.

[Cad97] J. Cadet, M. Berger, T. Douki, B. Morin, S. Raoul, J. L. Ravanat and S. Spinelli. *Effects of UV and visible radiation on DNA-final base damage.* Biological Chemistry 378(11) (Nov. 1997), pp. 1275–1286.

[Can05] C. Canuel, M. Mons, F. Piuzzi, B. Tardivel, I. Dimicoli and M. Elhanine. *Excited states dynamics of DNA and RNA bases: Characterization of a stepwise deactivation pathway in the gas phase.* The Journal of Chemical Physics 122(7) (Feb. 2005), p. 074316.

[CCK04] B. Cohen, C. E. Crespo-Hernández and B. Kohler. *Strickler-Berg analysis of excited singlet state dynamics in DNA and RNA nucleosides.* Faraday Discussions 127 (Aug. 2004), pp. 137–147.

[CCK05] C. E. Crespo-Hernández, B. Cohen and B. Kohler. *Base stacking controls excited-state dynamics in A·T DNA*. Nature 436(7054) (Aug. 2005), pp. 1141–1144.

[CDM01] G. J. Clydesdale, G. W. Dandie and H. K. Muller. *Ultraviolet light induced injury: immunological and inflammatory effects*. Immunology and Cell Biology 79(6) (Dec. 2001), pp. 547–568.

[Cha55] Chargaff, Erwin. *The nucleic acids: chemistry and biology*. I. New York: Academic Press, 1955.

[Che13] I. V. Chernyshova, E. J. Kontros, P. P. Markush and O. B. Shpenik. *Excitation of lowest electronic states of thymine by slow electrons*. Optics & Spectroscopy 115(5) (Nov. 2013), pp. 645–650.

[Cli10] T. Climent, I. González-Ramírez, R. González-Luque, M. Merchán and L. Serrano-Andrés. *Cyclobutane Pyrimidine Photodimerization of DNA/RNA Nucleobases in the Triplet State*. The Journal of Physical Chemistry Letters 1(14) (July 2010), pp. 2072–2076.

[Cre04] C. E. Crespo-Hernández, B. Cohen, P. M. Hare and B. Kohler. *Ultrafast Excited-State Dynamics in Nucleic Acids*. Chemical Reviews 104(4) (Apr. 2004), pp. 1977–2020.

[CS03] G. Cerullo and S. D. Silvestri. *Ultrafast optical parametric amplifiers*. Review of Scientific Instruments 74(1) (Jan. 2003), pp. 1–18.

[CSD05] J. Cadet, E. Sage and T. Douki. *Ultraviolet radiation-mediated damage to cellular DNA*. Mutation Research/Fundamental and Molecular Mechanisms of Mutagenesis. Biological Effects of Ultraviolet Radiation 571(1–2) (Apr. 2005), pp. 3–17.

[CT30] M. Czerny and A. F. Turner. *Über den Astigmatismus bei Spiegelspektrometern*. Zeitschrift für Physik 61(11-12) (Nov. 1930), pp. 792–797.

[Cuq11] M. C. Cuquerella, V. Lhiaubet-Vallet, F. Bosca and M. A. Miranda. *Photosensitised pyrimidine dimerisation in DNA*. Chemical Science 2(7) (June 2011), pp. 1219–1232.

[Dan94] V. I. Danilov, O. N. Slyusarchuk, J. L. Alderfer, J. J. P. Stewart and P. R. Callis. *A Theoretical Study of the Cytosine Excimer State: The Role of Geometry Optimization*. Photochemistry and Photobiology 59(1) (Jan. 1994), pp. 125–129.

[DC01] T. Douki and J. Cadet. *Individual Determination of the Yield of the Main UV-Induced Dimeric Pyrimidine Photoproducts in DNA Suggests a High Mutagenicity of CC Photolesions*. Biochemistry 40(8) (Feb. 2001), pp. 2495–2501.

[DD81] R. E. Dickerson and H. R. Drew. *Kinematic model for B-DNA.* Proceedings of the National Academy of Sciences of the United States of America 78(12) (Dec. 1981), pp. 7318–7322.

[DE02] B. Durbeej and L. A. Eriksson. *Reaction mechanism of thymine dimer formation in DNA induced by UV light.* Journal of Photochemistry and Photobiology A: Chemistry 152(1–3) (Sept. 2002), pp. 95–101.

[Dee14] A. A. Deeg, M. S. Rampp, A. Popp, B. M. Pilles, T. E. Schrader, L. Moroder, K. Hauser and W. Zinth. *Isomerization- and Temperature-Jump-Induced Dynamics of a Photoswitchable β-Hairpin.* Chemistry – A European Journal 20(3) (Jan. 2014), pp. 694–703.

[Des08] C. Desnous, B. R. Babu, C. Moriou, J. U. O. Mayo, A. Favre, J. Wengel and P. Clivio. *The Sugar Conformation Governs (6-4) Photoproduct Formation at the Dinucleotide Level.* Journal of the American Chemical Society 130(1) (Jan. 2008), pp. 30–31.

[DH71] M. Daniels and W. Hauswirth. *Fluorescence of the Purine and Pyrimidine Bases of the Nucleic Acids in Neutral Aqueous Solution at 300°K.* Science. New Series 171(3972) (Feb. 1971), pp. 675–677.

[DKV72] R. R. Dogonadze, A. M. Kuznetsov and M. A. Vorotyntsev. *On the Theory of Nonradiative Transitions in Polar Media II. Processes with "Nixing" of Quantum and Classical Degrees of Freedom.* physica status solidi (b) 54(2) (Dec. 1972), pp. 425–433.

[Doo13] G. W. Doorley, M. Wojdyla, G. W. Watson, M. Towrie, A. W. Parker, J. M. Kelly and S. J. Quinn. *Tracking DNA Excited States by Picosecond-Time-Resolved Infrared Spectroscopy: Signature Band for a Charge-Transfer Excited State in Stacked Adenine-Thymine Systems.* The Journal of Physical Chemistry Letters 4(16) (Aug. 2013), pp. 2739–2744.

[Dou03] T. Douki, A. Reynaud-Angelin, J. Cadet and E. Sage. *Bipyrimidine Photoproducts Rather than Oxidative Lesions Are the Main Type of DNA Damage Involved in the Genotoxic Effect of Solar UVA Radiation.* Biochemistry 42(30) (2003), pp. 9221–9226.

[Dre81] H. R. Drew, R. M. Wing, T. Takano, C. Broka, S. Tanaka, K. Itakura and R. E. Dickerson. *Structure of a B-DNA dodecamer: conformation and dynamics.* Proceedings of the National Academy of Sciences of the United States of America 78(4) (Apr. 1981), pp. 2179–2183.

[DT62] H. DeVoe and I. Tinoco Jr. *The hypochromism of helical polynucleotides.* Journal of Molecular Biology 4(6) (June 1962), pp. 518–527.

[DT79] T. G. Dewey and D. H. Turner. *Laser temperature-jump study of stacking in adenylic acid polymers.* Biochemistry 18(26) (Dec. 1979), pp. 5757–5762.

[DTW89] C. Doubleday, N. J. Turro and J. F. Wang. *Dynamics of flexible triplet biradicals.* Accounts of Chemical Research 22(6) (June 1989), pp. 199–205.

[EFM09] M. Etinski, T. Fleig and C. M. Marian. *Intersystem Crossing and Characterization of Dark States in the Pyrimidine Nucleobases Uracil, Thymine, and 1-Methylthymine.* The Journal of Physical Chemistry A 113(43) (Aug. 2009), pp. 11809–11816.

[Eis66] J. Eisinger, M. Guéron, R. G. Shulman and T. Yamane. *Excimer fluorescence of dinucleotides, polynucleotides, and DNA.* Proceedings of the National Academy of Sciences 55(5) (May 1966), pp. 1015–1020.

[EK91] T. Elsaesser and W. Kaiser. *Vibrational and Vibronic Relaxation of Large Polyatomic Molecules in Liquids.* Annual Review of Physical Chemistry 42(1) (1991), pp. 83–107.

[EL67] J. Eisinger and A. A. Lamola. *The excited-state precursor of the thymine dimer.* Biochemical and Biophysical Research Communications 28(4) (Aug. 1967), pp. 558–565.

[Elm07] S. Elmore. *Apoptosis: A Review of Programmed Cell Death.* Toxicologic Pathology 35(4) (June 2007), pp. 495–516.

[ElS63] M. A. El-Sayed. *Spin-Orbit Coupling and the Radiationless Processes in Nitrogen Heterocyclics.* The Journal of Chemical Physics 38(12) (June 1963), pp. 2834–2838.

[EM10] M. Etinski and C. M. Marian. *Ab initio investigation of the methylation and hydration effects on the electronic spectra of uracil and thymine.* Physical Chemistry Chemical Physics 12(19) (May 2010), pp. 4915–4923.

[Ema05] E. Emanuele, D. Markovitsi, P. Millié and K. Zakrzewska. *UV Spectra and Excitation Delocalization in DNA: Influence of the Spectral Width.* ChemPhysChem 6(7) (July 2005), pp. 1387–1392.

[Epe11] B. Epe. *DNA damage spectra induced by photosensitization.* Photochemical & Photobiological Sciences 11(1) (Dec. 2011), pp. 98–106.

[ES68] J. Eisinger and R. G. Shulman. *Excited Electronic States of DNA.* Science. New Series 161(3848) (Sept. 1968), pp. 1311–1319.

[Eti12] M. Etinski. *Investigation of the spin-forbidden process in thymine.* Hemijska industrija 66(2) (2012), pp. 165–170.

[Eti13] M. Etinski. *Effect of temperature on rate of a spin-forbidden transition in uracil and thymine.* Journal of the Serbian Chemical Society 78(1) (Jan. 2013), pp. 65–73.

[Ezr77] F. S. Ezra, C.-H. Lee, N. S. Kondo, S. S. Danyluk and R. H. Sarma. *Conformational properties of purine-pyrimidine and pyrimidine-purine dinucleoside monophosphates.* Biochemistry 16(9) (May 1977), pp. 1977–1987.

[Fan10] J.-C. Fan, Z.-C. Shang, J. Liang, X.-H. Liu and H. Jin. *Systematic theoretical investigations on the tautomers of thymine in gas phase and solution.* Journal of Molecular Structure: THEOCHEM 939(1–3) (Jan. 2010), pp. 106–111.

[FG53] R. E. Franklin and R. G. Gosling. *Molecular Configuration in Sodium Thymonucleate.* Nature 171(4356) (Apr. 1953), pp. 740–741.

[FH65] G. Felsenfeld and S. Z. Hirschman. *A neighbor-interaction analysis of the hypochromism and spectra of DNA.* Journal of Molecular Biology 13(2) (Sept. 1965), pp. 407–427.

[FJ70] G. J. Fisher and H. E. Johns. *Ultraviolet Photochemistry of Thymine in Aqueous Solution.* Photochemistry and Photobiology 11(6) (1970), pp. 429–444.

[FK55] T. Förster and K. Kasper. *Ein Konzentrationsumschlag der Fluoreszenz des Pyrens.* Zeitschrift für Elektrochemie, Berichte der Bunsengesellschaft für physikalische Chemie 59(10) (1955), pp. 976–980.

[FKH07] T. Fleig, S. Knecht and C. Hättig. *Quantum-Chemical Investigation of the Structures and Electronic Spectra of the Nucleic Acid Bases at the Coupled Cluster CC2 Level.* The Journal of Physical Chemistry A 111(25) (June 2007), pp. 5482–5491.

[FKS90] L. A. Frederico, T. A. Kunkel and B. R. Shaw. *A sensitive genetic assay for the detection of cytosine deamination: determination of rate constants and the activation energy.* Biochemistry 29(10) (Mar. 1990), pp. 2532–2537.

[Fre31] J. Frenkel. *On the Transformation of Light into Heat in Solids. II.* Physical Review 37(10) (May 1931), pp. 1276–1294.

[Fre87] S. E. Freeman, R. W. Gange, J. C. Sutherland, E. A. Matzinger and B. M. Sutherland. *Production of Pyrimidine Dimers in DNA of Human Skin Exposed In Situ to UVA Radiation.* Journal of Investigative Dermatology 88(4) (Apr. 1987), pp. 430–433.

[Fri03] M. Frisch, G. Trucks, H. Schlegel, G. Scuseria et al. *Gaussian 03, Revision C.02.* 2003.

[GG12] H. Günzler and H.-U. Gremlich. *IR-Spektroskopie Eine Einführung*. Weinheim: Wiley-VCH, 2012.

[Giu13] A. Giussani, L. Serrano-Andrés, M. Merchán, D. Roca-Sanjuán and M. Garavelli. *Photoinduced Formation Mechanism of the Thymine-Thymine (6–4) Adduct*. The Journal of Physical Chemistry B 117(7) (Jan. 2013), pp. 1999–2004.

[GKM01] F. R. de Gruijl, H. J. van Kranen and L. H. Mullenders. *UV-induced DNA damage, repair, mutations and oncogenic pathways in skin cancer*. Journal of Photochemistry and Photobiology. B, Biology 63(1-3) (Oct. 2001), pp. 19–27.

[Gon09] J. González-Vázquez, L. González, E. Samoylova and T. Schultz. *Thymine relaxation after UV irradiation: the role of tautomerization and $\pi\sigma^*$ states*. Physical Chemistry Chemical Physics 11(20) (Apr. 2009), pp. 3927–3934.

[Gon10a] R. González-Luque, T. Climent, I. González-Ramírez, M. Merchán and L. Serrano-Andrés. *Singlet-Triplet States Interaction Regions in DNA/RNA Nucleobase Hypersurfaces*. Journal of Chemical Theory and Computation 6(7) (July 2010), pp. 2103–2114.

[Gon10b] I. González-Ramírez, D. Roca-Sanjuán, T. Climent, J. J. Serrano-Pérez, M. Merchán and L. Serrano-Andrés. *On the photoproduction of DNA/RNA cyclobutane pyrimidine dimers*. Theoretical Chemistry Accounts 128(4-6) (Nov. 2010), pp. 705–711.

[Göp09] M. Göppert-Mayer. *Elementary processes with two quantum transitions*. Annalen der Physik 18(7-8) (2009), pp. 466–479.

[Gou90] I. R. Gould, D. Ege, J. E. Moser and S. Farid. *Efficiencies of photoinduced electron-transfer reactions: role of the Marcus inverted region in return electron transfer within geminate radical-ion pairs*. Journal of the American Chemical Society 112(11) (May 1990), pp. 4290–4301.

[Gru03] F. R. de Gruijl, J. Longstreth, M. Norval, A. P. Cullen, H. Slaper, M. L. Kripke, Y. Takizawa and J. C. van der Leun. *Health effects from stratospheric ozone depletion and interactions with climate change*. Photochemical & Photobiological Sciences: Official Journal of the European Photochemistry Association and the European Society for Photobiology 2(1) (Jan. 2003), pp. 16–28.

[GS78] G. Gupta and V. Sasisekharan. *Theoretical calculations of base-base interactions in nucleic acids: II Stacking interactions in polynucleotides*. Nucleic Acids Research 5(5) (May 1978), pp. 1655–1673.

[GSM02] T. Gustavsson, A. Sharonov and D. Markovitsi. *Thymine, thymidine and thymidine 5'-monophosphate studied by femtosecond fluorescence upconversion spectroscopy.* Chemical Physics Letters 351(3–4) (Jan. 2002), pp. 195–200.

[Guc00] K. M. Guckian, B. A. Schweitzer, R. X.-F. Ren, C. J. Sheils, D. C. Tahmassebi and E. T. Kool. *Factors Contributing to Aromatic Stacking in Water: Evaluation in the Context of DNA.* Journal of the American Chemical Society 122(10) (Mar. 2000), pp. 2213–2222.

[Gus02] T. Gustavsson, A. Sharonov, D. Onidas and D. Markovitsi. *Adenine, deoxyadenosine and deoxyadenosine 5'-monophosphate studied by femtosecond fluorescence upconversion spectroscopy.* Chemical Physics Letters 356(1–2) (Apr. 2002), pp. 49–54.

[Gus06a] T. Gustavsson, Á. Bányász, E. Lazzarotto, D. Markovitsi, G. Scalmani, M. J. Frisch, V. Barone and R. Improta. *Singlet Excited-State Behavior of Uracil and Thymine in Aqueous Solution: A Combined Experimental and Computational Study of 11 Uracil Derivatives.* Journal of the American Chemical Society 128(2) (Jan. 2006), pp. 607–619.

[Gus06b] T. Gustavsson, N. Sarkar, E. Lazzarotto, D. Markovitsi and R. Improta. *Singlet excited state dynamics of uracil and thymine derivatives: A femtosecond fluorescence upconversion study in acetonitrile.* Chemical Physics Letters 429(4–6) (Oct. 2006), pp. 551–557.

[Gus07] T. Gustavsson, N. Sarkar, Á. Bányász, D. Markovitsi and R. Improta. *Solvent Effects on the Steady-state Absorption and Fluorescence Spectra of Uracil, Thymine and 5-Fluorouracil.* Photochemistry and Photobiology 83(3) (May 2007), pp. 595–599.

[Gus08] T. Gustavsson, Á. Bányász, N. Sarkar, D. Markovitsi and R. Improta. *Assessing solvent effects on the singlet excited state lifetime of uracil derivatives: A femtosecond fluorescence upconversion study in alcohols and D_2O.* Chemical Physics. Femtochemistry and FemtobiologyPapers associated with the 8th International Conference on Femtochemistry and Femtobiology 350(1–3) (June 2008), pp. 186–192.

[Gus11] T. Gustavsson, A. Banyasz, R. Improta and D. Markovitsi. *Femtosecond fluorescence studies of DNA/RNA constituents.* Journal of Physics: Conference Series 261(1) (Jan. 2011), p. 012009.

[GWR96] I. G. Gut, P. D. Wood and R. W. Redmond. *Interaction of Triplet Photosensitizers with Nucleotides and DNA in Aqueous Solution at Room Temperature.* Journal of the American Chemical Society 118(10) (Jan. 1996), pp. 2366–2373.

[Hai12a] Haiser, Karin. *Femtosekunden-Infrarotspektroskopie von UV-induzierten Photoschäden in Nukleinsäuren.* PhD Thesis. Munich: Ludwig-Maximilians-Universität, 2012.

[Hai12b] K. Haiser, B. P. Fingerhut, K. Heil, A. Glas et al. *Mechanism of UV-Induced Formation of Dewar Lesions in DNA.* Angewandte Chemie International Edition 51(2) (Jan. 2012), pp. 408–411.

[Har08] P. M. Hare, C. T. Middleton, K. I. Mertel, J. M. Herbert and B. Kohler. *Time-resolved infrared spectroscopy of the lowest triplet state of thymine and thymidine.* Chemical Physics. Ultrafast Photoinduced Processes in Polyatomic Molecules Electronic Structure, Dynamics and Spectroscopy 347(1–3) (May 2008), pp. 383–392.

[HCK07] P. M. Hare, C. E. Crespo-Hernández and B. Kohler. *Internal conversion to the electronic ground state occurs via two distinct pathways for pyrimidine bases in aqueous solution.* Proceedings of the National Academy of Sciences 104(2) (Jan. 2007), pp. 435–440.

[HKR11] C. Homann, N. Krebs and E. Riedle. *Convenient pulse length measurement of sub-20-fs pulses down to the deep UV via two-photon absorption in bulk material.* Applied Physics B 104(4) (Aug. 2011), pp. 783–791.

[HL94] M. J. Horsfall and C. W. Lawrence. *Accuracy of Replication Past the T-C (6-4) Adduct.* Journal of Molecular Biology 235(2) (Jan. 1994), pp. 465–471.

[HM97] P. S. Ho and B. H. Mooers. *Z-DNA crystallography.* Biopolymers 14(1) (1997), pp. 65–90.

[HMS71] E. J. Hart, B. D. Michael and K. H. Schmidt. *The Absorption Spectrum of e_{aq}^- in the Temperature Range -4 to 390°.* The Journal of Physical Chemistry 75(18) (1971), pp. 2798–2805.

[HOZ97] P. Hamm, S. M. Ohline and W. Zinth. *Vibrational cooling after ultrafast photoisomerization of azobenzene measured by femtosecond infrared spectroscopy.* The Journal of Chemical Physics 106(2) (Jan. 1997), pp. 519–529.

[Imp09] R. Improta, V. Barone, A. Lami and F. Santoro. *Quantum Dynamics of the Ultrafast $\pi\pi^*/n\pi^*$ Population Transfer in Uracil and 5-Fluoro-Uracil in Water and Acetonitrile.* The Journal of Physical Chemistry B 113(43) (Oct. 2009), pp. 14491–14503.

[Imp12] R. Improta. *Photophysics and Photochemistry of Thymine Deoxy-Dinucleotide in Water: A PCM/TD-DFT Quantum Mechanical Study.* The Journal of Physical Chemistry B 116(49) (Dec. 2012), pp. 14261–14274.

[Ism02] N. Ismail, L. Blancafort, M. Olivucci, B. Kohler and M. A. Robb. *Ultrafast Decay of Electronically Excited Singlet Cytosine via a π,π^* to n_O,π^* State Switch.* Journal of the American Chemical Society 124(24) (June 2002), pp. 6818–6819.

[JF77] F.-Y. Jou and G. R. Freeman. *Shapes of optical spectra of solvated electrons. Effect of pressure.* The Journal of Physical Chemistry 81(9) (1977), pp. 909–915.

[JF79] F.-Y. Jou and G. R. Freeman. *Temperature and isotope effects on the shape of the optical absorption spectrum of solvated electrons in water.* The Journal of Physical Chemistry 83(18) (1979), pp. 2383–2387.

[JH04] J. M. Jean and K. B. Hall. *Stacking-Unstacking Dynamics of Oligodeoxynucleotide Trimers.* Biochemistry 43(31) (Aug. 2004), pp. 10277–10284.

[JIT72] W. C. Johnson, M. S. Itzkowitz and I. Tinoco. *Circular dichroism of polynucleotides: Dimers as a function of conformation.* Biopolymers 11(1) (Jan. 1972), pp. 225–234.

[Jor76] J. Jortner. *Temperature dependent activation energy for electron transfer between biological molecules.* The Journal of Chemical Physics 64(12) (June 1976), pp. 4860–4867.

[JT93] N. Jiang and J. S. Taylor. *In vivo evidence that UV-induced C–T mutations at dipyrimidine sites could result from the replicative bypass of cis-syn cyclobutane dimers or their deamination products.* Biochemistry 32(2) (Jan. 1993), pp. 472–481.

[JW07a] A. T. Johnson and O. Wiest. *Structure and Dynamics of Poly(T) Single-Strand DNA: Implications toward CPD Formation.* The Journal of Physical Chemistry B 111(51) (Dec. 2007), pp. 14398–14404.

[JW07b] A. T. Johnson and O. Wiest. *Structure and Dynamics of Poly(T) Single-Strand DNA: Implications toward CPD Formation.* The Journal of Physical Chemistry B 111(51) (Dec. 2007), pp. 14398–14404.

[JW71] H. E. Johns and D. W. Whillans. *Properties of the triplet states of thymine and uracil in aqueous solution.* Journal of the American Chemical Society 93(6) (Mar. 1971), pp. 1358–1362.

[Kap06] U. P. Kappes, D. Luo, M. Potter, K. Schulmeister and T. M. Rünger. *Short- and Long-Wave UV Light (UVB and UVA) Induce Similar Mutations in Human Skin Cells.* Journal of Investigative Dermatology 126(3) (Jan. 2006), pp. 667–675.

[Kea11] P. M. Keane, M. Wojdyla, G. W. Doorley, G. W. Watson et al. *A Comparative Picosecond Transient Infrared Study of 1-Methylcytosine and 5'-dCMP That Sheds Further Light on the Excited States of Cytosine Derivatives.* Journal of the American Chemical Society 133(12) (Mar. 2011), pp. 4212–4215.

[Kea12] P. M. Keane, M. Wojdyla, G. W. Doorley, J. M. Kelly et al. *Ultrafast IR spectroscopy of polymeric cytosine nucleic acids reveal the long-lived species is due to a localised state.* Physical Chemistry Chemical Physics 14(18) (2012). WOS:000302951500021, pp. 6307–6311.

[KG61] W. Kaiser and C. G. B. Garrett. *Two-Photon Excitation in CaF_2:Eu^{2+}.* Physical Review Letters 7(6) (Sept. 1961), pp. 229–231.

[Kim94] S. T. Kim, K. Malhotra, C. A. Smith, J. S. Taylor and A. Sancar. *Characterization of (6-4) photoproduct DNA photolyase.* Journal of Biological Chemistry 269(11) (Mar. 1994), pp. 8535–8540.

[Kle62] D. A. Kleinman. *Laser and Two-Photon Processes.* Physical Review 125(1) (Jan. 1962), pp. 87–88.

[KLJ74] N. R. Kestner, J. Logan and J. Jortner. *Thermal electron transfer reactions in polar solvents.* The Journal of Physical Chemistry 78(21) (Oct. 1974), pp. 2148–2166.

[KMP06] W.-M. Kwok, C. Ma and D. L. Phillips. *Femtosecond Time- and Wavelength-Resolved Fluorescence and Absorption Spectroscopic Study of the Excited States of Adenosine and an Adenine Oligomer.* Journal of the American Chemical Society 128(36) (Sept. 2006), pp. 11894–11905.

[KMP08] W.-M. Kwok, C. Ma and D. L. Phillips. *A Doorway State Leads to Photostability or Triplet Photodamage in Thymine DNA.* Journal of the American Chemical Society 130(15) (Mar. 2008), pp. 5131–5139.

[Koo01] E. T. Kool. *Hydrogen Bonding, Base Stacking, and Steric Effects in Dna Replication.* Annual Review of Biophysics and Biomolecular Structure 30(1) (2001), pp. 1–22.

[Kos09] K. Kosma, C. Schröter, E. Samoylova, I. V. Hertel and T. Schultz. *Excited-State Dynamics of Cytosine Tautomers.* Journal of the American Chemical Society 131(46) (Nov. 2009), pp. 16939–16943.

[KRA65] M. Kasha, H. R. Rawls and M. Ashraf El-Bayoumi. *The exciton model in molecular spectroscopy.* Pure and Applied Chemistry 11(3-4) (Jan. 1965).

[Kra97] K. H. Kraemer. *Sunlight and skin cancer: Another link revealed.* Proceedings of the National Academy of Sciences 94(1) (Jan. 1997), pp. 11–14.

[Kub09] Kubon, Julia Katharina. *Untersuchung von Photoschäden der DNA und RNA mit Femtosekunden IR-Spektroskopie*. Diploma thesis. Munich: Ludwig-Maximilians-Universität, 2009.

[KWC72] J. F. R. Kerr, A. H. Wyllie and A. R. Currie. *Apoptosis: A Basic Biological Phenomenon with Wideranging Implications in Tissue Kinetics*. British Journal of Cancer 26(4) (Aug. 1972), pp. 239–257.

[Lak10] J. R. Lakowicz. *Principles of fluorescence spectroscopy*. 3. ed., corr. 4. print. New York, NY: Springer, 2010.

[Lam67] A. A. Lamola, M. Guéron, T. Yamane, J. Eisinger and R. G. Shulman. *Triplet State of DNA*. The Journal of Chemical Physics 47(7) (Oct. 1967), pp. 2210–2217.

[Lan32] L. D. Landau. *Zur Theorie der Energieubertragung. II*. Physics of the Soviet Union 2 (1932).

[LBC00] J.-H. Lee, S.-H. Bae and B.-S. Choi. *The Dewar photoproduct of thymidylyl(3'→5')- thymidine (Dewar product) exhibits mutagenic behavior in accordance with the "A rule"*. Proceedings of the National Academy of Sciences 97(9) (Apr. 2000), pp. 4591–4596.

[LBL91] J. E. LeClerc, A. Borden and C. W. Lawrence. *The thymine-thymine pyrimidine-pyrimidone(6-4) ultraviolet light photoproduct is highly mutagenic and specifically induces 3' thymine-to-cytosine transitions in Escherichia coli.* Proceedings of the National Academy of Sciences 88(21) (Nov. 1991), pp. 9685–9689.

[LE68] A. A. Lamola and J. Eisinger. *On the Mechanism of Thymine Photodimerization*. Proceedings of the National Academy of Sciences 59(1) (Jan. 1968), pp. 46–51.

[Lee76] C.-H. Lee, F. S. Ezra, N. S. Kondo, R. H. Sarma and S. S. Danyluk. *Conformational properties of dinucleoside monophosphates in solution: dipurines and dipyrimidines*. Biochemistry 15(16) (Aug. 1976), pp. 3627–3639.

[LF66] M. Leng and G. Felsenfeld. *A study of polyadenylic acid at neutral pH*. Journal of Molecular Biology 15(2) (Feb. 1966), pp. 455–466.

[LFR95] J. Lorentzon, M. P. Fuelscher and B. O. Roos. *Theoretical Study of the Electronic Spectra of Uracil and Thymine*. Journal of the American Chemical Society 117(36) (Sept. 1995), pp. 9265–9273.

[LGT87] R. Letellier, M. Ghomi and E. Taillandier. *Normal coordinate analysis of 2'-deoxythymidine and 2'-deoxyadenosine*. European biophysics journal: EBJ 14(7) (1987), pp. 423–430.

[LHC99] J.-H. Lee, G.-S. Hwang and B.-S. Choi. *Solution structure of a DNA decamer duplex containing the stable 3' T·G base pair of the pyrimidine(6–4)pyrimidone photoproduct [(6–4) adduct]: Implications for the highly specific 3' T → C transition of the (6–4) adduct.* Proceedings of the National Academy of Sciences 96(12) (June 1999), pp. 6632–6636.

[Lit05] G. Litfin. *Technische Optik in der Praxis.* Berlin; New York: Springer, 2005.

[Liu15] L. Liu, B. M. Pilles, A. M. Reiner, J. Gontcharov and W. Zinth. *2'-Methoxyacetophenone: An Efficient Photosensitizer for Cyclobutane Pyrimidine Dimer Formation.* ChemPhysChem 16(16) (Nov. 2015), pp. 3483–3487.

[Liu16] L. Liu, B. M. Pilles, J. Gontcharov, D. B. Bucher and W. Zinth. *Quantum Yield of Cyclobutane Pyrimidine Dimer Formation Via the Triplet Channel Determined by Photosensitization.* The Journal of Physical Chemistry B 120(2) (Jan. 2016), pp. 292–298.

[Liv01] Z. Livneh. *DNA Damage Control by Novel DNA Polymerases: Translesion Replication and Mutagenesis.* Journal of Biological Chemistry 276(28) (July 2001), pp. 25639–25642.

[LR01] R. Laenen and T. Roth. *Generation of solvated electrons in neat water: new results from femtosecond spectroscopy.* Journal of Molecular Structure 598(1) (Oct. 2001), pp. 37–43.

[LRH08] A. W. Lange, M. A. Rohrdanz and J. M. Herbert. *Charge-Transfer Excited States in a pi-Stacked Adenine Dimer, As Predicted Using Long-Range-Corrected Time-Dependent Density Functional Theory.* The Journal of Physical Chemistry B 112(20) (May 2008), pp. 6304–6308.

[LRL00] R. Laenen, T. Roth and A. Laubereau. *Novel Precursors of Solvated Electrons in Water: Evidence for a Charge Transfer Process.* Physical Review Letters 85(1) (July 2000), pp. 50–53.

[LSO61] P. Lengyel, J. F. Speyer and S. Ochoa. *Synthetic Polynucleotides and the Amino Acid Code.* Proceedings of the National Academy of Sciences of the United States of America 47(12) (1961), pp. 1936–1942.

[LY67] A. A. Lamola and T. Yamane. *Sensitized photodimerization of thymine in DNA.* Proceedings of the National Academy of Sciences 58(2) (Aug. 1967), pp. 443–446.

[Mar03] D. Markovitsi, A. Sharonov, D. Onidas and T. Gustavsson. *The Effect of Molecular Organisation in DNA Oligomers Studied by Femtosecond Fluorescence Spectroscopy.* ChemPhysChem 4(3) (Mar. 2003), pp. 303–305.

[Mar05] C. M. Marian. *A new pathway for the rapid decay of electronically excited adenine.* The Journal of Chemical Physics 122(10) (Mar. 2005), p. 104314.

[Mar06] D. Markovitsi, F. Talbot, T. Gustavsson, D. Onidas, E. Lazzarotto and S. Marguet. *Molecular spectroscopy: Complexity of excited-state dynamics in DNA.* Nature 441(7094) (June 2006), E7–E7.

[Mar56a] R. A. Marcus. *Electrostatic Free Energy and Other Properties of States Having Nonequilibrium Polarization. I.* The Journal of Chemical Physics 24(5) (May 1956), pp. 979–989.

[Mar56b] R. A. Marcus. *On the Theory of Oxidation-Reduction Reactions Involving Electron Transfer. I.* The Journal of Chemical Physics 24(5) (May 1956), pp. 966–978.

[Mar60] R. A. Marcus. *Exchange reactions and electron transfer reactions including isotopic exchange. Theory of oxidation-reduction reactions involving electron transfer. Part 4.–A statistical-mechanical basis for treating contributions from solvent, ligands, and inert salt.* Discussions of the Faraday Society 29 (Jan. 1960), pp. 21–31.

[Mar63] R. A. Marcus. *ON THE THEORY OF OXIDATION–REDUCTION REACTIONS INVOLVING ELECTRON TRANSFER. V. COMPARISON AND PROPERTIES OF ELECTROCHEMICAL AND CHEMICAL RATE CONSTANTS.* The Journal of Physical Chemistry 67(4) (Apr. 1963), pp. 853–857.

[Mar93] R. A. Marcus. *Electron transfer reactions in chemistry. Theory and experiment.* Reviews of Modern Physics 65(3) (July 1993), pp. 599–610.

[Mas92] P. E. Maslen, N. C. Handy, R. D. Amos and D. Jayatilaka. *Higher analytic derivatives. IV. Anharmonic effects in the benzene spectrum.* The Journal of Chemical Physics 97(6) (Sept. 1992), pp. 4233–4254.

[MAS99] M. A. Morsy, A. M. Al-Somali and A. Suwaiyan. *Fluorescence of Thymine Tautomers at Room Temperature in Aqueous Solutions.* The Journal of Physical Chemistry B 103(50) (Dec. 1999), pp. 11205–11210.

[Mat04] S. Matsika. *Radiationless Decay of Excited States of Uracil through Conical Intersections.* The Journal of Physical Chemistry A 108(37) (2004), pp. 7584–7590.

[Mat62] J. H. Matthaei, O. W. Jones, R. G. Martin and M. W. Nirenberg. *CHARACTERISTICS AND COMPOSITION OF RNA CODING UNITS.* Proceedings of the National Academy of Sciences of the United States of America 48(4) (Apr. 1962), pp. 666–677.

[McC52] H. McConnell. *Effect of Polar Solvents on the Absorption Frequency of n→π Electronic Transitions.* The Journal of Chemical Physics 20(4) (Apr. 1952), pp. 700–704.

[MCK07] C. T. Middleton, B. Cohen and B. Kohler. *Solvent and Solvent Isotope Effects on the Vibrational Cooling Dynamics of a DNA Base Derivative.* The Journal of Physical Chemistry A 111(42) (Oct. 2007), pp. 10460–10467.

[MEK01] J. M. Martínez, S. K. C. Elmroth and L. Kloo. *Influence of Sodium Ions on the Dynamics and Structure of Single-Stranded DNA Oligomers: A Molecular Dynamics Study.* Journal of the American Chemical Society 123(49) (Dec. 2001), pp. 12279–12289.

[Mer06] M. Merchán, R. González-Luque, T. Climent, L. Serrano-Andrés, E. Rodríguez, M. Reguero and D. Peláez. *Unified Model for the Ultrafast Decay of Pyrimidine Nucleobases.* The Journal of Physical Chemistry B 110(51) (2006), pp. 26471–26476.

[MGL75] K. Mutai, B. A. Gruber and N. J. Leonard. *Synthetic spectroscopic models. XIV. Intramolecular stacking interactions between indole and connected nucleic acid bases. Hypochromism and fluorescence.* Journal of the American Chemical Society 97(14) (July 1975), pp. 4095–4104.

[Mid09] C. T. Middleton, K. de La Harpe, C. Su, Y. K. Law, C. E. Crespo-Hernández and B. Kohler. *DNA Excited-State Dynamics: From Single Bases to the Double Helix.* Annual Review of Physical Chemistry 60(1) (2009), pp. 217–239.

[MK11] S. Matsika and P. Krause. *Nonadiabatic Events and Conical Intersections.* Annual Review of Physical Chemistry 62(1) (2011), pp. 621–643.

[MM05] S. Marguet and D. Markovitsi. *Time-Resolved Study of Thymine Dimer Formation.* Journal of the American Chemical Society 127(16) (Apr. 2005), pp. 5780–5781.

[Mou06] S. Mouret, C. Baudouin, M. Charveron, A. Favier, J. Cadet and T. Douki. *Cyclobutane pyrimidine dimers are predominant DNA lesions in whole human skin exposed to UVA radiation.* Proceedings of the National Academy of Sciences 103(37) (Sept. 2006), pp. 13765–13770.

[Mou10] S. Mouret, C. Philippe, J. Gracia-Chantegrel, A. Banyasz, S. Karpati, D. Markovitsi and T. Douki. *UVA-induced cyclobutane pyrimidine dimers in DNA: a direct photochemical mechanism?* Organic & Biomolecular Chemistry 8(7) (Mar. 2010), pp. 1706–1711.

[MS85] R. A. Marcus and N. Sutin. *Electron transfers in chemistry and biology.* Biochimica et Biophysica Acta (BBA) - Reviews on Bioenergetics 811(3) (Aug. 1985), pp. 265–322.

[MT86] J. Michl and E. W. Thulstrup. *Spectroscopy with polarized light: solute alignment by photoselection, in liquid crystals, polymers, and membranes.* VCH, 1986.

[MVH99] J. B. Mills, E. Vacano and P. J. Hagerman. *Flexibility of single-stranded DNA: use of gapped duplex helices to determine the persistence lengths of Poly(dT) and Poly(dA).* Journal of Molecular Biology 285(1) (Jan. 1999), pp. 245–257.

[Nac11] D. Nachtigallová, A. J. A. Aquino, J. J. Szymczak, M. Barbatti, P. Hobza and H. Lischka. *Nonadiabatic Dynamics of Uracil: Population Split among Different Decay Mechanisms.* The Journal of Physical Chemistry A 115(21) (June 2011), pp. 5247–5255.

[Nak13] A. Nakayama, G. Arai, S. Yamazaki and T. Taketsugu. *Solvent effects on the ultrafast nonradiative deactivation mechanisms of thymine in aqueous solution: Excited-state QM/MM molecular dynamics simulations.* The Journal of Chemical Physics 139(21) (Dec. 2013), p. 214304.

[Nik90] D. Nikogosyan. *Two-quantum UV Photochemistry of Nucleic Acids: Comparison with Conventional Low-intensity UV Photochemistry and Radiation Chemistry.* International Journal of Radiation Biology 57(2) (Jan. 1990), pp. 233–299.

[NL83] D. N. Nikogosyan and V. S. Letokhov. *Nonlinear laser photophysics, photochemistry and photobiology of nucleic acids.* La Rivista del Nuovo Cimento 6(8) (Aug. 1983), pp. 1–72.

[Nor11] M. Norval, R. M. Lucas, A. P. Cullen, F. R. de Gruijl, J. Longstreth, Y. Takizawa and J. C. van der Leun. *The human health effects of ozone depletion and interactions with climate change.* Photochemical & Photobiological Sciences: Official Journal of the European Photochemistry Association and the European Society for Photobiology 10(2) (Feb. 2011), pp. 199–225.

[NOR83] D. N. Nikogosyan, A. A. Oraevsky and V. I. Rupasov. *Two-photon ionization and dissociation of liquid water by powerful laser UV radiation.* Chemical Physics 77(1) (May 1983), pp. 131–143.

[Ola06] G. Olaso-González, D. Roca-Sanjuán, L. Serrano-Andrés and M. Merchán. *Toward the understanding of DNA fluorescence: The singlet excimer of cytosine.* The Journal of Chemical Physics 125(23) (Dec. 2006), p. 231102.

[Oni02] D. Onidas, D. Markovitsi, S. Marguet, A. Sharonov and T. Gustavsson. *Fluorescence Properties of DNA Nucleosides and Nucleotides: A Refined Steady-State and Femtosecond Investigation.* The Journal of Physical Chemistry B 106(43) (Oct. 2002), pp. 11367–11374.

[ORH94] J. C. Owrutsky, D. Raftery and R. M. Hochstrasser. *Vibrational Relaxation Dynamics in Solutions.* Annual Review of Physical Chemistry 45(1) (1994), pp. 519–555.

[Ost03] T. Ostrowski, J.-C. Maurizot, M.-T. Adeline, J.-L. Fourrey and P. Clivio. *Sugar Conformational Effects on the Photochemistry of Thymidylyl(3'-5')thymidine.* The Journal of Organic Chemistry 68(17) (Aug. 2003), pp. 6502–6510.

[Pan09] S. Pandelov, B. M. Pilles, J. C. Werhahn and H. Iglev. *Time-Resolved Dynamics of the OH Stretching Vibration in Aqueous NaCl Hydrate.* The Journal of Physical Chemistry A 113(38) (Sept. 2009), pp. 10184–10188.

[Pan10] S. Pandelov, J. C. Werhahn, B. M. Pilles, S. S. Xantheas and H. Iglev. *An Empirical Correlation between the Enthalpy of Solution of Aqueous Salts and Their Ability to Form Hydrates.* The Journal of Physical Chemistry A 114(38) (Sept. 2010), pp. 10454–10457.

[Pan11] Z. Pan, J. Chen, W. J. Schreier, B. Kohler and F. D. Lewis. *Thymine Dimer Photoreversal in Purine-Containing Trinucleotides.* The Journal of Physical Chemistry B 116(1) (2011), pp. 698–704.

[PBH05] T. S. C. Poon, R. S. C. Barnetson and G. M. Halliday. *Sunlight-induced immunosuppression in humans is initially because of UVB, then UVA, followed by interactive effects.* The Journal of Investigative Dermatology 125(4) (Oct. 2005), pp. 840–846.

[Per74] S. Person, J. A. McCloskey, W. Snipes and R. C. Bockrath. *Ultraviolet Mutagenesis and Its Repair in an Escherichia Coli Strain Containing a Nonsense Codon.* Genetics 78(4) (Dec. 1974), pp. 1035–1049.

[Pes89] M. Pessot, D. J. Harter, J. Squier and G. Mourou. *Chirped-pulse amplification of 100-fsec pulses.* Optics Letters 14(15) (Aug. 1989), pp. 797–799.

[Pil14a] B. M. Pilles, D. B. Bucher, L. Liu, P. Clivio, P. Gilch, W. Zinth and W. J. Schreier. *Mechanism of the Decay of Thymine Triplets in DNA Single Strands.* The Journal of Physical Chemistry Letters 5(9) (May 2014), pp. 1616–1622.

[Pil14b] B. M. Pilles, D. B. Bucher, L. Liu, P. Gilch, W. Zinth and W. J. Schreier. *Identification of charge separated states in thymine single strands*. Chemical Communications 50(98) (Nov. 2014), pp. 15623–15626.

[Ple00] R. Plessow, A. Brockhinke, W. Eimer and K. Kohse-Höinghaus. *Intrinsic Time- and Wavelength-Resolved Fluorescence of Oligonucleotides: A Systematic Investigation Using a Novel Picosecond Laser Approach*. The Journal of Physical Chemistry B 104(15) (Apr. 2000), pp. 3695–3704.

[PMM87] M. Pessot, P. Maine and G. Mourou. *1000 times expansion/compression of optical pulses for chirped pulse amplification*. Optics Communications 62(6) (June 1987), pp. 419–421.

[PPK00] J.-M. L. Pecourt, J. Peon and B. Kohler. *Ultrafast Internal Conversion of Electronically Excited RNA and DNA Nucleosides in Water*. Journal of the American Chemical Society 122(38) (Sept. 2000), pp. 9348–9349.

[PPK01] J.-M. L. Pecourt, J. Peon and B. Kohler. *DNA Excited-State Dynamics: Ultrafast Internal Conversion and Vibrational Cooling in a Series of Nucleosides*. Journal of the American Chemical Society 123(42) (Oct. 2001), pp. 10370–10378.

[Pre09] Pregl, Sebastian Philipp. *Integration und Erprobung eines Vielkanal-Detektorsystems im mittleren infraroten Wellenlängenbereich zur Untersuchung ultraschneller Schwingungs-Relaxationsprozesse*. Diploma thesis. Munich: Ludwig-Maximilians-Universität, 2009.

[Pre74] B. Prescott, R. Gamache, J. Livramento and G. J. Thomas. *Raman studies of nucleic acids. XII. Conformations of oligonucleotides and deuterated polynucleotides*. Biopolymers 13(9) (Sept. 1974), pp. 1821–1845.

[PS96] W. Peng and B. R. Shaw. *Accelerated Deamination of Cytosine Residues in UV-Induced Cyclobutane Pyrimidine Dimers Leads to CC→TT Transitions*. Biochemistry 35(31) (Jan. 1996), pp. 10172–10181.

[PSD05] S. Perun, A. L. Sobolewski and W. Domcke. *Ab Initio Studies on the Radiationless Decay Mechanisms of the Lowest Excited Singlet States of 9H-Adenine*. Journal of the American Chemical Society 127(17) (2005), pp. 6257–6265.

[PSD06] S. Perun, A. L. Sobolewski and W. Domcke. *Conical Intersections in Thymine*. The Journal of Physical Chemistry A 110(49) (Dec. 2006), pp. 13238–13244.

[Qui07] S. Quinn, G. W. Doorley, G. W. Watson, A. J. Cowan et al. *Ultrafast IR spectroscopy of the short-lived transients formed by UV excitation of cytosine derivatives.* Chemical Communications (21) (May 2007), pp. 2130–2132.

[RDC01] J.-L. Ravanat, T. Douki and J. Cadet. *Direct and indirect effects of UV radiation on DNA and its components.* Journal of Photochemistry and Photobiology B: Biology. Consequences of exposure to sunlight:elements to assess protection 63(1–3) (Oct. 2001), pp. 88–102.

[Reu00] A. Reuther, H. Iglev, R. Laenen and A. Laubereau. *Femtosecond photo-ionization of nucleic acid bases: electronic lifetimes and electron yields.* Chemical Physics Letters 325(4) (July 2000), pp. 360–368.

[Rho61] W. Rhodes. *Hypochromism and Other Spectral Properties of Helical Polynucleotides.* Journal of the American Chemical Society 83(17) (Sept. 1961), pp. 3609–3617.

[Rie00] E. Riedle, M. Beutter, S. Lochbrunner, J. Piel, S. Schenkl, S. Spörlein and W. Zinth. *Generation of 10 to 50 fs pulses tunable through all of the visible and the NIR.* Applied Physics B 71(3) (June 2000), pp. 457–465.

[RNL96] A. Reuther, D. N. Nikogosyan and A. Laubereau. *Primary Photochemical Processes in Thymine in Concentrated Aqueous Solution Studied by Femtosecond UV Spectroscopy.* The Journal of Physical Chemistry 100(13) (1996), pp. 5570–5577.

[Roc03] P. J. Rochette, J.-P. Therrien, R. Drouin, D. Perdiz, N. Bastien, E. A. Drobetsky and E. Sage. *UVA-induced cyclobutane pyrimidine dimers form predominantly at thymine–thymine dipyrimidines and correlate with the mutation spectrum in rodent cells.* Nucleic Acids Research 31(11) (June 2003), pp. 2786–2794.

[Rod09] C. T. Rodgers. *Magnetic field effects in chemical systems.* Pure and Applied Chemistry 81(1) (2009), pp. 19–43.

[Sal07] B. E. A. Saleh. *Fundamentals of photonics.* 2nd ed. Wiley series in pure and applied optics. Hoboken, N.J: Wiley Interscience, 2007.

[San03] A. Sancar. *Structure and Function of DNA Photolyase and Cryptochrome Blue-Light Photoreceptors.* Chemical Reviews 103(6) (June 2003), pp. 2203–2238.

[San13] F. Santoro, R. Improta, F. Avila, M. Segado and A. Lami. *The interplay between neutral exciton and charge transfer states in single-strand polyadenine: a quantum dynamical investigation.* Photochemical & Photobiological Sciences 12(8) (Aug. 2013), pp. 1527–1543.

[Sat04] Satzger, Helmut. *Untersuchung initialer Schritte der Peptidfaltung mit Ultrakurzzeitspektroskopie*. PhD Thesis. Munich: Ludwig-Maximilians-Universität, 2004.

[Sat06] H. Satzger, D. Townsend, M. Z. Zgierski, S. Patchkovskii, S. Ullrich and A. Stolow. *Primary processes underlying the photostability of isolated DNA bases: Adenine*. Proceedings of the National Academy of Sciences 103(27) (July 2006), pp. 10196–10201.

[SB62] S. J. Strickler and R. A. Berg. *Relationship between Absorption Intensity and Fluorescence Lifetime of Molecules*. The Journal of Chemical Physics 37(4) (Aug. 1962), pp. 814–822.

[SB75] C. Salet and R. Bensasson. *Studies on Thymine and Uracil Triplet Excited State in Acetonitrile and Water*. Photochemistry and Photobiology 22(6) (1975), pp. 231–235.

[SBB79] C. Salet, R. Bensasson and R. S. Becker. *TRIPLET EXCITED STATES OF PYRIMIDINE NUCLEOSIDES AND NUCLEOTIDES*. Photochemistry and Photobiology 30(3) (Sept. 1979), pp. 325–329.

[SBI07] F. Santoro, V. Barone and R. Improta. *Influence of base stacking on excited-state behavior of polyadenine in water, based on time-dependent density functional calculations*. Proceedings of the National Academy of Sciences 104(24) (June 2007), pp. 9931–9936.

[SBI09] F. Santoro, V. Barone and R. Improta. *Excited States Decay of the A–T DNA: A PCM/TD-DFT Study in Aqueous Solution of the (9-Methyl-adenine)$_2$·(1-methyl-thymine)$_2$ Stacked Tetramer*. Journal of the American Chemical Society 131(42) (Oct. 2009), pp. 15232–15245.

[Sch07] W. J. Schreier, T. E. Schrader, F. O. Koller, P. Gilch et al. *Thymine Dimerization in DNA Is an Ultrafast Photoreaction*. Science 315(5812) (Feb. 2007), pp. 625–629.

[Sch08] Schreier, Wolfgang Johannes. *UV-Strahlung und DNA-Schäden – Untersuchung UV-induzierter Prozesse in Nukleinsäuren mit Femtosekunden-Infrarotspektroskopie*. PhD Thesis. Munich: Ludwig-Maximilians-Universität, 2008.

[Sch09] W. J. Schreier, J. Kubon, N. Regner, K. Haiser, T. E. Schrader, W. Zinth, P. Clivio and P. Gilch. *Thymine Dimerization in DNA Model Systems: Cyclobutane Photolesion Is Predominantly Formed via the Singlet Channel*. Journal of the American Chemical Society 131(14) (Apr. 2009), pp. 5038–5039.

[Sch11] Schuster, Benjamin Johannes. *Integration einer IR-Vielkanaldetektion in ein bestehendes Anreg-Abtast-Experiment und Femtosekundenspektroskopie an Azobenzol Dabcyl Säure.* Diploma thesis. Munich: Ludwig-Maximilians-Universität, 2011.

[Ser07] J. J. Serrano-Pérez, R. González-Luque, M. Merchán and L. Serrano-Andrés. *On the Intrinsic Population of the Lowest Triplet State of Thymine.* The Journal of Physical Chemistry B 111(41) (Oct. 2007), pp. 11880–11883.

[SG81] J. C. Sutherland and K. P. Griffin. *Absorption Spectrum of DNA for Wavelengths Greater than 300 nm.* Radiation Research 86(3) (June 1981), pp. 399–410.

[SH84] M. J. Scanlan and I. H. Hillier. *An ab initio study of tautomerism of uracil, thymine, 5-fluorouracil, and cytosine.* Journal of the American Chemical Society 106(13) (June 1984), pp. 3737–3745.

[Sha03] A. Sharonov, T. Gustavsson, V. Carré, E. Renault and D. Markovitsi. *Cytosine excited state dynamics studied by femtosecond fluorescence upconversion and transient absorption spectroscopy.* Chemical Physics Letters 380(1–2) (Oct. 2003), pp. 173–180.

[Sha89] Z. Shakked, G. Guerstein-Guzikevich, M. Eisenstein, F. Frolow and D. Rabinovich. *The conformation of the DNA double helix in the crystal is dependent on its environment.* Nature 342(6248) (Nov. 1989), pp. 456–460.

[She03] Y. R. Shen. *The principles of nonlinear optics.* Wiley classics library ed. Wiley classics library. Hoboken, N.J: Wiley-Interscience, 2003.

[SL02] M. K. Shukla and J. Leszczynski. *Phototautomerism in Uracil: A Quantum Chemical Investigation.* The Journal of Physical Chemistry A 106(37) (Sept. 2002), pp. 8642–8650.

[SLG04] I. H. M. van Stokkum, D. S. Larsen and R. van Grondelle. *Global and target analysis of time-resolved spectra.* Biochimica et Biophysica Acta (BBA) - Bioenergetics 1657(2–3) (July 2004), pp. 82–104.

[SM85] D. Strickland and G. Mourou. *Compression of amplified chirped optical pulses.* Optics Communications 56(3) (Dec. 1985), pp. 219–221.

[SMB06] L. Serrano-Andrés, M. Merchán and A. C. Borin. *Adenine and 2-Aminopurine: Paradigms of Modern Theoretical Photochemistry.* Proceedings of the National Academy of Sciences of the United States of America 103(23) (June 2006), pp. 8691–8696.

[SMD64] A. B. Shafer, L. R. Megill and L. Droppleman. *Optimization of the Czerny-Turner Spectrometer.* Journal of the Optical Society of America 54(7) (July 1964), p. 879.

[Son98] Q. Song, W. Lin, S. Yao and N. Lin. *Comparative studies of triplet states of thymine components by acetone sensitization and direct excitation in aqueous solution at room temperature.* Journal of Photochemistry and Photobiology A: Chemistry 114(3) (Apr. 1998), pp. 181–184.

[Spö01] Spörlein, Sebastian. *Femtosekunden-Spektroskopie schnellster Strukturänderungen in Peptid-Chromophor-Komplexen.* Diploma thesis. Munich: Ludwig-Maximilians-Universität, 2001.

[SS15] J.-Y. Salpin and D. Scuderi. *Structure of protonated thymidine characterized by infrared multiple photon dissociation and quantum calculations.* Rapid Communications in Mass Spectrometry 29(20) (Oct. 2015), pp. 1898–1904.

[SSK14] O. A. Stasyuk, H. Szatylowicz and T. M. Krygowski. *Tautomerisation of thymine acts against the Hückel 4N + 2 rule. The effect of metal ions and H-bond complexations on the electronic structure of thymine.* Organic & Biomolecular Chemistry 12(33) (July 2014), pp. 6476–6483.

[Ste94] P. J. Stephens, F. J. Devlin, C. F. Chabalowski and M. J. Frisch. *Ab Initio Calculation of Vibrational Absorption and Circular Dichroism Spectra Using Density Functional Force Fields.* The Journal of Physical Chemistry 98(45) (Nov. 1994), pp. 11623–11627.

[Stü32] E. Stückelberg. *Theory of inelastic collisions between atoms(Theory of inelastic collisions between atoms, using two simultaneous differential equations).* Helv. Phys. Acta,(Basel) 5 (1932), pp. 369–422.

[SU89] U. E. Steiner and T. Ulrich. *Magnetic field effects in chemical kinetics and related phenomena.* Chemical Reviews 89(1) (Jan. 1989), pp. 51–147.

[Szy09] J. J. Szymczak, M. Barbatti, J. T. Soo Hoo, J. A. Adkins, T. L. Windus, D. Nachtigallová and H. Lischka. *Photodynamics Simulations of Thymine: Relaxation into the First Excited Singlet State.* The Journal of Physical Chemistry A 113(45) (Nov. 2009), pp. 12686–12693.

[Tak08] T. Takaya, C. Su, K. d. L. Harpe, C. E. Crespo-Hernández and B. Kohler. *UV Excitation of Single DNA and RNA Strands Produces High Yields of Exciplex States between Two Stacked Bases.* Proceedings of the National Academy of Sciences of the United States of America 105(30) (July 2008), pp. 10285–10290.

[Tan01] K. Tanimura. *Femtosecond time-resolved spectroscopy of the formation of self-trapped excitons in CaF2.* Physical Review B 63(18) (Apr. 2001), p. 184303.

[Tay94] J. S. Taylor. *Unraveling the Molecular Pathway from Sunlight to Skin Cancer*. Accounts of Chemical Research 27(3) (Mar. 1994), pp. 76–82.

[Tin60] I. Tinoco. *Hypochromism in Polynucleotides*. Journal of the American Chemical Society 82(18) (Sept. 1960), pp. 4785–4790.

[TK93] D. C. Thomas and T. A. Kunkel. *Replication of UV-irradiated DNA in human cell extracts: evidence for mutagenic bypass of pyrimidine dimers*. Proceedings of the National Academy of Sciences 90(16) (Aug. 1993), pp. 7744–7748.

[Tre69] E. Treacy. *Optical pulse compression with diffraction gratings*. IEEE Journal of Quantum Electronics 5(9) (Sept. 1969), pp. 454–458.

[Tsu02] T. Tsujibayashi, K. Toyoda, S. Sakuragi, M. Kamada and M. Itoh. *Spectral profile of the two-photon absorption coefficients in CaF2 and BaF2*. Applied Physics Letters 80(16) (Apr. 2002), pp. 2883–2885.

[TTM05] K. Tomić, J. Tatchen and C. M. Marian. *Quantum Chemical Investigation of the Electronic Spectra of the Keto, Enol, and Keto-Imine Tautomers of Cytosine*. The Journal of Physical Chemistry A 109(37) (Sept. 2005), pp. 8410–8418.

[UJ75] J. Ulstrup and J. Jortner. *The effect of intramolecular quantum modes on free energy relationships for electron transfer reactions*. The Journal of Chemical Physics 63(10) (Nov. 1975), pp. 4358–4368.

[Vay10] I. Vayá, T. Gustavsson, F.-A. Miannay, T. Douki and D. Markovitsi. *Fluorescence of Natural DNA: From the Femtosecond to the Nanosecond Time Scales*. Journal of the American Chemical Society 132(34) (Sept. 2010), pp. 11834–11835.

[Vay12] I. Vayá, T. Gustavsson, T. Douki, Y. Berlin and D. Markovitsi. *Electronic Excitation Energy Transfer between Nucleobases of Natural DNA*. Journal of the American Chemical Society 134(28) (July 2012), pp. 11366–11368.

[VR01] A. A. Vink and L. Roza. *Biological consequences of cyclobutane pyrimidine dimers*. Journal of Photochemistry and Photobiology B: Biology 65(2–3) (Dec. 2001), pp. 101–104.

[Wal95] G. C. Walker. *SOS-regulated proteins in translesion DNA synthesis and mutagenesis*. Trends in Biochemical Sciences 20(10) (Oct. 1995), pp. 416–420.

[Wan83] A. H.-J. Wang, S. Fujii, J. H. v. Boom and A. Rich. *Right-handed and Left-handed Double-helical DNA: Structural Studies*. Cold Spring Harbor Symposia on Quantitative Biology 47 (Jan. 1983), pp. 33–44.

[WB68] P. J. Wagner and D. J. Bucheck. *Causes for the low efficiency of thymine and uracil photodimerization in solution.* Journal of the American Chemical Society 90(23) (Nov. 1968), pp. 6530–6532.

[WB70] P. J. Wagner and D. J. Bucheck. *Photodimerization of thymine and uracil in acetonitrile.* Journal of the American Chemical Society 92(1) (Jan. 1970), pp. 181–185.

[WC53a] J. D. Watson and F. H. Crick. *Molecular structure of nucleic acids; a structure for deoxyribose nucleic acid.* Nature 171(4356) (Apr. 1953), pp. 737–738.

[WC53b] J. D. Watson and F. H. C. Crick. *Genetical Implications of the Structure of Deoxyribonucleic Acid.* Nature 171(4361) (May 1953), pp. 964–967.

[WC70] M. M. Warshaw and C. R. Cantor. *Oligonucleotide interactions. IV. Conformational differences between deoxy- and ribodinucleoside phosphates.* Biopolymers 9(9) (Sept. 1970), pp. 1079–1103.

[Web02] S. Weber, C. W. M. Kay, H. Mögling, K. Möbius, K. Hitomi and T. Todo. *Photoactivation of the flavin cofactor in Xenopus laevis (6–4) photolyase: Observation of a transient tyrosyl radical by time-resolved electron paramagnetic resonance.* Proceedings of the National Academy of Sciences 99(3) (Feb. 2002), pp. 1319–1322.

[Web05] S. Weber. *Light-driven enzymatic catalysis of DNA repair: a review of recent biophysical studies on photolyase.* Biochimica et Biophysica Acta (BBA) - Bioenergetics. Functional Redox Radicals in Proteins 1707(1) (Feb. 2005), pp. 1–23.

[WJ72] D. W. Whillans and H. E. Johns. *Triplet state studies of the nucleoside and nucleotide derivatives of uracil and thymine.* Biochimica et Biophysica Acta (BBA) - Nucleic Acids and Protein Synthesis 277(1) (Aug. 1972), pp. 1–6.

[WPR97] T. Wilhelm, J. Piel and E. Riedle. *Sub-20-fs pulses tunable across the visible from a blue-pumped single-pass noncollinear parametric converter.* Optics Letters 22(19) (Oct. 1997), pp. 1494–1496.

[WS97] M. C. Wahl and M. Sundaralingam. *Crystal structures of A-DNA duplexes.* Biopolymers 44(1) (1997), pp. 45–63.

[WSW53] M. H. F. Wilkins, A. R. Stokes and H. R. Wilson. *Molecular Structure of Nucleic Acids: Molecular Structure of Deoxypentose Nucleic Acids.* Nature 171(4356) (Apr. 1953), pp. 738–740.

[Wu90] P. Wu, T. M. Nordlund, B. Gildea and L. W. McLaughlin. *Base stacking and unstacking as determined from a DNA decamer containing a fluorescent base.* Biochemistry 29(27) (July 1990), pp. 6508–6514.

[YT11] S. Yamazaki and T. Taketsugu. *Nonradiative Deactivation Mechanisms of Uracil, Thymine, and 5-Fluorouracil: A Comparative ab Initio Study.* The Journal of Physical Chemistry A 116(1) (Dec. 2011), pp. 491–503.

[Yua11] S. Yuan, W. Zhang, L. Liu, Y. Dou, W. Fang and G. V. Lo. *Detailed Mechanism for Photoinduced Cytosine Dimerization: A Semiclassical Dynamics Simulation.* The Journal of Physical Chemistry A 115(46) (Nov. 2011), pp. 13291–13297.

[YZE11] Z. b. Yang, R. b. Zhang and L. A. Eriksson. *A triplet mechanism for the formation of thymine-thymine (6-4) dimers in UV-irradiated DNA.* Physical Chemistry Chemical Physics 13(19) (Apr. 2011), pp. 8961–8966.

[ZB08] G. Zechmann and M. Barbatti. *Photophysics and Deactivation Pathways of Thymine.* The Journal of Physical Chemistry A 112(36) (Sept. 2008), pp. 8273–8279.

[ZE06] R. B. Zhang and L. A. Eriksson. *A Triplet Mechanism for the Formation of Cyclobutane Pyrimidine Dimers in UV-Irradiated DNA.* The Journal of Physical Chemistry B 110(14) (Apr. 2006), pp. 7556–7562.

[Zen32] C. Zener. *Non-Adiabatic Crossing of Energy Levels.* Proceedings of the Royal Society of London A: Mathematical, Physical and Engineering Sciences 137(833) (Sept. 1932), pp. 696–702.

[Zew00] A. H. Zewail. *Femtochemistry: Atomic-Scale Dynamics of the Chemical Bond.* The Journal of Physical Chemistry A 104(24) (2000), pp. 5660–5694.

[Zew93] A. H. Zewail. *Femtochemistry.* The Journal of Physical Chemistry 97(48) (1993), pp. 12427–12446.

[ZH14] X. Zhang and J. M. Herbert. *Excited-State Deactivation Pathways in Uracil versus Hydrated Uracil: Solvatochromatic Shift in the $^1n\pi^*$ State is the Key.* The Journal of Physical Chemistry B 118(28) (July 2014), pp. 7806–7817.

List of Publications

- S. Pandelov, B. M. Pilles, J. C. Werhahn and H. Iglev. *Time-Resolved Dynamics of the OH Stretching Vibration in Aqueous NaCl Hydrate*. The Journal of Physical Chemistry A 113(38) (Sept. 2009), pp. 10184–10188

- S. Pandelov, J. C. Werhahn, B. M. Pilles, S. S. Xantheas and H. Iglev. *An Empirical Correlation between the Enthalpy of Solution of Aqueous Salts and Their Ability to Form Hydrates*. The Journal of Physical Chemistry A 114(38) (Sept. 2010), pp. 10454–10457

- K. Haiser, B. P. Fingerhut, K. Heil, A. Glas, T. T. Herzog, B. M. Pilles, W. J. Schreier, W. Zinth, R. de Vivie-Riedle and T. Carell. *Mechanism of UV-Induced Formation of Dewar Lesions in DNA*. Angewandte Chemie International Edition 51(2) (Jan. 2012), pp. 408–411

- D. B. Bucher, B. M. Pilles, T. Pfaffeneder, T. Carell and W. Zinth. *Fingerprinting DNA Oxidation Processes: IR Characterization of the 5-Methyl-2'-Deoxycytidine Radical Cation*. ChemPhysChem 15(3) (Feb. 2014), pp. 420–423

- D. B. Bucher, B. M. Pilles, T. Carell and W. Zinth. *Charge separation and charge delocalization identified in long-living states of photoexcited DNA*. Proceedings of the National Academy of Sciences 111(12) (Mar. 2014), pp. 4369–4374

- A. A. Deeg, M. S. Rampp, A. Popp, B. M. Pilles, T. E. Schrader, L. Moroder, K. Hauser and W. Zinth. *Isomerization- and Temperature-Jump-Induced Dynamics of a Photoswitchable β-Hairpin*. Chemistry – A European Journal 20(3) (Jan. 2014), pp. 694–703

- B. M. Pilles, D. B. Bucher, L. Liu, P. Clivio, P. Gilch, W. Zinth and W. J. Schreier. *Mechanism of the Decay of Thymine Triplets in DNA Single Strands*. The Journal of Physical Chemistry Letters 5(9) (May 2014), pp. 1616–1622

- B. M. Pilles, D. B. Bucher, L. Liu, P. Gilch, W. Zinth and W. J. Schreier. *Identification of charge separated states in thymine single strands*. Chemical Communications 50(98) (Nov. 2014), pp. 15623–15626

- D. B. Bucher, B. M. Pilles, T. Carell and W. Zinth. *Dewar Lesion Formation in Single- and Double-Stranded DNA is Quenched by Neighboring Bases.* The Journal of Physical Chemistry B 119(28) (July 2015), pp. 8685–8692
- L. Liu, B. M. Pilles, A. M. Reiner, J. Gontcharov and W. Zinth. *2'-Methoxyacetophenone: An Efficient Photosensitizer for Cyclobutane Pyrimidine Dimer Formation.* ChemPhysChem 16(16) (Nov. 2015), pp. 3483–3487
- L. Liu, B. M. Pilles, J. Gontcharov, D. B. Bucher and W. Zinth. *Quantum Yield of Cyclobutane Pyrimidine Dimer Formation Via the Triplet Channel Determined by Photosensitization.* The Journal of Physical Chemistry B 120(2) (Jan. 2016), pp. 292–298

Danksagung

Einige Menschen haben durch ihre Unterstützung sehr zum Gelingen dieser Arbeit beigetragen. Ihnen möchte ich an dieser Stelle danken:

Prof. Dr. Wolfgang Zinth für die Gelegenheit am BMO meine Doktorarbeit zu machen, seine Unterstützung und Hilfsbereitschaft, sein Interesse an der Forschung und an seinen Mitarbeitern und das hervorragende Arbeitsklima.

Prof. Dr. Peter Gilch für die Übernahme des Zweitgutachtens, die vielen Diskussionen über die Interpretation der Daten und seine Unterstützung beim Publizieren derselben.

Dr. Wolfgang Schreier für die Starthilfe am Anfang meiner Promotion und die andauernde Unterstützung beim Diskutieren und Veröffentlichen der Daten.

Dem Z20 Team Dr. Karin Haiser, Dr. Teja Herzog, Dr. Andreas Deeg, Dr. Dominik Bucher, Benjamin März, Benjamin Schuster, Michael Rampp und Lizhe Liu für die angenehme Zusammenarbeit im Labor.

Dem IT Team Dr. Karl-Heinz Mantel und Florian Trommer für ihre kompetente Hilfe bei allen Computerfragen.

Julia Gontcharov für das aufopferungsvolle Korrekturlesen meiner Doktorarbeit und ihre Hilfe bei allen Formatierungsproblemen, hauptsächlich jedoch für die Unterstützung in allen Lebenslagen.

Anne Reiner und Ilvana Turkanovic für das Korrekturlesen meiner Arbeit und die konstruktive Kritik.

Der AG Zinth für die gute Zusammenarbeit und das hervorragende Betriebsklima.

Dem Sekretariat and damit Alexandra Michaelis und Marianne Widmann-Diermeier für die stets freundliche Hilfe bei allen Verwaltungsangelegenheiten.

Der Werkstatt und damit Rudolf Schwarz, Alfons Stork, Christian Hausmann und Harald Hoppe für die zügige Ausführung aller Aufträge.

Meiner Familie für die andauernde Unterstützung vor allem während des Studiums. Ohne sie wäre es nicht zu dieser Arbeit gekommen.